



Evolution of the ultrastructure, parietal composition and mechanical properties of flax fibres over time: when history meets science

Alessia Melelli

► To cite this version:

Alessia Melelli. Evolution of the ultrastructure, parietal composition and mechanical properties of flax fibres over time: when history meets science. Materials. Université de Bretagne Sud, 2021. English. NNT : 2021LORIS606 . tel-03613043

HAL Id: tel-03613043

<https://theses.hal.science/tel-03613043>

Submitted on 18 Mar 2022

HAL is a multi-disciplinary open access archive for the deposit and dissemination of scientific research documents, whether they are published or not. The documents may come from teaching and research institutions in France or abroad, or from public or private research centers.

L'archive ouverte pluridisciplinaire **HAL**, est destinée au dépôt et à la diffusion de documents scientifiques de niveau recherche, publiés ou non, émanant des établissements d'enseignement et de recherche français ou étrangers, des laboratoires publics ou privés.

THESE DE DOCTORAT DE

L'UNIVERSITE BRETAGNE SUD

ECOLE DOCTORALE N° 602
Sciences pour l'Ingénieur
Spécialité : Génie des Matériaux

Par

Alessia MELELLI

Evolution of the ultrastructure, parietal composition and mechanical properties of flax fibres over time: when history meets science

Évolution de l'ultrastructure, de la composition des parois et des propriétés mécaniques des fibres de lin au fil du temps: quand l'histoire rencontre la science

Thèse présentée et soutenue à Lorient, le 29 novembre 2021

Unité de recherche : IRDL

Thèse N° : 606

Rapporteurs avant soutenance :

Anne BERGERET
Anita QUILLES

Professeur des Universités, C2MA, IMT Mines Alès
Ingénieur de Recherche, HDR, IFAO, Le Caire

Composition du Jury :

Président : Ludovic BELLOT-GURLET
Examineurs : Olivier ARNOULD
Giulia CANEVA

Professeur des Universités, MONARIS, Sorbonne Université
Maître de Conférences, LMGC, Université Montpellier
Professeur des Universités, Département des sciences, Université Rome III

Dir. de thèse : Alain BOURMAUD
Co-dir. de thèse : Johnny BEAUGRAND
Frédéric JAMME

Ingénieur de Recherche, HDR, IRDL, Université Bretagne Sud
Directeur de Recherche, BIA, INRAE, Nantes
Ingénieur de Recherche, ligne de lumière DISCO, Synchrotron SOLEIL

*<< Tu mostri non aver posto mente che la vita di quest'universo è un
perpetuo circuito di produzione e distruzione, collegate ambedue tra sé
di maniera, che ciascheduna serve continuamente all'altra, ed alla
conservazione del mondo; il quale sempre che cessasse o l'una o l'altra
di loro, verrebbe parimente in dissoluzione.>>*

Dialogo della Natura e di un Islandese- Giacomo Leopardi, 1824



*<< Evidently, you have not considered that in this universe life is a
perpetual cycle of production and destruction, both functions being so
closely bound together that one is continuously working toward the
other, thus bringing about the conservation of the world, which, if either
one of them were to cease, would likewise dissolve>>*

Dialogue between Nature and an Iclander- Giacomo Leopardi

*Operette Morali: Essays and Dialogues by Giacomo Leopardi,
Translated by Giovanni Cecchetti, University of California Press, US, 1983*

REMERCIEMENTS

Cette partie est souvent la moins considérée mais nous oublions que des travaux de recherche ne sont jamais effectués par une seule personne.

Je souhaite remercier mes trois encadrants, Alain, Johnny et Frédéric qui m'ont soutenue, par ailleurs, supportée durant ces trois années.

Ils se sont vite aperçus que je suis une personne têtue, parfois même un peu trop. L'étude des fibres anciennes n'était pas l'objectif initial de leur recherche, mais ils m'ont fait confiance pour le développement de cette idée et ensemble nous avons construit un nouveau chemin qui nous a amené vers des nouvelles frontières méconnues.

Je tiens également à remercier Olivier Arnould, la colonne portante pour toute la partie théorique d'AFM et nanoindentation. Je l'ai considéré comme un quatrième encadrant qui a suivi chaque préparation d'échantillons, chaque article, chaque CSI et chaque étape depuis le début. Sans ces quatre personnes, cette recherche n'aurait jamais pu être réalisée et aboutir.

Je voudrais, aussi, remercier Sylvie Durand, Camille Alvarado et toute l'équipe INRAE de Nantes pour tout le support pour la préparation des échantillons, la session DISCO et toutes les analyses biochimiques effectuées dans une course contre la montre.

Un gros merci à Antoine Kervoëlen pour toute la partie des tests mécaniques sur fibres élémentaires et qui a dû m'aider à extraire et à coller une centaine des fibres unitaires (désolée, mais j'ai découvert que je n'étais vraiment pas faite pour l'extraction des fibres). Anthony Magueresse, pour l'énormité du temps passé au MEB en essayant de comprendre ce que je voulais, quand moi non plus je ne savais pas trop quoi chercher. Eric Balnois, pour les journées passées à discuter et lutter ensemble pour comprendre tous les réglages de l'AFM.

Je remercie Chloé Joly et Lise Dugor pour leur patience, car je suis tellement tête-en-l'air que sans elles j'aurais, sans doute, oublié la moitié des démarches administratives à faire.

Je remercie les partenaires du projet, en premier lieu, Darshil Shah de l'université de Cambridge et toute son énergie positive. Le groupe Depestele pour avoir cultivé mes plantes de lin avec autant d'amour, et l'université de Portsmouth, Ecotechnilin, Howa Tramico et Kaïros pour leur investissement dans le projet.

Je remercie le musée du Louvre, Noemi Proietti du CNR, Carlo Santulli de l'Université de Camerino, ENI Tarbes et FEMTO-ST, que nous ont permis de collaborer avec eux et donner vie à cette recherche multidisciplinaire et je les remercie pour cela.

Je remercie Delphin, Emmanuelle et Maxime qui ont été avec moi dans le projet FLOWER. Nous aurions dû passer plus de temps ensemble à s'amuser aux conférences et aux FLOWER meetings, mais le Covid est passé par là et nous a privé de ces beaux moments d'échanges. Je vous souhaite bon courage pour la suite !

Mais également, mes collègues et ex-collègues, à commencer par ceux de mon bureau. Chloé, en premier, qui depuis le début s'est révélée être ma fée bleue personnelle, capable de résoudre tous mes problèmes et de m'écouter quand j'avais besoin de parler (j'ai encore ta cire d'abeille sous mon bureau). Je remercie Guillaume et Claire, qui m'ont tenu compagnie pendant tout ce temps. Anaïs qui vient de commencer mais qui a déjà trouvé sa place avec son caractère extraverti.

Je tiens aussi à remercier tous mes collègues de l'UBS qui ont passé avec moi un peu de temps entre pause et soirées.

Et enfin je souhaite remercier toutes les personnes qui m'ont aidé et soutenu en restant dans l'ombre.

Ma sœur Erica avant tout, à laquelle j'ai demandé de l'aide pour les figures, pour divers conseils, à qui j'ai demandé d'aller chercher des bestioles dans les caves pour prendre des photos. À elle, que j'ai embêté avec tous mes doutes sur la grammaire anglaise.

Un gros merci à tous mes amis en Italie, qui, même loin, ont été précieux. À Julien et Hélène les seules personnes capables de me faire arrêter de travailler et me convaincre de prendre un peu de temps libre. Je remercie Anton Loïc avec lequel j'ai partagé une partie de mon travail, d'échange d'idée et aussi des hobbies.

Enfin, pour finir, je remercie tout le personnel d'université : Béatrice, Lénaïck, Marie, Noluenn, Roseline et toutes les autres personnes qui ont été toujours là pour n'importe quel problème ou quelles questions. Chacun, à sa manière, m'ont permis de mener à bien ce travail durant ces trois ans.

The birth of an idea

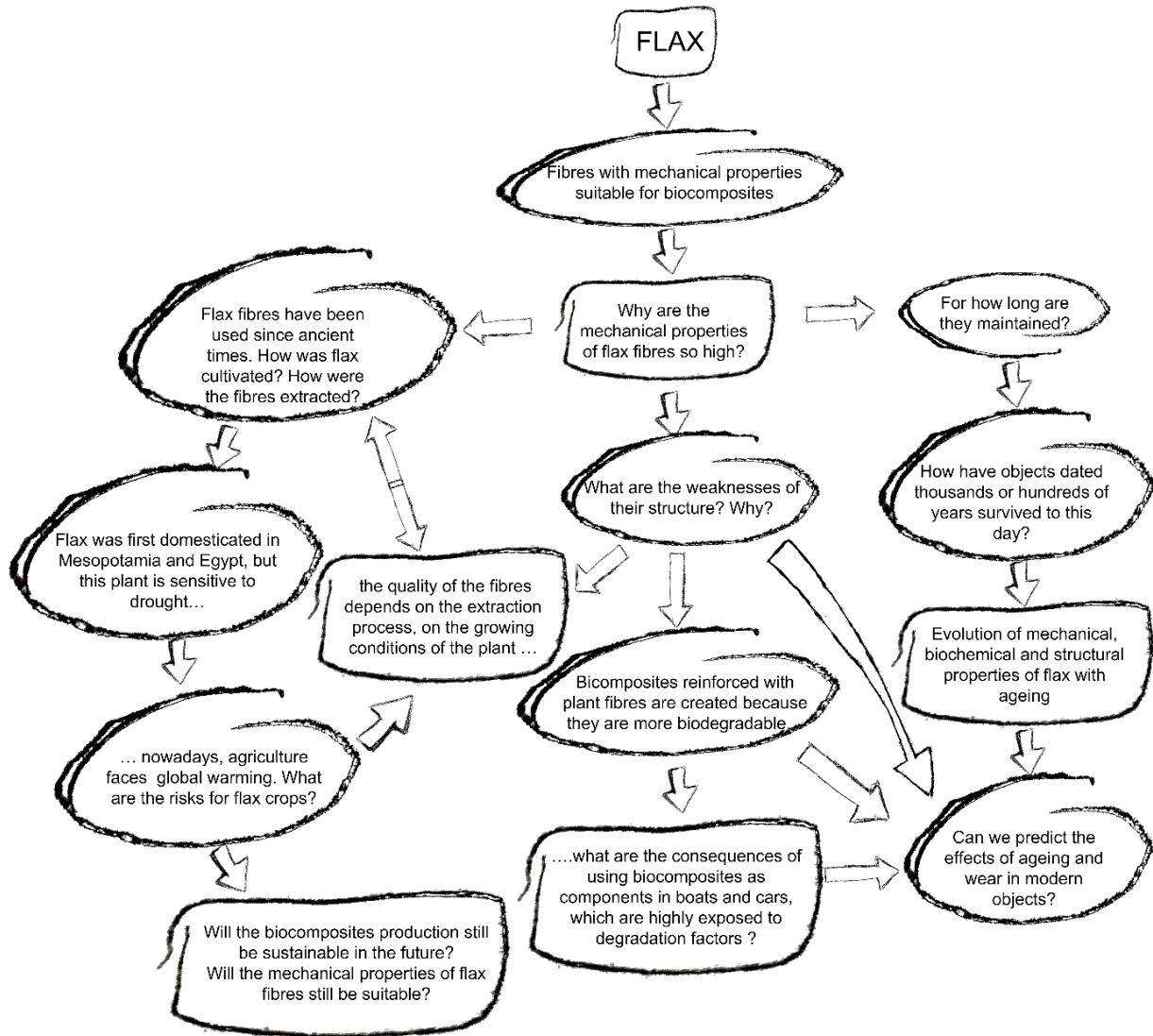


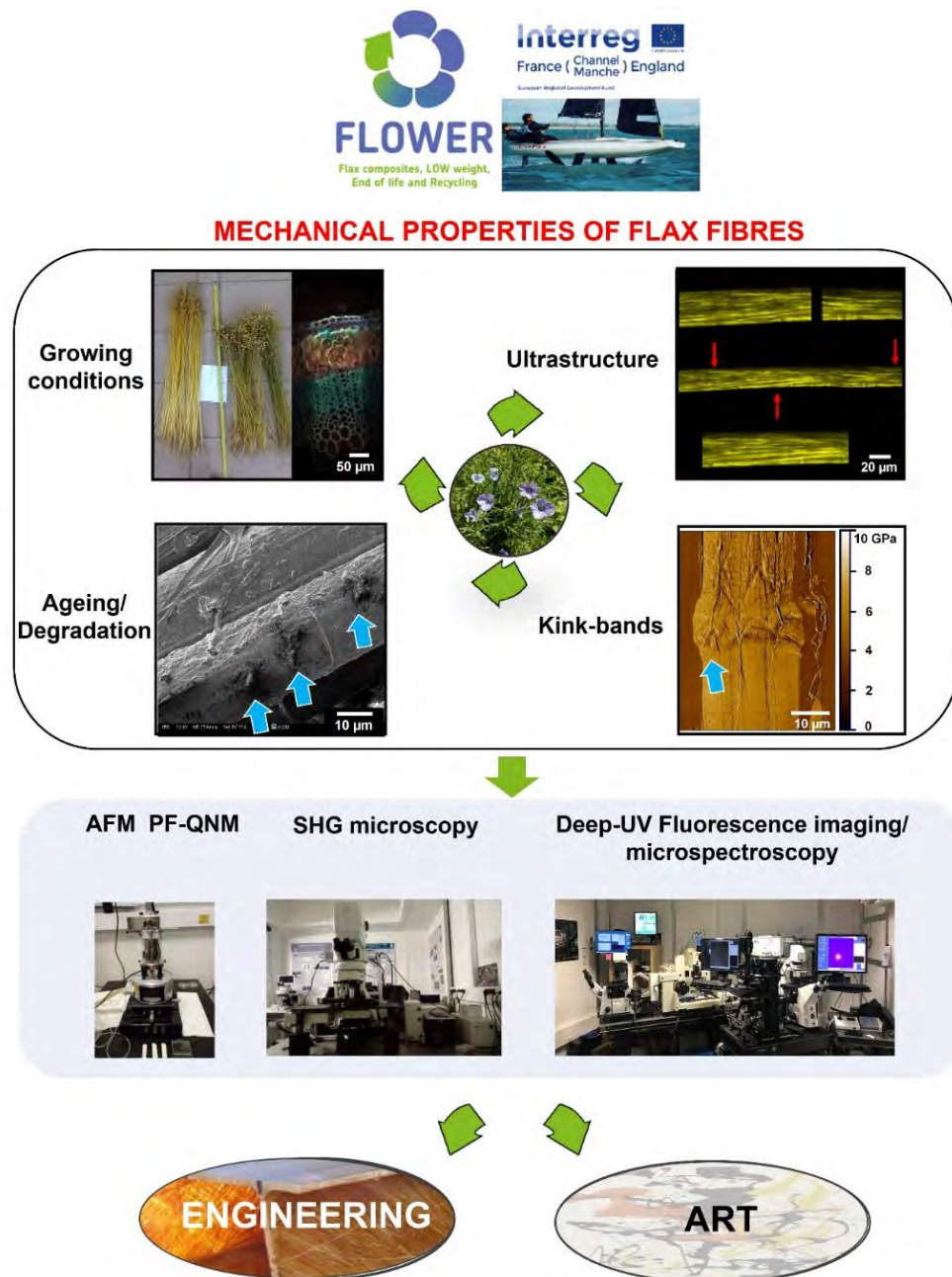
TABLE OF CONTENTS

Graphical Abstract	1
GENERAL INTRODUCTION	3
Bibliography	7
CHAPTER I. LITERATURE REVIEW	9
Graphical Abstract	11
1. Introduction: flax plants and flax fibres	13
1.1 Stem organisation and plant growth	14
1.2 Fibre organisation and properties	16
2. Flax through the Millennia in Europe and the Middle East	22
2.1 Evolution of the flax variety and geographical localisation in Europe and the Middle East	22
2.2 Ancient cultivation and extraction methods	27
2.3 Actual sowing, production, and extraction methods and application	33
3. Degradation of flax fibres: problems in modern and ancient objects	38
3.1 Two main factors of the flax fibre degradation process: water and temperature	38
3.2 Biodegradation, light and pollution: other degradation mechanisms linked with water and temperature	39
4. Characterisation techniques to study ancient and modern flax yarns	43
4.1 Morphological analysis	43
4.2 Study of parietal composition	44
4.3 Ultrastructural modifications	46
4.4 Multiscale estimation of mechanical properties	47
4.5 Dating	48
4.6 Innovative techniques	48
5. Summary and Conclusions	51
Bibliography	53
CHAPTER II. GENERAL INFORMATION ON THE MAIN METHODS USED	69
Graphical Abstract	71
1. Introduction	73
2. Atomic Force Microscopy in Peak Force mode	73
3. Second-harmonic generation imaging microscopy	77
4. DEEP-UV Fluorescence imaging and microspectroscopy	81
Bibliography	85

CHAPTER III. INVESTIGATION OF THE ULTRASTRUCTURE OF FLAX FIBRES THROUGH ADVANCED MICROSCOPIC TECHNIQUES	89
Graphical Abstract	91
1. The middle lamella of plant fibres used as composite reinforcement: investigation by atomic force microscopy	93
1.1 Introduction	93
1.2 Materials	95
1.3 AFM investigations	96
1.4 Results and Discussion	97
1.5 Conclusions	106
2. Microfibril angle of elementary flax fibres investigated with polarised second-harmonic generation microscopy	108
2.1 Introduction	108
2.2 Materials	110
2.3 SHG analysis	110
2.4 Result and discussion	112
2.5 Conclusions	117
3. Extensive investigation of the ultrastructure of kink-bands in flax fibres	119
3.1 Introduction	119
3.2 Materials	121
3.3 Methods	121
3.4 Results and discussion	123
3.5 Kink-band areas, a complex and sensitive structure	132
3.6 Three investigative techniques but also three scales of measurement; what are the cell wall elements measured?	135
3.7 Conclusions	137
Bibliography	139
CHAPTER IV. AGEING AND DEGRADATION	149
Graphical Abstract	151
1. Lessons on textile history and fibre durability from a 4000-year-old Egyptian flax yarn	153
1.1 Introduction	153
1.2 Materials	155
1.3 Methods	156
1.4 Results and Discussion	161
1.5 Conclusions	167
2. Chemical, morphological and mechanical study of the ageing of textile flax fibres from 17th/18th-century paintings on canvas	168
2.1 Introduction	168
2.2 Samples	169
2.3 Experimental methods	171
2.4 Results and Discussion	175
2.5 Conclusions	188

3. Investigations by AFM of ageing mechanisms in PLA-flax fibre composites during garden composting	189
3.1 Introduction	189
3.2 Materials	190
3.3 Methods	191
3.4 Results and discussion	192
3.5 Conclusions	199
Bibliography	200
 CHAPTER V. THE EFFECT OF THE DROUGHT STRESS ON FLAX PLANTS AND FIBRES EXTRACTED	 209
Graphical Abstract	211
1. Introduction	213
2. Materials: flax plants and fibres	216
3. Methods	217
4. Results	223
5. Discussion	234
6. Conclusion	240
Bibliography	241
 GENERAL CONCLUSION AND FURTHER WORKS	 247
Conclusion générale et perspectives	253

Graphical Abstract



GENERAL INTRODUCTION

Over the last few decades, our society has developed new technologies and new materials that have led to progress thanks to the use of fossil carbon and petroleum-derived substances. Nevertheless, the use of this fossil fuel and the non-biodegradable materials are the main causes of pollution and climate change, which are problems that have become evident especially since the beginning of the last century.

With the Kyoto Protocol first and the Paris Climate Agreements in 2015 then, one of the objectives was to reduce carbon emissions on a global scale. During this current year, 194 states have signed the agreements. The global economy is slowly shifting its attention from synthetic to natural and renewable materials, rediscovering ancient knowledge.

Flax fibres are one of these materials, which have been used since ancient times for different purposes, such as clothing or sailing, and that are currently taking on new importance because of the production of biobased materials.

This thesis is a part of the FLOWER project, a European project carried out with funding by Interreg, that aims to study flax fibres and flax plants in order to use technical flax fibres in biocomposite materials for industrial purposes, with a particular focus on the production of a boat prototype, automotive headliners and advertising panels.

The FLOWER project is a collaboration between France and England, consisting of four academic groups (University of Portsmouth, University of Cambridge, Université de Bretagne Sud and INRAE of Nantes with four PhD students) and four industrial companies (EcoTechnilin, Kaïros, Howa Tramico, Depestele), with the aim to study fundamental and applied research levels, the mechanical, chemical and morphological properties of raw flax fibres and the coupling between flax and polymer resins to produce prototypes of final products for various applications (automotive, advertising and sailing).

Being one of the four theses, the one herein presented is principally focused on the study of raw flax fibres and plants, with particular attention to the micro-mechanic and ultrastructure of flax fibres, not only for engineering and industrial purposes but also to study the effects of the ageing process in fibres naturally aged from artefacts of the cultural heritage field.

Chapter I is an overview that put in relationship the life cycle of flax plants and the structure and mechanical properties of flax fibres, presented in **Section 1**, with the history of the cultivation and use of this plant for fibres extraction from the past to the present day, described in **Section 2**. **Sections 3** and **4** summarize the main degradation mechanisms of flax fibres explored in cultural heritage and engineering fields and the most important techniques used to investigate this type of cellulosic material. **Section 5** concludes with some points on future perspectives, and some of them will be treated in this PhD manuscript.

Chapter II briefly describes the three main techniques used to study flax fibres at micro and nano-scale level in this thesis: atomic force microscopy in PeakForce mode (AFM PF-QNM), second-harmonic generation imaging microscopy (SHG) and deep-UV imaging/microspectroscopy. Other techniques are occasionally used, and some parameters adapted case by case will be described in the respective sections of each chapter.

Chapter III explores some critical points of the flax fibres ultrastructure that are still debated in the literature and considered essential because they actively play a role in the fibres mechanical properties and plant fibre composites damage and ageing. These three points are i) the layer called middle lamella between fibres (**Section 1**), with a comparison of its mechanical properties from several plant species, ii) the microfibril angle that cellulose microfibrils form with respect to the fibre axis (**Section 2**) and, iii) the kink-bands defects all along the fibres axis (**Section 3**). Their study is mainly performed at nano-scale and micro-scale levels.

Chapter IV focuses on investigating ageing and degradation mechanisms of different artefacts: i) a piece of mortuary linen fabric from Egypt dated 2140–1976 BC (**Section 1**) and ii) four Italian paintings on canvas dated between the seventeenth and eighteenth century (**Section 2**). Furthermore, a modern flax/polylactic acid (PLA) biocomposite left in homemade compost for four weeks has been explored (**Section 3**).

Chapter V links the past with the present day because ancient populations have been forced to adapt their cultivation methods. Some ancient populations have totally abandoned or almost completely replaced the use of flax fibres materials in favour of other materials to face drought environmental conditions, which is an adverse condition for flax crops. However, nowadays, this topic is relevant because the current flax fibres production is limited to a restricted area in Europe, mainly located in the north-west of France and mainly Normandy, that will probably face severe climate change and the increase of drought events in the coming decades. This chapter explores the effects of the drought conditions on flax plants and flax fibres at morphological, biochemical and mechanical levels.

Conclusions and perspectives summarize the results and discuss the questions still open at the end of this three-year research project, which paves the way for future works both in engineering and cultural heritage domains.

The chapters in this thesis have been already published in several international journals or are still under review in a peer-review process. The overview presented in **Chapter I** has been submitted to Industrial Crops and Products journal in a review format and is still under peer-review process [1]. **Chapter II** is composed of several “material&methods” chapters from published and not yet published articles related to this work [2–5] to describe the basic principles of the techniques used. **Chapter III** is composed of three original articles already published and available online [2–4]; **Chapter IV** is composed of three original articles, two accepted [5,6] and one under the final review process [7]. **Chapter V** is an original article in the first step of the per-review process [8].

CHAPTER I

- ❖ A. Melelli, J. Beaugrand, F. Jamme, A. Bourmaud, Evolution of the ultrastructure and parietal composition of flax fibres over time, *Ind. Crops Prod.* (under review).

CHAPTER II

- ❖ Selected parts of the “methods” section from all the original articles

CHAPTER III

- ❖ A. Melelli, O. Arnould, J. Beaugrand, A. Bourmaud, The Middle Lamella of Plant Fibers Used as Composite Reinforcement: Investigation by Atomic Force Microscopy, *Molecules*. 25 (2020) 632. <https://doi.org/10.3390/molecules25030632>
- ❖ A. Melelli, F. Jamme, D. Legland, J. Beaugrand, A. Bourmaud, Microfibril angle of elementary flax fibres investigated with polarised second harmonic generation microscopy, *Ind. Crops Prod.* 156 (2020) 112847. <https://doi.org/10.1016/j.indcrop.2020.112847>
- ❖ A. Melelli, S. Durand, O. Arnould, E. Richely, S. Guessasma, F. Jamme, J. Beaugrand, A. Bourmaud, Extensive investigation of the ultrastructure of kink-bands in flax fibres, *Ind. Crops Prod.* 164 (2021) 113368. <https://doi.org/10.1016/j.indcrop.2021.113368>

CHAPTER IV

- ❖ A. Melelli, D. Shah, G. Hapsari, R. Cortopassi, S. Durand, O. Arnould, V. Placet, D. Benazeth, J. Beaugrand, F. Jamme, A. Bourmaud, Lessons on textile history and fibre durability from a 4000-year-old Egyptian flax yarn, *Nat. Plants*. (2021). <https://doi.org/10.17863/CAM.71495>
- ❖ A. Melelli, G. Roselli, N. Proietti, A. Bourmaud, O. Arnould, F. Jamme, J. Beaugrand, A. Migliori, G. Di Girolami, P. Cinaglia, C. Santulli, Chemical, morphological and mechanical study of the ageing of textile flax fibres from 17th/18th-century paintings on canvas, *J. Cult. Herit.* (under review).
- ❖ A. Melelli, D. Pantaloni, E. Balnois, O. Arnould, F. Jamme, C. Baley, J. Beaugrand, D.U. Shah, A. Bourmaud, Investigations by AFM of Ageing Mechanisms in PLA-Flax Fibre Composites during Garden Composting, *Polymers*. 13 (2021) 2225. <https://doi.org/10.3390/polym13142225>

CHAPTER V

- ❖ A. Melelli, S. Durand, C. Alvarado, A. Kervoëlen, L. Foucat, M. Grégoire, O. Arnould, X. Falourd, F. Callebert, P. Ouagne, A. Geairon, S. Daniel, F. Jamme, A. Bourmaud, J. Beaugrand, Anticipating global warming effects: a comprehensive study of drought impact of both flax plants and fibres, *Ind. Crops Prod.* (under review).

Bibliography

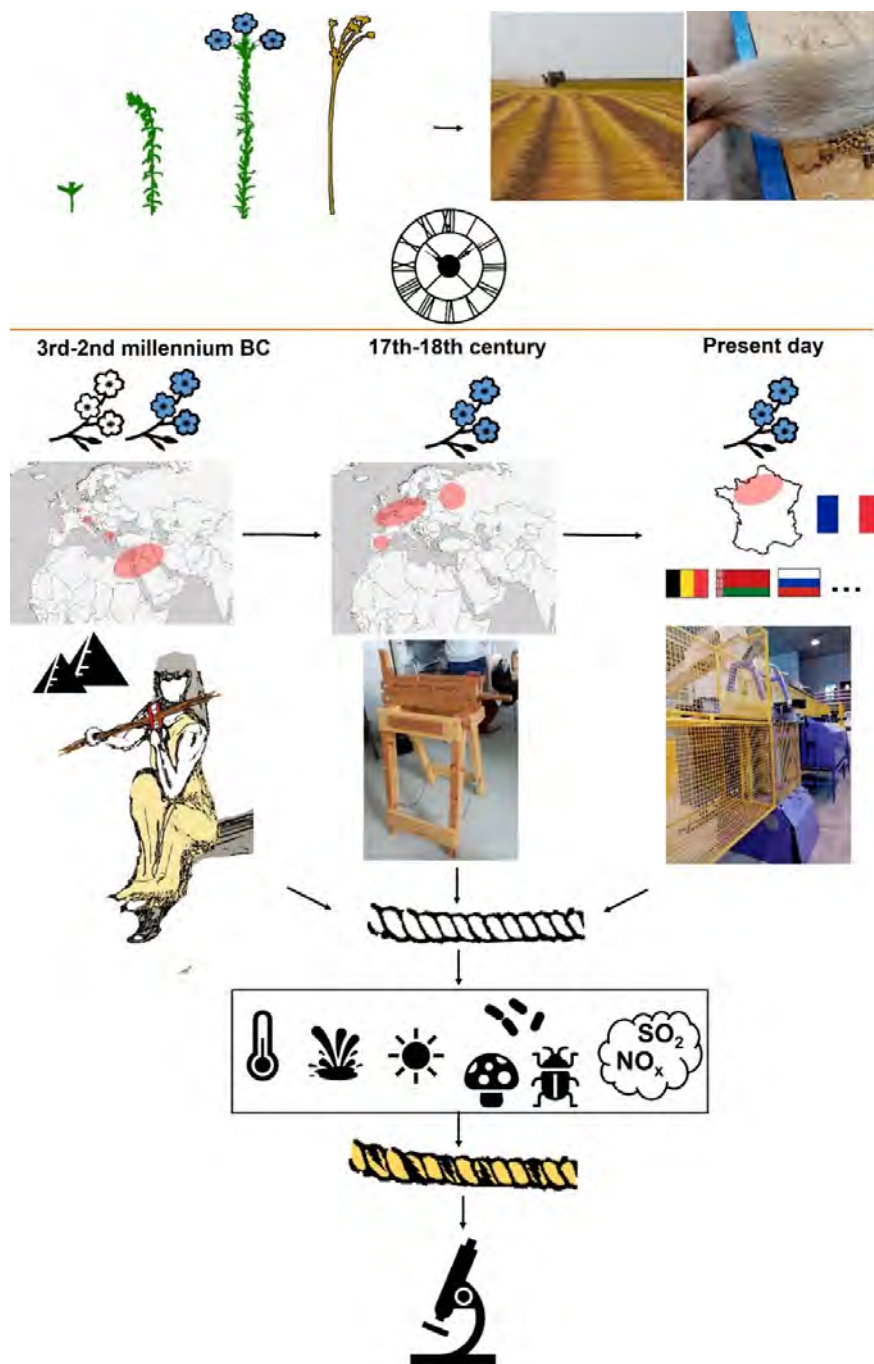
- [1] A. Melelli, J. Beaugrand, F. Jamme, A. Bourmaud, Evolution of the ultrastructure and parietal composition of flax fibres over time, *Ind. Crops Prod.* (under review).
- [2] A. Melelli, O. Arnould, J. Beaugrand, A. Bourmaud, The Middle Lamella of Plant Fibers Used as Composite Reinforcement: Investigation by Atomic Force Microscopy, *Molecules*. 25 (2020) 632. <https://doi.org/10.3390/molecules25030632>.
- [3] A. Melelli, F. Jamme, D. Legland, J. Beaugrand, A. Bourmaud, Microfibril angle of elementary flax fibres investigated with polarised second harmonic generation microscopy, *Ind. Crops Prod.* 156 (2020) 112847. <https://doi.org/10.1016/j.indcrop.2020.112847>.
- [4] A. Melelli, S. Durand, O. Arnould, E. Richely, S. Guessasma, F. Jamme, J. Beaugrand, A. Bourmaud, Extensive investigation of the ultrastructure of kink-bands in flax fibres, *Ind. Crops Prod.* 164 (2021) 113368. <https://doi.org/10.1016/j.indcrop.2021.113368>.
- [5] A. Melelli, D. Pantaloni, E. Balnois, O. Arnould, F. Jamme, C. Baley, J. Beaugrand, D.U. Shah, A. Bourmaud, Investigations by AFM of Ageing Mechanisms in PLA-Flax Fibre Composites during Garden Composting, *Polymers*. 13 (2021) 2225. <https://doi.org/10.3390/polym13142225>.
- [6] A. Melelli, D. Shah, G. Hapsari, R. Cortopassi, S. Durand, O. Arnould, V. Placet, D. Benazeth, J. Beaugrand, F. Jamme, A. Bourmaud, Lessons on textile history and fibre durability from a 4000-year-old Egyptian flax yarn, *Nat. Plants*. (2021). <https://doi.org/10.17863/CAM.71495>.
- [7] A. Melelli, G. Roselli, N. Proietti, A. Bourmaud, O. Arnould, F. Jamme, J. Beaugrand, A. Migliori, G. Di Girolami, P. Cinaglia, C. Santulli, Chemical, morphological and mechanical study of the ageing of textile flax fibres from 17th/18th-century paintings on canvas, *J. Cult. Herit.* (under review).
- [8] A. Melelli, C. Alvarado, S. Durand, A. Kervoëlen, L. Foucat, M. Grégoire, O. Arnould, X. Falourd, F. Callebert, P. Ouagne, A. Geairon, S. Daniel, F. Jamme, A. Bourmaud, J. Beaugrand, Anticipating global warming effects: a comprehensive study of drought impact on both flax plants and fibres, *Ind. Crops Prod.* (under review).



CHAPTER I. LITERATURE REVIEW



Graphical Abstract



A. Melelli, J. Beaugrand, F. Jamme, A. Bourmaud, Evolution of the ultrastructure and parietal composition of flax fibres over time, *Ind. Crops Prod.* (under review).

1. Introduction: flax plants and flax fibres

Textiles are important inventions in human history, and the use of plant fibres, such as flax and hemp, have been used to produce not only clothes but also sails in sailing ships, flags, carpets or canvases, which are considered cultural heritage. Several of the first houses built by ancient civilisations were made with clay and straw in the form of mud bricks, which can be considered as the first biocomposite material in building construction. The use of mud bricks persists even today in several African countries as well as in India. Currently, there is renewed interest in the *know-how* and technologies of plant fibre composites for use in the material construction, automotive, sport and design industries as ecological, sustainable and cost-effective alternatives to common synthetic materials. This discovery and rediscovery of cellulosic fibres exhibits continuity in terms of technological progress. Consequently, an active exchange can be established between the engineering and cultural heritage to resolve problems in both domains and supplement the missing information, such as that of the evolution of degradation mechanisms.

Linum usitatissimum L., which is the scientific name of the common flax plant, is derived from the Latin word “*usitatus*”, which means “commonly used” [1]. The Latin name of this plant highlights the importance of this plant throughout the history of civilisation. Flax is one of the oldest domesticated plants [2] because its oil and fibres can be exploited, and it has been fundamental in both ancient and modern times to create clothes and objects. Despite the continuity of its plantation and application from the ancient era to the contemporary era, the cultivation and fibre extraction methods have been improved, and the plant morphology has evolved. Currently, textile flax is mainly cultivated in Western Europe; however, for thousands of years, this plant has been cultivated from the Mediterranean region to India, as well as in the Fertile Crescent area. The habitat of this plant varies from moderately cold to moderately warm regions [3], which is an adaptive advantage contributing to its widespread use.

Through human selection, flax plants have been optimised to obtain two main types of flax, the former suitable to produce linseed oil and the latter for fibres. In this context, several morphological characteristics of this plant have been modified. For example, the types of flax used to prepare fibres are taller with smaller capsules and fewer branches than those used to extract linseed oil [3].

Every year, new varieties of flax are commercialised, and the fibre yield and behaviour of each variety, as related to biotic (fungi, insects) or abiotic (wind, drought) stresses, are evaluated on an average of one to four years [4,5]. Therefore, this plant undergoes substantial changes annually, which accentuates the difference between the linseed and fibre producing varieties and between the ancient and modern varieties.

To understand the evolution of this plant and its fibres in terms of morphology, cultivation and extraction methods, as well as the geographical areas involved and current application in different fields, the historical aspects must be considered.

Archaeological artefacts and historical objects can highlight the origin and use of flax and its fibres and explain the evolution of human interest in this plant, the reasons for the survival of the artefacts made from this organic material for several millennia and the type of techniques that can be used to study ancient and modern objects to compare them, describe their structure and quantify their quality. Considering these aspects, this review summarises the history of the use, cultivation and extraction of flax, compares these aspects in the present and past contexts, highlights the ageing mechanisms that can change the initial structure, morphology and chemistry of flax fibres and clarifies the characterisation techniques available at present to study these features.

1.1 Stem organisation and plant growth

Similarly to other vascular plants, flax stems have different histological tissues, as shown in **Figure I-1a**, which illustrates both young and mature steps. In this figure, it is possible to identify 1) the epidermis and cuticle, 2) cortical parenchyma, 3) sclerenchyma fibres, 4) phloem, 5) vascular cambium, 6) xylem and 7) pith.

1.1.1 *Tissues and their roles: an overview of the flax stem*

Each tissue in the plant has a specific role, and the corresponding chemical composition is adapted according to this function. Xylem and phloem are vascular tissues. Xylem conducts water and raw sap and also contributes to the mechanical support of the stem [6]. Thus, the high lignin content of this tissue can help ensure the rigidity of the structure and hydrophobicity of the cells [7,8]. The phloem tissue has two types of cells: certain cells transport food resources such as the elaborated sap, while the primary sclerenchyma phloem fibres, which are flexible, support the structure of the stem. Flax fibres are grouped in 30–40 units and radially distributed in the whole stem. The chemical distribution examined through microspectroscopic techniques indicates that cellulose is more abundant in bast fibres than in the rest of the stem, while the content of lignin is lower but still detectable [9,10]. Moreover, the lignin present in fibres is mainly a G condensed epitope. In contrast, the lignin in the xylem is mainly a less condensed GS epitope [11].

The flax stem is composed of a vascular cambium (**Figure I-1a**) responsible for the secondary growth of the stem and which generates new xylem and phloem tissues. The cortical parenchyma, also called cortex or bark parenchyma, is richer in chlorophyll than xylem and bast fibres [12], and, for this reason, it is easily distinguishable from fibres and epidermis.

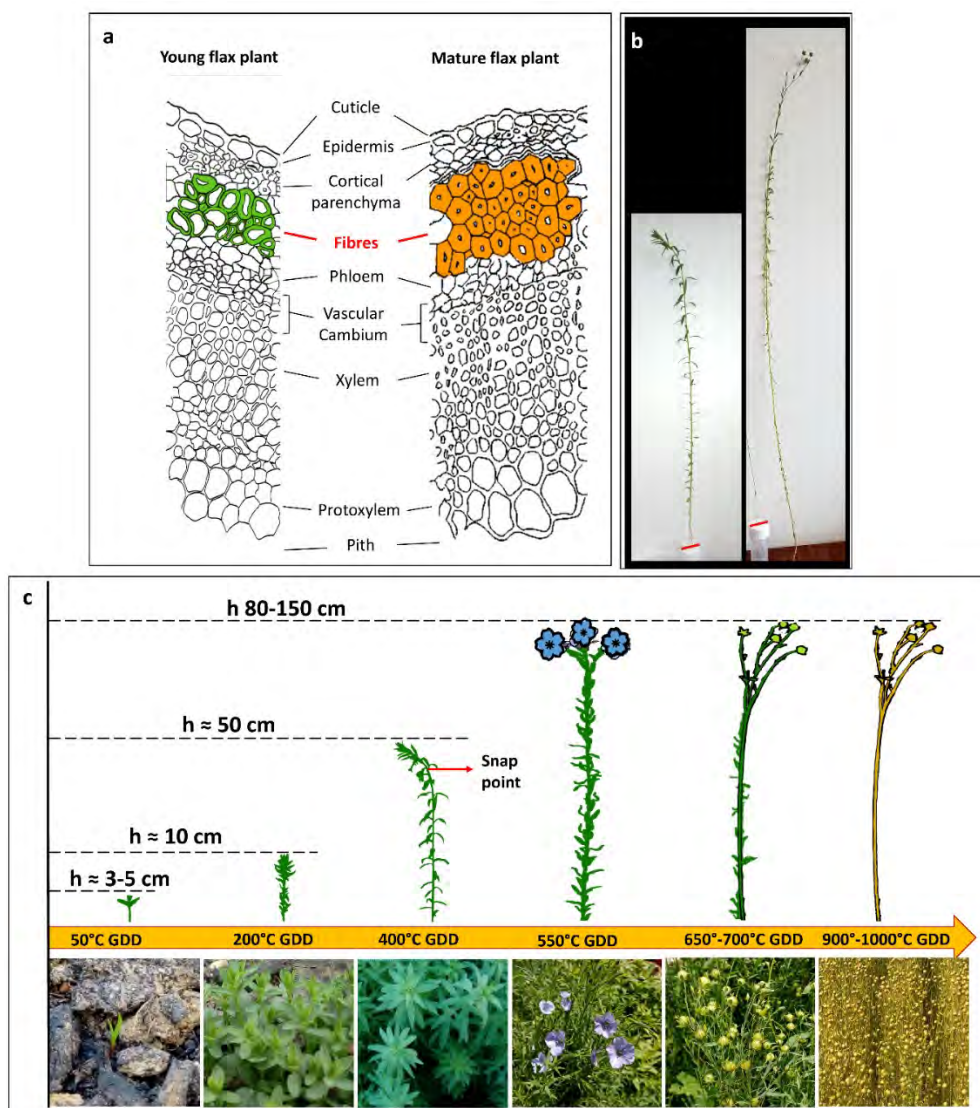


Figure I-1a) Schema of a young flax stem at approximately 400 °C GDD and mature stem at 1000 °C GDD (© Erica Melelli); **b)** photo of two flax plants pulled out at 400 °C and 1000 °C GDD in the real scale; **c)** plant growth over time with flowering and browning of the capsules.

The epidermis and cuticle, which are the external layers, are abundant in wax and phenolic groups, as they provide mechanical support and protect the innermost tissues of the stem from abiotic and biotic stress that may occur during plant growth [13]. Consequently, when the plant is injured, lignification occurs in the tissues involved [14] as lignin is a complex mixture of polyphenols and generally more difficult to metabolise by microorganisms than carbohydrates [15].

The epidermis is rich in polygalacturonates, which are components of pectins, the molecules responsible for plant elongation and porosity regulation. As a plant matures, pectins become less methylated and form more cross-links with Ca^{2+} ; these cross-links reduce the sensitivity to the polygalacturonase enzyme responsible for the degradation of cortical tissue during retting [16]. The pith, xylem, phloem [6] and epidermis of flax stems are commonly referred to as woody tissues. During fibre extraction, these parts of the stems are sacrificed and reduced in shives.

During plant growth, the biochemistry of the different tissues of the flax plant changes, and thus, it is important to consider the maturity of the stem to determine when the flax crop should be harvested and fibres must be extracted.

1.1.2 Flax: a fast-growing plant

Flax plants go through different steps of growth before becoming mature, and the cumulative growing degree day (GDD) value can be calculated to identify flowering, capsule browning and complete plant maturation. The GDD can be calculated as reported in **Eq.I-1**:

$$\text{GDD} = \left(\frac{T_{\max} + T_{\min}}{2} \right) - T_b \quad (\text{Eq.I-1})$$

The maximum temperature is added to the minimum value and divided by two to determine the mean value, and the temperature base (T_b), which is the minimum temperature at which a specific plant can grow, is subtracted [17,18]. T_b for flax plants is 5 °C. The first emergence after sowing occurs at approximately 50 °C growing degree days, flowering starts at 550 °C, followed by the growth of capsules, which are initially green, at approximately 650–700 °C. The capsules become brown at plant maturity (**Figures I-1b, c**) [19,20]. Flax plants reach fibre maturity between 850 °C and 1000 °C GDD, while the seeds are considered mature at 1000–1100 °C [20]. Thus, it can be estimated that flax maturity can be achieved at approximately 110 d after sowing in Europe [21].

During the growth of flax plants, it is possible to recognise the “snap point” as a transition point between the rigid stem stage, in which the fibres reach maximum elongation, and the thickening process, which occurs at the top of the stems. The top of the stem is thus flexible because fibres are still involved in the elongation process and have not yet been lignified [22,23]. In general, the height of a flax plant may range from 80 to 150 cm at maturity (**Figures I-1b, c**), and this value also depends on the variety [4,21]. The root system is also of significance. The roots of flax cannot reach deep soils and therefore exploit the nutrients present in the first 70 cm of soil. Consequently, flax and linseed plants are sensitive to drought stress [24,25].

1.2 Fibre organisation and properties

1.2.1 General information on flax fibres

Flax fibres are single unit cells that originate from the phloem region of the flax plant and, like jute and hemp, are among the commonly used bast fibres [26].

Cells are the fundamental units of living organisms. In the context of technical fibres, the cell wall is of interest because it is responsible for the rigid structure of a plant and contributes to its mechanical

properties [27], allowing the use of the fibres as raw materials with suitable properties, for example, as composite material reinforcement.

The diameter of flax fibres generally ranges from 8 to 25 μm [28], and its value changes throughout the cell [29]. The mean diameter can vary with several factors, such as the stage of maturity [30], variety, year and retting degree [31]. The diameter can vary depending on the fibre position in the stem. Fibres in the basal region have a larger diameter (approximately $25.2 \pm 10.00 \mu\text{m}$) than those on the top near the snap point (diameter of $11.4 \pm 3.4 \mu\text{m}$) [32].

Although the length changes across varieties, the fibre length is usually between 5 and 80 mm [33,32] with an average value of approximately 20–30 mm. Ageeva *et al.* demonstrated that fibres with the smallest length lie in the basal part of the stem, and the longest fibres are present at the top of the stem [34].

1.2.2 Hierarchical structure and ultrastructure of the fibre

Flax fibres, like all cellulosic fibres, have a hierarchical structure composed of several layers (**Figure I-2a**). In engineering science, conventionally, the flax cell wall is divided into the primary layer (P), which is the outer layer and is approximately 0.2 μm thick [28], and the secondary layer, which is 5–15 μm thick [35]. Moreover, the secondary wall is divided into three sublayers labelled S_1 , S_2 and S_3 , specified for the first time by Roelofsen in 1951, who analysed flax, hemp and ramie fibres under a microscope in a polarised light environment after swelling in cuprammonium [36].

Botanically, flax is a type of plant with gelatinous cell walls and well-defined characteristics. The difference between lignified fibres (type S, with common distinction among S_1 , S_2 and S_3) and gelatinous fibres (type G) has been described by [37], and the characteristics of the G layer can be summarised as follows [38,39]: i) the lignin and xylan content of the layer is extremely low or nearly zero, ii) the layer is rich in water, and cellulose is its main component, iii) in contrast to the S layers, the cellulose microfibrils in the G layer have a small microfibril angle and are nearly parallel to the fibre axis. A recent model by Gorshkova *et al.* [39], from which **Figure I-2a** is inspired and partially readapted, indicated the presence of a flax structure with a secondary wall composed of cellulose ~ 40%, lignin ~30%, xylan ~25% and the inner layer, also known as the tertiary layer [39,40], and identified as the G layer, with a cellulose content of up to 85% and the presence of rhamnogalacturonan-I (approximately 5–7%) with short galactan chains if the layer is mature and long chains if the layer is newly deposited [39].

During plant growth, two mechanisms occur in flax fibre cells: intrusive growth and thickening of the cell wall layers. In the intrusive growth phenomenon, the elongation of certain flax fibres occurs faster than that of the surrounding fibres, and these fibres can penetrate adjacent fibres [23,34], forcing the growing fibre to push the other cells to find adequate space until the elongation process is complete.

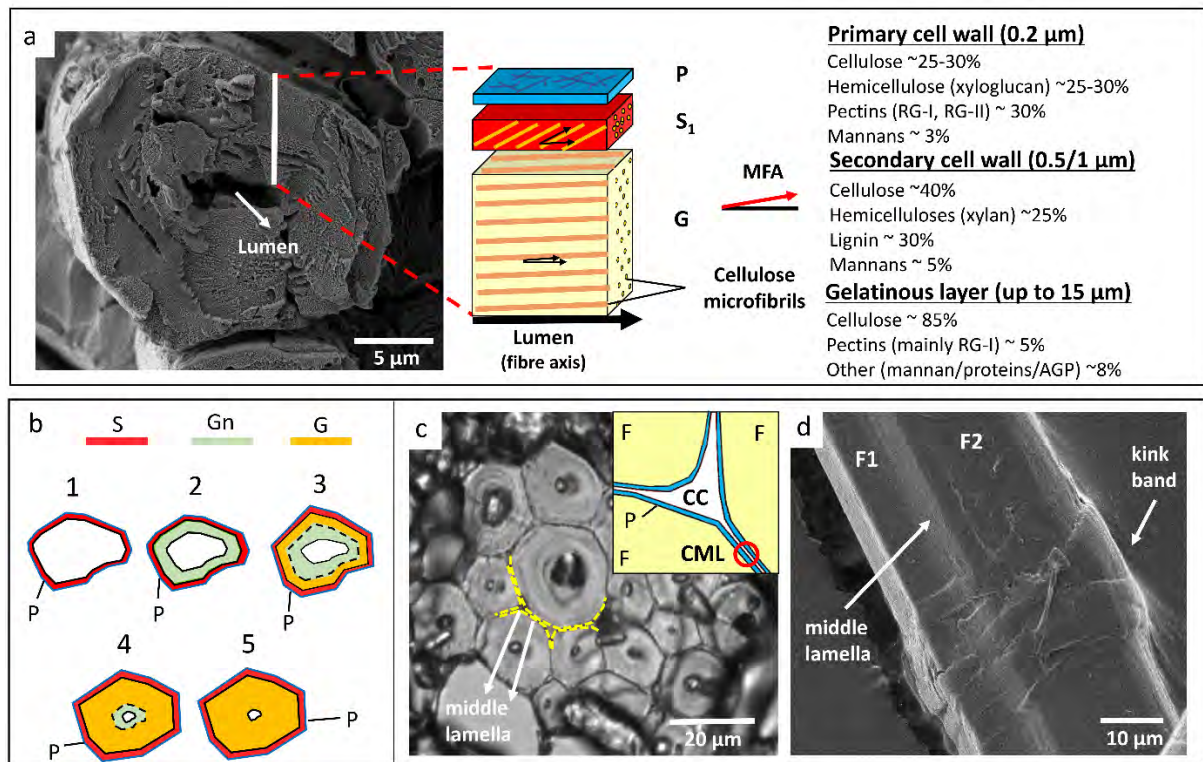


Figure I-2a) Schema of flax fibre ultrastructure and chemical composition, inspired and partially readapted from [39,41] and data from [19]; **b)** formation of the cell wall layers, inspired by [30], and the progressive filling and thickening with the Gn layer transformed to G; **c)** transversal section of a flax fibre bundle, in which the middle lamella is highlighted in yellow. A schema representing the cell corner (CC) between three fibres (F) is shown, along the compound middle lamella (CML) composed of the primary wall (P) and middle lamella between two adjacent fibres; **d)** bundle of two fibres (F1 and F2) with a visible kink-band and outermost primary cell wall layer.

In the thickening process, the inner cell wall is divided into a mature layer, designated G, with Gn indicating the newly deposited layer (See **Figures I-2a, b**). During the development of the plant fibre, G and Gn coexist. Initially, only the Gn layer constitutes the cell wall, together with the S layer and the primary wall. However, with the maturity of the fibre, the Gn layer is subjected to a gradual thickening process that starts from the outer side and moves to the inner side of the cell, and this layer transforms to the G layer [30,42,43]. During this growing process, the lumen diameter is progressively reduced, in certain cases, almost replaced by the cell wall. As long as the fibre is alive, the lumen is filled with cytoplasm, which disappears upon cell death, leaving the lumen empty [44,45].

The different cell wall layers also have different chemistry [19,39], which also depends on the maturity of the fibre, as indicated by His *et al.* through immunogold localisation [46]. Since it is difficult to clarify the biochemical composition for each cell wall layer separately due to their reduced thickness, in the literature, a global percentage is usually defined as the total contribution of all the layers [47,26]. **Table I-1** lists certain percentages reported in the literature. In addition to biochemistry, a key characteristic of the cell wall ultrastructure is the microfibril angle (MFA).

Table I-1 Literature review of the biochemical global composition of the considered bundles of fibres.

	Cellulose (%)	Hemicellulose (%)	Lignin (%)	Reference
<i>Linum usitatissimum</i> L. (Flax)	60–85	14.0–20.6	1–3	[48–50]
<i>Cannabis sativa</i> (Hemp)	55–90	12	2–5	[51–54]
<i>Corchorus capsularis</i> (Jute)	58.0–71.5	13.6–24.0	11.8–16	[55,56]

Cell wall layers are composed of several cellulose chains known as microfibrils, the size of which is of the order of a few nanometres [57], and assemblies of several microfibrils, realised through hemicellulose, pectin and variable amounts of lignin [58], form bundles known as macrofibrils. Each cell wall layer has microfibrils with different orientations against the fibre axis. This angle that cellulose microfibrils form with the fibre axis is known as the microfibril angle (MFA), illustrated in **Figure I-2a**.

In general, the primary wall is represented by a random orientation of the microfibrils [59–61]; however, certain recent studies indicated that mature flax fibres reorient the microfibrils inside the primary cell wall due to cell elongation [62,63].

The secondary wall has a complex structure and transition zones in which the microfibril angle gradually changes have been observed [32,64]. The S₁ layer has a crisscrossed pattern of cellulose microfibrils [65,66]; however, for the secondary wall, a MFA between 5° and 10° for dry flax fibres has been reported in the literature associated with engineering [67,68] and botany [39]. In engineering, the S layer is considered the thickest main layer, and thus it should coincide with the G layer, as in the models reported by [26,32]. In botany, the microfibril angle of the G layer is close to 0° and almost parallel to the fibre axis, which is one of the main characteristics of gelatinous fibres that allow them to be distinguished from other S-fibres [23,37,39].

1.2.3 Middle lamella: the adhesive between fibres

Several tens of flax fibres are grouped in bundles in the phloem region of the stem. These fibres are glued through another layer, known as the middle lamella (**Figure I-2c**), which is mainly composed of pectic polysaccharides (58%), lignin (38%), and a small amount of protein (approximately 4%) [69,70]. Moreover, it is possible to distinguish the tricellular junction or cell corner (CCML), which links three or four fibres, and the compound middle lamella (CML), which aggregates the middle lamellae and primary cell wall, thereby forming a composite system of both layers (**Figure I-2c**).

The middle lamella has often been considered the weakest layer, in which fractures can start to propagate when flax fibres are used in biocomposite materials and mechanically tested [71,72]. Nevertheless, certain researchers reported that fractures occur more often between the S₁ layer and G layer or between the S₁ layer and the primary wall than in the middle lamella [11,69].

1.2.4 Kink-bands: defects along the fibres that influence the mechanical properties of modern and historical objects

An important characteristic of certain plant fibres, such as hemp and flax, is the local deformation of the cell wall along the axis. The associated defects are known as kink-bands, have a precise geometry (**Figure I-2d**) and often involve several fibres of the single bundle. These defects can be attributed to the environmental conditions during the growth of the plant and the fibre extraction process [73]. Hughes *et al.* demonstrated that hemp fibres carefully extracted from green stems have fewer kink-bands than the common fibres extracted in an automated extraction line [73].

The geometry of kink-bands is different from that of the remaining fibre, and according to Thygesen and Gierlinger's work on *Cannabis sativa* (hemp), kink-bands have a less ordered microfibril network and higher microfibril angles [74]. Through FIB-SEM tomographic reconstruction, another team observed cavities in the kink-bands in flax fibres [75]. The abovementioned aspects are likely why kink-bands are the weakest points of plant fibres from a chemical viewpoint, although they are the preferred points at which enzymatic hydrolysis can be initiated [76]. The density of these regions considerably influences the mechanical properties of fibres and composite materials [77–80] and has been known to limit the fibre strength in historical textiles and artworks [81,82]. The nature and structure of these defects along the fibres must be extensively investigated to confirm these observations.

1.2.5 Small and strong: the mechanical properties of flax fibres

Despite the presence of kink-bands, flax fibres exhibit remarkable mechanical properties, which have been deeply investigated [33,83]. **Table I-2** presents a comparison of the mechanical properties of flax fibres reported in the literature and those of other natural and synthetic fibres. The G layer is the main layer responsible for the mechanical behaviour of cellulosic fibres, especially in the longitudinal direction [43]. According to the existing studies, a small microfibril angle, small lumen and small fibre diameter lead to a high Young's modulus and superior performance [67,84]. For instance, although cotton has a high cellulose content (82–98%), its MFA ranges from 20° to 30° [26,68], and thus, the Young's modulus and tensile strength are low; in contrast, the strain at break (in %) is high due to the increase in its MFA when subjected to tensile stress. Therefore, in ancient times, flax was used to prepare not only clothes but also sails that could resist the wind stress.

Table I-2 Typical mechanical properties of E-glass compared to flax, hemp and cotton. Mean values modified from [26,85–88].

Fibre	Density (g/cm ³)	Strain at break (%)	Tensile strength (MPa)	Stiffness/Young's modulus (GPa)	Moisture sorption (%)
E-glass	2.6	2.5–3	2000–3400	70–81	/
Flax	1.4–1.5	1.3–3.6	595–1500	45–60	8–12
Hemp	1.4–1.5	0.8–3.3	285–900	25–40	6–12
Cotton	1.5–1.6	3.0–10	287–800	5.5–13	8–25

Several studies have demonstrated that the variety [5,67] and growing conditions of the plant [89] and the fibre extraction process [90] can affect the fibre performance. In recent years, mechanical properties have been recorded at the cell level. For flax, the indentation modulus lies between 15 and 24 GPa for a mature G layer and between 9 and 15.9 GPa for a newly deposited Gn layer [30,43]; these values also depend on the fibre position in the stem. When the flax plant is young, the thickness and local indentation moduli of flax fibres drastically change and increase from the bottom near the roots to the top near the snap point. However, the local indentation moduli and thickness become uniform when the plant reaches maturity [30]. Once the stem is cut and undergoes retting, the indentation modulus of flax fibres increases with the increase in the retting degree, defined in terms of days of retting [65].

2. Flax through the Millennia in Europe and the Middle East

The interest in and use of flax plants for oil or fibres have been prevalent for several millennia. The domestication of flax has influenced the plant structure and properties as well as the area of cultivation and production. In this section, the history of flax cultivated for fibres and the evolution of the extraction methods are summarised from the origin of the use of flax through the contemporary era.

2.1 Evolution of the flax variety and geographical localisation in Europe and the Middle East

The first evidence of the use of *Linum usitatissimum* is dated between 9,000 and 8,000 BC in the Near East, with other instances of flax seeds observed in Turkey and Syria [91]. Only later did the use of these seeds spread in Egypt [92–94]. However, in 2009, Kvavadze *et al.* published an article on several flax fibres discovered in Dzudzuana Cave, Georgia, dated to Upper Palaeolithic period (30,000 years before present) through the radiocarbon dating of soil deposits [95]. The fibres were coloured, which suggests the beginning of a manufacturing process. This discovery can backdate the use of flax other than as a food source; however, the identification of these bast fibres is highly debated. The entire scientific community is not in consensus regarding the attribution to flax fibres, and this aspect must thus be further investigated [96].

Although the use of flax is evident through archaeological findings, plant domestication likely occurred later in civilisations such as Mesopotamia and Egypt. These civilisations grew both domesticated and wild flax (or pale flax) as crops, as shown in **Figure I-3**, which illustrates the natural distribution of pale flax in addition to the approximate areas of dated archaeological findings.

The history of the domestication and cultivation of this plant is not clear, and genetic diversity seems to suggest that independent episodes of domestication likely occurred in different geographical areas from Asia to the Mediterranean regions because of the vast geographical range of pale flax [92,97]. Before 1975, a hypothesis was presented regarding the relationship between *Linum usitatissimum*, which is domesticated flax, and *Linum bienne* as its wild progenitor, and van Zeist et Bakker-Heeres suggested that the first cultivations of flax were performed in dry soils as the natural habitat of *Linum bienne* [2].

Diederichsen et Hammer compared the characteristics of the first progenitor pale flax (*L. angustifolium* Huds.) and cultivated flax *L. usitatissimum* [97]. Morphological evaluations were performed through direct observation of the plants cultivated and analysed for three years with different accession geographic origins.

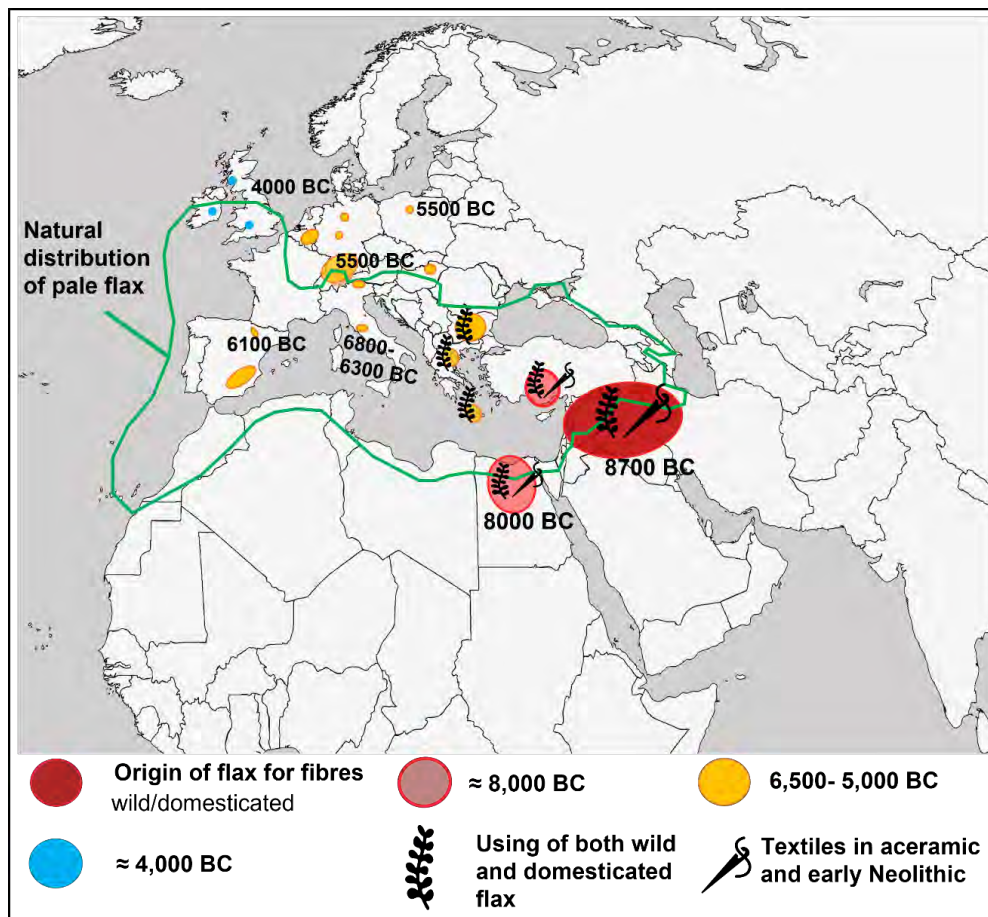


Figure I-3 Map with the natural distribution of wild (pale) flax (in green) and the origin of the use of flax and its spread in Europe along with the first fabrics dated to the early Neolithic. The distribution of pale flax (green) has been obtained from [97–99]. The centres of archaeological findings have been adapted from [100–102].

The following aspects were considered: the length and width of petals, size of seeds, colour and shape of the flower, the height of plants and number of days until emergence from the soil or flowering. The authors concluded that most of the considered aspects for the two flax species were distinguishable, which highlighted the influence of the domestication of the plant on its morphology [97].

Muravenko *et al.* extracted the DNA of *L. angustifolium* (Huds.), *L. bienne* and *L. usitatissimum*, and performed evaluations considering the genetic polymorphism and the comparison of the chromosome C-banding and molecular markers [103]. The authors clarified the relationship between the three species, which are often confused and considered subspecies of one another: a dendrogram, as illustrated in **Figure I-4**, indicated that *L. angustifolium* (Huds.) was similar to the ancient cultivated flax, and *L. bienne* was considered a subspecies of *L. usitatissimum* [103]. Two years after this publication, another team of researchers used DNA extraction, PCR amplification and sequencing to analyse the cultivated and pale flax [92]. The authors suggested that a single pale flax plant (*L. angustifolium*) was likely domesticated and was the only progenitor of the cultivated flax. In Europe, the domestication of flax fibres is dated to the Neolithic period with the Linearbandkeramik Culture (5500-4500 BC) ([104],

quoted in [100]). According to the map presented by Karg *et al.*, simplified and readapted in **Figure I-3**, in contrast to that in the Middle East, only the domesticated plant was cultivated in southern and western Europe [100].

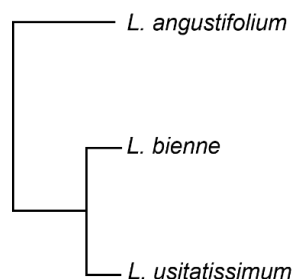


Figure I-4 Dendrogram from [103]. *L. angustifolium* appeared as the progenitor of both *L. bienne* and *L. usitatissimum*.

The use of cultivated flax increased rapidly and spread across Europe, and traces were observed in Switzerland [105] and Greece [106] during the Neolithic period.

Herbig et Maier measured the size of several flax seeds and evaluated capsules and shives from different archaeological sites located around Lake Constance and Upper Swabia. The authors hypothesise that different varieties of flax were used for linseed and fibres [107]. The variety of flax linked to the Pfyn culture was mainly used in 4,000–3,800 BC, and despite the presence of shives and linen found in the archaeological sites, the larger number of capsules and seeds and larger seeds suggests that this flax variety was principally used to produce oil. Seeds with a drastically reduced size were observed along with a higher quantity of shives and threshing traces only in a later period, during the middle and latest phases of the Late Neolithic (3,400–2,500 BC). This finding supported the hypothesis that a new variety of flax, linked with the Horogen culture and likely introduced from the Balkans, was cultivated for fibre extraction [107]. Even in the present era, the size of capsules and seeds, as well as their number in the tillers, are important characteristics that allow flax to be distinguished from the linseed varieties [3]. The work performed by Herbig et Maier presented one of the earliest pieces of evidence of the use of different flax varieties for different purposes.

The extensive use of flax began with Egyptians during the dynastic period, in which flax fibres were widely used for cloth and sail production and in funerary rites. The production of these objects required considerable effort to produce linen, and Egypt emerged as the “land of linen”. The 1st dynasty (3,000 BC) corresponded to the first attempts at mummification, which was initially performed only for pharaohs and then successively extended to the remaining population [108]. This practice persisted across all subsequent dynasties and for a certain period even beyond the conquering of Egypt by the Romans and its annexure into the Roman Empire. The case of the mummy of Grottarossa discovered in Rome and dated between 150 and 200 A.D. must be mentioned; an embalmed young girl was found to

be treated with ancient knowledge of Egyptian mummification, and bandages of linen were identified [109].

In ancient Mesopotamia and other areas of the Near East, considered the cradle of flax cultivation, the use of flax crops gradually disappeared as this plant required highly fertile soils to grow, and, consequently, aggressive expansion policies, or due to a long period of drought, which occurred in the last part of the Middle Bronze Age and the first part of the Late Bronze Age [110,111]. In Mesopotamia, in the 4th–3rd millennium, flax fibres were replaced with wool fibres [110], while drought during the Bronze Ages seemed to have favoured a change of crops towards drought-tolerant plants [111].

Due to the flourishing trade between populations located in the Mediterranean regions, historians find it challenging to determine whether Romans or Phoenicians first introduced the use of linen in Europe; however, it is generally agreed that the expansion of the Roman Empire promoted the use of this plant for fibre extraction throughout northern Europe. In northern Europe, flax was primarily used to produce oil, and the most ancient remains of linen seem to suggest that they were originally imported from the Germans or Romans (Hald, 1950 as cited in [112] and Bender Jørgensen, 1986 as cited in [113]). In Denmark, there is evidence of linen fabric dated to 800 BC, and in Sweden, the first textile production is dated to approximately 200–300 AD [112–114].

In the 1st century BC, Pliny the Elder wrote the *Naturalis Historia* and dedicated a part of his opera to flax (*Liber XIX*), highlighting the importance of this plant in the production of sails that allowed commerce and contacts between populations around the Mediterranean Sea. Despite the flax cultivations in Europe, Egypt maintained primacy for centuries in the production and exportation of flax with the most advanced technology and expertise. Egyptian linen was cheaper and more abundant than other types of linen produced in the same period in Italy or by the Gallic population located in southwestern France (*Carduci*); however, Pliny the Elder also reported that the quality of this flax was inferior to that of the linen produced in Europe (NH 19, 13–14). This difference may have occurred because Egyptians sowed flax during the winter season, while to the north of the Mediterranean regions, flax was cultivated during spring [115], which likely facilitated the development of diversity in summer and winter varieties. Musselman reported that although flax was known to be used for both oil and fibres in the Bible, it was only associated with linen [116], which suggests the importance of these plant fibres in antiquity.

Between the 9th and 10th centuries, in Zeeland and Flanders linen was generally preferred to wool for clothes because wool, although more easily produced, was considered too coarse, and Flanders became an important linen manufacturing centre [117]. As reported by Dixon in his opera dated 1854, at the end of the 13th century, Beatrice de Gaule introduced the coutil fabric in both northwestern France (Brittany, Main, Angers) and Flanders, where flax grew naturally [118]. During the Middle Ages, the fustian fabric, a mix of linen and cotton that probably originated from Egypt and was successively produced in Italy and Spain, emerged as an important entity throughout Europe, especially during the 14th century [119]. This fabric was manufactured also in Britain, Germany and Switzerland because

European spinners could not produce cotton yarns that were strong enough to be used in the warp direction [119,120].

Additionally, during the 14th century, flax fibres were largely used to prepare cloths, sails, bags and fishing equipment; however, at the end of this century, a new use appeared in Europe as painting support not only for banners but also for pictures mounted on frames. The use of canvases for paintings began during the Late Middle Age, and Cennini mentioned the preparation of canvas supports in his treatise *Il Libro dell'Arte* (Chapter CLXII), written between the end of the 14th century and the beginning of the 15th century. One of the most ancient paintings on canvas surviving to this day is “*The Madonna of Humility*” by Lippo di Dalmasio, dated 1390 ca. and displayed at the National Gallery. However, the use of canvases especially coupled with the oil technique, mostly linseed oil, was popularised only during the Renaissance, with Italy being the main centre. The “*Sistine Madonna*” of Raffaello, dated 1513–1514, is an example of oil on canvas.

In the 15th and 16th centuries, other important centres of flax and linen production emerged in northern Europe, Britain and the Hanseatic area [121] as well as in Rus lands [122].

With the Renaissance, the main cultural centre was displaced in Italy, and although the linen fabric was widely used and modest families had numerous luxurious linens and tablecloths, as reported in [123], flax was mainly produced in central Europe. In the 16th century, Poland, Bohemia and Moravia became important areas of linen manufacture [124], while Brittany, one of the main centres of flax cultivation, established major imports of flax seeds from Zeeland and Baltic countries [125].

In approximately 1670, the Huguenots from France, Protestants who moved in large numbers to England and Ireland as well as Switzerland, Holland and Germany as religious refugees, introduced knowledge in England regarding textile production, as indicated by Louis Crommelin, a French Huguenot expert in linen manufacture, in the documents cited in [126,127]. During the 17th century in France, flax cultivations reached 300,000 ha, over double the area of cultivation in 2021 (140,000 ha) [128]. Baltic countries specialised in flaxseed production and supplied the product to the remaining European countries [125,128]. Between 1660 and 1700 in England, considerable quantities of flax and hemp were imported from Norway, Denmark and the Baltic, while linen and textile yarns were principally imported from Germany, Holland, Flanders and France [129].

In the *Encyclopédie* dated 1751–1765, Diderot and D’Alembert reported the presence of three varieties of flax in the market: cold, medium and warm [130]. Although the warm variety grew faster during the first phases of plant growth, at maturity, the plant was lower in height than the other two varieties and produced numerous branches with seeds; therefore, the yield of the flax fibres was low. In contrast, the ‘cold’ flax grew slower but was stronger and more resistant to cold environments. At maturity, the flax plant of this variety produced fewer branches and capsules and was taller than the other varieties; therefore, fibre extraction was optimal [130]. The highest quality of seeds of the ‘cold’ flax variety came from Riga, but as this variety of flax plants produced a small number of seeds at

maturity, so farmers in France were obliged to buy the seeds from Riga once every three or four years [130].

In the second half of the 19th century, Holland and Belgium specialised in the luxury market with high-quality flax fibres, while Russia became the leader of the common quality of flax fibres for all uses with a monopoly in the West European market [131].

At the beginning of the 20th century, several main centres of linen manufacturing were located in Ireland, Scotland, France, Belgium, Germany and Bohemia [131]. Moreover, Ollerenshaw reported that with the Russian Revolution, Russian and Baltic flax production almost disappeared and re-emerged only after 1920, while the German occupation of northern Europe during the First World War affected the flax production in Belgium and France [131]. In both World Wars, the production of flax was of primary importance to supply the army; further details can be found in Ollerenshaw's paper, as previously cited. In the Second World War, flax was widely used to build aeroplanes, parachutes and other military supplies [132], and sustained production was observed. Kozłowski *et al.* reported that Egypt doubled its cultivation to support the flax demand of the United Kingdom [132].

It must be highlighted that in Asia, India was one of the origins and/or diversification centres of flax, and production spread in the remaining continent between 5000–0 BC. In America and Australia, flax was introduced only with colonisation. The French exported flax cultivations and knowledge in Quebec approximately 400 y ago, and the English exported it in Australia less than 150 y ago [99].

2.2 Ancient cultivation and extraction methods

Following the previous section, the history of flax cultivation is supplemented by a brief description of sawing practices and details of the extraction methods adopted by different populations across the centuries in Europe and the Middle East.

Today, as in the past, several steps must be implemented to obtain long fibres from flax. Once flax plants are sown and reach maturity, they are pulled out. To extract the fibres, a retting stage is implemented in which stems are laid on the soil and subjected to the action of rain, sun and microorganisms (dew retting) for several weeks or immersed in water (water retting) for several days. The two retting modes have the common objective of degrading the pectic middle lamellae in the bast fibre bundles to facilitate their extraction. After the retting step, the woody part of the stem is mechanically broken (breaking), and the woody part of the stem and fibres are separated (scutching). Finally, the fibres are combed to remove the residual middle lamellae and separate the fibres (hackling or combing); see **Section 2.3** of this **Chapter**.

Starting from ancient Mesopotamia, flax was considered one of the most important plants and, as illustrated in the *Warka* vase (dated to c. 3200–3000 BC), it was often associated with dates as a symbol of fertility [133] because of its needs for rich soils and high moisture, which required irrigation.

Apparently, in ancient Mesopotamia, only small plots of lands were dedicated to flax as a winter crop [110,134]. However, Miller *et al.* [133] reported that, in ancient texts, flax was associated with concepts of both “field” and “garden”, while other important plants, for example, barley, were cultivated only in crop fields. Flax was associated with the goddess Inanna [133], and in general, weaving work was a prerogative of women, especially slaves and prisoners of war, as reported in [110] and its relative comments. In contrast, sowing and stem preparation, as well as fibre extraction, involved both women and men.

In the 4th–3rd millennium, Mesopotamians used both dew and water retting, and the textiles were left under the sun to bleach fibres [110]. Moreover, the textiles were treated with certain plants that grow in the Middle East, such as *Salsola kali* and *S. soda*, *Salicornia europaea* and other glassworts and saltworts used to produce soda ash [116,135], as well as mineral clays such as Fuller’s earth [135].

In ancient Egypt, flax was cultivated in mid-November after the seasonal flood of the Nile River in August–September [110,136]. In the beginning, only water from floods and rainfall was used in cultivations without any human intervention. However, due to the scarce rainfall that did not promote crop growth and the vital Nile flood, which decided the state of abundance or famine for the whole population [137], a system of basins (probably starting from the Middle Kingdom) was built to channel the water from the Nile inundation into crops [138].

The water was allowed to enter the basins for almost one month to saturate the soil, which also promoted the deposition of fertile clays and silts, and then allowed to flow out [138]. Sowing occurred after this operation, and both *Linum bienne* and *usitatissimum* were sown [139]. At maturity, the stems were pulled out (not cut), grouped in bundles, and dried under the sun. Then the capsules were removed. As in Mesopotamia, stems were retained in flowing water between 10 and 14 d (water-retted) to eliminate pectin, and subsequently, the stems were successively broken with wooden mallets using stones as a work surface and a wooden knife to eliminate the rest of the bark [115,139]. Unfortunately, these work steps are not illustrated in ancient tombs or mentioned in texts, and no tools have been found in archaeological sites because of the high degradability of cellulosic objects [115,139].

In contrast, in the Egyptian Tombs of Dagi (Middle Kingdom TT103, details shown in **Figure I-5**) and Thutnefer (New Kingdom, TT104), the scutching process was illustrated: flax stems were passed through two sticks, and a wooden fan (or knife) was used as an alternative [139].



Figure I-5 Details of wall painting from Tombs of Dagi (TT103), where two women are shown to scutch flax stems (from the left) and probably splice flax into threads (right). Illustration from [139].

Finally, the hackling step was implemented. In certain cases, this step was optional, especially when the thread was spliced rather than spun [115]. In general, an indicator of spliced thread is if two or more threads, which are composed of twisted fibres, are plied. If the thread is spun, the yarn is generally used alone [140]. Ancient Egyptian threads were prepared through S-direction twisting and plying, and a wet rotation technique was used [139,141].

In terms of the use of flax in ancient Egypt, flax threshing and shives were used in mud brick construction, and a mix of silt, clay, sand, straw and water was used to create blocks as building materials [142,143]. Linen was employed in cloths and tunics, such as the fabric investigated in [144] to prepare sails [145,146] and as bandages in the embalming process of dead bodies. As reported by Vogeslang-Eastwood, clothes were mended or retransformed and reused in other ways if they were excessively worn and torn [139], and because linen production was particularly laborious, the same principle was likely also applied to other objects made of linen, as in the case of the linen shroud of a mummy that may have been previously used as a sail [147].

Another important use was in cartonnage, a multi-layered painted support made of different layers, with the first layer made of linen, as shown in [148], followed by plaster and paint. The first condoms were likely made of linen in ancient Egypt [149], but the attribution of that function to small pieces of ancient linen fabric is still controversial.

As the use of flax spread from Europe through Egypt, the processing methods of flax were similar. In Upper Swabia and Lake Constance, during the Late Neolithic, the Horogen culture cultivated flax plants for fibres and oil [107]. Similar to Egypt and Mesopotamia, flax plants were pulled out and not cut, allowing the use of the entire length of the stem to extract fibres as long as possible. No traces of epidermis, cortex or phloem were found at the surface of the fibres, and Maier et Schlichtherle hypothesised that this could be attributed to the use of the retting process before the extraction of the fibre [150]. The same authors also observed that certain archaeological remains of the stems were flattened and broken at different points, suggesting the use of a breaking tool to beat them [150]. The combs for hackling and spindles found in the same sites indicate the use of a reasonably advanced method to produce linen. As reported by Maier et Schlichtherle and other authors cited in their paper, objects such as fabrics and fishing nets were preserved at the Constance Lake site.

In Italy, during the pre-Roman period and successively during the Republic, flax was mainly exported from Egypt, although Spain and Gaul exported a certain amount as well. Although a small amount of flax was also cultivated and processed in Italy, the greatest quantity was produced in the Roman colonies and used not only for clothes but also as war material to prepare tents and sail clothes [151]. The climate in Italy can be divided according to the country shape: northern Italy has a climate similar to central Europe, and South Italy has an arid Mediterranean climate. In ancient times, in the northern half of the country, sowing was performed during spring, while in the southern half, sowing more closely followed Egyptian practices and was performed in autumn with abundant rainfall [151]. Additionally, as

Margarita Gleba reported, not all the soils in Italy were suitable for the cultivation of flax, and because linen production required more work than wool fibres, it was economically disadvantageous to produce it [151]. Furthermore, flax cultivation depletes the soil of resources, and thus, crop rotation was performed [152]. At present, due to the implementation of dew-retting and the release of organic matter during this stage, an opposite trend is observed and the soil is enriched.

Similar to Egyptians, Romans used combs to remove capsules and wooden clubs to break stems after the dew or water retting process. To bleach the fibres, Margarita Gleba reported the exploitation of sun exposure, as in ancient Mesopotamia and Egypt, as well as the use of a sulfuric treatment [151] and it is known in the literature that also urine was used for this purpose [153].

Several spindles of different shapes were found in northern Italy [154], and in contrast to Egypt, in Europe, linen threads were mostly produced with a Z-twist [140] as noted in the Etruscan textile examined by Carroll [141]. Moreover, the fabric mainly appeared in-plane waves [151].

Tools similar to those used by the Romans to extract fibres were found in northern Europe. Because the use of flax fibres spread with the Romans, expectedly, at least initially, similar tools, such as clubs to beat the stems (**Figures I-6a**) and knives for scutching or combs for heckling (**Figures I-6b**), were adopted. An example pertains to the possible reconstruction and use of wooden clubs, as shown in **Figure I-6a** found in Sweden and dated to the Roman Iron Age (Item 447267. SHM 23159: K12, Historiska Museet), likely used to break flax stems.

Between the period of the Roman Empire and the Middle Age, several instruments and methods to extract fibres were improved. For example, in the Middle Age, Vikings likely used breakers mounted on a stand with serrated teeth, such as that illustrated in **Figure I-6a** with missing legs [112]. Surprisingly, not even the symbols linked with this plant changed through populations, and in Sweden and Norway and the Norse religion, as reported by Viklund, flax was associated with femininity and goddesses and used in magical rituals linked with fertility and funerary rites [114].

Two miniatures of manuscripts created in Belgium, one dated 1515 (*Book of hours - Da Costa hours* MS M.399 fol. 12v [155]) and the other dated 1525–1530 ca. (*Book of hours* MS M.1175 Fol. 014r [156]), currently available at the Pierpont Morgan Library, show two men surrounded by a circle of flax stems, breaking fibres with a manual tool (a schematic reproduction of the *Book of hours* dated 1515 is presented in **Figure I-6c**). In both miniatures, a woman scutches the broken flax stems placed in a wooden column by hitting them with a wooden tool. This action was reported to be performed during November, and therefore, in the manuscript of Bruges MS M.1175, the miniature of the fibre extraction process has been associated with a second miniature with the sagitta zodiac sign. However, another miniatures manuscript from France, *Livre d'heures* (L'Escalopier 22), dated 1555 and created for King Henri II, shows two women working on flax fibre extraction: the first woman is using a wooden breaking tool mounted on a stand to break the stems, while the other woman is scutching the fibres with a wooden knife, and the flax fibres are placed on a circular support (**Figure I-6d**). Apart from this difference, the extraction method did not seem to change across centuries.

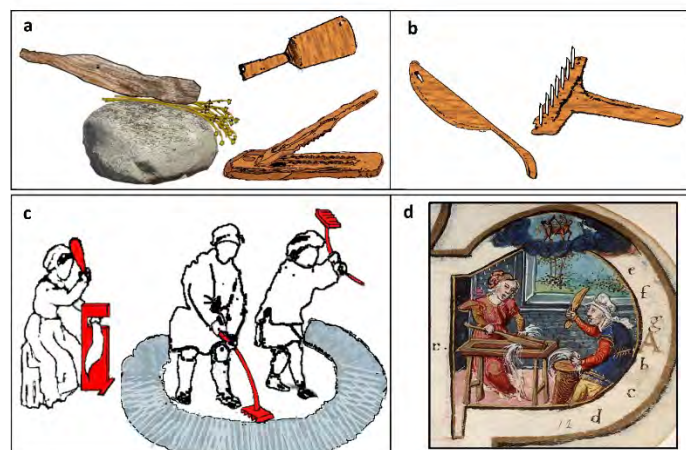


Figure I-6 a) Left: reconstruction of the use of wooden clubs in Sweden to beat the flax stems on a plane surface (rock or wood). The club is schematised from the archaeological tool displayed at the Historiska Museet, original photo © Gabriel Hildebrand and right: another shape of a wooden club inspired from [112,157], and a schema of the breaking tool mounted on a stand found in Norway and reported in [112]; **b)** from the left: schema of a wooden knife found in Gloucestershire and dated to the middle Bronze Age (original photo © Cotswold Archaeology), and reconstruction of a heckle dated between 850–1000 AD found in Shetland, Scotland (Item X. HSA 318 © National Museums Scotland); **c)** schematic representation of the Miniature of the Book of Hours, 1515, Belgium (original photo © The Morgan Library & Museum, New York). On the left, a woman scutches a bundle of flax fibres with a wooden tool and a wooden column (highlighted in red) while two men beat the stems with breaking tools; **d)** Detail of the “Livre d’heures” L’Escalopier, hours in Latin with calendar, parchment of 16th century, f. 12 Ms LES 22 A, reproduced with the kind permission of © Bibliothèques d’Amiens Métropole and IRHT-CNRS.

In *L’Encyclopédie*, Diderot and D’Alembert indicate that in France, at the end of the 18th century, flax flowering occurred in June [130]. Next, plants were pulled out based on the maturity and quality of the fibres that the farmers wished to obtain. The stems were left to dry in the field for 24 h on soil and successively grouped in bundles. The bundles were placed on the ground, in an upright position, leaning against one another to form an inverted V-shape chain of stems to enhance the airflow. The authors also reported that a shorter chain corresponded to better airflow. Dried stems were successively placed in the granary, and once the seeds were dry, capsules were removed by beating the stems. For the retting process, three months were optimal: March, May and September. The retting process was performed in flowing water in which stems were left for approximately 8 d and turned every day at the same hour of the day. The retting step was judged to be optimal by extracting three or four stems, pulling them and observing if the woody part was easily separated from the fibres. Retted stems were arranged on the ground to dry and bleached under the sun for eight days (the stems were turned after four days). Once the stems were dry, they were broken using a breaking tool mounted on a stand. A wooden knife with a dull wooden blade was used to eliminate the remaining straw, and finally, the flax fibres were combed [130]. Diderot described another interesting method: flax was placed in a pot with boiling sea water, lime and ash in alternate layers, and the mixture was boiled for 10 h, with the addition of sea water when necessary. This method was used to prepare flax fibres to make them similar to cotton, and at the end of the process, flax fibres were ready for carding [130].

William Hincks performed a series of twelve lithography on linen manufacturing in Ireland for King George III of Great Britain, dated 1783. The author represented the process of flax fibre extraction. In plate II (**Figure I-7a**) two women harvest the flax crop in the background, while two other women eliminate the capsules. The man in the foreground places the stems in water. Plate III (**Figure I-7b**) illustrates the successive step when stems are extracted from the water by the man in the foreground. In the background, a woman and two men dry the retted stems near a fire and break them using breaking tools such as the tools illustrated in the miniatures shown in **Figure I-6c, d** and described by Diderot [130].

In plate IV, ‘*The Common Method of Beetling, Scutching and Hackling the Flax*’ (**Figure I-7c**), a family is involved in the extraction process using the same tools as those in the Renaissance: a young girl uses a wooden mallet with stems placed in a plane support, two other women scutch the fibres on wooden columns using wooden knives and a man combs the fibres through several combs mounted on a wooden stand. In plate V, ‘*Interior view of a Scutch Mill*’ (**Figure I-7d**), the first automated industrial process is illustrated.

Thus, even after the Industrial Revolution, manual extraction occurred. The French painter Jean-François Millet in ‘*Breaking Flax*’ dated 1850–51 represented a woman performing the breaking process with the breaking tool mounted on a stand, although the tool appeared to be made of a larger and less elaborate wood piece. Fedot Vasilevich Sychkov, in the painting “Flax Combers” (Мяльщицы льна) dated 1905, represented a group of women breaking fibres using the same type of breaking tool.

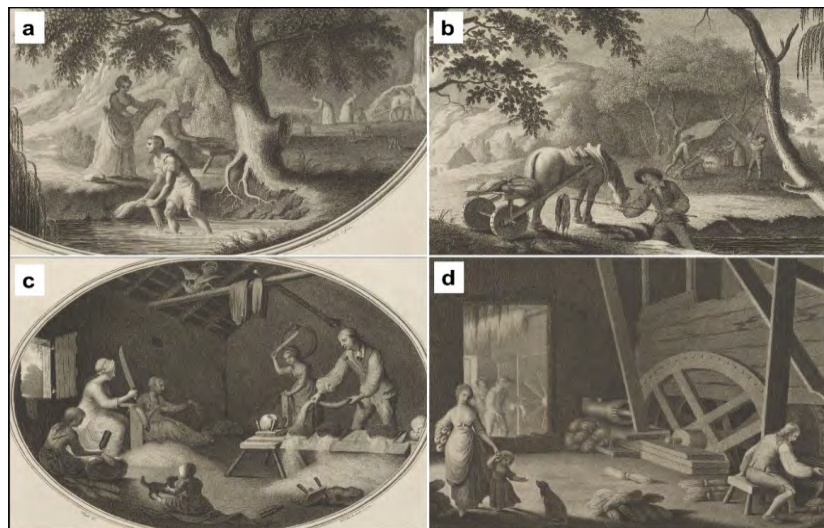


Figure I-7 Four lithography by William Hincks, dated 1783 **a)** Plate II “View near Hillsborough in the country of Downe, representing pulling the flax when grown, hooking or putting it up to dry, rippling or saving the seed, and bogging or burying it in water”. Two women remove the capsules and prepare the stems for water retting, while a man places bundles of stems in water. In the background, two other women harvest the flax plants, group them in bundles and place them upright with respect to the ground to dry before the retting step; **b)** Plate III “View in the county of Louth representing taking the flax out of the bog”. After the retting process, the retted stems are moved near a campfire to be dried. In the background, two men are breaking the dried stems; **c)** Plate IV “The common method of beetling, scutching and hackling the flax”. A family is represented as breaking the stems and combining the fibres; **d)** Plate V “A perspective view of a scutch mill, with the method of breaking the flax” represents one of the earliest industrial scutching mills. The four images are reproduced with the kind permission of the © British Library Board.

2.3 Actual sowing, production, and extraction methods and application

The global supply of fibres has grown yearly since the end of the 20th century; however, the demand for synthetic fibres, such as polyester fibres, has decisively attracted more importance than natural fibres. In 2020, approximately 120 million tons of natural and synthetic fibres were produced, and while cotton production was about 26 million tons, flax reached slightly over 1 million tons [158].

The global supply at present demands a high quantity of production, which requires several hectares of fertile, cultivable soil and industries that can process flax and sell fabrics and semi-finished products. According to the FAOSTAT data (www.fao.org), flax production is mainly concentrated in Europe, which alone produced 97.1% of the flax supply between 2018 and 2019, followed by Asia (1.6%), Africa (0.8%) and America (0.6%). The world leader is France, while Belgium, Belarus and Russia together cover approximately 16.5%, and the production of all the other countries completes the rest of the global supply (**Table I-3**).

Table I-3 Summary of the world production of flax fibres and tows in year 2019. Data from FAOSTAT [159].

Country	Tonnes
France	850,350
Belgium	94,000
Belarus	46,245
Russian Federation	38,464
China, mainland	17,550
Netherlands	13,360
United Kingdom	8,199
Egypt	7,525
Chile	3,201
Argentina	2,695
Total	1,081,589

Several flax varieties are currently in use, which can be divided into winter and summer types. The choice of the variety is extremely important, with each variety having a specific fibre yield, sensitivity to pests (oïdium and fusarium), sensitivity to drought stress and wind (lodging) and precocity to maturity [160]. Research teams of several laboratories have focused on genetic modifications. For example, Musialak *et al.* improved the retting process by reducing the pectin content; their transgenic flax was not only easier to ret but also more resistant to fusarium [161], but the cultivation of GMOs is prohibited or strictly limited in Europe, making it an exception for research purposes [162].

After selecting the variety, seeds are sown with an optimal density between 1600 and 1800 plants/m². This density avoids competition between plants, which reduces the stem diameter and degrades the fibre mechanical properties and makes the plants sensitive to lodging [163]. For example, no remedy exists for *Fusarium oxysporum* f. sp. *lini*, which is a fungus that can penetrate from the soil to the root system and spread into vascular tissues (xylem and phloem) [164]. The plant dies slowly, and the fungus can affect the nearby plants. In other words, not only the mechanical properties of flax fibres are compromised, but fungal attacks can also cause the loss of the entire crop. Even if the diseased plants are eliminated, *Fusarium* can survive in the soil for several years. Therefore, crop rotation for flax is necessary, and a six-years interval between two flax cultivations is suggested [165].

At maturity, the plants are pulled out, and dew-retted between 3 and 6 weeks: the stems are left on the ground and turned to ensure retting in the whole stem. In Europe, the practice of water retting has been forbidden since the beginning of the 20th century due to induced water eutrophication, which refers to the pollution of freshwater with a high content of organic material generated by the action of anaerobic bacteria [166]; nevertheless, this practice is currently in use in other countries. Moreover, the cost of this process is high because fibres should be well dried once the retting is completed [167]. Thus, dew retting is preferred, although this process is highly dependent on the weather, and warm temperatures and rainfall with alternating sunny days are essential to ensure satisfactory retting [160,168]. Several countries that produce linen, such as England or Scandinavia, cannot implement dew retting because of their unfavourable climate [169]; climate change has also been responsible for inhomogeneous retting, especially in Western Europe in recent years.

If the environment is excessively dry, the dew retting process is slow, and inferior retting yields stems with fibres that are difficult to extract; moreover, the well-glued cortical parenchyma is difficult to eliminate from the fibre surface, resulting in a low fibre quality (extremely coarse) and degraded mechanical properties [170,171]. In this case, the fibre bundles appear gold-coloured. In contrast, when fibres are over-retted for more time than necessary or excessive rainfall occurs, the extracted fibres are weak [171] and appear black. In extreme cases, the cellulose can be excessively degraded and the fibre properties are inadequate to be used [172]. Thus, although the retting process is the fundamental step, it cannot be controlled and evaluated only by an expert. Five organoleptic criteria are selected, based on the senses of sight and touch, listed in **Table I-4**: nature of flax (unctuous or dry), colour, strength, fineness, and homogeneity of retting with presence/absence of woody parts. For each criterion, a value between 1 and 7 is assigned, where 7 represents the highest quality [173].

To improve this step and render it more reproducible, enzyme retting has been studied; however, currently, this alternative is expensive [169,174] and cannot be applied at the industrial scale, although the resulting fibres exhibit enhanced mechanical properties. Additionally, the use of fungal cultures was examined for the retting process. Akin *et al.* reported that among *Rhizomucor pusillus*, *Fusarium lateritium* and *Epicoccum nigrum* isolated from dew-retted flax, *R. pusillus* exhibited the highest

performance because it did not attack the flax fibre cell walls and divide them from the remaining stem, in contrast to the other two fungi that led to over-retting [175].

Table I-4 Five organoleptic criteria to establish the flax fibre quality. Table readapted from [173].

Criteria		Value assigned					
Nature	/	/	3 dry fibres or diseased fibres	4 fatigued fibres	5 standard	6 unctuous	7 unctuous/ silvered
Colour	1 blue/black (over-retted)	2 bright yellow (under-retted)	3 diseased fibres (e.g., fusarium)	4 golden tonality	5 blue	6 bright blue	7 grey/silvered
Strength	1 non-resistant	2 medium	3 satisfactory	4 highly resistant	/	/	/
Fineness	1 low	2 medium	3 satisfactory	4 highest fineness	/	/	/
Homogeneity of retting (colour)	1 large defect in colour (notable presence of straw)	2 a slight defect in colour (relative presence of straw)	3 high homogeneity	4 highly homogeneous	/	/	/

In addition to the possibility of damaging flax cell walls, certain fungi are also pathogens, such as *R. pusillus* [175]. Moreover, fungal spores are difficult to control and eliminate and can potentially grow even after the fibre extraction process. Another way to ret the stem is by chemical retting with reagents [176]; however, this process is also expensive and cannot be used on an industrial scale [174].

Once flax fibres are retted and well dried, they are processed in a scutching/heckling line similar to that described by Gregoire *et al.* and shown in **Figure I-8a** [177]. Industrial extraction lines are based on ancient extraction methods transformed at a large scale and automated. The whole line is divided into different modules, as illustrated in **Figure I-8a**: a breaking module made of several rollers that crash the stems, a scutching module with turbines that scrap the broken shives from the fibres and a hackling module with combs in the last part of the line. For further explanation of the flax fibre extraction process, readers can refer to the review by Manian *et al.* [41]. After their extraction, fibres can be transformed into woven or non-woven preforms. An advantage is that the same lines can be used for the extraction of other bast fibres, such as jute and hemp.

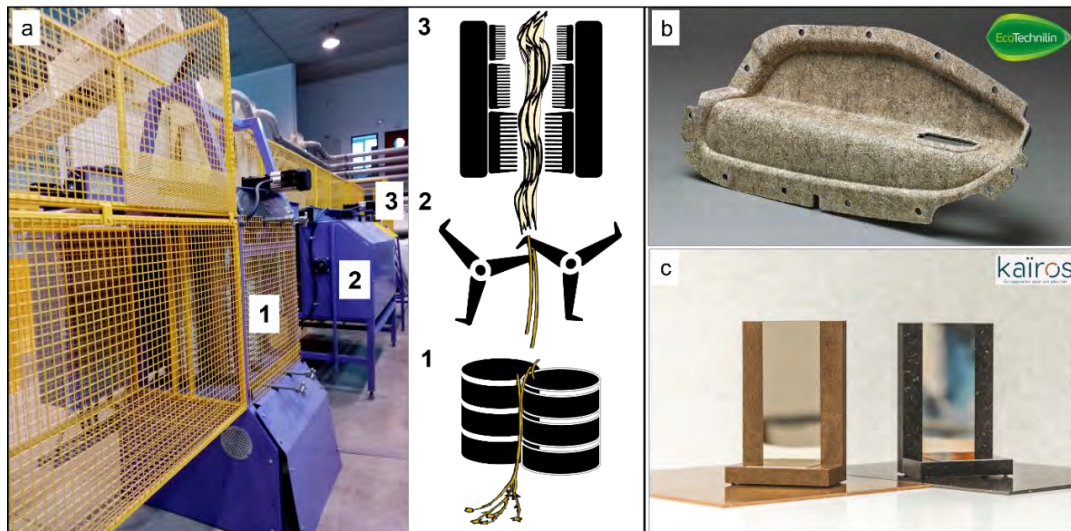


Figure I-8 **a)** Taproot extraction line with three modules, and a schematic representation of the steps involved in general industrial extraction lines: 1. breaking module, 2. scutching module and 3. combing module; **b)** biocomposite made of flax fibres for automotive (© Ecotechnilin) and **c)** biocomposites reinforced with flax fibres employed for applicators used in cosmetic showrooms (© Kairos).

After fibre extraction, several products are obtained: dust, shives and tow, short fibres and long fibres. Although technical fibres are the products with the highest quality and strength, the other subproducts are currently considered for use in the industry in the context of recycling [6]. At present, long flax fibres are mainly used in the manufacturing industry, household linen and design objects, although a new market of biocomposites and technical textiles has begun emerging.

The definition of biocomposite is generally extended to the coupling between synthetic or mineral materials, which have a matrix function, and natural fibres, in this case flax fibres, used to enhance the mechanical properties of the matrix.

Countries worldwide are attempting to modify the practices in the industrial economy to reduce waste and carbon impacts, which are mainly responsible for climate change. This effort also involves substituting synthetic materials with natural materials when possible, such as the biodegradable plastic bags used presently for food waste [178]. Consequently, biocomposites have attracted interest to promote widespread use in the future.

In contrast to blocks for building construction, such as kaolin and earth reinforced with plant fibres, the progenitors of which are ancient mud bricks [179–182], biocomposites created from a mixture of polymer resins and plant fibres are materials developed in the contemporary era. These biocomposites are used for automotive and sporting goods such as bicycles but also for musical instruments and other objects used in daily life, such as those shown in **Figures I-8b, c**. Hybrid fabric with mixed carbon and plant fibres has been also developed [183]. Because such biocomposites are novel products, their mechanical properties, durability and life cycle are not well known and are being collaboratively examined in the academic and industrial domains.

Additionally, agricultural practices have been influenced by global warming and the consequent climate change. Flax is highly sensitive to drought, and almost all flax production is localised in France, especially in north-west of France. According to the recent ARVALIS data, in 2020, almost all regions of flax production had less than 125 mm of rainfall between April and July compared to the mean calculated from the same period (April–July) of the last 20 y [160]. In addition to drought, extreme weather events are uncertain, and in the future, the production of flax in France may be threatened.

3. Degradation of flax fibres: problems in modern and ancient objects

Flax fibre is an organic material with a complex structure and is naturally sensitive to changes over time. Consequently, the natural ageing process can easily modify the chemical composition, and such fibres are more susceptible to biological attacks and structural damage compared to inorganic materials.

In the context of artworks, this phenomenon can lead to problems for museums, restorers and conservation scientists focused on stabilising and preserving objects. Moreover, the engineering domain is interested in understanding the plant fibre ultrastructure responsible for their high performance and biochemical changes that occur after exposure to thermal treatments, humidity and artificial ageing processes, as well as the modifications due to coupling with materials of different natures.

This section summarises the factors that can contribute to the morphological, structural and chemical changes of flax fibres.

3.1 Two main factors of the flax fibre degradation process: water and temperature

In conservation science, water and high temperatures are the basis for almost all damage mechanisms of materials, and they mostly contribute to the ageing process. In particular, at high relative humidity and temperatures, several other degradation processes, such as biodegradation and chemical reactions, may occur.

A direct effect of high relative humidity is fibre swelling, caused by new bonds formed between water molecules with hydroxyl groups present in hemicelluloses and amorphous celluloses in cell walls [184–186] and carboxyl groups of pectins, especially in the middle lamella, that lead to mechanical and structural changes [185]. Garat et al. indicated that at RH <10%, this type of absorption is prevalent, while at higher RH, between 10% and 65%, water is absorbed by pores and lumen through capillarity, leading to the abundance of free water, which are water molecules that are not chemically bonded [185].

In the context of museums and art galleries, a low relative humidity, RH 5–40%, causes the materials to become dry and brittle [187–189] in addition to the structural deformation due to the loss of water molecules. The effect is accentuated if several materials of different natures are coupled, such as in oil paintings [190]. In contrast, a relative humidity higher than 60% promotes the development of microorganisms: the first moulds appear after three months at RH 70% and after a few days at RH 90% [189]. Furthermore, to eliminate the stress that repetitive humidity cycles can cause on the fibre structure, fluctuations of the relative humidity should be avoided in museums.

In Italy, the UNI10829 presented by Ente Italiano di Normazione suggests that ancient clothes, tapestries, natural fibres, etc. should be preserved at RH 30–50% with daily fluctuations limited to approximately 6%. Easel paintings on canvas (oils, tempera, gouache) should be preserved at RH 45–60% with fluctuations limited to approximately 6%, as cited in [191].

The effect of temperature is often associated with relative humidity because of its strong correlation. High temperatures can break the cellulose chain of plant fibres, which acquire a brown colour [192]. In museums, following UNI10829, ancient clothes, tapestries and other artworks made of natural fibres and easel paintings on canvas should be preserved at T 19–24 °C with daily fluctuations limited to approximately 1.5 °C [191]. In the context of higher temperatures, Gassan and Bledzki reported that at 60 °C, amorphous cellulose forms hydrogen bonds. At 150 °C, recrystallisation occurs, and hemicelluloses are more sensitive to the degradation process than lignin or α -cellulose [193]. The authors also observed that until 170 °C, only a slight difference occurs in the tenacity and degree of polymerisation (DP). Above this limit, the degree of crystallinity increases, indicating recrystallisation after chain breakage. However, the tenacity and degree of polymerisation dramatically decrease [193]. This change in flax fibres due to extremely high temperatures was also recorded through nanoindentation and atomic force microscopy tests. At 190 °C, the indentation modulus was approximately 21 GPa, and at higher temperatures, the fibre stiffness was noted to be 16 and 14 GPa at 210 °C and 250 °C, respectively [194].

3.2 Biodegradation, light and pollution: other degradation mechanisms linked with water and temperature

Biodegradation is the first of the indirect effects of water and temperature on natural cellulosic fibres and the reason why the hygrometry and temperatures must be meticulously controlled in museums. Warm temperatures and high humidity content are ideal conditions for the development of most microorganisms and parasites that can degrade plant fibres. However, other parameters, such as pH, the presence of oxygen, light and availability of nutrients, may favour the growth of certain microorganisms and inhibit others, according to their limits of tolerance.

Two notable studies on jute fibres performed by Basu and Ghose [195,196] demonstrated that different fungi can lead to different types of degradation and have different spread methods. Considering the type of spread, the authors divided the fungal species into two categories: one group can penetrate into the lumen, whereas the other group cannot [196].

Nugari *et al.* presented detailed tables of certain bacteria and fungi most frequently isolated from cellulose artworks and air of museums [197], and other research teams summarised the methods of identification of fungi [198,199] and bacteria [199] isolated from dew-retting, water retting and standing retting flax fibres.

Table I-5, presents the fungi and bacteria found in common between the retted flax and isolated from artworks. Fungi are more largely represented.

Table I-5 Fungi and bacteria in common between fresh retted flax stems and cultural heritage objects made of cellulosic fibres. Table adapted from [197–199].

FUNGI	BACTERIA
<i>Alternaria solani</i>	<i>Bacillus cereus</i>
<i>Alternaria tenuissima</i>	<i>Bacillus subtilis</i>
<i>Aspergillus flavus</i>	<i>Pseudomonas aeruginosa</i>
<i>Aspergillus niger</i>	
<i>Botrytis cinerea</i>	
<i>Cladosporium cladosporioides</i>	
<i>Cladosporium herbarum</i>	
<i>Epicoccum nigrum</i>	
<i>Fusarium oxysporum</i>	
<i>Humicola grisea</i>	
<i>Trichoderma virens</i>	
<i>Verticillium nigrescens</i>	

Water activity a_w (or free water) is essential to the growth of microorganisms and is expressed as the ratio of the partial vapour pressure of water in equilibrium with a solution (p^{equ}) to the water vapour pressure of pure water (p°). Therefore, $a_w = p^{\text{equ}}/p^\circ$, with $a_w=1$ for pure water [200–202]. For materials such as food and other surfaces, the equilibrium relative humidity (ERH) indicates the capacity of a material to absorb and desorb water molecules in air at given temperature and under a total pressure of 1 atm. Therefore, $\text{ERH} = (p^{\text{equ}}/p^{\text{sat}})_T$, $p = 1$ atm, where p^{equ} is the partial pressure of water vapour in equilibrium, and p^{sat} is the saturation partial pressure of water [200].

In general, fungi need lower water activity (a_w between 0.75–0.99) than bacteria ($a_w > 0.90$) to grow, and a higher fungal activity is expected in air [15,201]. In contrast, if artefacts, objects or biocomposites are buried in soil or compost, bacterial activity is generally prevalent [15]. However, in burial contexts, fungi (especially soft rot fungi) and bacteria may coexist [15] by attacking the same cellulosic materials and fibre cells [203]. **Figures I-9a, b** show certain over-retted fibres attacked by bacteria visible on the surface of the fibre and fungi; the hyphae, in the case of flax fibres, are almost completely embedded in a biofilm.

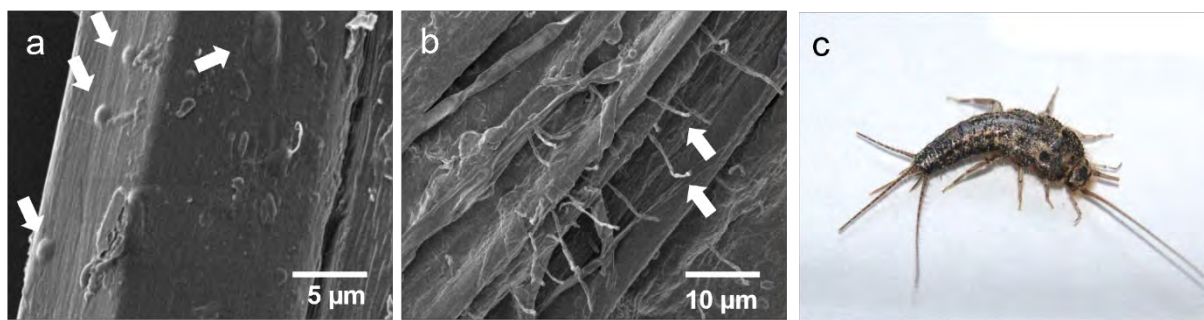


Figure I-9 **a)** Bacterial and **b)** fungal colonisation on the surface of over-retted fibres and **c)** silverfish *Ctenolepisma lineata* (© Erica Melelli). Unpublished images.

In summary, fungi and bacteria may lead to mechanical and structural damage of the fibre through the formation of tunnels, erosion and fractures in the cell wall. Moreover, these organisms can lead to changes in the pH (generally to more acidic) due to substances secreted due to the metabolic activities and pigmented spots [192,204]. This change in acidity caused by enzymes can promote the acid hydrolysis of cellulosic fibres, which is one of the most destructive processes for textiles and paper.

Insects may also damage linen fabric, although their action is less frequent than that of fungi and bacteria. Two of the most well-known insects that can infest linen are silverfish (*Lepisma saccharina*, *Ctenolepisma longicudata* and *Ctenolepisma lineata*), shown in **Figure I-9c**, and firebrats (*Thermobia domestica*) [205,206]. The action of these insects is generally limited to hole production because they feed on cellulose fibres; however, silverfish can also produce yellowing spots [205].

Other indirect impacts of water and temperatures are chemical reactions, especially due to air pollution, and, in the case of seawater and aerosols, salt deposition. Air pollution is a current problem that has gained increasing attention in society. SO_2 and NO_x , generated because of oxygen in air and water molecules in moisture, can produce sulfuric and nitric acids, respectively, which react with cellulose fibres in the acid hydrolysis process [192]. Moreover, the complexity of artworks can also promote these chemical reactions because of the several layers of different natures often coupled in the same object, for example, in the form of pigments.

The presence of moisture, together with the constant contact of cellulosic fibres with metals, can cause another phenomenon known as mineralisation. Metal corrosion caused by the reaction of water with metal cations creates minerals within cellulose fibres and leads to a partial substitution of the organic material [207–209]. Although fibre mineralisation causes structural modification of cellulose fibres such as flax, which become stiffer and brittle, metal cations, such as copper cations, can contribute to the preservation of textiles due to their biocidal activity, which limits the development of microorganisms [207–209].

In terms of salt deposition, water can contain dissolved salts, of which the most common salt is sodium chloride as in seawater. Salty water can penetrate between the cellulosic fibres, and into their pores and their lumen. The subsequent evaporation of the aqueous medium deposits salt, which

crystallises and the formed crystals exert pressure, causing fractures in the cell walls and cavities between fibres [210]. This phenomenon requires alternate wetting and drying cycles, and salt, being hygroscopic, modifies the hygroscopic stability of the whole object, together with its structure, in a self-perpetuating process. Wood degraded with salt is also known as “fuzzy” wood because of its appearance [210].

In general, the problem does not arise because these conditions do not allow the preservation of cultural artefacts made of bast fibres. For example, cotton immersed in sea water can degrade in three weeks [211]. Therefore, although salt growth is documented in stone [212] and wood [213] conservation, this phenomenon is not considered for bast fibres. Notably, this aspect is considered to be examined in the engineering field in the future because one of the applications of plant fibre-reinforced composites is the production of aquatic sports equipment such as surfboards [214] and sailing equipment.

The last parameter is light. Together with water and temperature, light can promote the growth of microorganisms and cause heating damage. UV radiation is particularly dangerous, especially in the presence of water molecules, because it causes photo-oxidation of cellulosic fibres, which not only alters the original colour but also produces carboxylic acid and breaks the cellulose chains [192,215]. Furthermore, oxidised cellulose promotes hydrolysis [216]. Therefore, UNI10829:1999 established illumination limits similar to the temperature and humidity parameters. Textiles and tapestries can be exposed to a maximum luminance of 50 lux (luminous flux to square metre = lm/m^2), with a maximum UV radiation of $75 \mu\text{W}/\text{lm}$ and a maximum annual light dose of $0.2 \text{ Mlx} \cdot \text{h}/\text{y}$. Different values are indicated for paintings on canvases, which are less sensitive to light than pure textiles ($E=150 \text{ lx}$, $\text{UV max}=75$, annual light dose $\text{LO}=0.2$) [191].

4. Characterisation techniques to study ancient and modern flax yarns

Several techniques are currently being used to characterise plant fibres at different scales and are briefly introduced in this section, followed by the types of information that can be obtained using these techniques.

4.1 Morphological analysis

The simplest characterisation method is optical microscopy using visible light. Compound and stereo microscopes, which are fast, inexpensive and available in every laboratory, are suitable to obtain a global view of the sample. Optical microscopy can be adopted to measure the average diameter of flax fibres and evaluate the presence/absence of kink-bands and defects along the fibres (**Figure I-10a**). In the case of fabrics, this technique can be used to evaluate the thread count and type of weaving, as indicated by Helmi *et al.* [217]. As shown in **Figure I-10b**, polarised light microscopy enables the identification of kink-bands from different bast fibres [96] and their quantification through image processing [218,219]. For further explanation of the investigation of kink-bands under polarised light, Thygesen and Hoffmeyer's paper is suggested [218].

Scanning electron microscopy (SEM) is one of the most commonly used characterisation techniques. This approach is principally used to scan the fibre surface (**Figure I-10c**) and, in the case of artworks, it can provide information regarding the elemental composition of foreign materials if coupled with energy-dispersive X-ray spectroscopy (EDX) or wavelength-dispersive X-ray spectroscopy (WDX) systems (<https://www.eesemi.com/edxwdx.htm> for more details). SEM analysis can be used to clarify the fibre shape and kink-band shape, signs of ageing [82] and presence of foreign materials and biological attacks [220]. Richter reported that textile fibres can be washed in boiling water and ether at 40–60 °C to extract dust and foreign materials before SEM analysis [220]; however, this step is not always possible and is not exempt from the risk of causing further damage to the fibres. Additionally, certain important pieces of information that can be obtained from foreign materials may be lost. Consequently, this step is rarely executed for ancient textiles and is not necessary when modern samples are considered.

Furthermore, although transmission electron microscopy (TEM) analysis is important, it is not commonly adopted because of the difficult sample preparation process; the sample must be as thin as possible (less than 100–150 nm). In contrast to SEM, this technique highlights the cell wall layers in sample cross-sections and can be used to investigate the biodegradation of the cell wall in archaeological findings [15,221].

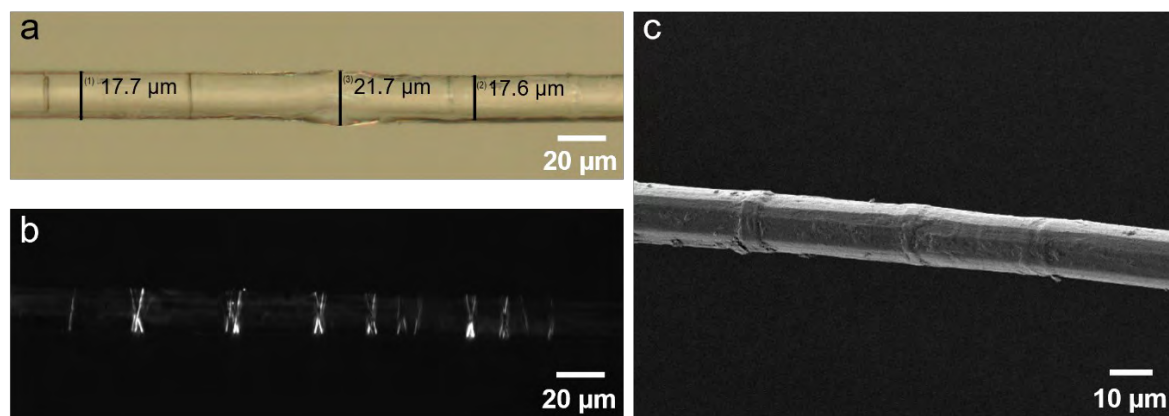


Figure I-10 *a)* Elementary flax fibre under optical microscopy and diameter calculation *b)* elementary flax fibre under polarised light that highlights kink-bands in white and *c)* SEM microscopy of an elementary flax fibre with three visible kink-bands.

4.2 Study of parietal composition

FTIR and Raman spectroscopies are vibrational spectroscopic techniques that are extensively used to analyse bast fibres, and these approaches are well known in the cultural heritage field because of their non-destructive nature. Nevertheless, in the case of plant fibre analysis, FTIR spectroscopy is generally preferred because the recorded spectrum is not influenced by the presence of fluorescence emission; in contrast, in the case of Raman analysis, fluorescence can hide signals of interest from the sample structure. Therefore, Raman spectroscopic analysis of bast fibres is generally preferred using an excitation wavelength of 785 nm in the case of micro-Raman spectroscopy [222,223] or 1064 nm for FT-Raman spectroscopy [224] to reduce fluorescence. Another method to decrease fluorescence, which is extremely high in ancient textiles, is the photo-bleaching method, which involves irradiating the sample with a laser for long periods, for example, 30 min, before the acquisition [223].

Micro-Raman spectroscopy performed using an excitation wavelength of 532 nm and a 100x oil immersion objective can have a spatial resolution of approximately 240 nm [74]. Infrared spectroscopy can be performed at the microscale level through μ -FTIR/ATR, which is an IR spectrometer technique involving a germanium crystal that allows a contact area of 100 μm with the sample surface [225].

With excitation wavelengths in the visible radiation or NIR (for Raman spectroscopy) range and IR range (for FTIR spectroscopy), the abovementioned techniques allow to obtain information on the sample molecular structure through the inelastic scattering of photons in the case of Raman, or absorption of the incident radiation that activate particular molecular vibrational modes of molecules present in the sample, in the case of FTIR. For further information regarding the application of vibrational spectroscopic techniques to plant cells, Gierlinger's work is suggested [226]. Vibrational spectroscopic analysis of bast fibres allows to recognize plant species [223,224,227] and study ageing

process [222,228], biodegradation [229,230] and evaluate presence or absence of foreign materials, such as pigments and binders.

These two spectral techniques can also be used to calculate relative intensity ratios between peaks to evaluate the crystallinity index ($X_{\text{CFT-Raman}}/\% = (I_{1481}/I_{1481}+I_{1462}) \times 10^2$ in the Schenzel method or I_{380}/I_{1096} in the Agarwal method, $X_{\text{CFTIR}} = I_{1372}/I_{2900}$) [229,231,232] and lateral order index ($LOI_{\text{FTIR}} = I_{1430}/I_{897}$) [233,234], which can reflect the state of preservation of cellulose chains in the fibres.

^{13}C cross polarisation magic angle spinning nuclear magnetic resonance spectroscopy (^{13}C CP-MAS NMR) is another technique used to evaluate cellulosic objects. NMR uses nuclei, such as ^1H or ^{13}C , and maps their position in the molecules by applying an external magnetic field that induces the nucleus resonance. An advantage of solid-state NMR is the possibility of studying solid samples in their native form. A recent and exhaustive review of the solid-state NMR technique can be found in [235]. This technique provides complementary information to that obtained using vibrational spectroscopy, regarding the abundance or change in the molecular composition of the sample. For example, for cellulosic materials, ^{13}C NMR CP-MAS analysis was performed to evaluate naturally aged and artificially oxidised cotton and linen fibres to simulate fibres in ancient paper [236]. A notable parameter that can be calculated using the ^{13}C NMR CP-MAS technique is the crystalline to amorphous ratio of cellulose. The values are calculated using the integrated areas of crystalline C4c ($\delta \sim 87\text{--}93$ ppm) and amorphous C4a ($\delta \sim 80\text{--}85$ ppm) cellulose, through the formula $R = I(\text{C4c})/I(\text{C4a})$ [237,238]. Moreover, the cellulose I_α and I_β allomorphs [239–241] can be evaluated, along with the effects of mechanisms such as hydrolysis [242].

Other complementary information regarding the fibre structure can be obtained by the calculation of the average lateral fibril dimension [242], which is an estimate of the ultrastructure of the cellulosic fibres and their microfibril network. NMR is micro-destructive, and at least 30 mg of sample is needed, which is a key limitation of this technique in the cultural heritage field [243]. Other techniques, such as gas chromatography/mass spectrometry (GC/MS) or pyrolysis–gas chromatography/mass spectrometry (Py-GC/MS) can be used to obtain information regarding fibre treatments [244,245] or pigments [246] present at the fibre surface; however, the use of these approaches is limited. In botany and engineering fields, gas chromatography is widely applied, for example to determine the polysaccharide composition, but notably, the minimum amount of sample required is 5 mg and its destructive [247,248].

The last technique presented here that can be used to obtain information regarding the state of preservation and ageing of cellulose fibres is the degree of polymerisation (DP) [249–251]. This technique quantifies the monomers present in the cellulose chains through viscosity or sedimentation-diffusion measurements [252]; thus, the technique is destructive and requires a considerably high amount of sample, i.e. between 60 and 120 mg [250]. In the past, there was disagreement regarding the polymerisation degree calculated using nitrate or cuprammonium and the preference for sedimentation-diffusion and viscosity. However, at present, protocols have been established through norms as the ISO 5351:2010, UNI 8282: 1994 in Italy or DIN 54270 in Germany, according to which, copper (II)

ethylenediamine is used for sample dissolution and successive calculation of relative viscosity. As reported by Rossi, for raw cotton and linen, the degree of polymerisation is higher than 2000–2500 DPw, while for bleached fibres, the degree of polymerisation is higher than 1200–1300 DPw. In ancient paintings, values less than 500 DPw are considered critical and a sign that cellulose fibres have lost their strength [250]. An interesting example of this application can be found in [249].

Notably, in the engineering field, other destructive techniques, such as thermogravimetric analysis TGA and derivative thermogravimetry DTG, can provide indirect and approximate information regarding the chemical composition of cellulose fibres and enable the comparison of the quantity of water, cellulose components and non-cellulosic material between two samples [253]. Flax fibres, heated at a well-defined interval of 10 °C to high temperatures (600 °C) with constant monitoring of their weight, exhibit loss of water at 60 °C, and successive degradation of cellulose and hemicellulose at 300 °C, followed by lignin and pectin degradation at 400 °C [253,254].

4.3 Ultrastructural modifications

X-ray diffraction (XRD) is based on a collimated and monochromatic X-ray beam that hits the sample and interacts with electrons of the atoms in the sample. The X-rays are elastically scattered, and if the sample has a crystalline and well-ordered structure, the crystalline lattice generates a diffraction pattern due to the constructive and destructive interferences following Bragg's law: $2d\sin\theta=n\lambda$. XRD analysis, performed with synchrotron radiation (SR-XRD) [82,255], can be used to examine the crystallinity index of cellulose fibres [256], microfibril angle of cellulose microfibrils [257], mineralisation process [258] and presence of unknown fibres [259].

XRD can provide data in two formats: representations of the 2D diffraction pattern, and one-dimensional profiles extracted from these representations. Flax fibres yield the typical signal of cellulose I with reflections at 110, $1\bar{1}0$ and 200 [255]. Based on these reflection peaks in the one-dimensional profile extracted from the pattern, three methods can be used to calculate the crystallinity index: i) using height ratios between the reflection peak at 200 and minimum reflection intensity between the 110 and 200 reflection peaks, ii) deconvolution of the reflection peaks and iii) amorphous subtraction. For more details regarding these three methods, readers can refer to the review presented by Rogpipi *et al.* [260] or the paper written by Park *et al.* [261].

Notably, the crystallinity index measured using the three methods differs, and both the deconvolution and subtraction methods yield results closer to the NMR than the height method [261]. To study plant fibres, small-angle (SAXS) and wide-angle (WAXS) X-ray scattering techniques are used, as indicated by [262], to obtain information regarding the fibre structure. De Caro *et al.* performed WAXS analyses to realise the ageing characterisation of historical linen threads [251]. In engineering and botany, the use

of SAXS and WAXS is of significance to study the microfibril angle of cellulose microfibrils of plant fibres [257,262] because a lower angle corresponds to a higher tensile strength and modulus [263].

Another less common technique to investigate the internal structure of plant fibres is focused ion beam-scanning electron microscopy (FIB-SEM), which can be used to implement tomography on single elementary fibres [75,264].

4.4 Multiscale estimation of mechanical properties

As mentioned previously, the degree of polymerisation is a key method in the evaluation of the strength of cellulose fibres in cultural heritage fields, especially in the case of tapestries and canvases that are subjected to mechanical stress due to frames and/or their own weight due to the effect of gravity. This method has been used to evaluate the mechanical properties of Dalí's paintings by Oriola *et al.* In a set of several paintings, only one painting demonstrated DP <600 and was consequently considered at risk [265].

An interesting and innovative method to study the strain and structural modifications of tapestries in a generalised manner is digital imaging correlation (DIC). Khennouf *et al.* [266], Malesa *et al.* [267] and Malowany *et al.* [268] mounted a system of two cameras capable of recording images and correlated the deformations of canvases and tapestries with time and environmental conditions.

Other mechanical tests are less commonly performed in the cultural heritage field but are widely used in the engineering domains. A commonly employed test is the tensile test on unitary fibres. Between 30 and 50 elementary fibres are extracted from bundles, and each fibre is glued to a plastic support or in a paper frame, which has a gauge length of 10 mm according to ASTM C1557 [269]. The frame is successively mounted on a tensile testing machine, and a load cell of 2 N is used, which stretches the unitary fibre until rupture, allowing one to calculate its modulus and strength based on its diameter [163]. A larger number of elementary fibres leads to more reliable statistics and lower error; however, even few elementary fibres can indicate the fibre condition.

Tensile testing can also be performed for small pieces of fabric. Nechyporchuk *et al.* compared the mechanical behaviour of a fragment of an acrylic painting on canvas dated 15 y to a new modern canvas appositely prepared in the laboratory. The authors also considered the use of nanocellulose treatments to increase the canvas strength [270]. Recently, a combined method of digital imaging correlation and tensile testing has been applied to study historic tapestries made of silk [271].

Nanoindentation is a characterisation technique that can provide information regarding the mechanical properties of a sample at the nanoscale level. Notably, the use of this technique is increasing in the cultural heritage field [272], for example, the nanoindentation analysis performed by Salvant *et al.* on cross-sections of “*Portrait du Docteur Paul Gachet*” and “*La Salle de danse à Arles*” of Vincent Van Gogh [273]. Additionally, Tiennot *et al.* investigated a cross-section from a canvas painting using

nanoindentation, although the approach was different from that of Salvant *et al.*, as the authors mapped the mechanical properties of each tested layer and they concluded that the natural ageing process induce a stiffening of the painted layers [274].

4.5 Dating

The most commonly used dating method is radiocarbon dating using ^{14}C isotopes. Probably one of the most discussed and controversial works involving radiocarbon dating is that of the Turin shroud made from linen [275]. It was recently concluded that a new radiocarbon analysis should be performed again in the Turin shroud only after the development of a stricter protocol [276]. In the already cited work of De Caro *et al.*, the use of a new dating method by WAXS was proposed with promising results [251].

Bonizzoni *et al.* observed that more aged textile corresponded to a greater amount of fluorescence emission, and although the authors were cautious because they considered that fluorescence can also be generated from impurities, they used laser excited micro-fluorescence for dating and compared the results obtained using the μ -Raman spectra [222]. To elaborate μ -Raman spectra, the authors adopted the ratio between peaks I_{1121}/I_{1196} , which correspond to the vibrational modes of symmetric and anti-symmetric stretching of C-O-C of 1,4- β -glycosidic bond of cellulose [277,278], and correlated the values obtained with the age of the textiles [222].

Another method for dating cellulosic materials is the chemical method implemented using enzymatic biosensors developed by Campanella *et al.* [279,280]. These biosensors can recognize methyl and carboxyl groups of cellulosic materials, the amount of which increase with ageing. Notably, the authors warned that this type of method depends on the artwork conservation conditions, and the same analysis performed on fibres extracted in different parts of a single painting may give different results [280].

4.6 Innovative techniques

New technologies are being constantly developed, allowing the investigation of materials already studied for centuries, such as plant fibres, with novel methodologies and combinations.

Atomic force microscopy (AFM) is a cutting-edge technique, which is based on a tip mounted on a cantilever with a laser focused on the probe reflected in a photodiode. The technique can be used in several modes, and the most commonly used application is to investigate the topography of ancient materials at the nanoscale level [281]. AFM has also been used with a spherical probe functionalised with several consolidants, such as nanocellulose (CNF), before scanning the cotton fibres of an artificially aged canvas to test the adhesion between the treatments and cotton fibres [282].

Another example pertains to Reynaud *et al.*, who coupled the AFM probe with IR spectroscopy to investigate 5,000 y old, mineralised flax fibres. The authors simultaneously obtained morphological and chemical information and clarified the mineralisation phenomenon [209]. This particular system has already been tested on plant cell walls for botanical purposes [283].

In the engineering domain, another AFM mode known as the peak force quantitative mechanical property mapping (PF-QNM[®]) mode has been recently employed to scan cellulose fibres, as illustrated in **Figure I-11a** [30,43]. With a probe mounted on the cantilever, this technique allows to scan the sample surface and record force–distance curves that provide information on the mechanical properties of the sample at micro- and nanoscale levels. Further details are reported in **Chapter II**. This method can distinguish the mechanical properties of thermally treated fibres used as reinforcement in composites [194] and the effect of retting on the mechanical properties [65] or cells with different mechanical properties at different stages of growth [30]. Because this characterisation technique requires only a small amount of the sample (few millimetres of a yarn or few fibres) and can be used to investigate complex systems in which several materials are coupled, it seems promising and suitable to investigate samples from the cultural heritage field.

The second technique that is largely unknown in the cultural heritage and engineering fields despite its potential is the second-harmonic generation imaging microscopy (SHG). Based on a femtosecond pulsed laser in the NIR region, the non-centrosymmetric molecules in the sample can generate a second-harmonic response, a non-linear optic phenomenon, if they have a well-ordered structure. Cellulose microfibrils of plant fibres can generate SH, and several teams have already explored the ultrastructure of *Valonia* [284,285]. Furthermore, it is possible to clarify the effect of acid hydrolysis on cellulosic materials [286]. For further explanations and other applications of this technique, the book of Pavone and Campagnola is suggested [287]. Reynaud *et al.* applied SHG to archaeological flax fibres that have undergone mineralisation, as illustrated in **Figure I-11b** [209]. There are three advantages of using this technique: i) a single yarn or few fibres can be analysed, ii) the approach is a non-destructive method because an infrared excitation wavelength is used, and iii) the method can be used to scan a sample in depth (Z-stack), thereby providing information regarding the inner structure of a fibre, complementary to the SEM analysis. More details can be found in **Chapter II**.

Synchrotron radiation is a technique that is gaining increasing attention. FTIR vibrational spectroscopic analysis can be performed using synchrotron radiation to characterise ancient plant fibres. The work performed by Kavkler *et al.* on biodegraded historical textiles is a representative example: the authors compared conventional FTIR microspectroscopy and synchrotron FTIR microspectroscopy techniques [288].

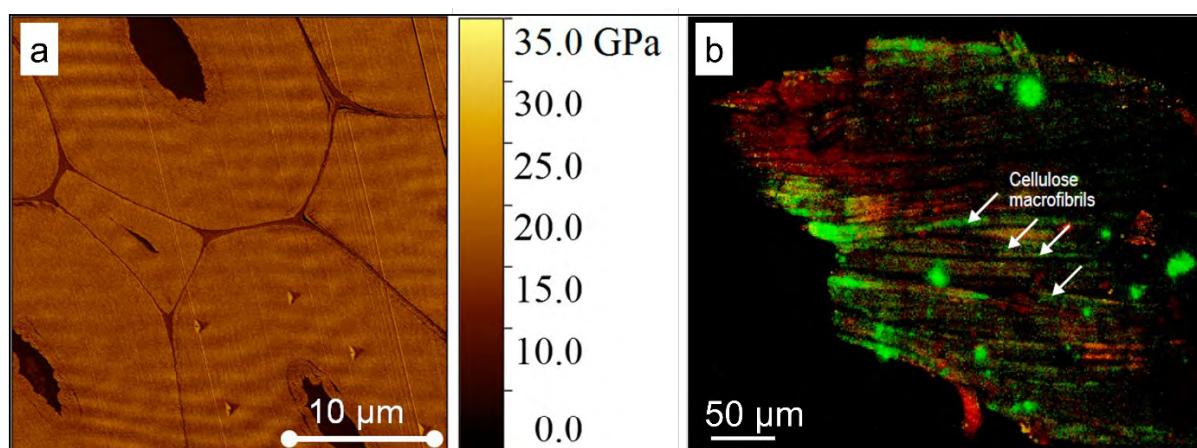


Figure I-11 a) Map of indentation moduli of flax fibres obtained by atomic force microscopy in PF-QNM to study the mechanical properties at the cell wall level in [30]. The mean indentation modulus is approximately 18 GPa; **b)** archaeological mineralised flax fibres investigated by second-harmonic generation microscopy from [209]. Cellulose macrofibrils from the internal fibre structure are highlighted.

In addition, at Synchrotron SOLEIL, the *Dichroism, Imaging and mass Spectrometry for Chemical and biOlogical systems* (DISCO) beamline has been specialised in the use of deep-UV (DUV) fluorescence to characterise plant cell walls. The autofluorescence present in plants due to waxes, protein, lignin and phenolics can be exploited through multi-spectral fluorescence imaging to compare cross-sections of flax stems grown in normal conditions or under gravitropism [289] or to track the effects of enzymes in maize. Maps of spectra can also be recorded by scanning fluorescence microspectroscopy and used to compare the chemical composition in different cells of the stems [290] as well as historical artefacts, as in the investigation of the coating of ancient lutes [291].

Finally, tomography is a characterisation technique useful for understanding the internal structure of samples and virtually reconstructing such structures. Using X-rays, it is possible to obtain high-resolution tomographic images. Single flax fibres [292,293] and bundles or fabric, such as mineralised archaeological textiles [294], have already been examined using this method, especially in the cultural heritage field. For details regarding the use of synchrotron radiation for plant investigation, the review written by Vijayan is suggested [295].

5. Summary and Conclusions

This review describes the historical timeline and problems encountered in the cultural heritage and engineering fields when flax fibres are employed to create objects.

Section 1 describes the composition and fibre structure of flax fibres and explains their desirable mechanical properties and limitations from the perspectives of cultural heritage applications. Notably, certain aspects, often interconnected, such as the microfibril angle, kink-bands or the mechanical properties of the middle lamella between fibres, are still not fully understood by the scientific community. The microfibril angle is one of the most important parameters that influence the mechanical properties of plant fibres; however, the real value for flax fibres is still debated. The MFA is generally accepted to be small (8°), even though the XRD and SAXS techniques usually used for its estimation involve certain physical limitations in calculating such small angles. Furthermore, knowledge regarding the internal structure of kink-bands, which are the weakest points of bast fibres and are directly correlated with the fibre extraction method, is limited. Therefore, a more extensive investigation should be performed to better comprehend why such bands are susceptible to breakage. The first part also briefly describes plant growth and all the steps from sowing until maturity.

Section 2 of the review discusses the history of flax cultivation and processes from the past to the contemporary era. This section highlights how and why the centres of flax production changed over the centuries in Europe and the Middle East which, in certain cases have been caused by episodes of drought or due to the adaptability of soils. The challenges in agricultural practices, especially in the case of flax crops in France, encountered due to climate change and increasingly frequent periods of drought are of interest even today. This section also treats the evolution of flax varieties and the methods used to extract the fibres from the first flax domestication to the present day. Today it is known that the extraction method impacts on the mechanical properties of flax fibres, in particular for the generation of kink-bands, so the study of ancient extraction methods can teach us something more about the fibre ultrastructure and its response to several mechanical stress made with various tools. Moreover, some uses of flax fibres have evolved, for example from sails used in antiquity to whole boats built today with flax/resin sandwich, and others are still the same, like the linen used in fashion.

Section 3 summarises the main degradation process of flax fibres, which is caused by several factors, such as water and temperature, with a focus on artworks. These degradation processes, which have been well studied in the cultural heritage field to preserve historical objects, are the same as those that flax fibres undergo when they are employed in the engineering field. Thus, artworks that have survived for centuries can be examined to predict the ageing process in new industrial objects.

Section 4 provides a brief overview of the main characterisation techniques used to investigate flax fibres and several cutting-edge techniques currently employed in engineering and botany fields, such as

AFM and SHG, that can also be used to investigate historical textiles. Thus, a new combination of techniques can provide novel insights regarding the ultrastructure and degradation process of cellulosic fibres. The findings are expected to be useful to evaluate their state of preservation and possible treatments. Future research should be focused on developing and adapting these techniques to the field of cultural heritage.

Bibliography

- [1] J. McDill, M. Repplinger, B.B. Simpson, J.W. Kadereit, The Phylogeny of *Linum* and Linaceae Subfamily Linoideae, with Implications for Their Systematics, Biogeography, and Evolution of Heterostyly, *Syst. Bot.* 34 (2009) 386–405. <https://doi.org/10.1600/036364409788606244>.
- [2] W. Van Zeist, J.A.H. Bakker-Heeres, Evidence for linseed cultivation before 6000 bc, *J. Archaeol. Sci.* 2 (1975) 215–219. [https://doi.org/10.1016/0305-4403\(75\)90059-X](https://doi.org/10.1016/0305-4403(75)90059-X).
- [3] C. Yu, Natural textile fibres: vegetable fibres, in: R. Sinclair (Ed.) *Textiles and Fashion*, Elsevier, 2015: pp. 29–56. <https://doi.org/10.1016/B978-1-84569-931-4.00002-7>.
- [4] ARVALIS Institut du végétal, *Lin fibre: résultats et préconisations*, ARVALIS, Paris, France, 2019.
- [5] C. Goudenhooft, A. Bourmaud, C. Baley, Varietal selection of flax over time: Evolution of plant architecture related to influence on the mechanical properties of fibers, *Ind. Crops Prod.* 97 (2017) 56–64. <https://doi.org/10.1016/j.indcrop.2016.11.062>.
- [6] L. Nuez, J. Beaugrand, D.U. Shah, C. Mayer-Laigle, A. Bourmaud, P. D'Arras, C. Baley, The potential of flax shives as reinforcements for injection moulded polypropylene composites, *Ind. Crops Prod.* 148 (2020) 112324. <https://doi.org/10.1016/j.indcrop.2020.112324>.
- [7] G. Neutelings, Lignin variability in plant cell walls: Contribution of new models, *Plant. Sci. J.* 181 (2011) 379–386. <https://doi.org/10.1016/j.plantsci.2011.06.012>.
- [8] L. Pereira, A.P. Domingues-Junior, S. Jansen, B. Choat, P. Mazzafera, Is embolism resistance in plant xylem associated with quantity and characteristics of lignin?, *Trees.* 32 (2018) 349–358. <https://doi.org/10.1007/s00468-017-1574-y>.
- [9] D.S. Himmelsbach, S. Khahili, D.E. Akin, Near-infrared–Fourier-transform–Raman microspectroscopic imaging of flax stems, *Vib. Spectrosc.* 19 (1999) 361–367. [https://doi.org/10.1016/S0924-2031\(98\)00065-4](https://doi.org/10.1016/S0924-2031(98)00065-4).
- [10] D.E. Akin, D.S. Himmelsbach, W. Herbert Morrison III, Biobased Fiber Production: Enzyme Retting for Flax/Linen Fibers, *J. Environ. Polym. Degrad.* 8 (2000) 103–109.
- [11] A. Day, K. Ruel, G. Neutelings, D. Crônier, H. David, S. Hawkins, B. Chabbert, Lignification in the flax stem: evidence for an unusual lignin in bast fibers, *Planta.* 222 (2005) 234–245. <https://doi.org/10.1007/s00425-005-1537-1>.
- [12] T. Gorshkova, Composition and Distribution of Cell Wall Phenolic Compounds in Flax (*Linum usitatissimum* L.) Stem Tissues, *Ann. Bot.* 85 (2000) 477–486. <https://doi.org/10.1006/anbo.1999.1091>.
- [13] H. Bargel, W. Barthlott, K. Koch, L. Schreiber, C. Neinhuis, Plant cuticles: multifunctional interfaces between plant and environment, in: A. R. Hemsley, I. Poole (Eds.), *The Evolution of Plant Physiology*, Academic Press, Amsterdam, 2004: pp. 171–III.
- [14] C. Paul-Victor, S. Dalle Vacche, F. Sordo, S. Fink, T. Speck, V. Michaud, O. Speck, Effect of mechanical damage and wound healing on the viscoelastic properties of stems of flax cultivars (*Linum usitatissimum* L. cv. Eden and cv. Drakkar), *PLoS ONE.* 12 (2017) e0185958. <https://doi.org/10.1371/journal.pone.0185958>.
- [15] Y.S. Kim, A.P. Singh, Micromorphological characteristics of wood biodegradation in wet environments: a review, *IAWA J.* 21 (2000) 135–155. <https://doi.org/10.1163/22941932-90000241>.
- [16] A. Jauneau, M. Quentin, A. Driouich, Micro-heterogeneity of pectins and calcium distribution in the epidermal and cortical parenchyma cell walls of flax hypocotyl, *Protoplasma.* 198 (1997) 9–19. <https://doi.org/10.1007/BF01282126>.
- [17] P. Miller, W. Lanier, S. Brandt, Using Growing Degree Days to Predict Plant Stages, *Montguide.* (2018). <https://landresources.montana.edu/soilfertility/documents/PDF/pub/GDDPlantStagesMT200103AG.pdf>.
- [18] C. Goudenhooft, Multi-scale characterization of flax stems and fibers: structure and mechanical performances, *génie des matériaux*, Université de Bretagne Sud, 2018.
- [19] C. Goudenhooft, A. Bourmaud, C. Baley, Flax (*Linum usitatissimum* L.) Fibers for Composite Reinforcement: Exploring the Link Between Plant Growth, Cell Walls Development, and Fiber Properties, *Front. Plant Sci.* 10 (2019) 411. <https://doi.org/10.3389/fpls.2019.00411>.

- [20] ARVALIS Institut du végétal, Lin fibre résultats et préconisation, ARVALIS, Paris, France, 2016.
- [21] A. Moudood, A. Rahman, A. Öchsner, M. Islam, G. Francucci, Flax fiber and its composites: An overview of water and moisture absorption impact on their performance, *J. Reinf. Plast. Compos.* 38 (2019) 323–339. <https://doi.org/10.1177/0731684418818893>.
- [22] T.A. Gorshkova, V.V. Sal'nikov, S.B. Chemikosova, M.V. Ageeva, N.V. Pavlencheva, J.E.G. van Dam, The snap point: a transition point in *Linum usitatissimum* bast fiber development, *Ind. Crops Prod.* 18 (2003) 213–221. [https://doi.org/10.1016/S0926-6690\(03\)00043-8](https://doi.org/10.1016/S0926-6690(03)00043-8).
- [23] O. Gorshkov, T. Chernova, N. Mokshina, N. Gogoleva, D. Suslov, A. Tkachenko, T. Gorshkova, Intrusive Growth of Phloem Fibers in Flax Stem: Integrated Analysis of miRNA and mRNA Expression Profiles, *Plants.* 8 (2019) 47. <https://doi.org/10.3390/plants8020047>.
- [24] D. Sertse, F.M. You, S. Ravichandran, S. Cloutier, The Complex Genetic Architecture of Early Root and Shoot Traits in Flax Revealed by Genome-Wide Association Analyses, *Front. Plant. Sci.* 10 (2019). <https://doi.org/10.3389/fpls.2019.01483>.
- [25] B.J. Soto-Cerda, S. Cloutier, H.A. Gajardo, G. Aravena, R. Quian, Identifying drought-resilient flax genotypes and related-candidate genes based on stress indices, root traits and selective sweep, *Euphytica.* 215 (2019) 41. <https://doi.org/10.1007/s10681-019-2362-0>.
- [26] A. Bourmaud, J. Beaugrand, D.U. Shah, V. Placet, C. Baley, Towards the design of high-performance plant fibre composites, *Prog. Mater. Sci.* 97 (2018) 347–408. <https://doi.org/10.1016/j.pmatsci.2018.05.005>.
- [27] K. Rogers, The cell, Britannica Educational Pub. in association with Rosen Educational Services, New York, NY, 2011: pp.55-60.
- [28] H.L. Bos, A.M. Donald, In situ ESEM study of the deformation of elementary flax fibres, *J. Mater. Sci.* 34 (1999) 3029–3034.
- [29] J.L. Thomason, J. Carruthers, J. Kelly, G. Johnson, Fibre cross-section determination and variability in sisal and flax and its effects on fibre performance characterisation, *Compos. Sci. Technol.* 71 (2011) 1008–1015. <https://doi.org/10.1016/j.compscitech.2011.03.007>.
- [30] C. Goudenhooft, D. Siniscalco, O. Arnould, A. Bourmaud, O. Sire, T. Gorshkova, C. Baley, Investigation of the Mechanical Properties of Flax Cell Walls during Plant Development: The Relation between Performance and Cell Wall Structure, *Fibers.* 6 (2018) 6. <https://doi.org/10.3390/fib6010006>.
- [31] I. Pillin, A. Kervoelen, A. Bourmaud, J. Goimard, N. Montrelay, C. Baley, Could oleaginous flax fibers be used as reinforcement for polymers?, *Ind. Crops Prod.* 34 (2011) 1556–1563. <https://doi.org/10.1016/j.indcrop.2011.05.016>.
- [32] C. Baley, C. Goudenhooft, M. Gibaud, A. Bourmaud, Flax stems: from a specific architecture to an instructive model for bioinspired composite structures, *Bioinspir. Biomim.* 13 (2018) 026007. <https://doi.org/10.1088/1748-3190/aaa6b7>.
- [33] C. Baley, A. Bourmaud, Average tensile properties of French elementary flax fibers, *Mater. Lett.* 122 (2014) 159–161. <https://doi.org/10.1016/j.matlet.2014.02.030>.
- [34] M.V. Ageeva, B. Petrovská, H. Kieft, V.V. Sal'nikov, A.V. Snegireva, J.E.G. van Dam, W.L.H. van Veenendaal, A.M.C. Emons, T.A. Gorshkova, A.A.M. van Lammeren, Intrusive growth of flax phloem fibers is of intercalary type, *Planta.* 222 (2005) 565–574. <https://doi.org/10.1007/s00425-005-1536-2>.
- [35] C. Morvan, C. Andème-Onzighi, R. Girault, D.S. Himmelsbach, A. Driouich, D.E. Akin, Building flax fibres: more than one brick in the walls, *Plant Physiol. Biochem.* 41 (2003) 935–944. <https://doi.org/10.1016/j.plaphy.2003.07.001>.
- [36] P.A. Roelofsen, Contradictory Data on Spiral Structures in the Secondary Cell Wall of Fibers of Flax, Hemp, and Ramie, *Text. Res. J.* 21 (1951) 412–418. <https://doi.org/10.1177/004051755102100605>.
- [37] E.J. Mellerowicz, T.A. Gorshkova, Tensional stress generation in gelatinous fibres: a review and possible mechanism based on cell-wall structure and composition, *J. Exp. Bot.* 63 (2012) 551–565. <https://doi.org/10.1093/jxb/err339>.
- [38] T. Gorshkova, N. Brutch, B. Chabbert, M. Deyholos, T. Hayashi, S. Lev-Yadun, E.J. Mellerowicz, C. Morvan, G. Neutelings, G. Pilate, Plant Fiber Formation: State of the Art, Recent and Expected Progress, and Open Questions, *Crit. Rev. Plant. Sci.* 31 (2012) 201–228. <https://doi.org/10.1080/07352689.2011.616096>.

- [39] T. Gorshkova, T. Chernova, N. Mokshina, M. Ageeva, P. Mikshina, Plant ‘muscles’: fibers with a tertiary cell wall, *New Phytol.* 218 (2018) 66–72. <https://doi.org/10.1111/nph.14997>.
- [40] A. Petrova, L. Kozlova, O. Gorshkov, A. Nazipova, M. Ageeva, T. Gorshkova, Cell Wall Layer Induced in Xylem Fibers of Flax Upon Gravistimulation Is Similar to Constitutively Formed Cell Walls of Bast Fibers, *Front. Plant. Sci.* 12 (2021) 485. <https://doi.org/10.3389/fpls.2021.660375>.
- [41] A.P. Manian, M. Cordin, T. Pham, Extraction of cellulose fibers from flax and hemp: a review, *Cellulose.* 28 (2021) 8275–8294. <https://doi.org/10.1007/s10570-021-04051-x>.
- [42] P. Mikshina, T. Chernova, S. Chemikosova, N. Ibragimova, N. Mokshina, T. Gorshkova, Cellulosic Fibers: Role of Matrix Polysaccharides in Structure and Function, in: T.G.M. Van De Ven (Ed.), *Cellulose - Fundamental Aspects*, IntechOpen, 2013: pp. 91–112.
- [43] O. Arnould, D. Siniscalco, A. Bourmaud, A. Le Duigou, C. Baley, Better insight into the nano-mechanical properties of flax fibre cell walls, *Ind. Crops Prod.* 97 (2017) 224–228. <https://doi.org/10.1016/j.indcrop.2016.12.020>.
- [44] E. Richely, S. Durand, A. Melelli, A. Kao, A. Magueresse, H. Dhakal, T. Gorshkova, F. Callebert, A. Bourmaud, J. Beaugrand, S. Guessasma, Novel Insight into the Intricate Shape of Flax Fibre Lumen, *Fibers.* 9 (2021) 24. <https://doi.org/10.3390/fib9040024>.
- [45] M.V. Ageeva, T.E. Chernova, T.A. Gorshkova, Processes of protoplast senescence and death in flax fibers: An ultrastructural analysis, *Russ. J. Dev. Biol.* 43 (2012) 94–100. <https://doi.org/10.1134/S1062360412020026>.
- [46] I. His, C. Andème-Onzighi, C. Morvan, A. Driouich, Microscopic Studies on Mature Flax Fibers Embedded in LR White: Immunogold Localization of Cell Wall Matrix Polysaccharides, *J. Histochem. Cytochem.* 49 (2001) 1525–1535. <https://doi.org/10.1177/002215540104901206>.
- [47] D. Jones, G.O. Ormondroyd, S.F. Curling, C.-M. Popescu, M.-C. Popescu, Chemical compositions of natural fibres, in: M. Fa, F. Fu (Eds.), *Advanced High Strength Natural Fibre Composites in Construction*, Woodhead Publishing., 2017: pp. 121–124. <https://doi.org/10.1016/C2014-0-03942-1>.
- [48] S. Alix, L. Lebrun, S. Marais, E. Philippe, A. Bourmaud, C. Baley, C. Morvan, Pectinase treatments on technical fibres of flax: Effects on water sorption and mechanical properties, *Carbohydr. Polym.* 87 (2012) 177–185. <https://doi.org/10.1016/j.carbpol.2011.07.035>.
- [49] J. Biagiotti, D. Puglia, J.M. Kenny, A Review on Natural Fibre-Based Composites-Part I: Structure, Processing and Properties of Vegetable Fibres, *J. Nat. Fibers.* 1 (2004) 37–68. https://doi.org/10.1300/J395v01n02_04.
- [50] J.M. Van Hazendonk, E.J.M. Reinerik, P. de Waard, J.E.G. van Dam, Structural analysis of acetylated hemicellulose polysaccharides from fibre flax (*Linum usitatissimum* L.), *Carbohydr. Res.* 291 (1996) 141–154. [https://doi.org/10.1016/S0008-6215\(96\)00160-7](https://doi.org/10.1016/S0008-6215(96)00160-7).
- [51] D. Crônier, B. Monties, B. Chabbert, Structure and Chemical Composition of Bast Fibers Isolated from Developing Hemp Stem, *J. Agric. Food Chem.* 53 (2005) 8279–8289. <https://doi.org/10.1021/jf051253k>.
- [52] K. Esau, *Plant anatomy*, Wiley, New York, 1953.
- [53] E. Gümüşkaya, M. Usta, M. Balaban, Carbohydrate components and crystalline structure of organosolv hemp (*Cannabis sativa* L.) bast fibers pulp, *Bioresour. Technol.* 98 (2007) 491–497. <https://doi.org/10.1016/j.biortech.2006.02.031>.
- [54] L. Marrot, A. Lefeuvre, B. Pontoire, A. Bourmaud, C. Baley, Analysis of the hemp fiber mechanical properties and their scattering (Fedora 17), *Ind. Crops Prod.* 51 (2013) 317–327. <https://doi.org/10.1016/j.indcrop.2013.09.026>.
- [55] F. Khan, S.R. Ahmad, Chemical modification and spectroscopic analysis of jute fibre, *Polym. Degrad. Stab.* 52 (1996) 335–340. [https://doi.org/10.1016/0141-3910\(95\)00240-5](https://doi.org/10.1016/0141-3910(95)00240-5).
- [56] A. Roy, S. Chakraborty, S.P. Kundu, R.K. Basak, S. Basu Majumder, B. Adhikari, Improvement in mechanical properties of jute fibres through mild alkali treatment as demonstrated by utilisation of the Weibull distribution model, *Bioresour. Technol.* 107 (2012) 222–228. <https://doi.org/10.1016/j.biortech.2011.11.073>.
- [57] G. Chinga-Carrasco, Cellulose fibres, nanofibrils and microfibrils: The morphological sequence of MFC components from a plant physiology and fibre technology point of view, *Nanoscale Res. Lett.* 6 (2011) 417. <https://doi.org/10.1186/1556-276X-6-417>.

- [58] L. Donaldson, Microfibril Angle: Measurement, Variation and Relationships – A Review, *IAWA J.* 29 (2008) 345–386. <https://doi.org/10.1163/22941932-90000192>.
- [59] A. Stamboulis, C.A. Baillie, T. Peijs, Effects of environmental conditions on mechanical and physical properties of flax fibers, *Compos. Part A Appl. Sci. Manuf.* 32 (2001) 1105–1115. [https://doi.org/10.1016/S1359-835X\(01\)00032-X](https://doi.org/10.1016/S1359-835X(01)00032-X)
- [60] M. John, S. Thomas, Biofibres and biocomposites, *Carbohydr. Polym.* 71 (2008) 343–364. <https://doi.org/10.1016/j.carbpol.2007.05.040>.
- [61] B. Madsen, M. Aslan, H. Lilholt, Fractographic observations of the microstructural characteristics of flax fibre composites, *Compos. Sci. Technol.* 123 (2016) 151–162. <https://doi.org/10.1016/j.compscitech.2015.12.003>.
- [62] C.J. Kennedy, A. Štuncová, M.C. Jarvis, T.J. Wess, Hydration effects on spacing of primary-wall cellulose microfibrils: a small angle X-ray scattering study, *Cellulose.* 14 (2007) 401–408. <https://doi.org/10.1007/s10570-007-9129-9>.
- [63] C. Rihouey, F. Paynel, T. Gorshkova, C. Morvan, Flax fibers: assessing the non-cellulosic polysaccharides and an approach to supramolecular design of the cell wall, *Cellulose.* 24 (2017) 1985–2001. <https://doi.org/10.1007/s10570-017-1246-5>.
- [64] J.-C. Roland, M. Mosiniak, D. Roland, Dynamique du positionnement de la cellulose dans les parois des fibres textiles du lin (*Linum usitatissimum*), *Acta Bot. Gall.* 142 (1995) 463–484. <https://doi.org/10.1080/12538078.1995.10515271>.
- [65] A. Bourmaud, D. Siniscalco, L. Foucat, C. Goudenhooff, X. Falourd, B. Pontoire, O. Arnould, J. Beaugrand, C. Baley, Evolution of flax cell wall ultrastructure and mechanical properties during the retting step, *Carbohydr. Polym.* 206 (2019) 48–56. <https://doi.org/10.1016/j.carbpol.2018.10.065>.
- [66] C. Wang, N. Wang, S. Liu, L.-P. Choo-Simth, H. Zhang, Z. Zhi, Investigation of Microfibril Angle of Flax Fibers Using X-Ray Diffraction and Scanning Electron Microscopy, *J. Nat. Fibers.* (2018) 1–10. <https://doi.org/10.1080/15440478.2018.1546639>.
- [67] A. Bourmaud, C. Morvan, A. Bouali, V. Placet, P. Perré, C. Baley, Relationships between micro-fibrillar angle, mechanical properties and biochemical composition of flax fibers, *Ind. Crops Prod.* 44 (2013) 343–351. <https://doi.org/10.1016/j.indcrop.2012.11.031>.
- [68] M.P. Ansell, L.Y. Mwaikambo, The structure of cotton and other plant fibres, in: S.J. Eichhorn, J.W.S. Hearle, M. Jaffe, T. Kikutani (Eds.), *Handbook of Textile Fibre Structure*, Woodhead Publishing, 2009: pp. 62–94. <https://doi.org/10.1533/9781845697310.1.62>.
- [69] M.S. Zamil, A. Geitmann, The middle lamella—more than a glue, *Phys. Biol.* 14 (2017) 015004. <https://doi.org/10.1088/1478-3975/aa5ba5>.
- [70] E. Richely, A. Bourmaud, V. Placet, S. Guessasma, J. Beaugrand, A critical review of the ultrastructure, mechanics and modelling of flax fibres and their defects, *Prog. Mater. Sci.* (2021) 100851. <https://doi.org/10.1016/j.pmatsci.2021.100851>.
- [71] A. Monti, A. El Mahi, Z. Jendli, L. Guillaumat, Mechanical behaviour and damage mechanisms analysis of a flax-fibre reinforced composite by acoustic emission, *Compos. Part A Appl. Sci. Manuf.* 90 (2016) 100–110. <https://doi.org/10.1016/j.compositesa.2016.07.002>.
- [72] S. Guessasma, J. Beaugrand, Damage Kinetics at the Sub-micrometric Scale in Bast Fibers Using Finite Element Simulation and High-Resolution X-Ray Micro-Tomography, *Front. Plant. Sci.* 10 (2019) 194. <https://doi.org/10.3389/fpls.2019.00194>.
- [73] M. Hughes, G. Sèbe, J. Hague, C. Hill, M. Spear, L. Mott, An investigation into the effects of micro-compressive defects on interphase behaviour in hemp-epoxy composites using half-fringe photoelasticity, *Compos. Interfaces.* 7 (2000) 13–29. <https://doi.org/10.1163/156855400300183551>.
- [74] L.G. Thygesen, N. Gierlinger, The molecular structure within dislocations in *Cannabis sativa* fibres studied by polarised Raman microspectroscopy, *J. Struct. Biol.* 182 (2013) 219–225. <https://doi.org/10.1016/j.jsb.2013.03.010>.
- [75] H. Zhang, T. Sui, L.G. Thygesen, P. O’Brien, A.M. Korsunsky, Multi-modal Microscopy Characterisation of Nodal Markings in Flax Fibre, in: *Proceedings of the World Congress on Engineering (WCE)*, London, U.K., 2015.

- [76] L.G. Thygesen, B.J. Hidayat, K.S. Johansen, C. Felby, Role of supramolecular cellulose structures in enzymatic hydrolysis of plant cell walls, *J. Ind. Microbiol. Biotechnol.* 38 (2011) 975–83. <https://doi.org/10.1007/s10295-010-0870-y>.
- [77] G. Davies, D. Bruce, Effect of environmental relative humidity and damage on the tensile properties of flax and nettle fibers, *Text. Res. J.* 68 (1998) 623–629. <https://doi.org/10.1177/004051759806800901>.
- [78] H. Bos, A. Van Den Oever, O. Peters, Tensile and compressive properties of flax fibres for natural fibre reinforced composites, *J. Mater. Sci.* 37 (2002) 1683–1692. <https://doi.org/10.1023/A:1014925621252>.
- [79] J. Andersons, E. Spārņiņš, E. Poriķe, Strength and Damage of Elementary Flax Fibers Extracted from Tow and Long Line Flax, *J. Compos. Mater.* 43 (2009) 2653–2664. <https://doi.org/10.1177/0021998309345035>.
- [80] J. Sliseris, L. Yan, B. Kasal, Numerical modelling of flax short fibre reinforced and flax fibre fabric reinforced polymer composites, *Compos. B. Eng.* 89 (2016) 143–154. <https://doi.org/10.1016/j.compositesb.2015.11.038>.
- [81] L.G. Thygesen, Dislocations in plant fibres and in Turin Shroud fibres, in: ENEA, Frascati, Italy, 2010: pp. 4–6.
- [82] L.K. Herrera, A. Justo, A. Duran, M.C.J. Haro, M.L. Franquelo, J.L. Perez Rodríguez, Identification of cellulose fibres belonging to Spanish cultural heritage using synchrotron high resolution X-ray diffraction, *Appl. Phys. A: Mater. Sci. Process.* 99 (2010) 391–398. <https://doi.org/10.1007/s00339-010-5626-z>.
- [83] C. Baley, Analysis of the flax fibres tensile behaviour and analysis of the tensile stiffness increase, *Compos. Part A Appl. Sci. Manuf.* 33 (2002) 939–948. [https://doi.org/10.1016/S1359-835X\(02\)00040-4](https://doi.org/10.1016/S1359-835X(02)00040-4).
- [84] S.K. Ramamoorthy, D. Åkesson, R. Rajan, A.P. Periyasamy, M. Skrifvars, Mechanical performance of biofibers and their corresponding composites, in: M. Jawaid, M. Thariq, N. Saba (Eds.), *Mechanical and Physical Testing of Biocomposites, Fibre-Reinforced Composites and Hybrid Composites*, Woodhead Publishing, 2019: pp. 259–292. <https://doi.org/10.1016/B978-0-08-102292-4.00014-X>.
- [85] M. Hughes, J. Carpenter, C. Hill, Deformation and fracture behaviour of flax fibre reinforced thermosetting polymer matrix composites, *J. Mater. Sci.* 42 (2007) 2499–2511. <https://doi.org/10.1007/s10853-006-1027-2>.
- [86] P. Wambua, J. Ivens, I. Verpoest, Natural fibres: can they replace glass in fibre reinforced plastics?, *Compos. Sci. Technol.* 63 (2003) 1259–1264. [https://doi.org/10.1016/S0266-3538\(03\)00096-4](https://doi.org/10.1016/S0266-3538(03)00096-4).
- [87] N. Lu, R.H. Swan, I. Ferguson, Composition, structure, and mechanical properties of hemp fiber reinforced composite with recycled high-density polyethylene matrix, *J. Compos. Mater.* 46 (2012) 1915–1924. <https://doi.org/10.1177/0021998311427778>.
- [88] A. Céline, S. Fréour, F. Jacquemin, P. Casari, The hygroscopic behavior of plant fibers: a review, *Front. Chem.* 1 (2014). <https://doi.org/10.3389/fchem.2013.00043>.
- [89] C. Goudenhooft, A. Bourmaud, C. Baley, Study of plant gravitropic response: Exploring the influence of lodging and recovery on the mechanical performances of flax fibers, *Ind. Crops Prod.* 128 (2019) 235–238. <https://doi.org/10.1016/j.indcrop.2018.11.024>.
- [90] C. Baley, M. Gomina, J. Breard, A. Bourmaud, P. Davies, Variability of mechanical properties of flax fibres for composite reinforcement. A review, *Ind. Crops Prod.* 145 (2020) 111984. <https://doi.org/10.1016/j.indcrop.2019.111984>.
- [91] C.A. Cullis, Flax, in: C. Kole (Ed.), *Oilseeds*, Springer Berlin Heidelberg, Berlin, Heidelberg, 2007: pp. 275–295. https://doi.org/10.1007/978-3-540-34388-2_8.
- [92] R.G. Allaby, G.W. Peterson, D.A. Merriwether, Y.-B. Fu, Evidence of the domestication history of flax (*Linum usitatissimum* L.) from genetic diversity of the sad2 locus, *Theor. Appl. Genet.* 112 (2005) 58–65. <https://doi.org/10.1007/s00122-005-0103-3>.
- [93] H. Helbaek, Joint efforts by botanists and archeologistsilluminate the obscure history of plant domestication., *Science.* 130 (1959) 365–372.
- [94] E. Weiss, D. Zohary, The Neolithic Southwest Asian Founder Crops: Their Biology and Archaeobotany, *Curr. Anthropol.* 52 (2011) S237–S254. <https://doi.org/10.1086/658367>.

- [95] E. Kvavadze, O. Bar-Yosef, A. Belfer-Cohen, E. Boaretto, N. Jakeli, Z. Matskevich, T. Meshveliani, 30,000-Year-Old Wild Flax Fibers, *Science*. 325 (2009) 1359–1359. <https://doi.org/10.1126/science.1175404>.
- [96] C. Bergfjord, S. Karg, A. Rast-Eicher, M.-L. Nosch, U. Mannering, R.G. Allaby, B.M. Murphy, B. Holst, Comment on “30,000-Year-Old Wild Flax Fibers,” *Science*. 328 (2010) 1634–1634. <https://doi.org/10.1126/science.1186345>.
- [97] A. Diederichsen, K. Hammer, Variation of cultivated flax (*Linum usitatissimum* L. subsp. *usitatissimum*) and its wild progenitor pale flax (subsp. *angustifolium* (Huds.) Thell.), *Genet. Resour. Crop Evol.* 42 (1995) 263–272. <https://doi.org/10.1007/BF02431261>.
- [98] R. Gutaker, M. Zaidem, Y.-B. Fu (符永碧), A. Diederichsen, O. Smith, R. Ware, R. Allaby, Flax latitudinal adaptation at *LuTFL1* altered architecture and promoted fiber production, *Sci. Rep.* 9 (2019) 976. <https://doi.org/10.1038/s41598-018-37086-5>.
- [99] D.S. Desta, Genomics of drought tolerance in flax (*Linum usitatissimum* L.), Biology, University of Ottawa, 2019.
- [100] S. Karg, New research on the cultural history of the useful plant *Linum usitatissimum* L. (flax), a resource for food and textiles for 8,000 years, *Veg. Hist. Archaeobotany*. 20 (2011) 507–508. <https://doi.org/10.1007/s00334-011-0326-y>.
- [101] S. Harris, Flax fibre: Innovation and Change in the Early Neolithic A Technological and Material Perspective, in: *Textile Society of America 2014 Biennial Symposium Proceedings: New Directions: Examining the Past, Creating the Future*, LA, California, 2014: p. 913.
- [102] S. Colledge, J. Conolly, eds., *The Origins and Spread of Domestic Plants in Southwest Asia and Europe*, Left Coast Press, Walnut Creek, CA, 2017. <https://doi.org/10.4324/9781315417615>.
- [103] O.V. Muravenko, V.A. Lemesh, T.E. Samatadze, A.V. Amosova, Z.E. Grushetskaya, K.V. Popov, O.Y. Semenova, L.V. Khotyuleva, A.V. Zelenin, Genome comparisons with chromosomal and molecular markers for three closely related flax species and their hybrid, *Russ. J. Genet.* 39 (2003) 414–421. <https://doi.org/10.1023/A:1023309831454>.
- [104] A. Kreuz, Archaeobotanical perspectives on the beginning of agriculture north of the Alps, in: In Colledge S, Conolly J (Eds) *The Origins and Spread of Domestic Plants in Southwest Asia and Europe*, Left Coast Press, 2007: pp. 259–294.
- [105] U. Leuzinger, A. Rast-Eicher, Flax processing in the Neolithic and Bronze Age pile-dwelling settlements of eastern Switzerland, *Veg. Hist. Archaeobotany*. 20 (2011) 535–542. <https://doi.org/10.1007/s00334-011-0286-2>.
- [106] S.M. Valamoti, Flax in Neolithic and Bronze Age Greece: archaeobotanical evidence, *Veget. Hist. Archaeobot.* 20 (2011) 549–560. <https://doi.org/10.1007/s00334-011-0304-4>.
- [107] C. Herbig, U. Maier, Flax for oil or fibre? Morphometric analysis of flax seeds and new aspects of flax cultivation in Late Neolithic wetland settlements in southwest Germany, *Veget. Hist. Archaeobot.* 20 (2011) 527–533.
- [108] R. Grilletto, *Il mistero delle mummie: dall’antichità ai nostri giorni attraverso il tempo e lo spazio*, 1st edition, Newton & Compton Editori, Rome, 2005.
- [109] A. Ascenzi, P. Bianco, G. CeccariniZ, M. FomaseriJ, G. Graziani, L. Ciuffarella, H. Granger-Taylor, The roman mummy of Grottarossa, in: K. Spindler, H. Wilfing, E. Rastbichler-Zissernig, D. ZurNedden, H. Nothdurfter (Eds.), *Human Mummies. The Man in the Ice*, Springer, Vienna, 1996: pp. 205–217.
- [110] J. McCorriston, Textile Extensification, Alienation, and Social Stratification in Ancient Mesopotamia, *Curr. Anthropol.* 38 (1997) 517–535. <https://doi.org/10.1086/204643>.
- [111] S. Riehl, Variability in ancient Near Eastern environmental and agricultural development, *J. Arid Environ.* 86 (2012) 113–121. <https://doi.org/10.1016/j.jaridenv.2011.09.014>.
- [112] B. Ejstrud, S. Andresen, A. Appel, S. Gjerlevsen, B. Thomsen, From flax to linen: experiments with flax at Ribe Viking Centre, Ribe Viking Centre ; University of Southern Denmark, Esbjerg, 2011.
- [113] S.T. Andresen, S. Karg, Retting pits for textile fibre plants at Danish prehistoric sites dated between 800 b.c. and a.d. 1050, *Veget. Hist. Archaeobot.* 20 (2011) 517–526. <https://doi.org/10.1007/s00334-011-0324-0>.

- [114] K. Viklund, Flax in Sweden: the archaeobotanical, archaeological and historical evidence, *Veget. Hist. Archaeobot.* 20 (2011) 509–515. <https://doi.org/10.1007/s00334-011-0325-z>.
- [115] E. Andersson Strand, The textile chaîne opératoire: Using a multidisciplinary approach to textile archaeology with a focus on the Ancient Near East, *Paleo.* 38 (2012) 21–40. <https://doi.org/10.3406/paleo.2012.5456>.
- [116] L.J. Musselman, A dictionary of Bible plants, 1st edition, Cambridge University Press, New York, 2012: pp. 57–58, 101–103.
- [117] D. Nicholas, *Medieval Flanders*, 2nd edition, Routledge, 1992: pp. 4, 38, 263.
- [118] E.S. Dixon, *Flax and Hemp: Their Culture and Manipulation*, G. Routledge, 1854: pp. 2–10.
- [119] P.V. Ulrich, From Fustian to Merino: The Rise of Textiles Using Cotton before and after the Gin, *Agric. Hist.* 68 (1994) 219–231.
- [120] F. A. Wood, G. A. F. Roberts, Natural Fibers and Dyes, in: G.T. Prance, M. Nesbitt (Eds.), *The cultural history of plants*, Routledge, New York, 2005: pp. 289–292.
- [121] A.L. Huang, Hanseatic Textile Production in 15th Century Long Distance Trade, in: *Textiles and the Medieval Economy: A. Ling Huang, C. Jahnke (Eds.), Production, Trade, and Consumption of Textiles, 8th_16th Centuries*, Oxbow Books, United Kingdom, 2014: pp. 204–214.
- [122] H.M. Sherman, From Flax to Linen in the Medieval Rus Lands, in: R. Netherton, G. R. Owen-Crocker (Eds.), *Medieval Clothing and Textiles*, 2008: pp. 1–20.
- [123] P.H. Erichsen, *Artisans, Objects and Everyday Life in Renaissance Italy: The Material Culture of the Middling Class*, Amsterdam University Press, NL Amsterdam, 2020. <https://doi.org/10.5117/9789463722629>.
- [124] J. Miller, *Urban Societies in East-Central Europe, 1500–1700*, Routledge, 2016: pp. 224–228.
- [125] P. Pourchasse, The Flaxseed trade between Courland and Brittany in the eighteenth century, in: G. Favero, M.-W. Serruys, M. Sugiura (Eds.), *The Urban Logistic Network: Cities, Transport and Distribution in Europe from the Middle Ages to Modern Times*, Springer International Publishing, Cham, 2019: pp. 193–207. https://doi.org/10.1007/978-3-030-27599-0_10.
- [126] W.R. Scott, The King's and Queen's Corporation for the Linen Manufacture in Ireland, *J. R. Soc. Antiq. Irel.*, Fifth Series. 31 (1901) 371–378.
- [127] W. Colquhoun, The Story of Linen, *Occup. Med.* 11 (1961) 177–178. <https://doi.org/10.1093/occmed/11.1.177>.
- [128] A. Bourmaud, L. Nuez, C. Goudenhoof, C. Baley, Multi-scale mechanical characterization of flax fibres for the reinforcement of composite materials, in: R.M. Kozłowski, M. Mackiewicz-Talarczyk (Eds.), *Handbook of Natural Fibres*, 2nd edition, Woodhead Publishing, 2020: pp. 205–226. <https://doi.org/10.1016/B978-0-12-818782-1.00006-7>.
- [129] R. Davis, English Foreign Trade, 1660–1700, *The Economic History Review New Series.* 7 (1954) 163–164.
- [130] D. Diderot, J.L.R. D'Alembert, *Encyclopédie ou Dictionnaire raisonné des sciences, des arts et des métiers. Tome neuvième, Ju-Mam / par une société de gens de lettres*, Bibliothèque nationale de France, 1751: pp.547–553 <https://gallica.bnf.fr/ark:/12148/bpt6k50541z> (accessed August 13, 2021).
- [131] P. Ollerenshaw, Textile Business in Europe During the First World War: The Linen Industry, 1914–18, *Bus. Hist.* 41 (1999) 63–87. <https://doi.org/10.1080/00076799900000202>.
- [132] R.M. Kozłowski, M. Mackiewicz-Talarczyk, K. Wielgusz, M. Praczyk, A.M. Allam, Bast fibres, in: R.M. Kozłowski, M. Mackiewicz-Talarczyk (Eds.), *Handbook of Natural Fibres*, Woodhead Publishing, 2020: pp. 93–162. <https://doi.org/10.1016/B978-0-12-818398-4.00006-2>.
- [133] N.F. Miller, P. Jones, H. Pittman, Sign and Image: Representations of Plants on the Warka Vase of Early Mesopotamia, in: N. F. Miller, H. Pittman, P. Jones (Eds.), *Origini*, Gangemi Editore international, Rome, 2016: pp. 53–73.
- [134] D. Bedigian, J.R. Harlan, Evidence for cultivation of sesame in the ancient world, *Econ. Bot.* 40 (1986) 137–154. <https://doi.org/10.1007/BF02859136>.
- [135] E. Soriga, A Diachronic View on Fulling Technology in the Mediterranean and the Ancient Near East: Tools, Raw Materials and Natural Resources for the Finishing of Textiles, in : S. Gaspa, C. Miche, M. L.

- Nosch (Eds.), *Textile Terminologies from the Orient to the Mediterranean and Europe, 1000 BC to 1000 AD*, Zea Books, Lincoln, NE, 2017, pp. 24–46. <https://doi.org/10.13014/K2CJ8BNP>.
- [136] E.C. Semple, *Ancient Mediterranean Agriculture: Part I*, *Agric. Hist.* 2 (1928) 61–98.
- [137] B. Bell, *Climate and the History of Egypt: The Middle Kingdom*, *Am. J. Archaeol.* 79 (1975) 223. <https://doi.org/10.2307/503481>.
- [138] W. Schenkel, *Les systèmes d'irrigation dans l'Égypte ancienne et leurs genèse*, *Archéo-Nil*. 4 (1994) 27–35.
- [139] G. Vogeslang-Eastwood, *Textiles*, in: P.T. Nicholson, I. Shaw (Eds.), *Ancient Egyptian Materials and Technology*, Cambridge University Press, 2000: pp. 268–297.
- [140] M. Gleba, S. Harris, *The first plant bast fibre technology: identifying splicing in archaeological textiles*, *Archaeol. Anthropol. Sci.* 11 (2019) 2329–2346. <https://doi.org/10.1007/s12520-018-0677-8>.
- [141] D.L. Carroll, *An Etruscan Textile in Newark*, *Am. J. Archaeol.* 77 (1973) 334–336. <https://doi.org/10.2307/503450>.
- [142] R.T.J. Cappers, *The reconstruction of agricultural practices in Ancient Egypt: an ethnoarchaeobotanical approach*, *Palaeohistoria*. 47/48 (2005) 429–446.
- [143] V.L. Emery, *Mud-Brick Architecture*, in: W. Willeke (Ed.), *UCLA Encyclopedia of Egyptology*, Los Angeles, 2011: pp. 1–9.
- [144] S. Landi, R.M. Hall, *The Discovery and Conservation of an Ancient Egyptian Linen Tunic*, *Stud. Conserv.* 24 (1979) 141–152. <https://doi.org/10.1179/sic.1979.017>.
- [145] E. Black, D. Samuel, *What were sails made of?*, *The Mariner's Mirror*. 77 (1991) 217–226. <https://doi.org/10.1080/00253359.1991.10656354>.
- [146] R.B. Partridge, *Transport, Pharaonic Egypt*, in: R.S. Bagnall, K. Brodersen, C.B. Champion, A. Erskine, S.R. Huebner (Eds.), *The Encyclopedia of Ancient History*, John Wiley & Sons, Inc., Hoboken, NJ, USA, 2012: pp. 6826–6829. <https://doi.org/10.1002/9781444338386.wbeah15402>.
- [147] J. Rougé, *E3 — La momie contenait-elle les fragments d'une voile ?*, *Nouvelles archives du Muséum d'histoire naturelle de Lyon*. 25 (1987) 91–96.
- [148] Sh. Abd El Aal, *Characterization and examination of pigments, grounds and media from ancient Egyptian cartonnage*, *Egypt. J. Archeol. Restor. Stud.* 4 (2018) 35–46. <https://doi.org/10.21608/ejars.2018.7272>.
- [149] L. Smith, *The history of contraception*, in: P. Briggs, G. Kovacs, J. Guillebaud (Eds.), *Contraception: A Casebook from Menarche to Menopause*, Cambridge University Press, 2013: pp. 18–25.
- [150] U. Maier, H. Schlichtherle, *Flax cultivation and textile production in Neolithic wetland settlements on Lake Constance and in Upper Swabia (south-west Germany)*, *Veget. Hist. Archaeobot.* 20 (2011) 567–578. <https://doi.org/10.1007/s00334-011-0300-8>.
- [151] M. Gleba, *Linen production in pre-roman and roman Italy*, in: C. Alfaro Giner, J.P. Wild, B. Costa (Eds.), *PURPUREAE VESTES*, Universitat de València, Ibiza, 2002: pp. 29–39.
- [152] E.C. Semple, *Ancient Mediterranean Agriculture: Part II. Manuring and Seed Selection*, *Agric. Hist.* 2 (1928) 129–156.
- [153] M. Bradley, *'It all comes out in the wash': Looking harder at the Roman fullonica*, *Journal of Roman Archaeology*. 15 (2002) 20–44.
- [154] M.S. Busana, A.R. Tricomi, *Textile Archaeology in the Roman Venetia (Italy)*, in: *Textiles, Basketry and Dyes in the Ancient Mediterranean World: Proceedings of the Vth International Symposium on Textiles and Dyes in the Ancient Mediterranean World*, Universitat de València, 2014: pp. 111–118.
- [155] Pierpont Morgan Library, *Book of hours (MS M.399) -Da Costa hours, (1515)*. <http://corsair.themorgan.org/vwebv/holdingsInfo?bibId=112362>.
- [156] Pierpont Morgan Library, *Book of hours (MS M.1175), (1525)*. <http://corsair.themorgan.org/vwebv/holdingsInfo?bibId=308001>.
- [157] K. Viklund, *Linet i Sverige*, *Sven. Bot. Tidskr.* 106 (2012) 3–4.
- [158] A.W. Engelhardt, *The Fiber Year 2020 – Deceleration along the textile chain*, *International Fiber Journal*. (2020). <https://fiberjournal.com/the-fiber-year-2020-deceleration-along-the-textile-chain/> (accessed August 16, 2021).

- [159] Crops and livestock products: flax fibre and tow, FAOSTAT. (2021). www.fao.org (accessed August 16, 2021).
- [160] ARVALIS Institut du végétal, Lin fibre: résultats et préconisations, ARVALIS, Paris, France, 2020.
- [161] M. Musialak, M. Wróbel-Kwiatkowska, A. Kulma, E. Starzycka, J. Szopa, Improving retting of fibre through genetic modification of flax to express pectinases, *Transgenic Res.* 17 (2008) 133–147. <https://doi.org/10.1007/s11248-007-9080-4>.
- [162] Directive (EU) 2015/412 of the European Parliament and of the Council of 11 March 2015 amending Directive 2001/18/EC as regards the possibility for the Member States to restrict or prohibit the cultivation of genetically modified organisms (GMOs) in their territory, 2015. <http://data.europa.eu/eli/dir/2015/412/oj/eng> (accessed August 16, 2021).
- [163] A. Bourmaud, M. Gibaud, C. Baley, Impact of the seeding rate on flax stem stability and the mechanical properties of elementary fibres, *Ind. Crops Prod.* 80 (2016) 17–25. <https://doi.org/10.1016/j.indcrop.2015.10.053>.
- [164] G.M.L.W. Kroes, R.P. Baayen, W. Lange, Histology of root rot of flax seedlings (*Linum usitatissimum*) infected by *Fusarium oxysporum* f.sp. lini, *Eur. J. Plant Pathol.* 104 (1998) 725–736.
- [165] F. Bert, Les maladies du lin fibre : La fusariose vasculaire, ARVALIS - Institut du végétal. (2011). <https://www.arvalis-infos.fr/lin-maladies-@/view-23663-arvarticle.html> (accessed July 19, 2021).
- [166] Z. Zawani, L.C. Abdullah, K. Abdan, Characterization of Kenaf Fibre-Retted Wastewater, *Int. J. Sci. Res.* 4 (2013) 314–317.
- [167] G. Henriksson, D.E. Akin, R.T. Hanlin, C. Rodriguez, D.D. Archibald, L.L. Rigsby, K.-E.L. Eriksson, Identification and Retting Efficiencies of Fungi Isolated from Dew-Retted Flax in the United States and Europe, *Appl. Environ. Microbiol.* 63 (1997) 3950–3956.
- [168] ARVALIS Institut du végétal, Lin fibre: résultats et préconisations, ARVALIS, Paris, France, 2017.
- [169] D.E. Akin, Linen Most Useful: Perspectives on Structure, Chemistry, and Enzymes for Retting Flax, *ISRN Biotechnology*. 2013 (2013) 1–23. <https://doi.org/10.5402/2013/186534>.
- [170] N. Martin, N. Mouret, P. Davies, C. Baley, Influence of the degree of retting of flax fibers on the tensile properties of single fibers and short fiber/polypropylene composites, *Ind. Crops Prod.* 49 (2013) 755–767. <https://doi.org/10.1016/j.indcrop.2013.06.012>.
- [171] W.J.M. Meijer, N. Vertregt, B. Rutgers, M. van de Waart, The pectin content as a measure of the retting and rettability of flax, *Ind. Crops Prod.* 4 (1995) 273–284. [https://doi.org/10.1016/0926-6690\(95\)00041-0](https://doi.org/10.1016/0926-6690(95)00041-0).
- [172] V. Placet, A. Day, J. Beaugrand, The influence of unintended field retting on the physicochemical and mechanical properties of industrial hemp bast fibres, *J. Mater. Sci.* 52 (2017) 5759–5777. <https://doi.org/10.1007/s10853-017-0811-5>.
- [173] A. Lefeuvre, Contribution à l'étude des propriétés mécaniques et morphologiques des fibres de lin – *Linum Usitatissimum* Linecea – variété Marylin et Andréa en fonction des pratiques culturales et comme renfort de matériaux composites, cas du plateau du Neubourg, Chimie des matériaux, Université de Rouen, 2014.
- [174] T.D. Tavares, J.C. Antunes, F. Ferreira, H.P. Felgueiras, Biofunctionalization of Natural Fiber-Reinforced Biocomposites for Biomedical Applications, *Biomolecules*. 10 (2020) 148.
- [175] D.E. Akin, L.L. Rigsby, G. Henriksson, K.-E.L. Eriksson, Structural Effects on Flax Stems of Three Potential Retting Fungi, *Text. Res. J.* 68 (1998) 515–519. <https://doi.org/10.1177/004051759806800708>.
- [176] A. Adamsen, D. Akin, L. Rigsby, Chemical Retting of Flax Straw Under Alkaline Conditions, *Text. Res. J.* 72 (2002) 789–794.
- [177] M. Gregoire, E. De Luycker, P. Ouagne, Étude de l'extraction des fibres de chanvre longs brins et impact sur leur potentiel de renfort, in: 24ème Congrès Français de Mécanique, Brest, 2019: p. 6.
- [178] K. Ghosh, B.H. Jones, Roadmap to Biodegradable Plastics—Current State and Research Needs, *ACS Sustainable Chem. Eng.* 9 (2021) 6170–6187. <https://doi.org/10.1021/acssuschemeng.1c00801>.
- [179] T. Vincelas, Caractérisation d'éco-matériaux terre-chanvre en prenant en compte la variabilité des ressources disponibles localement, Matériaux, Génie Civil, Université de Bretagne Sud, 2019.

- [180] T. Colinart, T. Vincelas, H. Lenormand, A.H.D. Menibus, E. Hamard, T. Lecompte, Hygrothermal properties of light-earth building materials, *J. Build. Eng.* 29 (2020) 101134. <https://doi.org/10.1016/j.jobbe.2019.101134>.
- [181] F. Menasria, A. Perrot, D. Rangeard, A.L. Duigou, Mechanical enhancement of casted and compacted earth-based materials by sand, flax fiber and woven fabric of flax, *AJCE*. 35 (2017) 148–153.
- [182] S. Fic, P. Brzyski, M. Szeląg, Composite based on foam lime mortar with flax fibers for use in the building industry, *Ecol. Chem. Eng. A*. 20 (2013) 899–907. [https://doi.org/10.2428/ecea.2013.20\(07\)084](https://doi.org/10.2428/ecea.2013.20(07)084).
- [183] M. Shamsuyeva, O. Hansen, H.-J. Endres, Review on hybrid carbon/flax composites and their properties, *Int. J. Polym. Sci.* 2019 (2019). <https://doi.org/10.1155/2019/9624670>.
- [184] B.M. Pejic, M.M. Kostic, P.D. Skundric, J.Z. Praskalo, The effects of hemicelluloses and lignin removal on water uptake behavior of hemp fibers, *Bioresour. Technol.* 99 (2008) 7152–7159. <https://doi.org/10.1016/j.biortech.2007.12.073>.
- [185] W. Garat, N. Le Moigne, S. Corn, J. Beaugrand, A. Bergeret, Swelling of natural fibre bundles under hygro- and hydrothermal conditions: Determination of hydric expansion coefficients by automated laser scanning, *Compos. Part A Appl. Sci. Manuf.* 131 (2020) 105803. <https://doi.org/10.1016/j.compositesa.2020.105803>.
- [186] A. Céline, O. Gonçalves, F. Jacquemin, S. Fréour, Qualitative and quantitative assessment of water sorption in natural fibres using ATR-FTIR spectroscopy, *Carbohydr. Polym.* 101 (2014) 163–170. <https://doi.org/10.1016/j.carbpol.2013.09.023>.
- [187] Museum Galleries Scotland, Museums Galleries Scotland - Temperature and humidity in museums, Museum Galleries Scotland. (2021). <https://www.museumsgalleriescotland.org.uk/advice/collections/temperature-and-humidity-in-museums/> (accessed March 22, 2021).
- [188] G. Pavlogeorgatos, Environmental parameters in museums, *Building and Environment*. 38 (2003) 1457–1462. [https://doi.org/10.1016/S0360-1323\(03\)00113-6](https://doi.org/10.1016/S0360-1323(03)00113-6).
- [189] Canadian Conservation Institute, Textiles and the Environment – Canadian Conservation Institute (CCI) Notes 13/1, (2013). <https://www.canada.ca/en/conservation-institute/services/conservation-preservation-publications/canadian-conservation-institute-notes/textiles-environment.html> (accessed March 22, 2021).
- [190] M.F. Mecklenburg, Determining the Acceptable Ranges of Relative Humidity And Temperature in Museums and Galleries, part 1, structural response to relative humidity, (2007).
- [191] S.P. Corgnati, V. Fabi, D. Raimondo, Conservazione preventiva e controllo microclimatico nel contesto degli standard museali, sms santa maria della scala, Siena, 2010.
- [192] F. Pertegato, I tessili: degrado e restauro, 3rd edition, Nardini Editore, Firenze, 2004: pp. 27-28. <https://www.bcin.ca/bcin/detail.app.jsessionid=675CDA9B57B2114DACB48D92F47B8ADB?id=139365&lang=fr&asq=&csq=&csa=&ps=100&pId=1435> (accessed June 29, 2021).
- [193] J. Gassan, A.K. Bledzki, Thermal degradation of flax and jute fibers, *J. Appl. Polym. Sci.* 82 (2001) 1417–1422. <https://doi.org/10.1002/app.1979>.
- [194] D. Siniscalco, O. Arnould, A. Bourmaud, A. Le Duigou, C. Baley, Monitoring temperature effects on flax cell-wall mechanical properties within a composite material using AFM, *Polym. Test.* 69 (2018) 91–99. <https://doi.org/10.1016/j.polymertesting.2018.05.009>.
- [195] S.N. Basu, R. Ghose, A Microscopical Study on the Degradation of Jute Fiber by Micro-Organisms, *Text. Res. J.* 32 (1962) 677–694. <https://doi.org/10.1177/004051756203200810>.
- [196] S.N. Basu, R. Ghose, Structural Changes Brought About in the Jute Fiber by Micro-Organisms and their Enzymes, *Text. Res. J.* 32 (1962) 932–942. <https://doi.org/10.1177/004051756203201109>.
- [197] M.P. Nugari, O. Maggi, A.M. Persiani, Problemi di biodeterioramento in relazione alla tipologia di ambienti: Musei, in: G. Caneva, M.P. Nugari, O. Salvadori (Eds.), *La Biologia Vegetale per i Beni Culturali: Biodeterioramento e Conservazione*, 2nd edition, Nardini Editore, Firenze, 2007: pp. 177–178.
- [198] J. Repeškienė, A. Lugauskas, Z. Jankauskiene, Diversity of fungal species on laid and stand-retted flax, *Bot. Lith.* 13 (2007) 51–59.
- [199] C. Djemiel, E. Goulas, N. Badalato, B. Chabbert, S. Hawkins, S. Grec, Targeted Metagenomics of Retting in Flax: The Beginning of the Quest to Harness the Secret Powers of the Microbiota, *Front. Genet.* 11 (2020). <https://doi.org/10.3389/fgene.2020.581664>.

- [200] T.M. Herrington, F.C. Vernier, Vapour pressure and water activity, in: S.T. Beckett (Ed.), *Physico-Chemical Aspects of Food Processing*, Springer US, Boston, MA, 1995: pp. 1–16. https://doi.org/10.1007/978-1-4613-1227-7_1.
- [201] G. Caneva, S. Ceschin, *Ecologia del biodeterioramento*, in: G. Caneva, M.P. Nugari, O. Salvadori (Eds.), *La Biologia Vegetale per i Beni Culturali: Biodeterioramento e Conservazione*, 2nd edition, Nardini Editore, Firenze, 2007: pp. 35–58.
- [202] C. Tiebe, M. Detjens, A. Fechner, S. Sielemann, A. Lorek, R. Wernecke, H. Stoltenberg, Development of a Device for Staged Determination of Water Activity and Moisture Content, *Proceedings*. 2 (2018) 881. <https://doi.org/10.3390/proceedings2130881>.
- [203] A.P. Singh, Y.S. Kim, T. Singh, Bacterial Degradation of Wood, in: Y. S. Kim, R. Funada and A. P. Singh (Eds.) *Secondary Xylem Biology*, Academic Press, 2016: pp. 169–190.
- [204] M.P. Nugari, *Dipinti mobili*, in: G. Caneva, M.P. Nugari, O. Salvadori (Eds.) *La Biologia Vegetale per i Beni Culturali: Biodeterioramento e Conservazione*, 2nd edition, Nardini editore, Firenze, 2007: pp. 156–159.
- [205] P.E. Sloderbeck, *Silverfish and Firebrats*, Kansas State University, (2004).
- [206] E.F. Phillips, J.L. Gillett-Kaufman, *Silverfish Lepisma saccharina Linnaeus (Insecta: Zygentoma: Lepismatidae)*, IFAS University of Florida, (2018). <https://doi.org/10.32473/edis-in1211-2018>.
- [207] R.D. Gillard, S.M. Hardman, R.G. Thomas, D.E. Watkinson, The Mineralization of Fibres in Burial Environments, *Stud. Conserv.* 39 (1994) 132–140. <https://doi.org/10.2307/1506562>.
- [208] E.E. Peacock, Il deterioramento biologico delle fibre tessili in contesti archeologici implicazioni per le scelte di conservazione, in: *Intrecci vegetali e fibre tessili da ambiente umido Analisi Conservazione e Restauro*, Incontri di Restauro 4, Trento, 2003: pp.11-31.
- [209] C. Reynaud, M. Thoury, A. Dazzi, G. Latour, M. Scheel, J. Li, A. Thomas, C. Moulhérat, A. Didier, L. Bertrand, In-place molecular preservation of cellulose in 5,000-year-old archaeological textiles, *PNAS*. 117 (2020) 19670–19676. <https://doi.org/10.1073/pnas.2004139117>.
- [210] G. Kirker, J. Glaeser, Techline: salt damage to wood, “Fuzzy Wood” often confused with fungal decay, forest products laboratory, USDA U.S. Department of Agriculture (2011).
- [211] C. Dorée, The Action of Sea Water on Cotton and other Textile Fibres, *Biochem J.* 14 (1920) 709–714.
- [212] T. Anson Cartwright, International Scientific Committee for Stone, eds., *ICOMOS-ISCS: Illustrated glossary on stone deterioration patterns*, ICOMOS, Paris, 2008.
- [213] X. Mi, T. Li, J. Wang, Y. Hu, Evaluation of Salt-Induced Damage to Aged Wood of Historical Wooden Buildings, *Int. J. Anal. Chem.* 2020 (2020) 1–11. <https://doi.org/10.1155/2020/8873713>.
- [214] L. Pil, F. Bensadoun, J. Pariset, I. Verpoest, Why are designers fascinated by flax and hemp fibre composites?, *Compos. Part A Appl. Sci. Manuf.* 83 (2016) 193–205. <https://doi.org/10.1016/j.compositesa.2015.11.004>.
- [215] C.Q. Yang, J.M. Freeman, Photo-Oxidation of Cotton Cellulose Studied by FT-IR Photoacoustic Spectroscopy, *Appl. Spectrosc.* 45 (1991) 1695–1698. <https://doi.org/10.1366/0003702914335274>.
- [216] R. Marini Bettolo, M.L. Migneco, M. Plossi Zappalà, I materiali cellulosici e le loro materie prime, in: *Chimica per l'arte*, Zanichelli, 2007: pp. 411–481.
- [217] F.M. Helmi, O.M. El-Feky, E.H. Salib, Identification and Characterization of Some Archaeological Coptic Textiles, *Coptic Museum, Cairo, Egypt, J. Anal. Chem.* 17 (2008) 53–62.
- [218] L.G. Thygesen, P. Hoffmeyer, Image analysis for the quantification of dislocations in hemp fibres, *Ind. Crops Prod.* 21 (2005) 173–184. <https://doi.org/10.1016/j.indcrop.2004.03.001>.
- [219] U.A. Mortensen, B. Madsen, Protocol for Quantification of Defects in Natural Fibres for Composites, *J. Text.* 2014 (2014) 1–9. <https://doi.org/10.1155/2014/929875>.
- [220] V. Richter, Indagine condotta con microscopia elettronica a scansione su materiali fibrosi cellulosici, in: G.C. Scicolone (Ed.), *Dipinti Su Tela: Metodologie d'indagine per i Supporti Cellulosici*, 2005th ed., Nardini Editore, Firenze, 2005: pp. 31–40.
- [221] Y.S. Kim, A.P. Singh, T. Nilsson, Bacteria as Important Degradors in Waterlogged Archaeological Woods, *Holzforschung.* 50 (1996) 389–392. <https://doi.org/10.1515/hfsg.1996.50.5.389>.

- [222] L. Bonizzoni, S. Bruni, G. Fanti, P. Tiberio, C. Zaffino, Ageing of flax textiles: Fingerprints in micro-Raman spectra of single fibres, *Microchem. J.* 125 (2016) 69–74. <https://doi.org/10.1016/j.microc.2015.11.011>.
- [223] K. Kavkler, A. Demšar, Examination of cellulose textile fibres in historical objects by micro-Raman spectroscopy, *Spectrochim. Acta A Mol. Biomol. Spectrosc.* 78 (2011) 740–746. <https://doi.org/10.1016/j.saa.2010.12.006>.
- [224] H.G.M. Edwards, D.W. Farwell, D. Webster, FT Raman microscopy of untreated natural plant fibres, *Spectrochim. Acta A Mol. Biomol. Spectrosc.* 53 (1997) 2383–2392. [https://doi.org/10.1016/S1386-1425\(97\)00178-9](https://doi.org/10.1016/S1386-1425(97)00178-9).
- [225] PerkinElmer Inc., Applications and Design of a Micro-ATR Objective, (2010). https://resources.perkinelmer.com/lab-solutions/resources/docs/TCH_MicroATR.pdf.
- [226] N. Gierlinger, New insights into plant cell walls by vibrational microspectroscopy, *Appl. Spectrosc. Rev.* 53 (2018) 517–551. <https://doi.org/10.1080/05704928.2017.1363052>.
- [227] P. Garside, P. Wyeth, Identification of Cellulosic Fibres by FTIR Spectroscopy - Thread and Single Fibre Analysis by Attenuated Total Reflectance, *Stud. Conserv.* 48 (2003) 269–275. <https://doi.org/10.1179/sic.2003.48.4.269>.
- [228] C. Margariti, The application of FTIR microspectroscopy in a non-invasive and non-destructive way to the study and conservation of mineralised excavated textiles, *Herit. Sci.* 7 (2019) 63. <https://doi.org/10.1186/s40494-019-0304-8>.
- [229] K. Kavkler, N. Gunde-Cimerman, P. Zalar, A. Demšar, FTIR spectroscopy of biodegraded historical textiles, *Polym. Degrad. Stab.* 96 (2011) 574–580. <https://doi.org/10.1016/j.polymdegradstab.2010.12.016>.
- [230] A. Elamin, K. Takatori, Y. Matsuda, M. Tsukada, F. Kirino, Fungal biodeterioration of artificial aged linen textile: evaluation by microscopic, spectroscopic and viscometric methods, *Mediterr. Archaeol. Archaeom.* 18 (2018) 103–120. <https://doi.org/10.5281/ZENODO.1461623>.
- [231] K. Schenzel, S. Fischer, E. Brendler, New Method for Determining the Degree of Cellulose I Crystallinity by Means of FT Raman Spectroscopy, *Cellulose.* 12 (2005) 223–231. <https://doi.org/10.1007/s10570-004-3885-6>.
- [232] U.P. Agarwal, R.S. Reiner, S.A. Ralph, Cellulose I crystallinity determination using FT-Raman spectroscopy: univariate and multivariate methods, *Cellulose.* 17 (2010) 721–733. <https://doi.org/10.1007/s10570-010-9420-z>.
- [233] M.L. Nelson, R.T. O'Connor, Relation of certain infrared bands to cellulose crystallinity and crystal lattice type. Part II. A new infrared ratio for estimation of crystallinity in celluloses I and II, *J. Appl. Polym. Sci.* 8 (1964) 1325–1341. <https://doi.org/10.1002/app.1964.070080323>.
- [234] M. Fan, D. Dai, B. Huang, Fourier Transform Infrared Spectroscopy for Natural Fibres, in: S. Salih (Ed.), *Fourier Transform - Materials Analysis*, InTech, 2012: pp.45-67. <https://doi.org/10.5772/35482>.
- [235] B. Reif, S.E. Ashbrook, L. Emsley, M. Hong, Solid-state NMR spectroscopy, *Nat. Rev. Methods Primers.* 1 (2021) 2. <https://doi.org/10.1038/s43586-020-00002-1>.
- [236] E. Princi, S. Vicini, N. Proietti, D. Capitani, Grafting polymerization on cellulose based textiles: A ¹³C solid state NMR characterization, *Eur. Polym. J.* 41 (2005) 1196–1203.
- [237] S. Park, D.K. Johnson, C.I. Ishizawa, P.A. Parilla, M.F. Davis, Measuring the crystallinity index of cellulose by solid state ¹³C nuclear magnetic resonance, *Cellulose.* 16 (2009) 641–647. <https://doi.org/10.1007/s10570-009-9321-1>.
- [238] K. Castro, E. Princi, N. Proietti, M. Manso, D. Capitani, S. Vicini, J.M. Madariaga, M.L. De Carvalho, Assessment of the weathering effects on cellulose based materials through a multianalytical approach, *Nucl. Instrum. Methods Phys. Res. B.* 269 (2011) 1401–1410. <https://doi.org/10.1016/j.nimb.2011.03.027>.
- [239] R.H. Atalla, D.L. VanderHart, Native Cellulose: A Composite of Two Distinct Crystalline Forms, *Science.* 223 (1984) 283–285. <https://doi.org/10.1126/science.223.4633.283>.
- [240] P.T. Larsson, K. Wickholm, T. Iversen, A CP/MAS ¹³C NMR investigation of molecular ordering in celluloses, *Carbohydr. Res.* 302 (1997) 19–25.

- [241] M. Foston, Advances in solid-state NMR of cellulose, *Curr. Opin. Biotechnol.* 27 (2014) 176–184. <https://doi.org/10.1016/j.copbio.2014.02.002>.
- [242] K. Wickholm, P.T. Larsson, T. Iversen, Assignment of non-crystalline forms in cellulose I by CP/MAS ¹³C NMR spectroscopy, *Carbohydr. Res.* 312 (1998) 123–129. [https://doi.org/10.1016/S0008-6215\(98\)00236-5](https://doi.org/10.1016/S0008-6215(98)00236-5).
- [243] D. Capitani, V. Di Tullio, N. Proietti, Nuclear Magnetic Resonance to characterize and monitor Cultural Heritage, *Prog. Nucl. Magn. Reson. Spectrosc.* 64 (2012) 29–69. <https://doi.org/10.1016/j.pnmrs.2011.11.001>.
- [244] E. Aracri, A. Fillat, J.F. Colom, A. Gutiérrez, J.C. del Río, Á.T. Martínez, T. Vidal, Enzymatic grafting of simple phenols on flax and sisal pulp fibres using laccases, *Bioresour. Technol.* 101 (2010) 8211–8216. <https://doi.org/10.1016/j.biortech.2010.05.080>.
- [245] G. Dorez, B. Otazaghine, A. Taguet, L. Ferry, J.M. Lopez-Cuesta, Use of Py-GC/MS and PCFC to characterize the surface modification of flax fibres, *J. Anal. Appl. Pyrolysis.* 105 (2014) 122–130. <https://doi.org/10.1016/j.jaap.2013.10.011>.
- [246] L. Degani, C. Riedo, O. Chiantore, Identification of natural indigo in historical textiles by GC–MS, *Anal. Bioanal. Chem.* 407 (2015) 1695–1704. <https://doi.org/10.1007/s00216-014-8423-2>.
- [247] F.A. Pettolino, C. Walsh, G.B. Fincher, A. Bacic, Determining the polysaccharide composition of plant cell walls, *Nat. Protoc.* 7 (2012) 1590–1607. <https://doi.org/10.1038/nprot.2012.081>.
- [248] A. Lefeuvre, C. Baley, C. Morvan, Analysis of Flax Fiber Cell-Wall Non-Cellulosic Polysaccharides Under Different Weather Conditions (Marylin Variety), *J. Nat. Fibers.* 15 (2018) 539–544. <https://doi.org/10.1080/15440478.2017.1349020>.
- [249] A.M. Seves, S. Sora, G. Scicolone, G. Testa, A.M. Bonfatti, E. Rossi, A. Seves, Effect of thermal accelerated ageing on the properties of model canvas paintings, *J. Cult. Herit.* 1 (2000) 315–322. [https://doi.org/10.1016/S1296-2074\(00\)01078-5](https://doi.org/10.1016/S1296-2074(00)01078-5).
- [250] E. Rossi, Misure del grado di polimerizzazione per la valutazione dello stato di deterioramento di un materiale fibroso cellulosico, in: G.C. Scicolone (Ed.), *Dipinti su Tela: metodologie d’indagine per i supporti cellulosici*, 2nd edition, Nardini Editore, Firenze, 2005: pp. 25–30.
- [251] L. De Caro, C. Giannini, R. Lassandro, F. Scattarella, T. Sibillano, E. Matricciani, G. Fanti, X-ray Dating of Ancient Linen Fabrics, *Heritage.* 2 (2019) 2763–2783. <https://doi.org/10.3390/heritage2040171>.
- [252] T.E. Timell, Chain length and chain-length distribution of untreated cotton, flax, and ramie celluloses, *Ind. Eng. Chem. Res.* 47 (1955) 2166–2172.
- [253] Y. Jiang, M. Lawrence, A. Hussain, M. Ansell, P. Walker, Comparative moisture and heat sorption properties of fibre and shiv derived from hemp and flax, *Cellulose.* 26 (2019) 823–843. <https://doi.org/10.1007/s10570-018-2145-0>.
- [254] C. Gourier, A. Le Duigou, A. Bourmaud, C. Baley, Mechanical analysis of elementary flax fibre tensile properties after different thermal cycles, *Compos. Part A Appl. Sci. Manuf.* 64 (2014) 159–166. <https://doi.org/10.1016/j.compositesa.2014.05.006>.
- [255] O. Paris, M. Müller, Scanning X-ray microdiffraction of complex materials: Diffraction geometry considerations, *Nucl. Instrum. Methods Phys. Res. B.* 200 (2003) 390–396. [https://doi.org/10.1016/S0168-583X\(02\)01728-7](https://doi.org/10.1016/S0168-583X(02)01728-7).
- [256] H. Zhao, J. Kwak, Z. Conradzhang, H. Brown, B. Arey, J. Holladay, Studying cellulose fiber structure by SEM, XRD, NMR and acid hydrolysis, *Carbohydr. Polym.* 68 (2007) 235–241. <https://doi.org/10.1016/j.carbpol.2006.12.013>.
- [257] M. Müller, C. Czihak, G. Vogl, P. Fratzl, H. Schober, C. Riekell, Direct Observation of Microfibril Arrangement in a Single Native Cellulose Fiber by Microbeam Small-Angle X-ray Scattering, *Macromolecules.* 31 (1998) 3953–3957. <https://doi.org/10.1021/ma980004c>.
- [258] H.L. Chen, D.W. Foreman, K.A. Jakes, X-ray Diffractometric Analyses of Microstructure of Mineralized Plant Fibers, in: M.V. Orna (Ed.), *Archaeological Chemistry*, American Chemical Society, Washington, DC, 1996: pp. 187–201. <https://doi.org/10.1021/bk-1996-0625.ch015>.

- [259] M. Müller, B. Murphy, M. Burghammer, I. Snigireva, C. Riekel, J. Gunneweg, E. Pantos, Identification of single archaeological textile fibres from the cave of letters using synchrotron radiation microbeam diffraction and microfluorescence, *Appl. Phys. A.* 83 (2006) 183–188. <https://doi.org/10.1007/s00339-006-3516-1>.
- [260] S. Rongpipi, D. Ye, E.D. Gomez, E.W. Gomez, Progress and Opportunities in the Characterization of Cellulose – An Important Regulator of Cell Wall Growth and Mechanics, *Front. Plant Sci.* 9 (2019) 1894. <https://doi.org/10.3389/fpls.2018.01894>.
- [261] S. Park, J.O. Baker, M.E. Himmel, P.A. Parilla, D.K. Johnson, Cellulose crystallinity index: measurement techniques and their impact on interpreting cellulase performance, *Biotechnol. Biofuels.* 3 (2010) 1–10.
- [262] M. Müller, C. Czihak, M. Burghammer, C. Riekel, Combined X-ray microbeam small-angle scattering and fibre diffraction experiments on single native cellulose fibres, *J. Appl. Crystallogr.* 33 (2000) 817–819. <https://doi.org/10.1107/S0021889800099751>.
- [263] M. Ioelovich, Cellulose: nanostructured natural polymer, LAP Lambert Academic Publishing, Saarbrücken, Germany, 2014.
- [264] T. Sui, H. Zhang, S. Ying, P. O’Brien, A.M. Korsunsky, FIB-SEM Serial Sectioning Nanotomography of Flax Fibres, in: *Proceedings of the International Multi Conference of Engineers and Computer Scientists*, 2, Hong Kong, 2015.
- [265] M. Oriola, A. Možir, P. Garside, G. Campo, A. Nualart-Torroja, I. Civil, M. Odlyha, M. Cassar, M. Strlič, Looking beneath Dalí’s paint: non-destructive canvas analysis, *Anal. Methods.* 6 (2014) 86–96. <https://doi.org/10.1039/C3AY41094C>.
- [266] D. Khennouf, J.M. Dulieu-Barton, A.R. Chambers, F.J. Lennard, D.D. Eastop, Assessing the Feasibility of Monitoring Strain in Historical Tapestries Using Digital Image Correlation, *Strain.* 46 (2010) 19–32. <https://doi.org/10.1111/j.1475-1305.2009.00637.x>.
- [267] M. Malesa, K. Malowany, L. Tyimińska-Widmer, E.A. Kwiatkowska, M. Kujawińska, B.J. Rouba, P. Targowski, Application of digital image correlation (DIC) for tracking deformations of paintings on canvas, in: *Optics for Arts, Architecture, and Archaeology III. International Society for Optics and Photonics*, Munich, Germany, 2011: p. 80840L. <https://doi.org/10.1117/12.889452>.
- [268] K. Malowany, L. Tyimińska-Widmer, M. Malesa, M. Kujawińska, P. Targowski, B.J. Rouba, Application of 3D digital image correlation to track displacements and strains of canvas paintings exposed to relative humidity changes, *Appl. Opt.* 53 (2014) 1739–1749. <https://doi.org/10.1364/AO.53.001739>.
- [269] ASTM C1557-20, ASTM International, West Conshohocken, PA, 2020. <https://doi.org/10.1520/C1557-20>.
- [270] O. Nechyporchuk, K. Kolman, A. Bridarolli, M. Odlyha, L. Bozec, M. Oriola, G. Campo-Francés, M. Persson, K. Holmberg, R. Bordes, On the potential of using nanocellulose for consolidation of painting canvases, *Carbohydr. Polym.* 194 (2018) 161–169. <https://doi.org/10.1016/j.carbpol.2018.04.020>.
- [271] P.M. Rocha, D. D’Ayala, C. Vlachou-Mogire, Methodology for tensile testing historic tapestries, *IOP Conf. Ser.: Mater. Sci. Eng.* 364 (2018) 012003. <https://doi.org/10.1088/1757-899X/364/1/012003>.
- [272] N.H. Faisal, R. Ahmed, S. Goel, G. Cross, Future of nanoindentation in archaeometry, *J. Mater. Res.* 33 (2018) 2515–2532. <https://doi.org/10.1557/jmr.2018.280>.
- [273] J. Salvant, E. Barthel, M. Menu, Nanoindentation and the micromechanics of Van Gogh oil paints, *Appl. Phys. A.* 104 (2011) 509–515. <https://doi.org/10.1007/s00339-011-6486-x>.
- [274] M. Tiennot, E. Paardekam, D. Iannuzzi, E. Hermens, Mapping the mechanical properties of paintings via nanoindentation: a new approach for cultural heritage studies, *Sci. Rep.* 10 (2020) 7924. <https://doi.org/10.1038/s41598-020-64892-7>.
- [275] P.E. Damon, D.J. Donahue, B.H. Gore, A.L. Hatheway, A.J.T. Jull, T.W. Linick, P.J. Sercel, L.J. Toolin, C.R. Bronk, E.T. Hall, R.E.M. Hedges, R. Housley, I.A. Law, C. Perry, G. Bonani, S. Trumbore, W. Woelfli, J.C. Ambers, S.G.E. Bowman, M.N. Leese, M.S. Tite, Radiocarbon dating of the Shroud of Turin, *Nature.* 337 (1989) 611–615. <https://doi.org/10.1038/337611a0>.
- [276] T. Casabianca, E. Marinelli, G. Pernagallo, B. Torrisi, Radiocarbon Dating of the Turin Shroud: New Evidence from Raw Data, *Archaeometry.* 61 (2019) 1223–1231. <https://doi.org/10.1111/arc.12467>.
- [277] A. Jähn, M.W. Schröder, M. Fütting, K. Schenzel, W. Diepenbrock, Characterization of alkali treated flax fibres by means of FT Raman spectroscopy and environmental scanning electron microscopy,

- Spectrochim. Acta A Mol. Biomol. Spectrosc. 58 (2002) 2271–2279. [https://doi.org/10.1016/S1386-1425\(01\)00697-7](https://doi.org/10.1016/S1386-1425(01)00697-7).
- [278] H.G.M. Edwards, N.F. Nikhassan, D.W. Farwell, P. Garside, P. Wyeth, Raman spectroscopic analysis of a unique linen artefact: the HMS Victory Trafalgar sail, *J. Raman Spectrosc.* 37 (2006) 1193–1200. <https://doi.org/10.1002/jrs.1609>.
- [279] L. Campanella, A. Antonelli, G. Favero, M. Tomassetti, New archeometric method for wood based on an enzymatic biosensor, *L'Act. Chim.* (2001) 14–20.
- [280] L. Campanella, F. Chicco, G. Favero, T. Gatta, M. Tomassetti, Further Applications of a New Biosensor Method for Dating Cellulosic Finds, *Ann. Chim.* 95 (2005) 133–141. <https://doi.org/10.1002/adic.200590015>.
- [281] A. Doménech-Carbó, M.T. Doménech-Carbó, V. Costa, Application of Instrumental Methods in the Analysis of Historic, Artistic and Archaeological Objects, in: A. Doménech-Carbó, M.T. Doménech-Carbó, V. Costa (Eds.), *Electrochemical Methods in Archaeometry, Conservation and Restoration*, Springer Berlin Heidelberg, Berlin, Heidelberg, 2009: pp. 1–32. https://doi.org/10.1007/978-3-540-92868-3_1.
- [282] A. Bridarolli, M. Odlyha, O. Nechyporchuk, K. Holmberg, C. Ruiz-Recasens, R. Bordes, L. Bozec, Evaluation of the Adhesion and Performance of Natural Consolidants for Cotton Canvas Conservation, *ACS Appl. Mater. Interfaces.* 10 (2018) 33652–33661. <https://doi.org/10.1021/acsami.8b10727>.
- [283] L. Pereira, D.N.A. Flores-Borges, P.R.L. Bittencourt, J.L.S. Mayer, E. Kiyota, P. Araújo, S. Jansen, R.O. Freitas, R.S. Oliveira, P. Mazzafera, Infrared Nanospectroscopy Reveals the Chemical Nature of Pit Membranes in Water-Conducting Cells of the Plant Xylem, *Plant Physiol.* 177 (2018) 1629–1638. <https://doi.org/10.1104/pp.18.00138>.
- [284] R.M. Brown, Jr., A.C. Millard, P.J. Campagnola, Macromolecular structure of cellulose studied by second-harmonic generation imaging microscopy, *Opt. Lett.* 28 (2003) 2207–2209. <https://doi.org/10.1364/OL.28.002207>.
- [285] O. Nadiarykh, R.B. LaComb, P.J. Campagnola, W.A. Mohler, Coherent and incoherent SHG in fibrillar cellulose matrices, *Opt. Express.* 15 (2007) 3348–3360. <https://doi.org/10.1364/OE.15.003348>.
- [286] A. Peciulyte, J. Kiskis, P.T. Larsson, L. Olsson, A. Enejder, Visualization of structural changes in cellulosic substrates during enzymatic hydrolysis using multimodal nonlinear microscopy, *Cellulose.* 23 (2016) 1521–1536. <https://doi.org/10.1007/s10570-016-0908-z>.
- [287] F.S. Pavone, P.J. Campagnola, eds., *Second Harmonic Generation Imaging*, 1st edition, CRC Press, Boca Raton, 2013.
- [288] K. Kavkler, Ž. Šmit, D. Jezeršek, D. Eichert, A. Demšar, Investigation of biodeteriorated historical textiles by conventional and synchrotron radiation FTIR spectroscopy, *Polym. Degrad. Stab.* 96 (2011) 1081–1086. <https://doi.org/10.1016/j.polymdegradstab.2011.03.011>.
- [289] J. Beaugrand, C. Alvarado, M.-F. Devaux, C. Rivard, S. Durand, H. Chauvet, M. Réfrégiers, F. Jamme, F. Guillon, A. Bourmaud, C. Baley, C. Goudenhooff, J. Beaugrand, Evolution of the Flax Cell Wall Composition During Development and After Gravitropism by Synchrotron Fluorescence Imaging, Preprint. (preprint). <https://doi.org/10.26434/chemrxiv.14665911.v1>.
- [290] F. Jamme, S. Kascakova, S. Villette, F. Allouche, S. Pallu, V. Rouam, M. Réfrégiers, Deep UV autofluorescence microscopy for cell biology and tissue histology, *Biol. Cell.* 105 (2013) 277–288. <https://doi.org/10.1111/boc.201200075>.
- [291] J.-P. Echard, M. Thoury, B.H. Berrie, T. Séverin-Fabiani, A. Vichi, M. Didier, M. Réfrégiers, L. Bertrand, Synchrotron DUV luminescence micro-imaging to identify and map historical organic coatings on wood, *Analyst.* 140 (2015) 5344–5353. <https://doi.org/10.1039/C5AN00483G>.
- [292] S. Eve, A. Thuault, B. Duchemin, K. Charlet, B. Abbey, A.M. Korsunsky, A synchrotron X-Ray study of the inner structure and the micro-mechanical behaviour of single flax fibres, in: *International Conference on Mechanics of Nano, Micro and Macro Composite Structures*, Politecnico di Torino, Italy, 2012.
- [293] B. Abbey, S. Eve, A. Thuault, K. Charlet, A. Korsunsky, Synchrotron X-Ray Tomographic Investigation of Internal Structure of Individual Flax Fibres, in: C.T. Lim, J.C.H. Goh (Eds.), *6th World Congress of Biomechanics (WCB 2010)*. August 1-6, 2010 Singapore, Springer Berlin Heidelberg, Berlin, Heidelberg, 2010: pp. 1151–1154. https://doi.org/10.1007/978-3-642-14515-5_292.

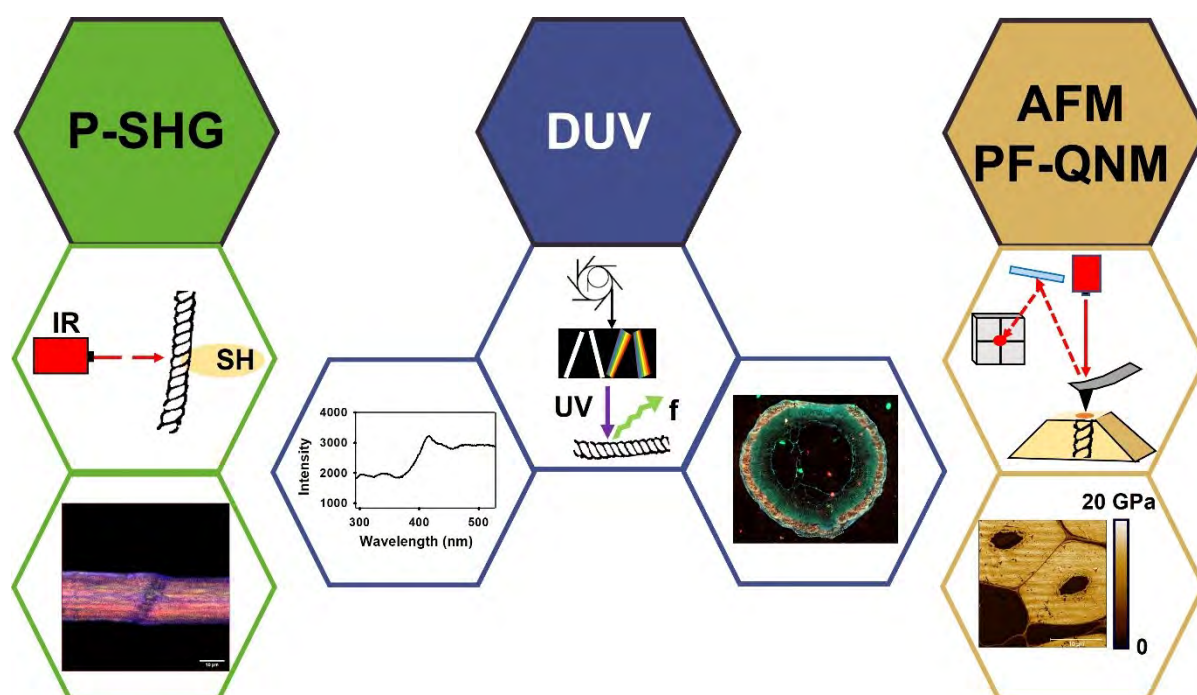
- [294] A. King, N. Guignot, J.-P. Deslandes, M. Pelerin, I. Joosten, D. De Looft, J. Li, L. Bertrand, E. Rosenberg, A. Dewaele, E. Boulard, Y. Le Godec, J.-P. Perrillat, E. Giovenco, G. Morard, T. Weitkamp, M. Scheel, J. Perrin, H. Chevreau, J.-P. Itié, Recent Tomographic Imaging Developments at the PSICHE Beamline, *Integr. Mater. Manuf. Innov.* 8 (2019) 551–558. <https://doi.org/10.1007/s40192-019-00155-2>.
- [295] P. Vijayan, I.R. Willick, R. Lahlali, C. Karunakaran, K.K. Tanino, Synchrotron Radiation Sheds Fresh Light on Plant Research: The Use of Powerful Techniques to Probe Structure and Composition of Plants, *Plant Cell Physiol.* 56 (2015) 1252–1263. <https://doi.org/10.1093/pcp/pcv080>.



CHAPTER II. General information on the main methods used



Graphical Abstract



1. Introduction

This chapter reports a simplified explanation of the techniques used and the parameters chosen to analyse the samples and the sample preparation. In each dedicated section of each chapter, the parameters that should have to be adjusted according to the sample and the calibration of each analysis session are reported. Besides, other characterisation techniques, which were occasionally used to examine the samples thanks to the collaboration with other external laboratories, will be described in each dedicated section.

2. Atomic Force Microscopy in Peak Force mode

The atomic force microscopy (AFM) is part of a large family of techniques regrouped under the name of scanning probe microscopies (SPMs). They all have in common the use of a sharp probe mounted on a micrometric cantilever to scan the sample surface [1]. The Peak Force quantitative nanomechanical property mapping (PF-QNM) mode is of particular interest for the present study.

A laser beam is focused on the probe mounted on a cantilever. During the scan of the sample surface, the cantilever is deflected due to attractive and repulsive interactions created between the surface and the probe. Consequently, the change in the reflection of the laser is then recorded by a 4-quadrant photodetector to measure cantilever bending and torsion (**Figures II-1a, b**).

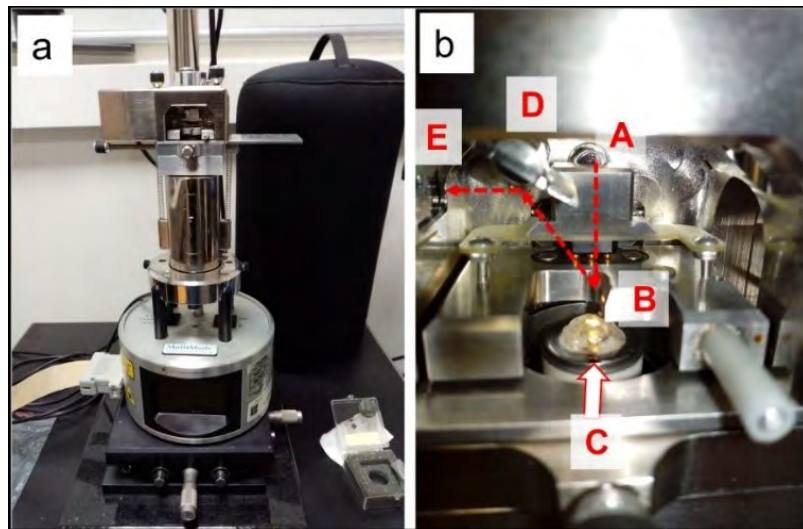


Figure II-1 a) AFM instrument Nanoscope 8 (Bruker) and **b)** focus on the sample-cantilever system and laser path. A = laser, B = cantilever with a RTESPA 525 probe mounted, C = sample, D = mirror to focus the laser into the photodetector, E = photodetector.

In AFM analysis, the cantilever deflection due to tip-sample interactions can be converted into a force-distance curve when the tip indents the surface. In PF-QNM, the recording of force-distance curves is performed at a high rate (2 kHz) for a limited maximum load and, thus, a limited indentation depth (on the order of a nanometre in this case). This method is similar to the TappingMode™, where the time of contact between the sample and the probe is not continuous but limited so that probe wear is limited, maps can be obtained in a reduced time and a recorded force-distance curve at each pixel.

In complement to the topography, several mechanical parameters such as the adhesion and modulus can be extracted from the force-curve (**Figure II-2 and Figures II-3a, b**).

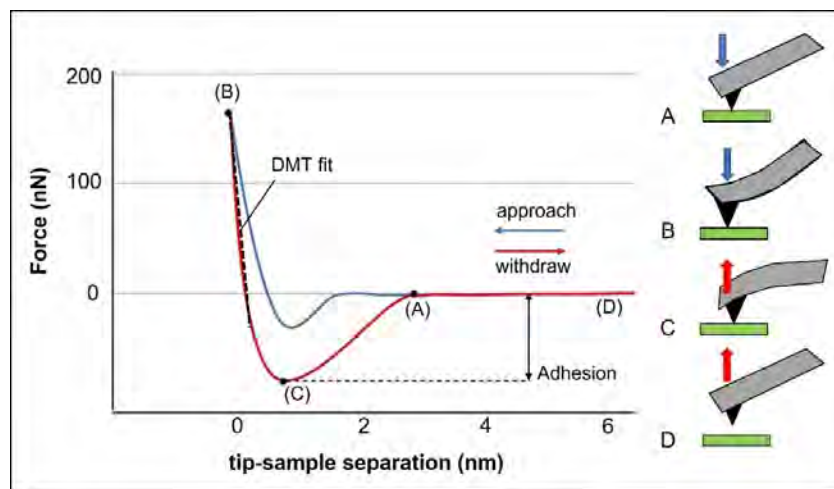


Figure II-2 example of a force-distance curve and relative information extracted at different moments of tip-sample interaction. Image inspired by [2].

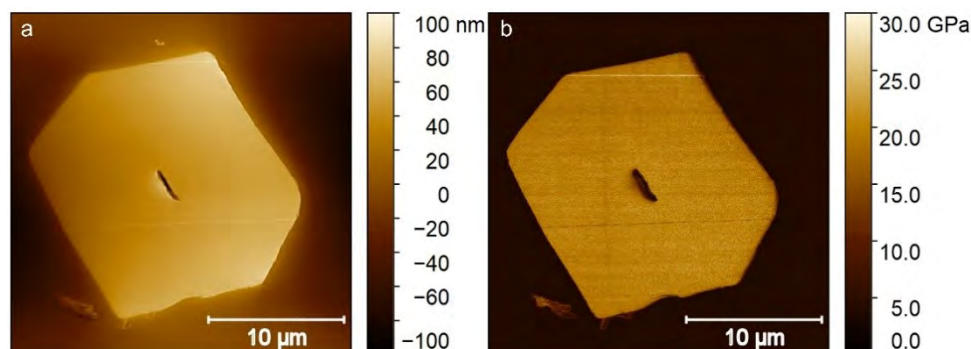


Figure II-3 topography (a) and indentation modulus (b) of an elementary flax fibre.

Several different probe tips and cantilevers can be selected and mounted to adapt the AFM to the expected modulus of the sample to investigate. Each cantilever is characterised by a spring constant (k) and each tip by a radius (R) whose combination is adapted to the sample stiffness, i.e., the stiffness of the cantilever sample must be in the same order of magnitude as the contact stiffness between the tip and the sample surface. Three examples of different probes with the relative range of moduli that can be investigated are reported in **Table II-1** [3].

Table II-1 comparison of three different probes provided by Bruker (CA, USA). Data from [3].

Sample modulus expected	Probe	Spring constant (k)	Tip radius (R)
200<E<2000 MPa	RTESPA-300	40 N/m	33 nm
1 GPa <E<50 GPa	RTESPA-525	200 N/m	33 nm
10 GPa<E< 100 GPa	Diamond probe (DNISP-HS)	450 N/m	40 nm

In the case of the study of plant cell walls, the probe used is a RTESPA 525 probe (Bruker, CA, USA), which is a silicon tip and cantilever with a (first) natural frequency in bending of 525 kHz and a small tip radius (generally around 33 nm at the beginning, but always less than 100 nm during the measurements).

The modulus from the plant cell walls can be extracted with several fitting contacts or indentation models. The tip apex, in this case, can be approximate as a sphere and the choice between the models to fit can be done thanks to the Tabor's parameter [4,5], which describes the ratio between the order of magnitude of the deformations of the sample surface, which is assumed in the normal direction and is related to the elastic modulus, and the spatial range of the interaction forces, i.e. adhesion forces, between the tip and the surface.

In the case of plant cell wall layers, there is a solid-solid adhesion with the tip [6,7]. The indentation depth is limited to the first 2–3 nm of the sample surface for the applied load, which is much less than the tip radius considered, while the adhesion force is small (few tens of nano-Newton) compared to the applied load (that in the case of the protocol used here, it is set at a maximum load of 200 nN). Thus, because both sample and tip are stiff, in the order of several GPa or higher, the adhesion forces that play a role are predominantly weak capillary forces, resulting in a small value of Tabor's parameter and allowing the use of the Derjaguin-Muller-Toporov (DMT) model (i.e., Hertz model including the effect of adhesion without any change in the contact behaviour because the adhesion forces are limited to the external zones of contact between the tip and the surface) [4–6,8] to process the force–distance curves and extract the indentation or reduced modulus.

The following equation (**Eq.II-1**) from [2] shows the relationship between the reduced modulus and Young's modulus in the case of an isotropic sample:

$$E^* = \left[\frac{1-\nu_s^2}{E_s} + \frac{1-\nu_{tip}^2}{E_{tip}} \right]^{-1} \quad (\text{Eq.II-1})$$

where E^* is the reduced modulus, ν_s and E_s are the Poisson's ratio and Young's modulus of the sample and ν_{tip} and E_{tip} are the Poisson's ratio and Young's modulus of the tip. The contribution of the tip is assumed to be negligible because its modulus is higher than the sample one. In the case of anisotropic materials, such as most of the wood cell wall layers that are transverse isotropic with a misalignment

angle (i.e., MFA), it is not possible to obtain a Young's modulus from the reduced, or indentation, modulus as this latter depends on several elastic constants (Young's and shear moduli, Poisson's ratios) [9–12]. Jäger *et al.* also concluded that the Poisson's ratios have a negligible effect on the indentation modulus calculated for typical wood cell walls [11]. Therefore, the Poisson's ratio was set to 0 in the AFM software to obtain the value of the indentation modulus.

It should be pointed out that the roughness of both sample and tip diminish the adhesion [4]. Furthermore, if the sample is highly rough and heterogeneous, the contact area between the sample and the tip, which ideally applies a load perpendicular to the sample surface, deviates from the ideal model and affecting the modulus calculated.

To calibrate the tip, it is necessary to calculate the cantilever's spring constant (k) first, and the Sader method is used thanks to the online application available in <https://sadermethod.org/> [13].

Successively the deflection sensitivity is calculated using a highly stiff sample, such as sapphire, that cannot be indented/deformed by the tip. The maximum load is chosen, which in this case was set to 200 nN as a trade-off to maximise the contact area and making the measurement stable enough to calculate the elastic modulus without damaging the cell walls or the tip. The tip radius is adjusted by using a standard sample with a well-known indentation modulus. The standard sample is dependent on the probe chosen and the sample to scan so that a standard sample with approximately the same range of moduli as those expected to be found in the real sample allows a better calibration.

For the analysis presented in this thesis, the probes were calibrated using highly oriented pyrolytic graphite (HOPG) of 18 GPa distributed by Bruker, or an internal standard of aramid fibres K305 Kevlar 21 Taffetas 305 g/m² (Sicomine epoxy systems-France) embedded in epoxy resin (Agar low viscosity resin (LV); Agar Scientific, UK) and appositely prepared like the flax samples. This second standard sample, with indentation moduli of the same order as the flax fibres cell walls, was previously measured by nanoindentation (24.3 ± 2.0 GPa and 5.4 ± 0.16 GPa for the centre of aramid fibres and embedded resin, respectively), following the method in [12]. Once the calibration is completed it is possible to investigate the unknown sample.

A Multimode 8 atomic force microscope (Bruker, Billerica, Massachusetts, USA) was equipped with an RTESPA-525 probe (Bruker probes, Billerica, Massachusetts USA) and used to perform the analyses presented in this work, with an oscillation frequency of 2 kHz and an acquisition angle of 90° with respect to the sample surface. The gain was set in automated mode. The peak force amplitude and the image resolution were adjusted based on the sample investigated, while the maximum fast scan velocity was constantly set at 8 $\mu\text{m/s}$. Nanoscope analysis (Bruker) and Gwyddion (<http://gwyddion.net/>, [14]) software were used, the former principally for data acquisition and the latter for data treatment. All the analyses have been performed in a room under a controlled atmosphere ($T = 23 \pm 2$ °C; %RH = 50 ± 4 %).

Sample preparation

Because the probe has a small radius, the technique is susceptible to the roughness of the sample. Therefore, the sample must be prepared to obtain a surface as flat as possible, at the nanometre scale, and, for this reason, it is generally embedded in resin, such as London Resin (LR)-white acrylic resin, Agar epoxy or other suitable resins, to minimise the sample deformation during its cutting. An interesting work compares the impact of different resins in the moduli obtained from wood cell walls [15].

For the samples examined in this work, a low viscosity epoxy resin kit by Agar Scientific (UK) was chosen (**Figure II-4a**).

Successively, the samples embedded are put in an oven at 60 °C overnight to ensure the correct polymerisation of the resin (**Figure II-4b**). Then, the surface of the resin block with the sample embedded is cut by an ultramicrotome equipped with diamond knives (Diatome Histo for trimming and Diatome Ultra AFM for final cutting) in thin sections of approximative 50 µm and at reduced speed (~1 mm/s) in order to have a roughness of the surface in the order of a few nanometres (**Figure II-4c**).

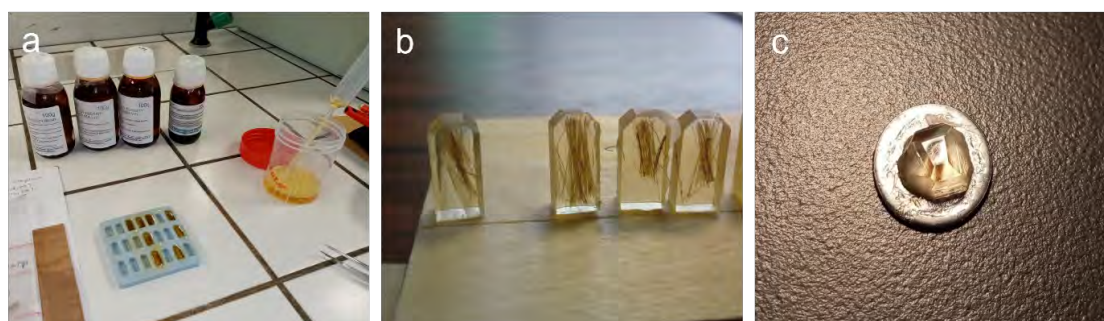


Figure II-4 resin and sample preparation **(a)** polymerised blocks **(b)** and sample prepared with a mirror surface **(c)**.

3. Second-harmonic generation imaging microscopy

Second-harmonic generation (SHG) is a coherent nonlinear optical phenomenon in which two photons, interacting with a nonlinear medium, are up-converted to a single photon with twice the incident frequency (2ω) as shown in **Figure II-5** [16,17]. This effect is possible provided that the sample has non-centrosymmetric molecules that can be polarised and that they are in a well-ordered structure. One of the main advantages of this technique, which is suitable to characterise biological materials, is the use of low energy excitation range (700–1000 nm) that reduces damages and photobleaching of the sample [18].

The SH signal is dependent on the wavelength of the laser pulse and its frequency. The second-harmonic generated has a wavelength equal to half of the wavelength chosen to excite the sample, and

the intensity is dependent on the pulse duration, which generates a higher SH when the duration is short [19,20].

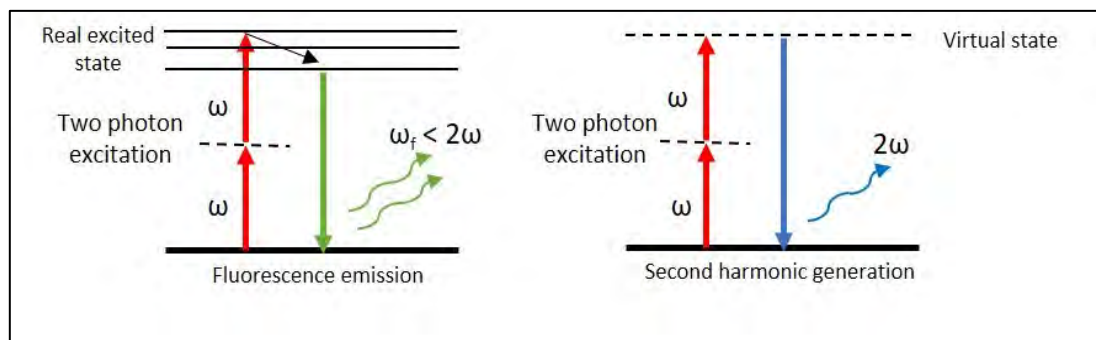


Figure II-5 On the left, the energy level diagram for fluorescence emission; on the right, the energy level diagram for second-harmonic generation. Inspired by Gauderon et al. [17].

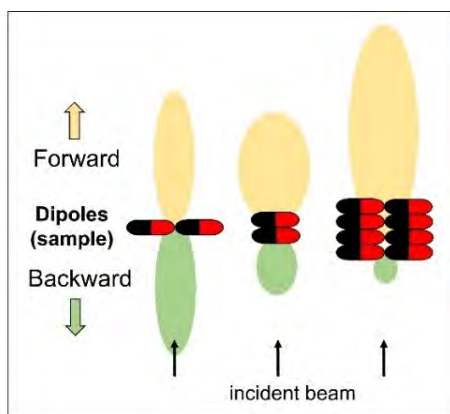


Figure II-6 Radiation pattern in backward and forward directions in different dipole arrays. Illustration inspired by Cox et Kable [18].

SH is generated in forward and backward directions. Although, in general, the forward direction shows the highest SH signal, the backward direction is used to obtain information on the sample structure by comparing the forward/backward radiations [21] or when the sample is too thick and the forward radiation cannot be detected. The well-known SHG radiation pattern is dependent on the dipole array (see **Figure II-6**).

Thus, the SH signal is dependent on many factors, including the polarisation of the light used for imaging and the organisation of the sample, such as the collagen fibres that form well-ordered structures and generate different intensity of SH signal according to the laser polarisation with respect to the orientation of the fibres [20]. Cellulose microfibrils in plant fibres show a similar behaviour of collagen fibres.

In the present work, a multiphoton Nikon A1 MP+ microscope (NIKON, France) equipped with a long working distance (LWD) 16x (NA 0.80) water immersion objective (NIKON, France) was used for the image acquisition, and a half-wave plate (MKS-Newport, USA) was rotated to change the laser

polarisation angle. The femtosecond laser used was a tuneable Mai Tai XF mode-locked Ti:sapphire femtosecond laser (SPECTRA PHYSICS, France), and an excitation wavelength of 810 nm was chosen. (The average power at 810 nm was 1.5 W.). All the tests were performed at a controlled temperature (21 °C), and **Figure II-7** illustrates the optical scheme of the microscope configuration.

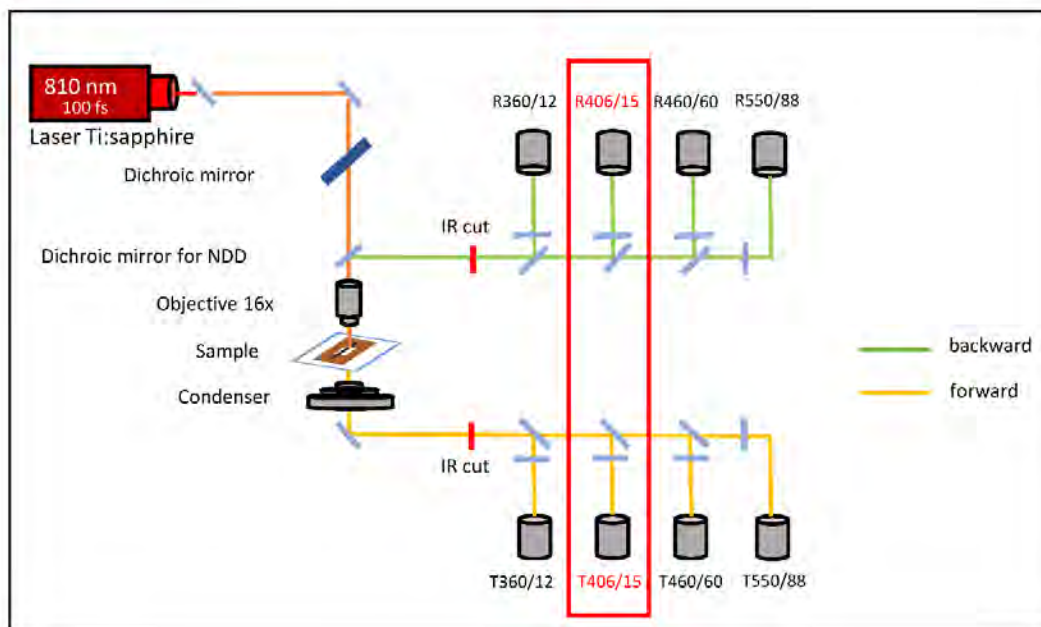


Figure II-7 Experimental setup of the multiphoton confocal microscope (NIKON, France). The two SHG channels are marked in red.

Both the backward and forward signals were collected with three bandpass filters at 460/60 nm (autofluorescence), 550/88 nm (autofluorescence) and 406/15 nm (SHG signal). GaAsP NDD (gallium arsenide non-descanned detectors) were used.

The first acquisitions were performed on flax fibres and cotton trichomes to establish the maximum average excitation laser power before damaging the surface by the laser beam. Furthermore, a series of images were acquired by changing the polarisation angle step by step with the half-wave plate (HWP) to find the polarisation degree that generates the highest intensity of the second-harmonic signal.

An average laser power percentage of 10% max was used for the acquisitions with a polarisation rotation step of 2°. However, damage due to the laser power was observed if the fibre had some thermolabile middle lamella pectic remnants on the surface in the case of under-retted fibres or the presence of small damages due to fibre extraction. Thus, to avoid any damage, the laser power was set at 5% for acquisitions obtained with a polarisation rotation step of 1°.

Successively, before sample experiment, a comparative test between flax fibres and maize starch grains was made. Microfibrils present in plant fibre ultrastructure are constituted of molecules of cellulose, which are non-centrosymmetric and generate second-harmonic emission that allows the study of plant cell walls [22]. Therefore, the specific structure and arrangement of cellulose within flax cell

walls fully justify the use of SHG for the investigation of the microfibril angle of plant fibres. However, because the SHG depends on the polarisation angle, a calibration method to define the polarisation at each sample plane at different angles in the polarised second-harmonic generation (P-SHG) technique had already been developed using starch granules [23,24].

Starch is mainly composed of amylopectins, amylose and other minor components, such as protein. Amylose is linear, while amylopectin has α (1–6) linked ramifications [25,26]. Consequently, in a starch grain, there are amorphous and semi-crystalline alternating layers called growth rings, and the radial distribution of amylopectins is the cause of the polarisation that can be detected with polarised light optical microscopy and P-SHG [23,24,27]. In **Figure II-8a**, a maize starch granule is illustrated, and the amylose and amylopectin structures are shown. Amylopectins are responsible for the SHG signals due to the crystallites arranged in a double helix structure [25]. Thus, a maize starch granule, accurately selected with a shape approximated as a sphere, can generate an SHG signal at each polarisation angle [24], allowing us to calibrate the laser polarisation at the sample plane (**Figure II-8b**).

Two steps were used for this experiment, and the rotation range of the half-wave plate was from 0° – 135° (step of 1°)/ 0° – 68° (step of 2°) for vegetal fibres and 0° – 190° (step of 1°)/ 0° – 68° (step of 2°) for the calibration with the maize starch grains. The scan line average was 8, the scan velocity was fixed at 1 (fps), and the scan size was 512×512 pixels. The software used for the imaging acquisition was NIS elements (NIKON, France), and the software used for the image processing was ImageJ (National Institute of Health, USA) [28].

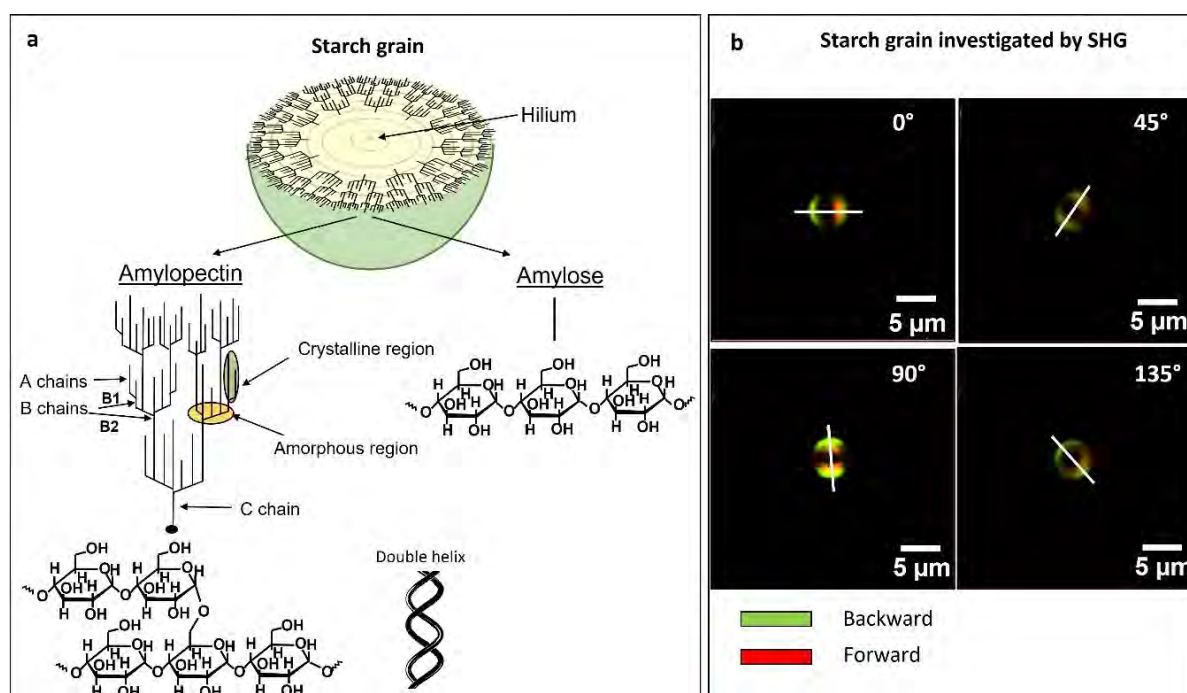


Figure II-8 a) Schematic structure of a starch grain, inspired by [26,29]; **(b)** Second-harmonic generated by an approximately spherical maize starch grain at controlled polarisation angle. The starch grain can generate second-harmonic at each polarisation angle, based on the laser position.

Sample preparation

Another advantage of the second-harmonic generation microscopy is that it does not require particular sample preparation, except for the thickness of the samples that can interfere with the generation of the second-harmonic in the forward direction.

Since plant fibres, such as flax fibres, are generally in the order of 20–30 μm thick, they can be examined without further manipulation. On the contrary, cross-sections of stems and wood tissues must be cut with a thickness of about 10–20 μm to be studied.

Each fibre or fibre bundle extracted from the samples investigated was directly mounted on a 150 μm thick paper support, commonly used for single fibre tensile tests (**Figure II-9a**) and the sample was placed between two coverslips to improve the observations and tuning of the microscope. **Figure II-9b** shows a single flax fibre glued on paper support commonly used for tensile tests according to ASTM C1557 [30] and the sample under the microscope (**Figure II-9c**).

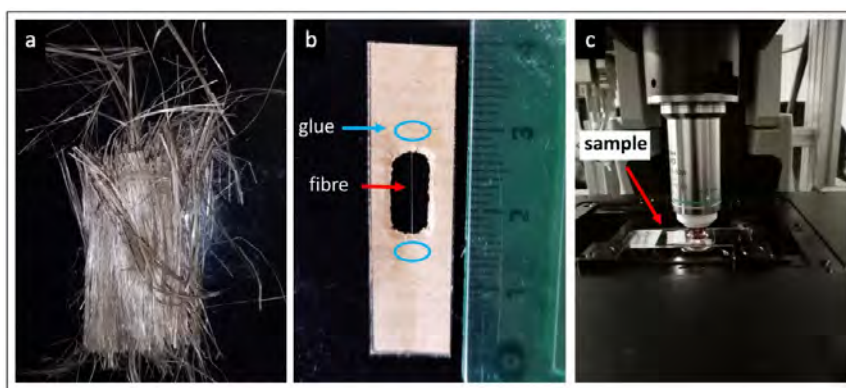


Figure II-9 Raw flax fibres (a), single flax fibre glued on a paper card for handling and testing (b) and SGH microscope (c).

4. DEEP-UV Fluorescence imaging and microspectroscopy

UV-visible excitation beam to obtain autofluorescence response from plant tissues has been widely used in the literature [31] and the reviews done by García-Plazaola *et al.* [32] and Donaldson [33] resume the fluorescence emission in plants.

Two different microscopes at Synchrotron SOLEIL (Source Optimisée de Lumière d'Energie Intermédiaire du LURE) (Gif-sur-Yvette, France), DISCO beamline, were used to obtain different information: a full-field microscope, called TELEMOS, that allows multispectral fluorescence imaging analysis and an inverted microscope adapted to perform scanning fluorescence microspectroscopy, called POLYPHEME (**Figure II-10**)

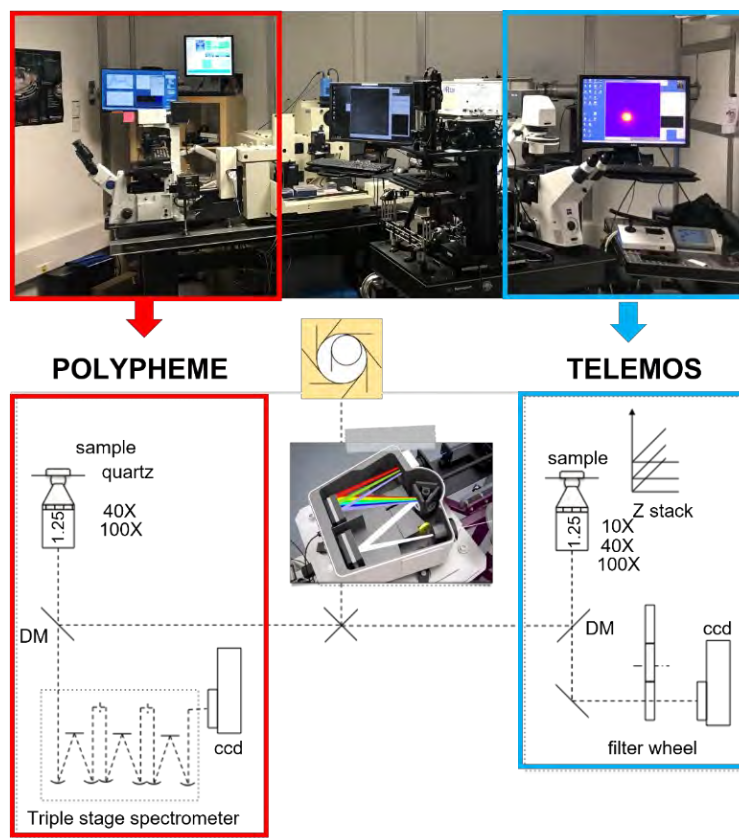


Figure II-10 Schema of the two microscopes at Synchrotron SOLEIL, POLYPHEME and TELEMOS respectively [34,35]. (©Frédéric Jamme, DISCO beamline).

4.1 TELEMOS parameters

The excitation wavelength used was in the deep UV range (275 nm), extracted from the white beam and monochromatised, thanks to a Czerny-Turner monochromator (iHR320, Jobin-Yvon, France) before reaching the end-stations, as described in [34–36]. The entire beamline is fully described in [37]. TELEMOS is a full field Axio Observer Z1 inverted microscope (Carl Zeiss GmbH, Germany) modified with quartz optic and equipped with a dichroic mirror at 300 nm (Omega Optical Inc., Brattleboro, USA), which allows the reflection of the excitation wavelength at 275 nm and cutting all the wavelengths above 300 nm, a back-illuminated CCD 16-bit camera (Pixis BUUV, Princeton Instrument, USA) and a motorised sample plate (MS-2000 XY, Applied Scientific Instrument, USA), which allows movements in the X- and Y-axes. The Z-axis is directly controlled by the microscope. More details about the equipment can be found in [34,36,38,39]. Specific objectives for UV transmission, 10x (N.A. 0.2) and 40x (N.A. 0.6) Ultrafluar (Zeiss) with chromatic correction were used to investigate the samples.

Three different passband filters at 327–353, 420–460, and 480–550 nm (Semrock, Rochester, USA) were used in this work to obtain information about: 1) protein, by probing their tyrosine and tryptophan amino acids, 2) small phenolic compounds called hydroxycinnamates (ferulic, *p*-coumaric and sinapic

acids), and 3) lignin, as a polymer composed of 3 phenyl propanoid units (G, H and S) respectively [38]. Time and offset for image acquisition were adjusted according to the objective used (**Table II-2**).

Table II-2 Deep UV acquisition parameters with TELEMOS microscope and possible attributions.

Filter	Acquisition time (s)	Objective	Main attribution	Channel
327–353 nm	8 sec	x10	proteins	Red
	20 sec	x40	(Tryptophan and Tyrosine)	
420–460 nm	8 sec	x10	Phenolic compounds	Green
	8 sec	x40	(hydroxycinnamic acids)	
480–550 nm	8 sec	x10	Lignin	Blue
	8 sec	x40	(phenylpropanoid units)	

The acquired images must be corrected to quantitatively calculate the fluorescence intensity. **Eq.II-2** is used to normalize the grey level to eliminate the variations linked to the CCD camera for each filter and acquisition time, as well as the heterogeneity of the intensity linked with the laser beam:

$$I_c = \frac{I_r - D_{(f,t)}}{W_{(z)} - D_{(w)}} \quad (\text{Eq.II-2})$$

where I_c is the grey level in the corrected image, I_r is the level in the raw image acquired, $D_{(f,t)}$ is the “dark” level of the camera acquired depending on the filter used and the acquisition time, $W_{(z)}$ is the “white” level of the beam without filters depending on the Z stack position and objective used and $D_{(w)}$ is the “dark” level acquired to record the noise of the instrument without any filter [39]. To perform the ‘white’ level, a small window of luminescent reference compound (Nd-YAG crystal) using only the dichroic mirror without any filter was used as a reference.

The images acquired were ultimately processed using ImageJ/Fiji software [40,41]. Segment and area tools were used to select ROI and calculate the intensity of each filter in regions of the image where the beam intensity is focused, i.e. the centre of the image.

4.2 POLYPHEME parameters

POLYPHEME is an Olympus IX71 inverted microscope modified with a quartz optic suitable for deep UV (DUV) spectroscopy equipped with a triple monochromator (T64000, Jobin-Yvon) in subtractive mode to suppress Rayleigh scattering and another 280 nm beam splitter. To collect spectra, an iDus CCD detector (Andor) was used (Peltier cooling to -70 °C). The detector is a 1024x256 pixel

with 26x26 μm pixels [34]. The objective used was a 40x Ultrafluar (Zeiss) objective with N.A. 0.6 and a laser spot diameter of approximately 4 μm (**Figure II-10**).

Before collecting the spectra, a calibration using the Nd-YAG crystal was performed. Due to limited time, only two cross-sections, one drought and one control, were examined under POLYPHEME. After acquisition, the spectra were processed using LabSpec 6 (Horiba Scientific) software and a program file written in MATLAB, Polypheme v2.0. Each spectrum was cut in the range of 294–529 nm. A correction of dead pixels at 323.7–323.2 nm was performed followed by spike correction. No smoothing operation was performed. Subsequently, MATLAB was used to calculate the principal component analysis after concatenating the two images acquired from the two different samples, and spectra were normalised using a unit vector ($\frac{x}{\sqrt{S^2}}$). The ‘modelling’ tool of LabSpec 5 (Horiba Scientific) software was successively used to create a normalised model where the score combination reached 100% by selecting three components identified as the three main signals of the spectra at approximately 335, 415 and 500–530 nm, obtaining separate cartographies of protein, phenolics and lignin.

Sample preparation for DEEP-UV analyses

To investigate the samples by deep-UV multi-spectral fluorescence imaging or microspectroscopy, the sample thickness must be limited to 10 μm . Since paraffin does not fluoresce, it can be used as a medium to include the samples successively cut under microtome to reach the right thickness. Further details of the method used to prepare the samples studied in this work can be found in **Chapter V**.

Bibliography

- [1] R.G. Reifenger, *Fundamentals of atomic force microscopy*, World Scientific, Hackensack, New Jersey, 2016.
- [2] B. Pittenger, N. Erina, C. Su, Quantitative mechanical property mapping at the nanoscale with PeakForce QNM, *Bruker Application Notes* 128, 1 (2010) 1–11.
- [3] Bede Pittenger, D.G. Yablon, Improving the Accuracy of Nanomechanical Measurements with Force-Curve-Based AFM Techniques, *Bruker Application Notes* 149. 1 (2017) 1–7.
<https://doi.org/10.13140/RG.2.2.15272.67844>.
- [4] D. Tabor, Surface Forces and Surface Interactions, in: M. Kerker, A. C. Zettlemoyer, R. L. Rowell (Eds.) *Plenary and Invited Lectures*, Academic Press, 1977: pp. 3–14. <https://doi.org/10.1016/B978-0-12-404501-9.50009-2>.
- [5] K.L. Johnson, J.A. Greenwood, An Adhesion Map for the Contact of Elastic Spheres, *J. Colloid Interface Sci.* 192 (1997) 326–333. <https://doi.org/10.1006/jcis.1997.4984>.
- [6] B.V. Derjaguin, V.M. Muller, Y.P. Toporov, Effect of contact deformations on the adhesion of particles, *J. Colloid Interface Sci.* 53 (1975) 314–326.
- [7] D. Xu, K.M. Liechti, K. Ravi-Chandar, On the modified Tabor parameter for the JKR–DMT transition in the presence of a liquid meniscus, *J. Colloid Interface Sci.* 315 (2007) 772–785.
<https://doi.org/10.1016/j.jcis.2007.07.048>.
- [8] R.C. Germanicus, D. Mercier, F. Agrebi, M. Fèbvre, D. Mariolle, P. Descamps, P. Leclère, Quantitative mapping of high modulus materials at the nanoscale: comparative study between atomic force microscopy and nanoindentation, *J. Microsc.* 290 (2020) 51–62. <https://doi.org/10.1111/jmi.12935>.
- [9] J.J. Vlassak, M. Ciavarella, J.R. Barber, X. Wang, The indentation modulus of elastically anisotropic materials for indenters of arbitrary shape, *J. Mech. Phys. Solids.* 51 (2003) 1701–1721.
[https://doi.org/10.1016/S0022-5096\(03\)00066-8](https://doi.org/10.1016/S0022-5096(03)00066-8).
- [10] A. Delafargue, F.-J. Ulm, Explicit approximations of the indentation modulus of elastically orthotropic solids for conical indenters, *Int. J. Solids Struct.* 41 (2004) 7351–7360.
<https://doi.org/10.1016/j.ijsolstr.2004.06.019>.
- [11] A. Jäger, Th. Bader, K. Hofstetter, J. Eberhardsteiner, The relation between indentation modulus, microfibril angle, and elastic properties of wood cell walls, *Compos. Part A Appl. Sci. Manuf.* 42 (2011) 677–685. <https://doi.org/10.1016/j.compositesa.2011.02.007>.
- [12] O. Arnould, D. Siniscalco, A. Bourmaud, A. Le Duigou, C. Baley, Better insight into the nano-mechanical properties of flax fibre cell walls, *Ind. Crops Prod.* 97 (2017) 224–228.
<https://doi.org/10.1016/j.indcrop.2016.12.020>.
- [13] J.E. Sader, R. Borgani, C.T. Gibson, D.B. Haviland, M.J. Higgins, J.I. Kilpatrick, J. Lu, P. Mulvaney, C.J. Shearer, A.D. Slattery, P.-A. Thorén, J. Tran, H. Zhang, H. Zhang, T. Zheng, A virtual instrument to standardise the calibration of atomic force microscope cantilevers, *Rev. Sci. Instrum.* 87 (2016) 093711.
<https://doi.org/10.1063/1.4962866>.
- [14] D. Nečas, P. Klapetek, Gwyddion: an open-source software for SPM data analysis, *Centr. Eur. j. Phys.* 10 (2012) 181–188. <https://doi.org/10.2478/s11534-011-0096-2>.
- [15] R. Coste, M. Soliman, N.B. Bercu, S. Potiron, K. Lasri, V. Aguié-Béghin, L. Tetard, B. Chabbert, M. Molinari, Unveiling the impact of embedding resins on the physicochemical traits of wood cell walls with subcellular functional probing, *Compos. Sci. Technol.* 201 (2021) 108485.
<https://doi.org/10.1016/j.compscitech.2020.108485>.
- [16] R.W. Boyd, *The Nonlinear Optical Susceptibility*, in: R. Boyd (Ed.) *Nonlinear Optics*, 3rd edition, Academic Press, Rochester, New York USA, 2008: pp. 5–8.
- [17] R. Gauderon, P.B. Lukins, C.J.R. Sheppard, Optimization of second-harmonic generation microscopy, *Micron.* 32 (2001) 691–700. [https://doi.org/10.1016/S0968-4328\(00\)00066-4](https://doi.org/10.1016/S0968-4328(00)00066-4).
- [18] G. Cox, E. Kable, Second-Harmonic Imaging of Collagen, in: D.J. Taatjes, B.T. Mossman (Eds.), *Cell Imaging Techniques: Methods and Protocols*, Humana Press, Totowa, NJ, 2006: pp. 15–35.
https://doi.org/10.1007/978-1-59259-993-6_2.

- [19] F.S. Pavone, P.J. Campagnola, eds., *Second Harmonic Generation Imaging*, 1st edition, CRC Press, Boca Raton, 2013.
- [20] P.J. Campagnola, L.M. Loew, Second-harmonic imaging microscopy for visualizing biomolecular arrays in cells, tissues and organisms, *Nat Biotechnol.* 21 (2003) 1356–1360. <https://doi.org/10.1038/nbt894>.
- [21] O. Nadiarnykh, R.B. LaComb, P.J. Campagnola, W.A. Mohler, Coherent and incoherent SHG in fibrillar cellulose matrices, *Opt. Express.* 15 (2007) 3348–3360. <https://doi.org/10.1364/OE.15.003348>.
- [22] Z. Heiner, I. Zeise, R. Elbaum, J. Kneipp, Insight into plant cell wall chemistry and structure by combination of multiphoton microscopy with Raman imaging, *J. Biophotonics.* 11 (2018) e201700164. <https://doi.org/10.1002/jbio.201700164>.
- [23] N. Mazumder, J. Qiu, M.R. Foreman, C.M. Romero, P. Török, F.-J. Kao, Stokes vector based polarization resolved second harmonic microscopy of starch granules, *Biomed. Opt. Express.* 4 (2013) 538–547. <https://doi.org/10.1364/BOE.4.000538>.
- [24] S. Psilodimitrakopoulos, I. Amat-Roldan, S. Santos, M. Mathew, A. Thayil K. N., D. Zalvidea, D. Artigas, P. Loza-Alvarez, Starch granules as a probe for the polarization at the sample plane of a high resolution multiphoton microscope, in: A. Periasamy, P.T.C. So (Eds.), *Multiphoton Microscopy in the Biomedical Sciences VIII*, San Jose, CA, 2008: p. 68600E. <https://doi.org/10.1117/12.763168>.
- [25] V. Nessi, A. Rolland-Sabaté, D. Lourdin, F. Jamme, C. Chevigny, K. Kansou, Multi-scale characterization of thermoplastic starch structure using Second Harmonic Generation imaging and NMR, *Carbohydr. Polym.* 194 (2018) 80–88. <https://doi.org/10.1016/j.carbpol.2018.04.030>.
- [26] A. Raguin, O. Ebenhöf, Design starch: Stochastic modeling of starch granule biogenesis, *Biochem. Soc. Trans.* 45 (2017) 1–9. <https://doi.org/10.1042/BST20160407>.
- [27] S. Pérez, E. Bertoft, The molecular structures of starch components and their contribution to the architecture of starch granules: A comprehensive review, *Starch/Stärke.* 62 (2010) 389–420. <https://doi.org/10.1002/star.201000013>.
- [28] C.A. Schneider, W.S. Rasband, K.W. Eliceiri, NIH Image to ImageJ: 25 years of image analysis, *Nat. Methods.* 9 (2012) 671–675. <https://doi.org/10.1038/nmeth.2089>.
- [29] E.C. O'Neill, R.A. Field, Underpinning Starch Biology with in vitro Studies on Carbohydrate-Active Enzymes and Biosynthetic Glycomaterials, *Front. Bioeng. Biotechnol.* 3 (2015) 136. <https://doi.org/10.3389/fbioe.2015.00136>.
- [30] ASTM C1557-20, ASTM International, West Conshohocken, PA, 2020. <https://doi.org/10.1520/C1557-20>.
- [31] G.A. Wagnieres, W.M. Star, B.C. Wilson, In Vivo Fluorescence Spectroscopy and Imaging for Oncological Applications, *Photochem. Photobiol.* 68 (1998) 603–632. <https://doi.org/10.1111/j.1751-1097.1998.tb02521.x>.
- [32] J.I. García-Plazaola, B. Fernández-Marín, S.O. Duke, A. Hernández, F. López-Arbeloa, J.M. Becerril, Autofluorescence: Biological functions and technical applications, *Plant Sci.* 236 (2015) 136–145. <https://doi.org/10.1016/j.plantsci.2015.03.010>.
- [33] L. Donaldson, Autofluorescence in Plants, *Molecules.* 25 (2020) 2393. <https://doi.org/10.3390/molecules25102393>.
- [34] F. Jamme, S. Villette, A. Giuliani, V. Rouam, F. Wien, B. Lagarde, M. Réfrégiers, Synchrotron UV Fluorescence Microscopy Uncovers New Probes in Cells and Tissues, *Microsc. Microanal.* 16 (2010) 507–514. <https://doi.org/10.1017/S1431927610093852>.
- [35] F. Jamme, S. Kascakova, S. Villette, F. Allouche, S. Pallu, V. Rouam, M. Réfrégiers, Deep UV autofluorescence microscopy for cell biology and tissue histology, *Biol. Cell.* 105 (2013) 277–288. <https://doi.org/10.1111/boc.201200075>.
- [36] T. Séverin-Fabiani, *Imagerie de photoluminescence synchrotron pour l'étude de matériaux anciens semi-conducteurs, optique/photonique*, Université Paris-Sud, 2016.
- [37] A. Giuliani, F. Jamme, V. Rouam, F. Wien, J.-L. Giorgetta, B. Lagarde, O. Chubar, S. Bac, I. Yao, S. Rey, C. Herbeaux, J.-L. Marlats, D. Zerbib, F. Polack, M. Réfrégiers, DISCO: a low-energy multipurpose beamline at synchrotron SOLEIL, *J. Synchrotron. Rad.* 16 (2009) 835–841. <https://doi.org/10.1107/S0909049509034049>.

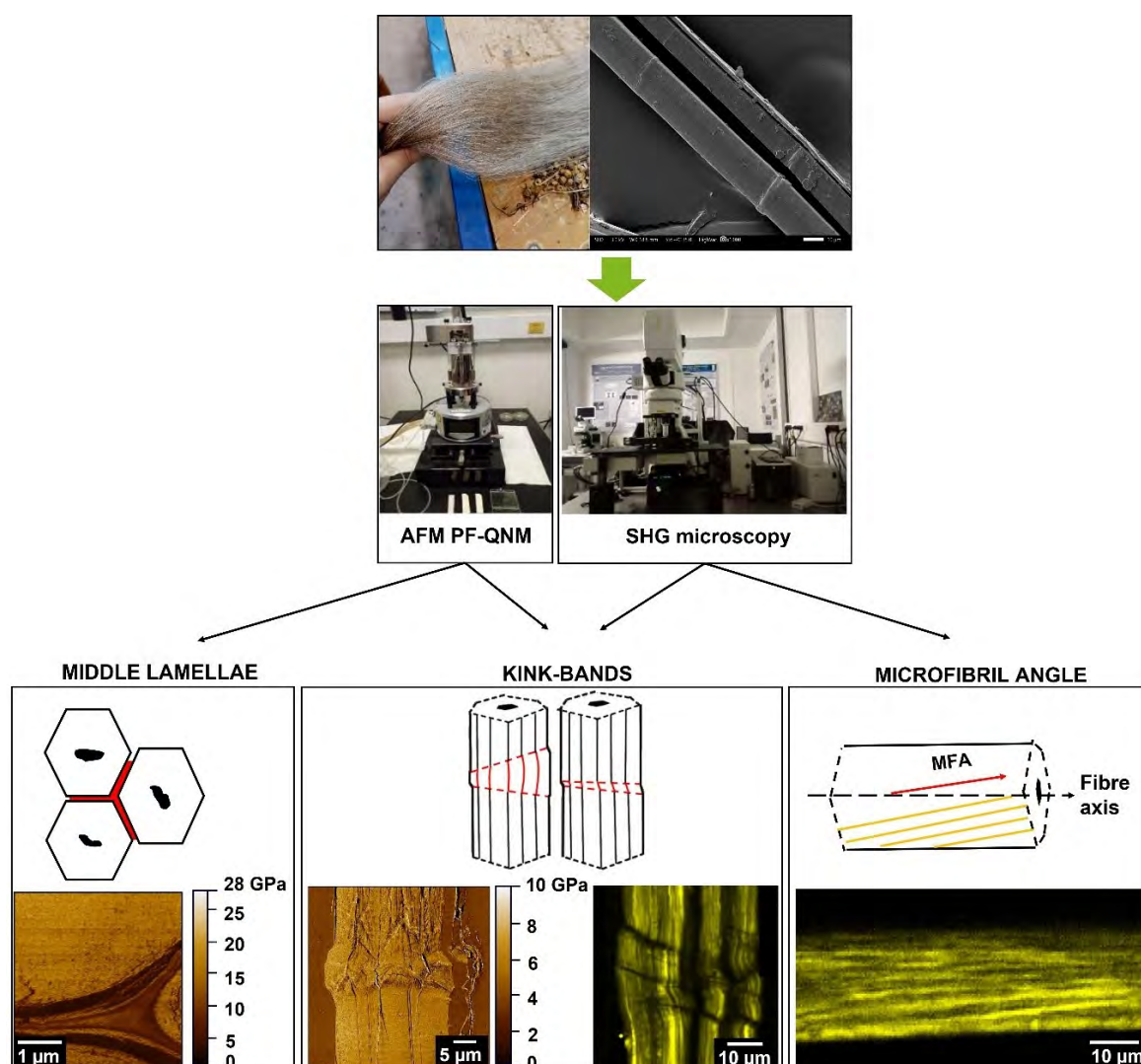
- [38] M.-F. Devaux, Synchrotron Time-Lapse Imaging of Lignocellulosic Biomass Hydrolysis: Tracking Enzyme Localization by Protein Autofluorescence and Biochemical Modification of Cell Walls by Microfluidic Infrared Microspectroscopy, *Front. Plant Sci.* 9 (2018) 16.
- [39] K. Vidot, M.-F. Devaux, C. Alvarado, S. Guyot, F. Jamme, C. Gaillard, R. Siret, M. Lahaye, Phenolic distribution in apple epidermal and outer cortex tissue by multispectral deep-UV autofluorescence cryo-imaging, *Plant Sci.*, 283 (2019) 51–59. <https://doi.org/10.1016/j.plantsci.2019.02.003>.
- [40] W.S. Rasband, ImageJ, National Institutes of Health, Bethesda, Maryland, USA, 1997. <https://imagej.nih.gov/ij/>.
- [41] J. Schindelin, I. Arganda-Carreras, E. Frise, V. Kaynig, M. Longair, T. Pietzsch, S. Preibisch, C. Rueden, S. Saalfeld, B. Schmid, J.-Y. Tinevez, D.J. White, V. Hartenstein, K. Eliceiri, P. Tomancak, A. Cardona, Fiji: an open-source platform for biological-image analysis, *Nat. Methods.* 9 (2012) 676–682. <https://doi.org/10.1038/nmeth.2019>



CHAPTER III. Investigation of the ultrastructure of flax fibres through advanced microscopic techniques



Graphical Abstract



A. Melelli, O. Arnould, J. Beaugrand, A. Bourmaud, The Middle Lamella of Plant Fibers Used as Composite Reinforcement: Investigation by Atomic Force Microscopy, *Molecules*. 25 (2020) 632.
<https://doi.org/10.3390/molecules25030632>.

A. Melelli, F. Jamme, D. Legland, J. Beaugrand, A. Bourmaud, Microfibril angle of elementary flax fibres investigated with polarised second harmonic generation microscopy, *Ind. Crops Prod.* 156 (2020) 112847.
<https://doi.org/10.1016/j.indcrop.2020.112847>.

A. Melelli, S. Durand, O. Arnould, E. Richely, S. Guessasma, F. Jamme, J. Beaugrand, A. Bourmaud, Extensive investigation of the ultrastructure of kink-bands in flax fibres, *Ind. Crops Prod.* 164 (2021) 113368.
<https://doi.org/10.1016/j.indcrop.2021.113368>.

1. The middle lamella of plant fibres used as composite reinforcement: investigation by atomic force microscopy

1.1 Introduction

In the last few decades, plant fibre-reinforced composites were progressively developed to replace composites where synthetic fibres are usually used or, in some cases, to create new families of composites having specific properties [1]. Their cost-effective production, low environmental impact, and specific mechanical properties, almost comparable to those of glass fibres, encourage industries to invest in this area [2,3].

Many plant species in nature produce fibres that can be employed for this purpose, but their structure, chemical composition, and properties differ greatly and depend on the type of plant [4–6]. An exhaustive summary of the plant fibres used for composite materials can be found in Bourmaud *et al.* [7]. The authors divided the fibres in wood and non-wood (e.g., bast), based on their location inside the plant. Bast fibres have high cellulose content, low microfibrillar angle (MFA), and consequently high mechanical performances in the fibre axis (or longitudinal) direction. Thus, they play a central role in new biocomposites, especially compared to leaf, xylem, or mesocarp fibres, and a clear example can be found in Wambua *et al.* [8]. The authors studied several poly-(propylene) composites reinforced with different plant fibres (sisal, kenaf, jute, hemp, and coir), and their results showed that coir fibres, extracted from seeds, have lower longitudinal mechanical properties than the others but, on the other hand, they exhibit a higher impact strength [8], which was also confirmed by Graupner *et al.* [9]. This result follows the functional evolution of the different types of cells in a plant; for example, bast fibres are responsible for the stiff structure of a plant and this specific role of mechanical support also explains their high mechanical performance.

Bast fibres have a similar ultrastructural model even if they originate from different plants. An elementary fibre is a single cell, and several fibres are linked to each other to form a bundle of several dozens of single fibres having a multilayer structure, as illustrated in **Figure III-1a** based on the flax fibre model generally used in the engineering domain: (1) the lumen is the central hollow part of the cell and its shape and diameter vary with the maturity of the plant and the environmental conditions during growth; (2) the secondary cell wall is the thickest layer, divided into two to three sub-layers (S_1 , S_2 or G , and S_3) rich in cellulose where the thinner and not always visible S_3 can also be assumed to be unmaturing G_n layer instead of a real S_3 [10]; (3) the primary cell wall is the external layer enriched in hemicelluloses, pectins, and lignin [11]. Between the fibres, there is another layer called middle lamella

(ML), which cements the primary cell walls of adjacent cells together and is mainly composed of pectic polysaccharides, lignin, and a small amount of protein [12–14]. This binder layer between two cells acts as a very thin and efficient interfacial matrix in the plant [13,15].

In biocomposites, the conventional interface level between a polymer matrix and plant fibres, which often coincides with the secondary wall, has been deeply investigated. However, middle lamellae are widely present in plant fibre composite materials due to the specific arrangement of the fibres in bundles in plants. The amount of middle lamellae depends on the retting process, the fibre extraction process and, when used in biocomposites, also on the material processing conditions that influence the shear rate and the temperature experienced by the fibres during composite processing [16–18].

Some studies demonstrated that this layer plays a central role in the mechanical behaviour of the final biocomposite product. Bourmaud *et al.* [19] noted several failure mechanisms in plant fibre biocomposite materials, and Monti *et al.* [20] showed that, in thermoset composites, cracks often propagate around the fibre bundles and through them, as illustrated in **Figure III-1b, c**. Recently, Beaugrand *et al.* showed that middle lamellae constitute an area of failure and that their behaviour is strongly related to their properties and cohesion with the fibres [21].

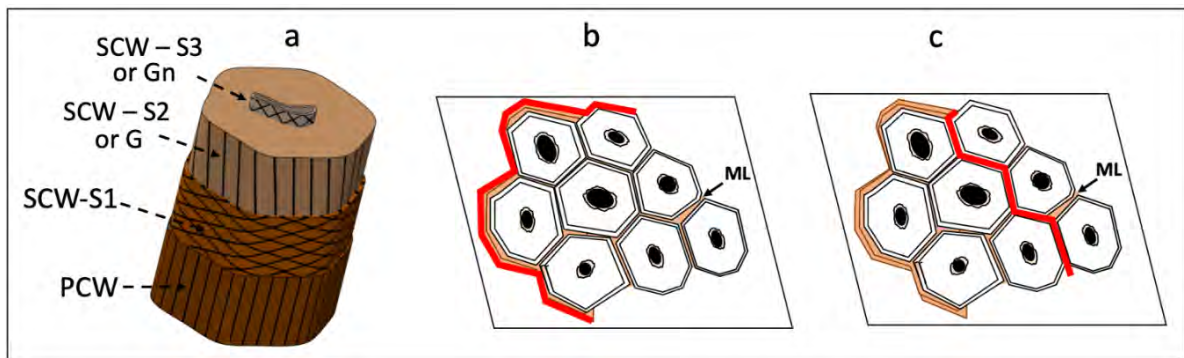


Figure III-1 *a)* Diagrams illustrating the structural arrangement of a single flax fibre from [7]; *(b)* a crack (in red) that propagates along the perimeter of a bundle and *(c)* through the bundle in a plant fibre-reinforced thermoset composite under tensile tests. SCW S_1 , S_2 or G, S_3 or Gn = secondary cell wall, PCW = primary cell wall, ML = middle lamella.

For a correct computational modelling of plant fibres, plant fibre bundles, and the mechanical behaviour of biocomposites, numerical values of mechanical properties of the middle lamella are required [22]. Some attempts were made to measure the mechanical properties of the ML of onion or flax cells using tensile tests [23,24], but this type of test remains challenging and difficult to interpret. Due to its reduced thickness in the order of the sub-micron, most of the measurements in the cell corner middle lamellae (CCML) were performed using micromechanical characterization techniques, such as nanoindentation, but, to the best of our knowledge, the studies are mainly limited to some wood samples [25–28]. In these cases, the average indentation modulus obtained ranges from around 5 to 11 GPa but with a generally high standard deviation.

Another technique used to investigate the middle lamellae is the atomic force microscopy (AFM) [28]. However, even though this technique is suitable for performing mechanical measurements in areas at the nanoscale level, like the CML layer, to the best of our knowledge, few researchers have focused on middle lamellae and often limited to wood using contact resonance-AFM (CR-AFM) [29,30] or AFM peak-force quantitative nanomechanical property mapping (PF-QNM) [31] with an average value ranging from 6 to 17 GPa, to bamboo with an average value around 14 GPa [32] or onion [23] obtaining moduli ranging from around 8 to 11 GPa. Nanoindentation and almost all the mechanical AFM methods make it possible to obtain an indentation modulus that depends on all the elastic constants of the material (Young's moduli, shear moduli, and Poisson's ratios) in a complex combination for materials with an anisotropic behaviour such as the secondary cell-wall layers [33,34]. However, in this case, middle lamellae can be considered as a material with an isotropic elastic behaviour as there are no microfibrils into their structure which is therefore quite random [35], and the indentation modulus depends on a single Young's modulus and a single Poisson's ratio.

In the case of an isotropic material, the indentation modulus M can be expressed according to the Hertz formula, $M = E/(1 - \nu^2)$, where E is the Young's modulus and ν is the Poisson's ratio. The Poisson's ratio of the middle lamella is not known but it should be lower than 0.5 like most amorphous polymer blends. Thus, in this case, the indentation modulus is quite close to the Young's modulus.

In previous papers, a protocol to study the mechanical properties of plant cells with the AFM PF-QNM method was already tested and the results were validated [36–39], and in the present section of this study, AFM PF-QNM was used to investigate middle lamellae. Thus, a set of plant fibres commonly used in biocomposites, i.e., flax, hemp, jute, kenaf, nettle, and date palm leaf sheath was investigated with the aim of creating a database of indentation moduli obtained from middle lamellae of different plant species and implementing the knowledge on this layer to help future computational modelling works.

1.2 Materials

Various plant fibres were considered to represent three of the main groups of fibres commonly used for biocomposite manufacturing, as reported in **Figure III-2**.

For flax (*Linum usitatissimum* L.), stems of the Eden variety cultivated in the year 2015 (Terre de Lin, Normandy, France) were chosen and cut after the first ramification (120 days) [38]. The nettle (*Urtica dioica*) samples were harvested in Lorraine (France) in 2014 and stored at room temperature in darkness; then, fibres were manually extracted. Hemp fibres from plants cultivated in 2016 (*Fedora 17* variety) in Bar-Sur-Aube (France) and field retted were chosen. Jute (*Corchorus capsularis* L) and kenaf (*Hibiscus cannabinus* L) fibres, provided by Derotex (Wielsbeke, Belgium), were grown in Bangladesh, and retted in water before being mechanically extracted from the stems; both were cultivated

in 2015 [36]. Date palm fibres (*Phoenix dactylifera* L.) were from Al-Ahsa (Eastern Province of Saudi Arabia), and the large bundle of the mesh surrounding the date palm tree stems were considered [40].

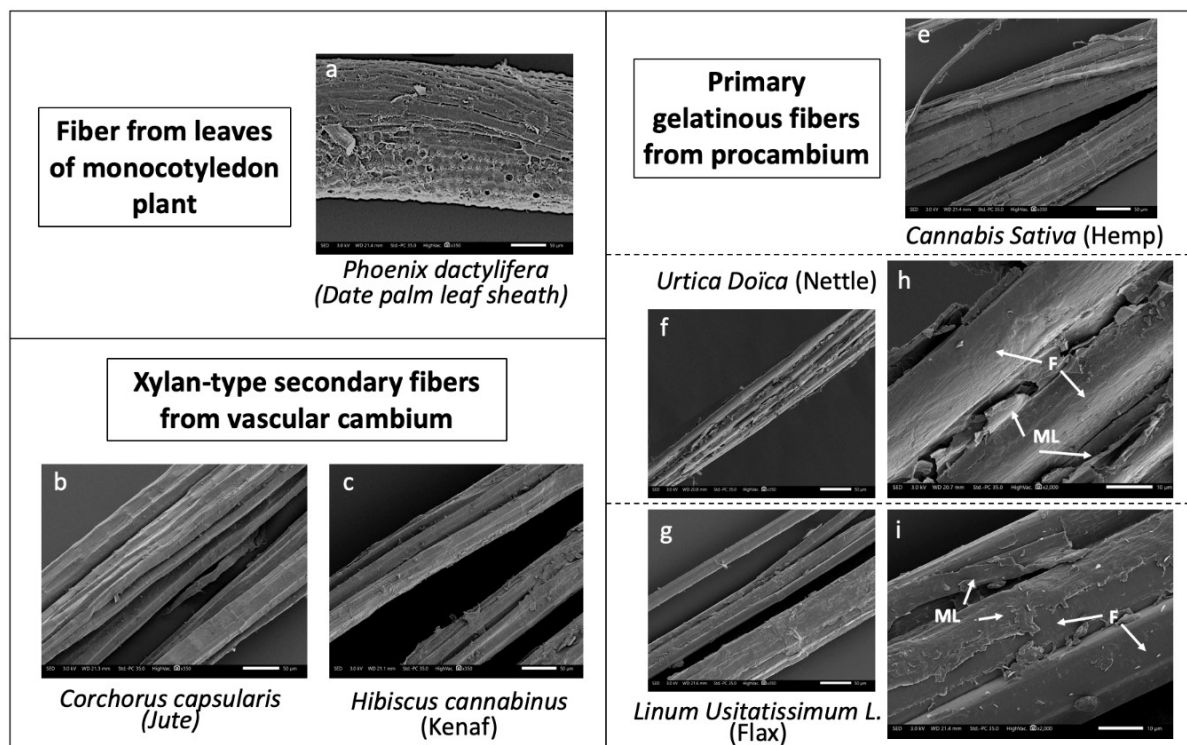


Figure III-2 SEM images and classification of date palm leaf sheath (a), jute (b), kenaf (c), hemp (d), nettle (e), flax (f) fibres investigated. (g) and (h) are zooms on middle lamellae area of nettle and flax, respectively (F = fibres, ML = middle lamella). Scale bars correspond to 50-µm lengths for all except (g) and (h) (10 µm).

All the samples were dried for 2 h in an oven at 60 °C to eliminate the moisture; then, they were dehydrated in a graded series of ethanol and included in London Resin (LR)-white acrylic resin. The final polymerization of the resin was made in the oven at 60 °C overnight. Further details on the sample preparation method can be found in **Chapter II**.

1.3 AFM investigations

AFM PF-QNM investigations were conducted with a tip radius between 15 and 50 nm for all the probes and the peak force amplitude was set to 75 nm. For each sample, 3–4 images were acquired with a verification of the value of the indentation modulus in the embedding resin, following the method in [39]. For further details, see **Chapter II**.

For each sample, some images were obtained at 512×512 pixels and other several images of 256×256 pixels were acquired and considered to have a good image resolution and a statistically significant average. A small area of each image was selected according to the morphology of the middle lamella, and only the cell corner (tricellular junctions) was considered, as shown in **Figure III-3**. A

mean of the indentation modulus of the selected area was calculated using the software's “statistical quantities” tool.

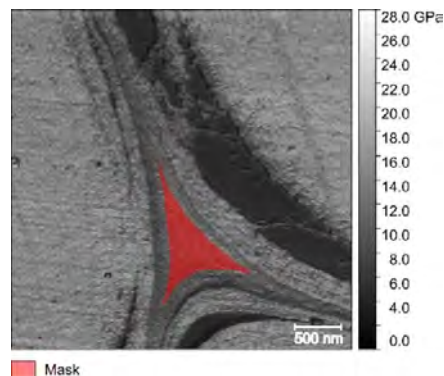


Figure III-3 Example of a flax middle lamella with a selected area masked to calculate the indentation modulus mean value and standard deviation.

1.4 Results and Discussion

Figure III-4 shows the topography and indentation modulus mapping obtained through AFM PF-QNM measurement of flax, nettle, jute, kenaf, hemp, and date palm fibres. These images provide values of the indentation modulus and information about the morphology of the middle lamellae. In the literature, the middle lamella (ML) is distinguished from the compound middle lamella (CML), especially referring to the wood cells [41,42], but this distinction is also applicable to other plant fibres [13]. In fact, the middle lamella between two primary cell walls of two different cells is often indistinguishable [13], and the small tripartite layer appears as a single layer, such as in **Figure III-4b** or **7a**, and consequently defined as compound middle lamella. Therefore, in the present research the indentation modulus was measured in the tricellular junctions, usually called the cell corner middle lamella (CCML), where the middle lamella is well discernible. Moreover, the biochemical composition of the CCML may differ from the ML [13].

In **Figure III-4a**, flax shows an interesting fracture (decohesion highlighted with white arrows), which probably occurred between the G and S₁ cell wall layers during the handling of the green flax stem. In several other images of the same section of the flax stem investigated, other cells showed this type of fracture between S₁ and G secondary layers, which was previously noted by Arnould *et al.* [39] and Goudenhoft *et al.* [38]. In addition, from Day *et al.*'s [43] pictures, it is possible to identify fractures, which occurred at the CML–S₁ or S₁–G level and their observations are in line with the results and conclusions reported in the present study. Le Duigou *et al.* [44] also observed peeling failures of the external fibre layer of flax fibres during a microdroplet debonding test, proving the low cohesion degree between structural layers.

Moreover, the images collected in the present study confirm the observations done by Zamil and Geitmann [13] and Raghavan *et al.* [15] in the ML and S_1 -G layers. In particular, the latter authors reported that the middle lamella is stronger than the primary or secondary cell wall layers and not damaged from a mechanical stretch; on the contrary, fractures take place in the adjacent primary or secondary cell-wall layers [15] and, thanks to our AFM analysis, in **Figure III-4a** it is possible to observe the damaged cell wall while the middle lamella remains intact. This fact reinforces the generally accepted assumption in the plant fibre community that the mechanical behaviour of the ML is far from the brittle behaviour associated with cell wall layers.

Middle lamellae in flax are well distinguishable and with an indentation modulus clearly lower than the other cell-wall layers, as can be expected given that middle lamella has a random organisation and composed of non-cellulosic polymers. For the same variety of flax investigated by our team [36,38], and although the measurements were done at a larger scale and not especially dedicated to the investigation of the ML, a similar contrast between values of indentation modulus obtained in G layer and ML was observed. Possible differences in thickness or arrangement of the ML area probably depend on the position of the fibres inside the same plant. In fact, as the lumen diameter and the cell wall thickness of flax fibres are influenced by the fibre position into the stem, it is possible to hypothesise that also the morphology, mechanical properties and biochemistry of middle lamella can change accordingly [45].

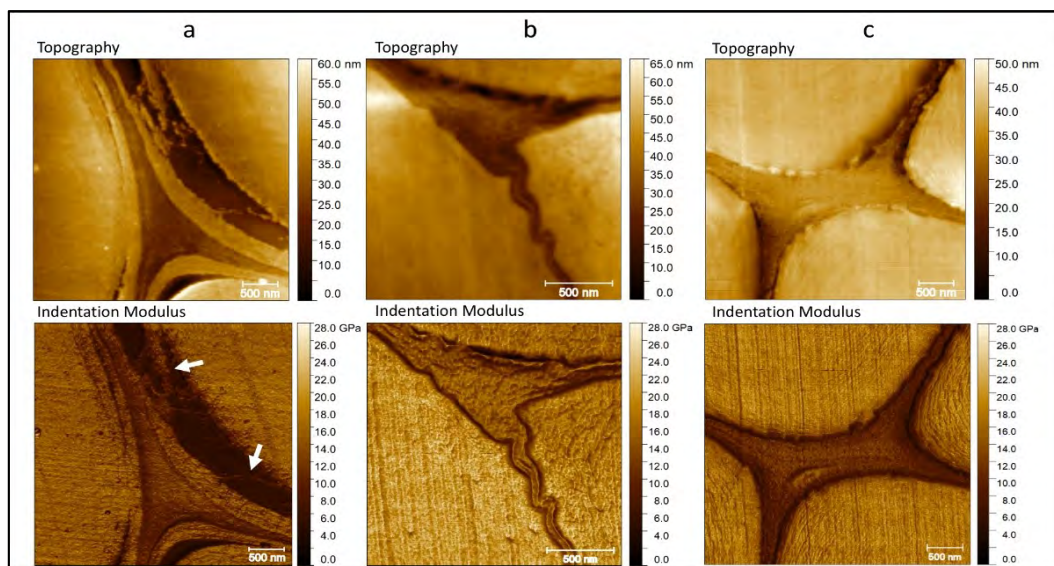


Figure III-4 Topography (top) and Indentation modulus (bottom) of the cell corners of **(a)** flax with illustration of decohesion (highlighted with white arrows) likely between S_1 and G cell wall layers; **(b)** nettle with values of indentation modulus close to the cell wall ones; **(c)** jute.

The middle lamella of nettle (**Figure III-4b**) clearly shows a high indentation modulus, almost comparable to the surrounding cell walls. In general, the indentation modulus is highly influenced by the anisotropic character of the considered material; thus, in this case, of quasi-isotropic non-cellulosic polymer (NCP) middle lamellae, the indentation modulus can be in the same range as the G layer, which

is underestimated due to the highly anisotropic nature of the secondary cell wall [33]. However, the indentation modulus in the middle lamella is remarkably high here and could be linked to a specific biochemical composition that should be investigated in future work.

The indentation modulus in the middle lamella is globally homogeneous, but one can note small areas where the indentation modulus is lower and other areas where it is higher, creating an irregular matrix like a grid or globular aspect. Considering the size of these nodules of a few tens of nanometers (**Figures III-5a, b** show zoomed-in view of the ML region, not corrected for the effect of tip dilation), they might be attributed to a high amount of lignin [31,46,47], or more likely to topographic effects that induce variations of the modulus measured in that area. As the roughness in that area is similar to the tip radius, it induces a strong correlation between the topography and the indentation modulus (**Figure III-5**), and consequently an apparently higher indentation modulus between two nodules and a lower one on top of them [48].

Bourmaud *et al.* [36] hypothesised that the degree of lignification is an important factor in the middle lamella morphology; however, although it is known in the literature that this layer is enriched in lignin, a direct quantification remains a challenge because of its sub-micrometric scale. Moreover, as previously mentioned, in nettle, the primary cell wall is not well distinguishable from the middle lamellae, and they appear as a single unitary layer between two fibres.

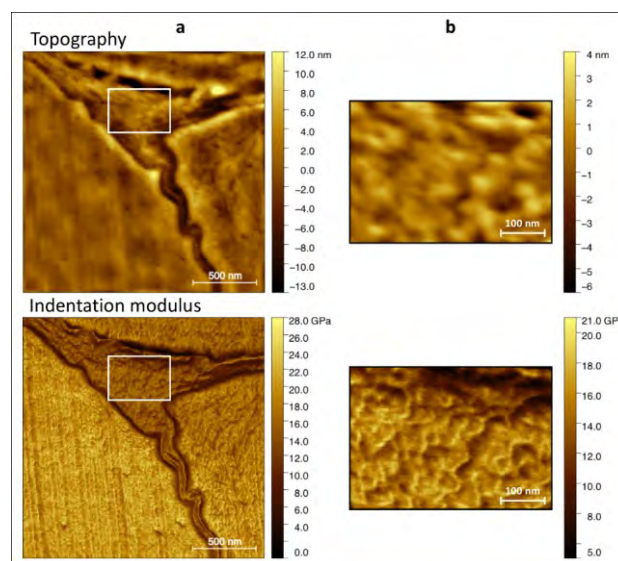


Figure III-5 (a) Surface topography and indentation modulus of nettle corresponding to those reported in **Figure III-4**. **(b)** Zoom of the ML region, corresponding to white rectangle in **(a)**, in order to highlight the correlation between topography and indentation modulus.

On the other hand, the middle lamellae of jute fibres are clearly distinguishable from the surrounding cell walls (**Figure III-4c**) thanks to their lower indentation modulus. In addition, the indentation modulus in CCML appears homogeneous with a fine texture that does not represent disconnections or asperities when compared with those of nettle. However, one can note that, in jute, there is a small

difference between the indentation modulus of the central area of the CCML and its edge (**Figure III-6**) that is not due to an effect of topography. The indentation modulus gradually increases from the edge to the centre of the tricellular junction; this singular phenomenon was noted on each jute CCML investigated but not for other middle lamellae investigated here, such as nettle and palm sheath fibres. The AFM PF-QNM method, thanks to its high resolution, is able to clearly highlight this type of gradient in a restricted area (**Figure III-6**), confirming its potential for ultra-local mechanical investigations.

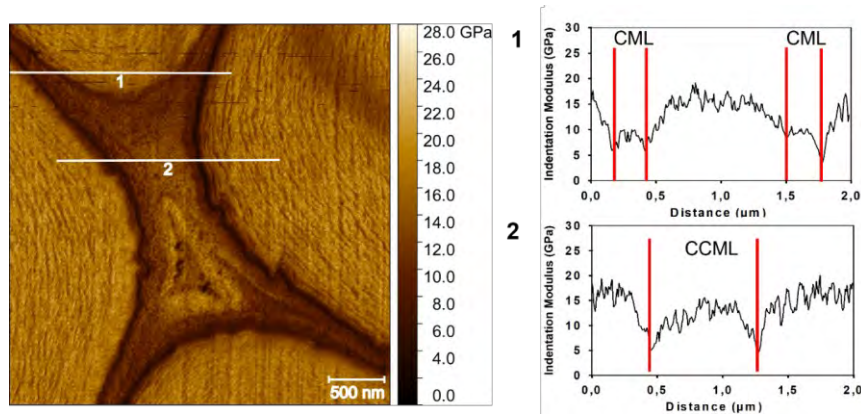


Figure III-6 Middle lamella cell corner in jute fibres. Two profiles (in white) are marked on the indentation modulus mapping and graphics extracted are shown on the right, respectively. The middle lamella cell corner (CCML) shows an increment of the values of indentation modulus from the edge, near the fibre cells, to the core.

In **Figure III-7a**, the primary walls of kenaf fibres show strong inhomogeneities with a globular aspect. In the present case, even more than in the nettle case, the nodules' topography induces a strong effect on the apparent indentation modulus. Moreover, the distinction between middle lamella and primary walls is difficult compared to other plant fibres.

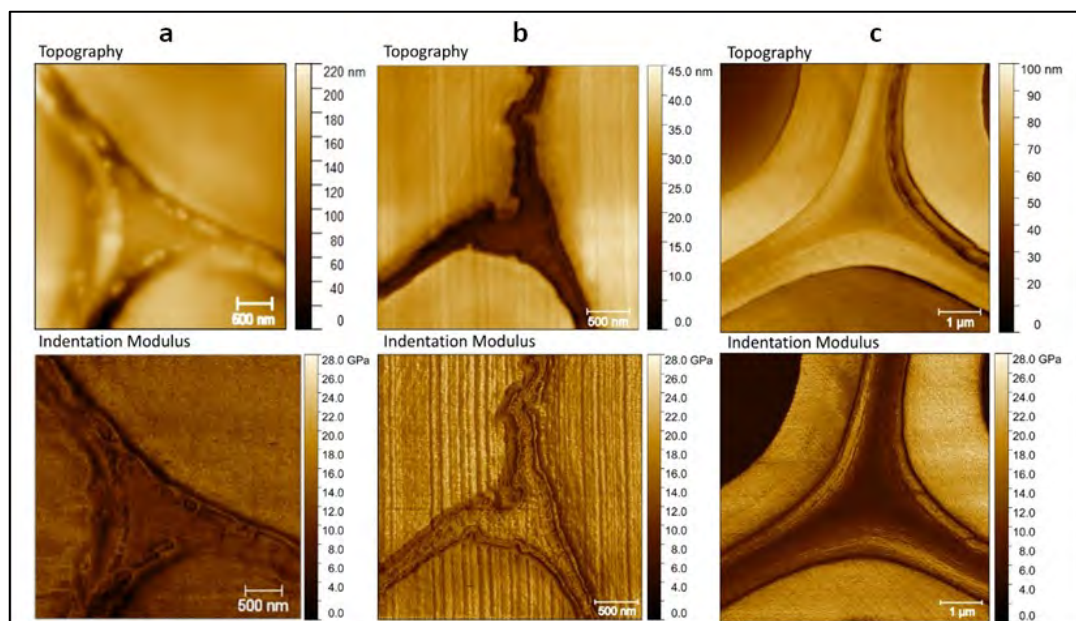


Figure III-7 Topography (top) and Indentation modulus (bottom) of the cell corners of (a) kenaf; (b) hemp that shows to have the highest indentation modulus and (c) date palm tree with the lowest indentation modulus but with a thicker and more homogeneous middle lamella.

The origin of these nodules is not clear but might be linked to the cutting behaviour and, therefore, to the mechanical properties of the different components of the cell wall layers during the sample surface preparation. Softer components make them harder to cut and leads to more irreversible deformation when cutting. These differences in behaviour induce variations in topography [29,49], such as steps between layers of the cell wall (as between S_1 and G layer or between G layer and the embedding resin) and roughness or nodules, as in the case of lignin, within a layer. However, biochemical investigations, like Raman or Infrared spectroscopy at cell level, e.g. by AFM-IR, must be done to better understand this phenomenon. **Figure III-7b** illustrates a tricellular junction between three hemp fibres. The middle lamella of hemp, together with the nettle, shows the highest values of indentation modulus that are also well correlated with values found by Bourmaud *et al.* [36] on several plant fibres studied by AFM PF-QNM mode. Nevertheless, both indentation modulus of middle lamella and fibre cell walls are high in nettle and hemp. The matrix inside the middle lamella of hemp is similar to the grid texture that was observed in nettle; however, in addition to this morphology and contrarily to the nettle, the primary cell wall is clearly distinguishable from the ML.

In **Figure III-7c**, date palm CCML has the lowest values and an extreme homogeneity of the indentation modulus with easily distinguishable layers. This is especially visible in **Figure III-8a-c** where the middle lamellae of kenaf and date palm fibres are highlighted and compared. Both graphical representations and distributions of the indentation modulus (**Figure III-8c**) underline significant differences in terms of indentation modulus between the two plants considered.

In kenaf (**Figure III-8a**), the non-uniformity of colour mapping clearly shows discontinuities with higher and lower values of the indentation modulus. These heterogeneities are partly due to a topography effect of the mechanical measurements caused by the huge globular aspect of the primary wall and possibly due to the cutting effects during the sample preparation between cell-wall layers or within a layer. Conversely, the indentation modulus in the date palm middle lamella is homogeneous, although the surface area analysed is larger than that for kenaf.

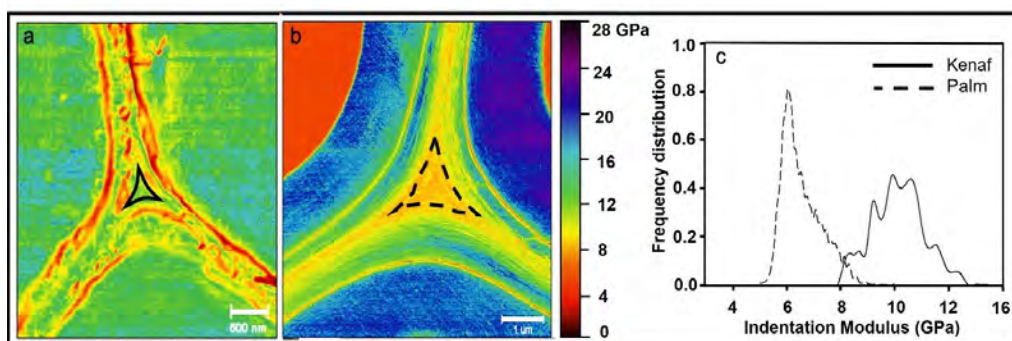


Figure III-8 (a) Kenaf middle lamella with a non-uniform indentation modulus; (b) date palm middle lamella with a more uniform indentation modulus distribution inside the middle lamella of the tricellular junction; (c) distribution of indentation modulus in middle lamella area of kenaf and palm, showing a high difference into spreading of values. The investigated area is highlighted using solid (kenaf) and dotted (palm) black lines.

For some fibres such as flax and palm, it is possible to trace and identify all the layers present in the fibre bundles, which are underlined thanks to their different modulus in **Figures III-9a, b**, highlighting the typical hierarchical structure. Average numerical values of the indentation modulus calculated in a selected area of each middle lamella are summarised in **Figure III-10** and **Table III-1** with their respective standard deviation.

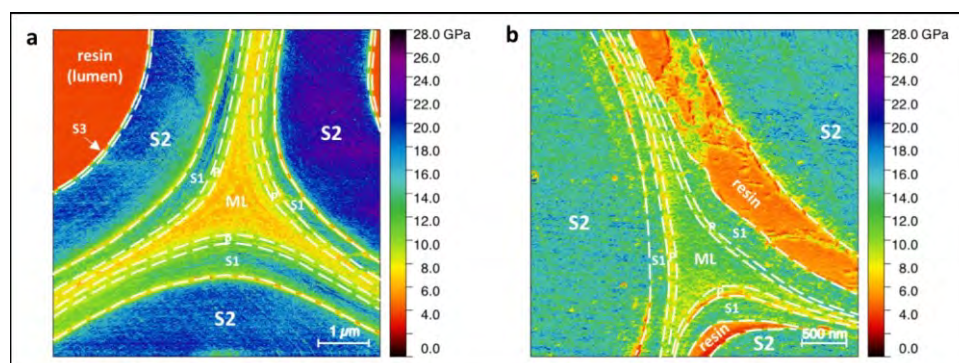


Figure III-9 **a)** date palm leaf sheath and **(b)** flax middle lamella area; limits between layers are clearly identified and highlighted by dot lines.

As previously mentioned, kenaf has the highest standard deviation since these measurements reflect the important inhomogeneity (see **Figure III-8a**) of the CCML region. Nevertheless, average values from flax, jute, and kenaf are comparable. Hemp and nettle have the highest indentation modulus for the middle lamellae. The morphology of these two ML is similar, probably because of the large amount of lignin. On the other hand, palm fibre CCML regions show the lowest indentation modulus. The different origin of the fibre elements is also visible in their overall chemical composition (**Table III-2**), which is related to their botanical functions or roles in the plant. Among the six plant species considered, some fibres ensure the role of conduction of raw or elaborated sap, while others support the stem and ensure its stability. For example, kenaf fibres are located in the bast (cortical layer) and core (woody) region.

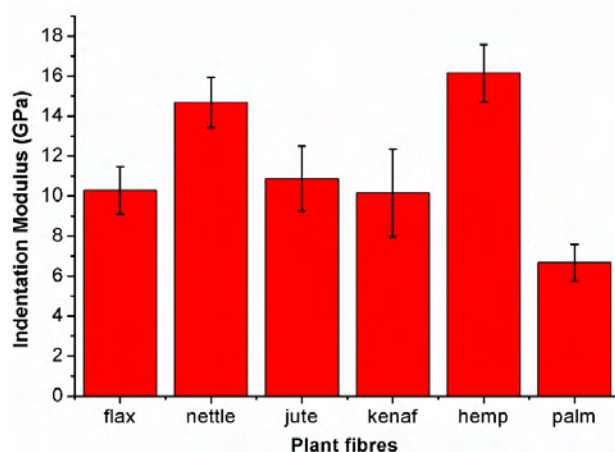


Figure III-10 Average values of indentation modulus calculated in each plant fibre middle lamella considered and respective standard deviation bars.

Table III-1 Mean and standard deviation of the indentation modulus obtained from the middle lamellae of the panel of the plant fibres considered.

Plant species	Indentation modulus (GPa)
<i>Linum usitatissimum</i> L. (Flax)	10.2 (\pm 1.2)
<i>Cannabis sativa</i> (Hemp)	16.1 (\pm 1.4)
<i>Corchorus capsularis</i> (Jute)	10.9 (\pm 1.6)
<i>Hibiscus cannabinus</i> (Kenaf)	10.2 (\pm 2.2)
<i>Urtica dioica</i> (Nettle)	14.7 (\pm 1.3)
<i>Phoenix dactylifera</i> (Date palm leaf sheath)	6.7 (\pm 0.9)

The bast fibres constitute around 40% of the total amount of the fibres. Primary phloic fibres (PPF) from procambium in the protophloem region and secondary phloic fibres (SPF) from cambium are both developed in both jute [50] and kenaf. Thus, in these two plants, the chemical composition of the fibres is highly dependent on the tissue from which they originate.

This type of cellular heterogeneity, in function of the tissue from which they arise, does not exist for flax and nettle, which have gelatinous and poorly lignified fibres that can be extracted only from the primary phloem region. In the case of hemp, a possible mix between primary and secondary fibres may occur; these two types of fibres have a role in the mechanical support of the plant. Consequently, their compositions and mechanical properties are fairly similar and the main difference is the length, which is significantly shorter for the secondary fibres because of their delayed growth that occurs after the structuration of the tissues.

Table III-2 Literature review of the biochemical global composition of the bundles of fibres studied, not reflecting the specific ML compositions.

Plant species	Cellulose (%)	Hemicellulose (%)	Lignin (%)	Reference
<i>Linum usitatissimum</i> L. (Flax)	60–85	14.0–20.6	1–3	[60–62]
<i>Cannabis sativa</i> (Hemp)	55–90	12	2–5	[63–66]
<i>Corchorus capsularis</i> (Jute)	58.0–71.5	13.6–24.0	11.8–16	[67,68]
<i>Hibiscus cannabinus</i> (Kenaf)	52.0–61.2	18.5–29.7	12.9–16.1	[69–71]
<i>Urtica dioica</i> (Nettle)	65.3–86.3	5.2–12.5	1.6–3.8	[72]
<i>Phoenix dactylifera</i> (Date palm leaf sheath)	34–45.1	27.7–28.9	16.9–18.2	[51,73]

For flax, hemp, and jute, middle lamellae are often reported as lignin-enriched domains, which are often highlighted to explain the mechanical stiffness and cohesion of the fibre bundles employed as composite reinforcement. Nevertheless, cell-wall lignification generally appears after seed maturity and can be strongly limited according to the cultivation management. For flax pulled out after flowering or seed maturity, Day *et al.* [43] reported a low lignin labeling in the CML area, absent in the cell corner and tricellular junctions, regardless of the epitope considered. The flax fibres investigated in the present study come from the plant stem and they were collected before the lignification of the middle lamella; in addition, no retting or scutching processes were performed contrary to the hemp fibres. In this case, the lignification and the retting effect could explain the higher indentation modulus of hemp fibres compared to flax.

As previously reported, the amount of lignin and the quality of links between the several layers influence the behaviour of the fibre bundles and, in the specific case of flax where decohesion between CML–S₁ or S₁–G level is noted, and these results are in line with the figure reported in Day *et al.*'s work [43]. These damages at the level of the middle lamella also have an impact on the biocomposite material when flax fibres are used as reinforcement. A second polymer well known to be an influent actor of the cell cohesion is the pectin family, precisely located in the ML. It has been demonstrated that the mechanical properties of the ML may vary with the degree of the esterified form of homogalacturonan [66]. This pectin is then more or less able to generate interchain interactions, for instance, by calcium cross-linking if homogalacturonans are de-esterified. From the panel of phenotype samples selected for this study, the backbone of the pectin methylation degree is arguably different, and some contrasting mechanical properties can be, therefore, expected due to susceptibility to cross-linking.

Dhakal *et al.* [37] investigated the damage mechanisms after impact testing on palm/PCL composites and they reported that, even after testing, the morphology of the date palm bundles remained unaltered. This is due to the high content in lignin and the homogeneity of the middle lamella (**Figure III-7f**) that strongly links the single palm fibres together, more than in other plant fibres, despite the soft middle lamella (**Figure III-10** and **Table III-1**). The silica-reinforced external paravascular or parafibrovacular parenchyma of palm bundles [40] is arguably too strong to be damaged, even after a high shear-rate process.

However, Baley *et al.* [67] observed an opposite behaviour of flax bundles used in a reinforced polyester composite and significant cracks were visible on the CML after transverse tensile tests. Indeed, the individualization of the fibres can be more or less pronounced, according to the process used to produce the composite material [18] and the scutching or hackling degree of the fibres [68] during the fibre extraction process. Consequently, all these factors can introduce significant changes in the mechanical performance of the final composite. Furthermore, when the composite contains a large number of flax fibre bundles, damage preferably occur in the bundles, and especially in the CML area, during loading [19,20]. In this case, the fibre–matrix interface is not the most critical, even when the polyolefin matrix, which has a weak fibre–matrix interface, is used. Thus, even if the indentation

modulus of flax ML is higher than the palm one (**Table III-1**), the individualization of flax fibres is facilitated thanks to the specific organisation of the bundles and preliminary action of retting and scutching.

However, as reported in Zamil et Geitmann's review [13], ML in flax are not directly involved in the failures, but the weak area seems to be between the different layers (S_1 -G) rather than in the middle lamella, even if ML exhibits a lower stiffness. A hypothesis for this result is that the softness and the cohesion of the ML are probably an advantage for the energy dissipation, and they limit the cell-wall damage during mechanical loading or shear rate stress. To support that assumption, a parallel can be done with the nacre, where the microstructure displays some homologies with the lignocellulosic bundles. Indeed, stiff and large structures of ceramic, as the fibre cell wall in the present study, are embedded in a thin and weak mortar made of unfolded protein and chitin biopolymers. The latter is the middle lamella of the bundles. During loading, in the nacre, the thin interface is able to deform, with most of the fracture occurring at the interfaces, providing more inelastic regions and favoring more energy dissipation and higher work of fracture, thereby giving nacre an elevated damage tolerance [69].

From the set of plant samples investigated in this study, palm sheath fibres, which have CCML with a lower indentation modulus, are probably less damaged in contrast to the flax fibres.

On the other hand, if we consider the jute fibres, it is clear that they have an indentation modulus similar to flax here investigated (see **Table III-1**), but their mechanical behaviour inside a composite material is very different. This is probably due to their high lignin content, as well as to their short length, and, as a consequence, high volume content of middle lamellae. The cohesion in bundles is strong, inducing a specific behaviour and a flow orientation in extrusion or injection molding [70]. Moreover, a high lignification is in favor of a good fibre-matrix interface, and Graupner *et al.* [71] noted that lignin may be an interesting adhesion promoter. Thus, flax, jute, and kenaf have similar CML indentation modulus (**Table III-1**), but their mechanical and morphological behaviour differs widely.

Finally, other fibres, such as hemp, have a strong tendency to be divided or fibrillated during the composite production process. This phenomenon was highlighted in extruded or injected compounds [72–74]. Interestingly, the difference between CML and G layer modulus is lower for hemp compared to other plants, and this might introduce a strong link between these two layers, whereby a weaker interface could possibly be identified at the intra G layer level.

Nevertheless, it is important to keep in mind that the morphology of the fibres may be involved in the breaking mechanism, and that the length of fibres and the ratio between the cell wall and lumen area may affect the critical shear rate, leading to irreversible damage. In addition, the indentation modulus is not necessarily correlated to the structural cohesion between layers, and the hardness investigated by the nano-indentation technique can be a better indicator even though it has a lower resolution than AFM PF-QNM. It is interesting to note that Wimmer *et al.* [28] studied the relationship between the longitudinal indentation modulus and hardness of CCML and S_2 in spruce wood, and they found a strong relationship between the indentation modulus of the CCML with its hardness, i.e., stiffer denoting

harder, unlike the S_2 . In this article, the indentation modulus of the CCML ranges from 4 to 12 GPa, whereas the hardness ranges from 0.12 to 0.47 GPa, with a mean value close to that of the S_2 . As the hardness depends on the inelastic behaviour of a material, it is linked to its plastic behaviour and property at break. If we assume that these results can be transposed here, it would mean that nettle and hemp fibre middle lamellae have a higher hardness in relation to a higher secondary wall longitudinal property, contrary to palm leaf sheath fibres. This seems to make sense mechanically, but needs to be confirmed by additional hardness measurements in the samples here investigated and mechanical strength tests of ML [23] or bioinspired films [31].

For this reason, the results presented here revealed huge differences in the indentation modulus of the middle lamella according to the plants considered, but it is difficult to correlate them directly to the differences in their mechanical behaviour or damage mechanisms when fibres are employed in biocomposites. In fact, these complex phenomena are impacted not only by the nature and cohesion of this middle lamella, but also by the morphology and the biochemical composition or structure of the fibres and bundles.

1.5 Conclusions

The results obtained in this section show differences in both the elastic mechanical behaviour and the morphology of the middle lamellae in fibre bundles from six different plants commonly used as biocomposite reinforcements: flax, hemp, jute, kenaf, nettle, and date palm leaf sheath. The AFM PF-QNM was used here as it is probably the only technique available today capable of providing semi-quantitative mechanical values of very thin layers at the nanoscale level, such as middle lamellae.

This allowed us to propose a comparative database of the indentation modulus of the cell corner middle lamella of the six plant fibres considered with three different groups: the first one (flax, jute and kenaf) with intermediate indentation modulus (on average between 8 and 12 GPa) close to values already obtained in previous studies on wood fibre middle lamellae, the second one (hemp and nettle) with very high values (in average between 13 and 17 GPa), surprisingly close to those of the secondary cell wall, and the last one (date palm leaf sheath) with low values (in average between 6 and 9 GPa), close to the lowest values obtained on wood fibre middle lamella. Moreover, the sample topography highlights morphological differences and heterogeneities between the middle lamella, as well as the primary and the secondary wall structure, with, on the one hand, very clear sublayers in the case of flax, date palm leaf sheath, and jute and, on the other hand, hardly distinguishable sublayers in the case of hemp and nettle with an irregular matrix like a grid for the cell corner middle lamella and sometimes a strong globular or nodular aspect for the primary wall in the case of kenaf.

The global biochemical composition or the origin and the role of each type of fibre in its respective plant does not completely explain the different type of CCML encountered here, and local biochemical

analysis will be necessary for the future. Nevertheless, the present results give complementary information for future modeling of plant fibre bundles and the design of better performing biocomposites. In addition to the semi-quantitative values provided, these results open new perspectives for future studies on the natural variability of the bundle intra plant (in the same stem all along its height) and inter plant (comparing similar locations in different stem samples) properties.

2. Microfibril angle of elementary flax fibres investigated with polarised second-harmonic generation microscopy

2.1 Introduction

Cellulose fibrils are cellulose crystallites assembled into longitudinal nanofibres, and hemicellulose and pectin glue several nanofibres together to form a single microfibril with a helical disposition [75–77]. The thickness of the layers and the orientation and morphology of the cellulose microfibrils vary between botanical species, as do the chemical composition and mechanical properties. For example, it is known that cotton trichomes have a microfibril angle of 25–30° in the S₂ layer [6,78], which is higher than that of flax. Moreover, the microfibrils in the G layer for flax have a diameter between 10 and 20 nm [79], and Ansell and Mwaikambo [6] reported that the thicknesses of cellulose microfibrils of different origin, for example, cotton or hemp, are of the same order of magnitude as that of flax.

Literature shows that plant fibres used for composite reinforcement exhibit strong differences into their intrinsic characteristics [80] and structure [7]. Chemical composition and structure of some varieties of flax were correlated with the mechanical properties [81]. The results showed a relationship between the MFA and Young's modulus, while there seems to be no correlation between the MFA and the strain at break of elementary fibres. Another study on hemp and sisal fibres highlighted the relationship of the MFA with the stress-strain curve, and the authors noted a linear trend for sisal (MFA=20°), while hemp has a less linear behaviour (MFA=10°) [82]. Thus, the MFA is strongly linked to the mechanical properties or behaviour of plant fibres and consequently to those of associated composites.

MFA of wood fibres has been extensively studied, from the role inside the plant to the mechanical properties correlated and the environmental impact on their variability [83]. This holistic review written by Donaldson offers a complete overview of MFA investigation methods; some, such as the pit method or confocal microscopy, are adapted to elementary fibres, but the most popular technique is X-ray Diffraction (XRD), despite it is mostly limited to fibre bundles. Thus, there is little information about the microfibril angle of bast fibres, particularly at the single fibre scale. In general, if the angle is too small, the resolution of the analytical techniques is often insufficient to evaluate it for an elementary fibre [81]. Nevertheless, Müller *et al.* successfully applied micro-small-angle X-ray scattering/wide-angle X-ray diffraction (μSAXS/WAXD) to elementary flax fibres [84,85]. In **Table III-3**, a summary of the MFA values found for flax fibres (measured at room temperature and relative humidity) are reported along with the method used. A more complete table with other methods used to evaluate

the microfibril angle of a range of plant fibres can be found in the chapter written by Ansell and Mwaikambo [6].

Recently, Wang *et al.* [86] mechanically removed the outer layer of flax fibre bundles to directly investigate the MFA by scanning electron microscopy (SEM) and X-ray diffraction (XRD); they reported MFA values between 5.8° and 7.3° , which is consistent with the literature data (**Table III-3**). They hypothesised that uncertainties in MFA values may be due not only to the use of fibre bundles but also to an additional signal induced by refraction effects at the fibre edge. Other differences in the MFA of flax were noted between dry and wet fibres and the results showed an increase in the angle when wet fibres were considered [87,85].

Table III-3 Some of the most used methods to calculate the microfibrillar angle of flax fibre elements.

Technique used	MFA of flax	References
μ SAXS	3.5° – 6.4°	[84,85]
SAXS	11°	[87]
XRD (Cu source)	6.2° – 9.5°	[86,81]
SEM/ESEM	5.8° – 10°	[86,88]

The development of new tools for material characterisation has provided the possibility of more accurately studying the ultrastructure of plant fibres. This is the case for second-harmonic generation (SHG) imaging, which can be considered as a new tool for accurately investigating the orientation of the microfibrils.

In the last decade, SHG imaging has emerged as a powerful tool in biology, and it has been applied to the study of collagen and in vivo samples [89–92]. In particular, in the study of rat-tendon fascicles, Goulam Housen *et al.* [93] concluded that a reconfiguration of the collagen microstructure occurs after mechanical tests (uniaxial tensile tests).

In plant research, some aspects have been already investigated using the second-harmonic generation imaging. Cellulose from two different organisms, the *Acetobacter xylinum* and the *Valonia* algae, can be detected thanks to the high SHG intensity due to the cellulose molecules that are chiral and in a well-ordered structure [94]. The same team also used the light polarisation control to investigate the dependence of the signal response of the cellulose microfibrils to the laser orientation and showed that this response is not linear, as expected from the nature of the SHG signal.

The objective of the study presented in this section is to estimate the MFA of single flax fibres using, unprecedented in the literature, a novel approach offered by the potential of SHG measurements. Detailed results are shown for flax fibres; besides, cotton trichomes were analysed due to the contrasted value of their MFA, which makes them clearly distinguishable from flax. The method is a direct

measurement of the MFA from an image of the cellulose microfibrils and showed heterogeneities of MFA that could be related to mechanical properties of the fibres.

2.2 Materials

Elementary flax fibres were extracted from a batch of the Bolchoï variety (year 2018, classification number 66233) cultivated in Normandy by the Depestele group. After growth, flax fibres were pulled out, dew-retted for 6 weeks and mechanically scutched. The diameter of each flax fibre was approximately 20 μm . Besides, cotton trichomes were investigated to increase the range of MFA measurements and validate the method. The cotton trichomes were issued from G3 BRS 293 and were cultivated in Ntarla, Mali, in 2017. For further details on the sample preparation, see **Chapter II**.

2.3 SHG analysis

2.3.1 SHG parameters and calibration

To avoid any damage, the laser power was set at 5%. The scan line average was 8, the scan velocity was fixed at 1 (fps) and the scan size was 512*512 pixels. For further details, see **Chapter II**.

To evaluate the microfibril angle, the half wave plate (HWP) was rotated to estimate the range of angles with the maximum intensity of the second-harmonic generation emitted for each flax fibre and cotton trichome. The signal was optimised to select the depth of the fibre that showed the maximum intensity, and finally, an image was collected at the rotation angle that better highlighted the pattern of the cellulose microfibrils. The four images collected at different polarisation angles illustrate a flax fibre with a starch granule of spherical shape deposited on the surface (**Figure III-11**).

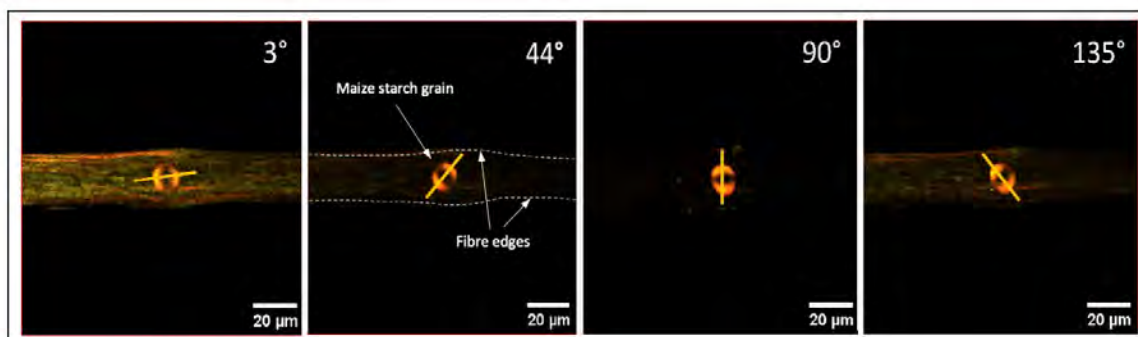


Figure III-11 Flax fibre with a maize starch grain manually deposited on the surface. It is possible to compare their signals at different polarisation angles. Backward (green) and forward (red) SHG signal combination. Acquisition parameters: 5% laser power and acquisition range of 0–135°, which represent the laser position as a function of the fibre axis. The edge of the fibre is highlighted with a dotted white line.

A maize starch grain can generate a second-harmonic signal at each angle of the HWP [95]. Thus, it is possible to compare the SHG signal of a maize starch grain with the SHG signal of fibres and trichomes, as reported in **Figure III-11**. The angle measured in the starch grain approximately corresponds to the angle of the cellulose microfibrils inside the fibre.

2.3.2 Development of a data processing method

To evaluate the microfibril angle, a MATLAB script has been written to identify and calculate the angles of microfibrils and create histograms of their frequency. The microfibril angle was evaluated by an image analysis procedure that computed the histogram of the preferred orientation of pixels, using an approach developed in Gager *et al.* [96]. Briefly, the preferred orientation is computed by (1) applying grey-level granulometry curves with various orientations, (2) computing a typical size in each direction, (3) and estimating the preferred orientation from typical sizes. Grey-level granulometry is an approach for image texture analysis based on the application of morphological operators (typically opening or closing) using a family of structuring elements of increasing size (**Figure III-12A-H**) [97–99]. Measuring the differences in grey levels of images after each opening or closing step results in a granulometry curve that depicts the size distribution of the structures within the image.

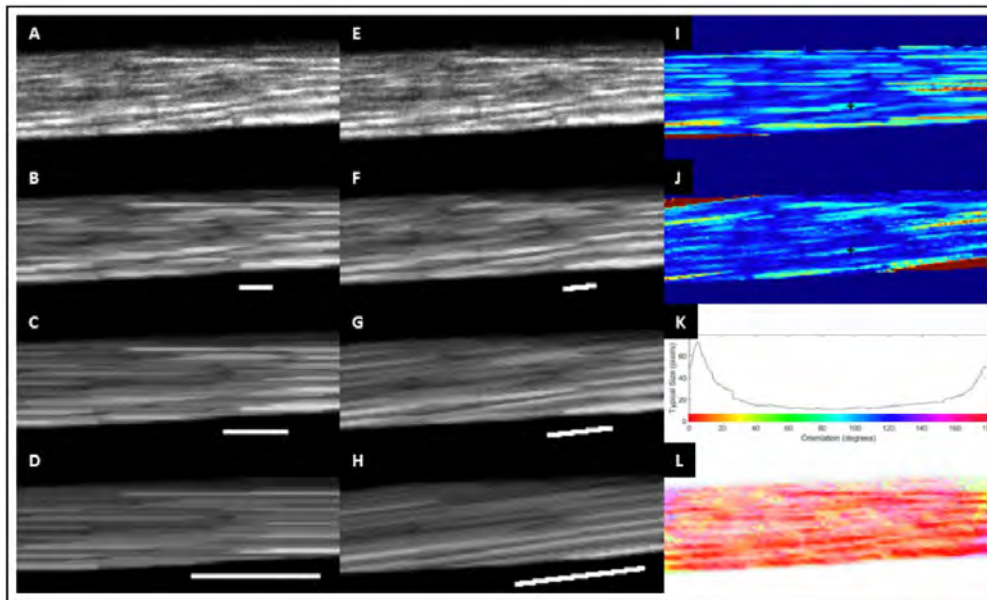


Figure III-12 Principle of the image analysis workflow for estimating preferred orientation of fibres. (A), (B), (C), (D): Results of morphological openings applied on image (A) using horizontal line structuring with lengths 10, 20 and 40 pixels. The size of the structuring elements is represented in the bottom part of each image. (E), (F), (G), (H): Results of morphological openings using 7-degrees oriented line structuring elements with the same sizes. (I), (J): Mapping of the typical linear size in the direction 0° and 7°, obtained by computing mean size from oriented granulometry curve of each pixel. (K) Profile of the typical linear size depending on the orientation for a sample pixel shown as a black cross in images (I) and (J). For this pixel, the profiles exhibit a peak around 5 degrees. (L) Parametric mapping of the preferred orientation for each pixel. Red colours correspond to preferred horizontal directions.

Granulometry curve computed for the whole image can be summarised by a grey-level mean size corresponding to the typical size of the structures within the image. The grey level mean size can also be computed for each pixel to investigate the typical size of the structure it belongs to, resulting in a local granulometry [99,100]. In order to assess the preferred orientation of the microfibrils, linear structuring elements with orientations ranging from 0 to 180 degrees were used [97,98,100,101]. The computation of granulometry curves for each orientation results in a function that depicts the typical size of each pixel depending on the orientation (**Figures III-12I, J**). For pixels belonging to a microfibril, this function presents a peak for the angle corresponding to the microfibril orientation (**Figure III-12K**). The preferred orientation of each pixel is estimated by integrating the typical size function over the range (0, 180) degrees, and represented using a colour code that considers both the orientation and the intensity of the pixel (**Figure III-12L**). Finally, the distribution of the microfibril angles is obtained by computing the histogram of the preferred orientation of the microfibril pixels.

2.4 Result and discussion

The SHG emitted in the forward direction is higher than the SHG emitted in the backward direction due to the coherent nature of the process [91,102]. The difference between backward and forward images from *Valonia* algae, which highlight differences in cellulose microfibrils, was already reported in [103].

In the present study, both flax fibres and cotton trichomes show a high intensity SH signal in the forward direction and therefore it was selected to investigate the samples (**Figure III-13**). In the images acquired, cellulose microfibrils present a characteristic pattern perpendicular to the microfibril length with alternating bands due to their highly ordered arrangement. A similar pattern was observed for nematode muscle by Campagnola *et al.* [104]. The authors reported that the lower limit for harmonic emission from the electric dipole interaction is $\lambda/10$; for a smaller distance, the asymmetric condition is broken, and SHG emission does not occur.

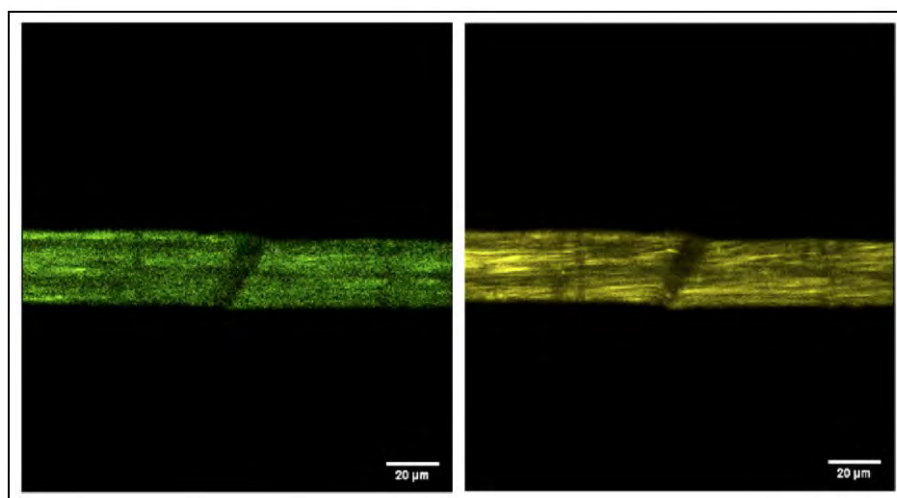


Figure III-13 Backward (green) and forward (yellow) SHG emission of a flax fibre at 2°.

Nevertheless, due to the MFA orientation, cellulose microfibrils are visible only over a specific range of the HWP rotation angle, and to identify this range, it is necessary to investigate flax fibres and trichomes at each polarisation angle using the P-SHG technique. As expected, it was found an angle of approximately 2° – 3° for flax and approximately 25° – 26° for cotton microfibrils. The microfibrils are well distinguishable, and it is possible to acquire images and precisely measure the orientation taking the fibre axis as the reference X-axis. The visible patterns of microfibrils of flax and cotton are shown in **Figures III-14a** and **14b**, respectively.

Besides, a range of elementary flax fibres was investigated, and even when their MFAs have a preferential orientation in agreement with the literature [81,87,85], it was observed that the microfibril orientation changes according to the area considered. This is particularly evident in flax fibre investigated in **Figures III-15a, b** where the MFA is close to 5° in some specific spots while in others it is almost parallel to the fibre axis (0°). This is a clear advantage of the SHG microscopic imaging technique where local areas of single elementary fibres can be analysed, oppositely to XRD, for example.

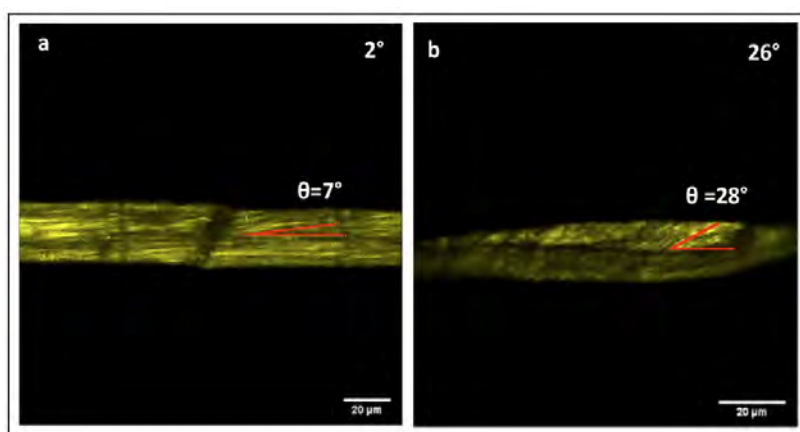


Figure III-14 Flax fibres **(a)** and cotton trichomes **(b)**. The angle θ marked on flax is 7° , while for cotton, it is 28° . Acquisition parameters: 10% laser power, acquisition range of 0 – 68° , and forward second-harmonic emission. The angle is defined based on the orientation of the fibre axis taken as X-axis.

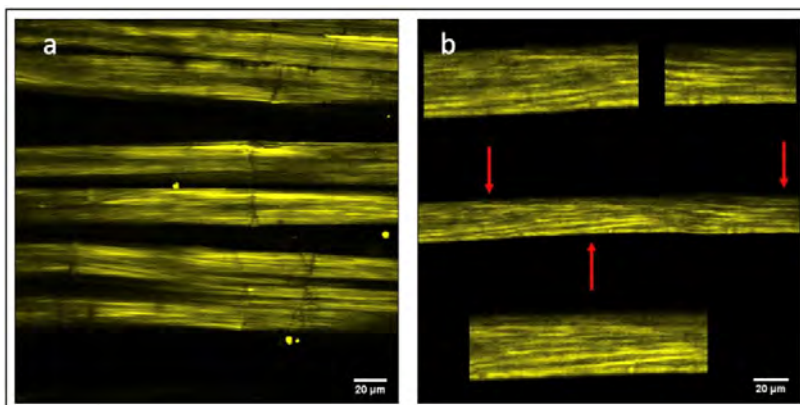


Figure III-15 SHG investigations of several flax fibres **(a)** and different areas of a single flax fibre **(b)**. One can observe the changes in the MFA depending on the zone (red arrows). Acquisition parameters: 5% laser power and forward emission (yellow), 2° HWP.

In **Figure III-16** the same image reported in **Figure III-15b** was processed thanks to a MATLAB script specifically created to estimate the local orientation of microfibrils and compute the histogram of the orientations.

The whole image has been processed, as well as the three sections separately, and slight heterogeneities in the orientation of microfibrils can be revealed. Ninety percent of the values measured are less than 10° with respect to the fibre axis (**Figure III-16A**) and the mean value over the whole area is $5.3 \pm 3.3^\circ$. Interestingly, the histograms highlight differences between zones with a progressive diminution of the microfibril angle (**Figures III-16E, F**) near a dislocation (kink-band) that is present along the fibre (**Figure III-16B**, grey arrow).

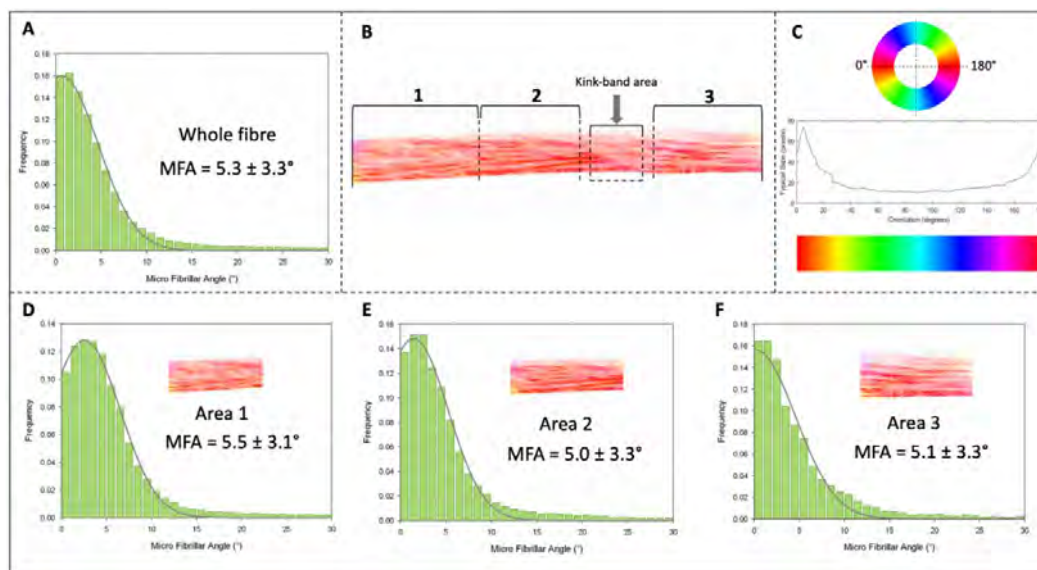


Figure III-16 Imaging process by MATLAB with histograms of the relative microfibril angle detected from the **Figure III-15b**. The first histogram (**A**) is related to the whole fibre (**B**); the grey arrow indicates the dislocation zone (kink-band). The areas 1, 2 and 3 (**D**, **E** and **F**) are processed separately. The scale of colours according to the orientation is shown in (**C**).

Under these observations, it is difficult to establish a single microfibril angle for a single elementary fibre and, consequently, for a fibre variety, as is often reported in the literature. This diversity in the organisation of cellulose cannot be determined by averaged measurements, as is the case with X-ray diffraction, for example; it is therefore rarely discussed in the literature. For example, for flax fibres, it has been shown by TEM analysis [105] that transition zones of angles exist, which also supports the hypothesis of misalignments such as those shown here. Thus, the relatively small angle value that was highlighted here compared to the data in the literature (**Table III-3**), takes on its full meaning when it is related to the inherent nature of flax walls.

The low values of microfibrillary angles found here, as well as their dispersion, are particularly important data, especially for the biocomposite community when fibres are used as reinforcements. Indeed, fibre stiffness and Young's modulus are inversely correlated with MFA [81], also demonstrated

by wood community using nanoindentation [33,106]. The results presented here allow to conceive a more detailed exploration of the evolution of MFA, whether it is a function of the varieties studied, but also of growing conditions, environmental stress and fibre extraction or processing conditions as in wood [83]. Finally, during a tensile test on elementary fibre, it has been shown that MFA decreases in the first part of the tensile stress, being marked by a reorientation of the cellulose macro fibrils [107]. This phenomenon results in a non-linearity at the beginning of the stress-strain curve, which represents a strong signature of single plant fibres mechanical behaviour.

For cotton trichomes, by changing the polarisation angle, two different and opposite orientations (right-handed Z and left-handed S helix, respectively) of the microfibrils were observed, forming a criss-cross pattern (see **Figures III-17a, b**). The sample plane in the Z direction (depth of the trichome) is the same, but, because the cotton trichomes are twisted [108], different layers can be involved, and their interpretation become more difficult.

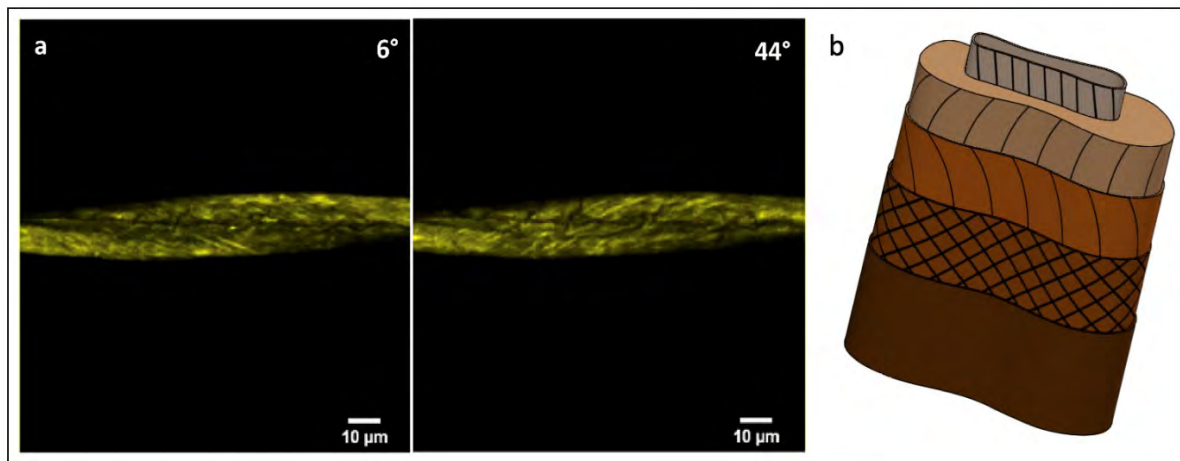


Figure III-17 a) Cotton trichomes observed at two different polarisation angles (6° and 44°), where two microfibril orientations (Z and S) are observed. Acquisition parameters: 10% laser power, acquisition range of 0-135°, and forward emission (yellow). **(b)** Cotton trichome structure from [7].

Other interesting information can be found by scanning at different Z values as second-harmonic microscopy is plane selective and allows the analysis of a single level without or with little interference from the other levels [94]. **Figures III-18a, b** shows that fibres are surrounded by an external layer on the edges, identified as the primary cell wall (P) and the S₁ layer.

The lumen in the middle (L) is delimited by the Gn layer that makes it visible. The lumen is visible only at a specific depth of the fibre. Interestingly, a fluorescent signal is observed at the edge of the lumen, helping in focusing and discerning this hollow structure. The origin of this fluorescence is arguably the vestiges of cytosolic fluorescent components left at the surface of the apoplasm through fibre senescence or apoptosis. Indeed, in such multinucleate fibres, it is likely that membrane-bound “apoptotic bodies” formed [109], were engulfed and more or less degraded into nucleic acid.

Additionally, fluorescence signals can be from mitochondria, which are well known to liberate many fluorescent cytochrome components after the programmed cell death [110].

The combination of the two SHG channels (forward and backward signals) does not show these details, and an autofluorescence signal is needed to highlight them. Indeed, in plant cell walls, suberin, lignin, cutin and a small number of proteins produce autofluorescence emission, as reported by Berg [111]. Day *et al.* measured the lignin inside the different layers of flax bast fibre cell walls and found GS lignin in the secondary cell wall as well as a significant amount of condensed G lignin in the S₁ layer together with the other two GS epitopes [43].

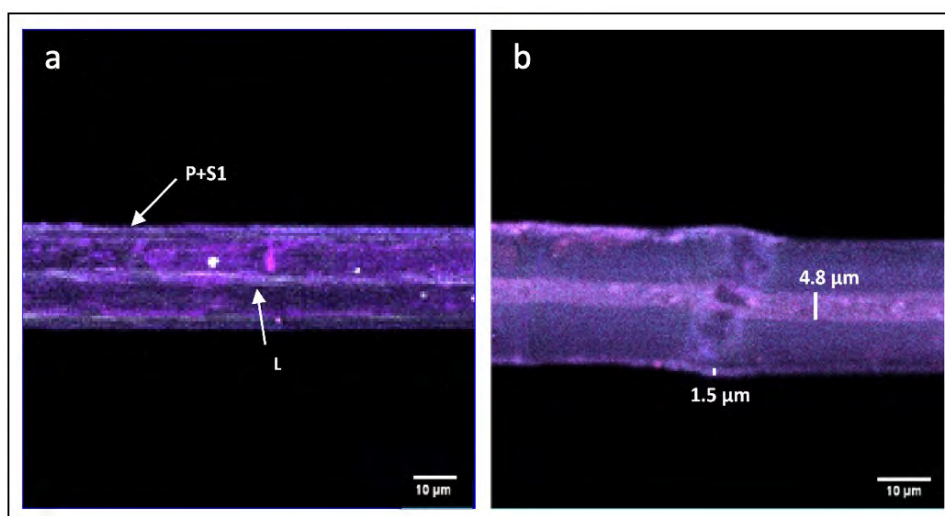


Figure III-18 Two different flax fibres investigated with different autofluorescence channels (R460/60 and T460/60 TNDD blue-cyan; R550/88 and T550/88 TNDD magenta) combined to highlight their different layers. It is possible to identify the lumen (L) in the middle (b) and two small layers at the edge of the fibre due to the primary cell wall (P) with the S₁ layer (a). The thicknesses of the lumen surrounded by the Gn layer and the P+S₁ layers (b) were measured with ImageJ software, and the different diameters of the lumen can be due to the different maturities of the fibres analysed.

Microfibrils are also present in the P and S₁ layers, but they cannot be detected and correctly visualised due to their small thicknesses.

Regarding the lumen, flax fibre cell walls change their structure during growth. In a not fully developed flax fibre, two types of layers have been identified: the G (S₂) layer, which is the mature part of the cell wall, and the Gn (S₃) layer, which is the newly deposited layer of the gelatinous cell wall [38]. The Gn layer is deposited from the outer to the inner side of the cell, and with maturation, the Gn layer changes its cell wall density and non-cellulosic polymer arrangement, becoming a mature G layer; these two layers mainly differ in the length of galactan chains, as reported by Rihouey *et al.* [10]. Thus, the more mature the fibre is, the smaller the lumen, and its diameter varies between fibres. The size of the lumen may also depend on environmental conditions. In the case of low temperature or the lodging phenomenon, conversion of Gn into the G layer may be stopped, inducing a large lumen. Nevertheless,

even for a fully developed fibre, a small part of the Gn layer is still present. Regarding both the macromolecules and the small size molecules that compose the cell wall, they are undoubtedly heterogeneously distributed over the layers described earlier [7]. In line with the scope of this study, phenolic structures are present in these layers, and with the particular G-rich lignin quantified and immunolocalised across flax fibres [43], these structures arguably emit fluorescence detectable at approximately 550 nm (pink). The literature also reported small molecules based on solid-state ^{13}C NMR [112], namely, anthocyanins and ferulates (hydroxycinnamics), which are supposed to emit a detectable fluorescence signal, for instance, a blue signal at approximately 460 nm.

This method has several important advantages: i) several areas of the same fibre can be investigated, so the variation in the microfibril organisation can be highlighted, ii) the MFA is measured and not estimated and iii) it is possible to change the environment and collect images to estimate the modification in the structure.

2.5 Conclusions

To date, researchers have used several techniques to evaluate the microfibril angle, such as X-ray diffraction (XRD), scanning electron microscopy (SEM) and microbeam small-angle X-ray scattering (μSAXS), but each of these techniques has some disadvantages.

In this section, the MFAs of elementary flax fibres and cotton trichomes were successfully calculated for the first time using second-harmonic microscopy under controlled polarisation light (P-SHG). The MFAs of flax and cotton were calculated using a direct evaluation of the microfibril angle observed in P-SHG images.

In fact, the resolution of this technique is such that macrofibrils are visible in the images collected, and their angles can be directly measured. This method not only allows us to obtain precise angles of the cellulose macrofibrils, when other techniques can only measure an average (confirming, however, the preferential orientations between 2° and 7° for flax fibres and approximately 26° for cotton trichomes already reported in the literature), but also allows us to investigate a length of several tens of micrometres for a single elementary fibre. Considering these new results, it is clear that the microfibril organisation in a fibre is inhomogeneous, depending on the zone analysed, and can have an orientation parallel to the axis of the flax fibre or a specific angle. This fact can also explain the large range of values found by other research teams, regardless of the methodology used.

Several planes in the Z-axis can also be analysed, and the second-harmonic emission for each position can be evaluated to compare the behaviour of the whole fibre. A limit we face is the need for non-twisted fibre elements, and the cotton trichome taken as a reference illustrates it with its numerous twists. However, if the whole length of the fibre elements cannot be observed, then a limited area is enough for the SHG measurement.

In conclusion, in this section, new important information on the ultrastructure of plant fibres is presented, and P-SHG demonstrates high potential for studying the variation in the MFA under different environmental conditions and at local defects, i.e., few μm kink-bands, owing to its high resolution. Future work will focus on evaluating the inhomogeneities of the microfibril organisation and, more specifically, the specific ultrastructure in critical areas, such as kink-bands and structural defects. Several environmental conditions will also be tested to investigate the reorganisation of the microfibrils, as well as possible MFA variation into the thickness of the fibre thanks to Z-stack explorations.

3. Extensive investigation of the ultrastructure of kink-bands in flax fibres

3.1 Introduction

Composites are often considered to be the materials of the future, owing to their high-performance mechanical properties, low weight and applicability in several domains, from buildings to automotive or sport and leisure fields [113]. To design eco-friendly composite materials, plant fibres, especially hemp and flax in Europe, have attracted attention as renewable, biodegradable and cost-effective resources [2,114,115]. Nevertheless, they exhibit certain limitations compared to synthetic fibres [114,116]. Moreover, the mechanical properties of plant fibres are dependent on the plant growing conditions and on the overall agricultural and mechanical extraction process (e.g., harvesting time, retting, scutching, hackling) where the decortication step has the main impact.

More specifically, living plants are subjected to specific abiotic stresses when growing, such as wind conditions or dried soils, which can cause deformations and damage to fibres [117–119]. Additional defects are also introduced during the retting and scutching processes [118,120–123]. Such defects appear under the optical microscope as local morphological deformations along the entire length of the cell, and they are commonly termed kink-bands, defects or dislocations, although several other terms have been used in the literature; a list of these terms can be found in [124]. In the present study, the term “kink-band” was chosen.

In this study, according to the poorly lignified and gelatinous characteristics and the low MFA of flax secondary cell walls and Gn, based on precise descriptions in the literature [125,126], the botanical model was adopted, which divided the layers in P, S₁ and G (see **Figure I-2** of **Chapter I**).

In the centre of a single elementary fibre, a lumen is present as an empty cavity, whose diameter depends on the botanical species, variety, maturity and location along the plant stem [7]. These layers differ from each other in terms of the chemical composition and cellulose microfibril orientation [127]. The microfibril angle (MFA) is defined as the angle between the cellulose microfibrils and the fibre axis and has been generally reported to be approximately 8° in the G layer of flax [81]. However, observations through SHG microscopy technique demonstrated that the MFA of the flax G layer varies between 0° and 7°, depending on the area examined (see **Section 2** of this **Chapter**).

Experimentally speaking, when SHG, scanning electron microscopy or atomic force microscopy are used, the observed angle does not directly correspond to the angle measured in microfibrils themselves but rather to the angle between the fibre axis and a bundle of microfibrils, i.e., a macrofibril, with diameter from 14 to 200 nm [128–130]. Indeed, in biology, a microfibril corresponds to several glucan chains (18–40 units) and to a diameter ranging from 2 to 4 nm [130,131]. They could be estimated in a

relevant way only by more in-depth investigative methods such as Nuclear Magnetic Resonance (NMR) [16].

However, this well-defined and ordered hierarchical structure present in flax cells can be modified when kink-bands occur. The inner structure of a kink-band in plant fibres has not yet been clarified. Thygesen and Gerlinger demonstrated that kink-bands have the same chemical composition as in the homogeneous areas of the hemp fibres [132]; however, around the largest kink-bands, transition areas were observed, in which the cellulose orientation was modified, and thus, the microfibrils were less oriented. The same authors also estimated that the MFA within and at the periphery of the kink-band in hemp was 30° and 10° – 15° , respectively [132].

The evolution of kink-band area behaviour and structure during mechanical loading has also been explored by various research groups. By using polarised light microscopy, Thygesen *et al.* evidenced a disappearance of kink-band areas on hemp fibre by realignment and straightening of macrofibrils under tensile loading [133] followed by a subsequent reappearance after one month. Another team developed numerical modelling of cellulose microfibrils with local misorientation under tensile loading and showed a slight realignment of dislocated chains after a specific strain in the kink-band region but without leading to the full recrystallisation of the dislocated regions [134].

Generally, the presence of significant kink-bands corresponds to a lower tensile strength inside the fibres because kink-bands are weak points at which the cracks begin to propagate until the elementary fibre breaks during tensile testing [133,135–137]. Aslan *et al.* hypothesised that fractures were initiated in the outer layer of the region with the largest kink-band and subsequently propagated inside the cell wall until they reached the nearest small kink-band [136]. Using a focused ion beam-scanning electron microscope (FIB-SEM), Zhang *et al.* observed that the kink-band regions in flax fibres consisted of a main cavity composed of several voids assembled and separated by membranes. Moreover, small pores were regrouped in the area close to the kink-band, and this phenomenon did not occur in other areas of the fibre [138].

The influence of the kink-bands is also demonstrated when fibres are used in biocomposites, as the kink-band geometry renders a single fibre strongly inhomogeneous. During mechanical testing, for example, stress concentration occurs in these areas, resulting in fibre-matrix debonding and matrix micro-cracking [118]. Le Duc *et al.* also demonstrated the sensitivity of the kink-band regions when flax fibres are compounded with a thermoplastic matrix [74]. The overall weakness of flax kink-bands was numerically confirmed by Sliseris *et al.* in both cases at both the isolated bundle and the composite scale [139]. This negative effect of kink-bands on plant fibres and associated composite material properties leads to a research path that aims at avoiding the formation of kink-bands by improving the fibre decortication process and investigating new extraction methods, such as the use of aqueous ammonia [122]. In parallel, the nature of kink-bands has been studied to describe the physical mechanism of their origin [140,141] and to artificially reproduce these bands by subjecting the fibres to bending or compression loads [135,142].

Despite all this research, only limited data are available in the literature on the internal ultrastructure or internal mechanical properties of the cell walls involved in kink-bands. For this reason, an extensive investigation of these specific regions is necessary. Therefore, in this section, a range of kink-bands of flax fibres, representing 8 bundles and 12 single fibres, were examined with the main objective of providing additional and more in-depth information by using two cutting-edge investigation methods: i) AFM in peak force quantitative nanomechanical mapping mode (AMF PF-QNM), to investigate the indentation modulus in kink- band regions at a microscale level, and ii) second-harmonic generation microscopy at polarised controlled light (P-SHG), to explore the MFA and ultrastructural changes in kink-band areas. In addition, SEM micrographs were acquired to obtain complementary information.

3.2 Materials

Flax fibres of the Bolchoï textile variety, organoleptic classification number 66233, cultivated in 2018, Normandy, France, by the Depestele group, were retted for 6 weeks and then mechanically scutched.

3.3 Methods

3.3.1 SEM

A fibre bundle with a thickness of a few millimetres was extracted and glued on the sample holder by using conductive carbon tape. A thin gold-sputter coating was performed for 180 s by using an Edwards Scancoat Six device, and the sample was successively scanned using a Jeol JSM 6460LV scanning electron microscope. Furthermore, observations on other flax bundles were carried out after cryofracturing; to induce cryofracturing, several flax bundles, different from those used in AFM and SHG, were embedded in agar resin (epoxy resin agar low viscosity resin (LV); Agar scientific UK) and placed in an oven at 60 °C overnight to ensure complete polymerisation. Subsequently, the blocks were frozen in liquid nitrogen and mechanically broken using hand pliers, with fibres submitted to a pull-out phenomenon. The broken sections were successively gold-sputtered and investigated.

3.3.2 SHG

To perform investigations using the SHG microscopy technique, flax single fibres and bundles were extracted from the Bolchoï fibre batch and mounted on paper support according to ASTM C1557.

The scan line average was set to 8 and 16, the scan velocity was fixed at 1 (fps), and the scan size was 512×512 pixels. Before each acquisition, the half-wave plate (HWP) was set parallel to the fibre axis, following the previous study presented in **Section 2** of this **Chapter**. Several images in air were acquired before adding distilled water between the two coverslips with a pipette and waiting for 5 min to saturate the fibres.

3.3.3 AFM in PF-QNM mode

Sample preparation

To perform the atomic force microscopy examination, another set of bundles embedded in resin without using ethanol bath and thus limit embedding resin penetration [143]. The flax bundles were cut to a length of less than 5 mm and placed in a flat silicone embedding mould (Polysciences) in the transverse direction (**Figure III-19**), and the surface was prepared by cutting several flax fibres along their length to highlight the inner structure. For further details on resin and sample preparation, see **Chapter II**.

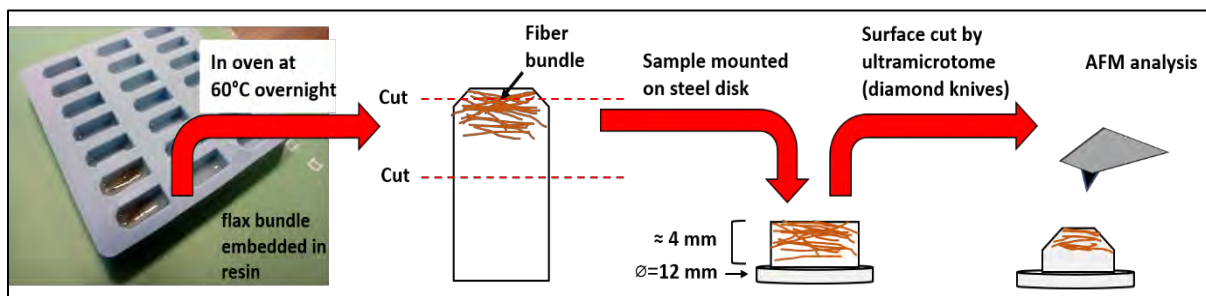


Figure III-19 Schematic illustrating the sample preparation process for the AFM PF-QNM analysis. Several nearly aligned fibre bundles were embedded in agar resin in the transverse direction. The thickness of the steel disc and the mounted block are not scaled to present an enlarged view of the fibre bundles.

AFM measurements

The average normal spring constant ranged between 147 and 203 N/m. The obtained tip radius ranged between 40 and 55 nm and the image resolution was 512×512 pixels. For further information see **Chapter II**. Different kink-band areas of the fibres were accurately selected and investigated; to design the distribution figures of the indentation modulus (IM), data were calculated for each AFM force curve, representing between 3,300 and 16,700 points for each image analysed.

3.4 Results and discussion

3.4.1 SEM results in the kink-band area

The surface of a bundle of flax fibres was initially analysed using the SEM technique; first, it is necessary to define the vocabulary and type of kink-bands investigated here. In the fibre bundle, kink-bands were present in the entire group of fibres and appeared as a single continuous deficient area (**Figures III-20a, b**), as already reported in the literature [144,137]. In Nyholm *et al.*, a fine description of the most common forms of kink-bands is listed [124]; schemes of the kink-band region in a flax fibre bundle and elementary flax fibres are depicted in **Figures III-20c** and **20d**, respectively. In the present work, kink-bands were distinguished according to their size using the terms type A (TA) and type B (TB) for the most and less pronounced, respectively.

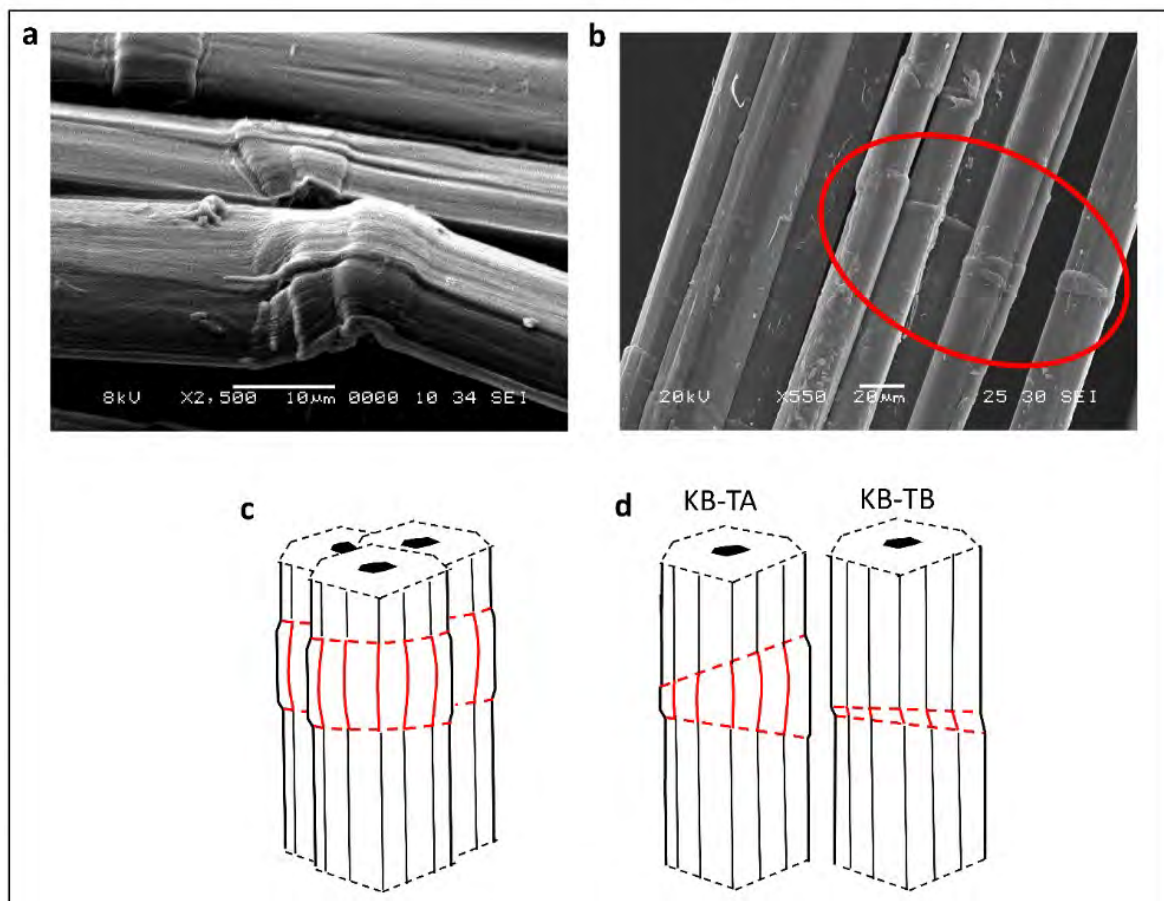


Figure III-20 SEM micrographs of a flax fibre bundle (**a, b**), in which all the fibres exhibit kink-bands located in the same area indicated by the red circle in (**b**); schematic representation (**c**) of a kink-band region in a bundle and (**d**) two different common types of kink-bands in a single fibre; the kink-band regions are indicated in red in (**c**) and (**d**).

Then, the local structure and defects in each type of kink-band were deeply investigated by SEM; SEM observations of peeled and cryo-fractured flax fibres and bundles are shown in **Figure III-21**. The significant differences in the organisation and orientation of the cellulose macrofibril network shown in **Figures III-21c, d and e** could suggest that different layers of the fibre are exposed. This observation allowed us to hypothesise a distinction of the visible layers by identifying them as primary cell walls (PCWs), S_1 and G. Indeed, the pattern of the surface of G appeared to have a highly ordered structure, which is in agreement with the one defined using almost all the existing models [127]. Regarding S_1 , several studies reported the presence of a crisscrossed network of cellulose microfibrils at a significant angle to the axis [86,145].

The images obtained in Zhang *et al.* by using FIB-SEM also suggested the presence of a layer with a similar pattern, although each pattern was not attributed to a corresponding layer [138]. This crisscrossed cellulose network in the layer expected to correspond to S_1 was less visible in the micrograph, although it is clearly observable that cellulose orientation is not homogenous (**Figure III-21c**) or even in the opposite direction (**Figure III-21d**) than that observed in the G layer (**Figure III-21e**). Nevertheless, both layers of the secondary wall exhibited a deviation in the orientation of their macrofibrils in the kink-band region. This deviation occurred with a well-defined angle, following the shape of the kink-band (**Figure III-21b**); it is clearly visible in **Figure III-21e** with a significant local orientation change for G layer macrofibrils.

Figure III-21h shows a typical flax fibre after a cryofracture process, with the innermost cell wall layers exposed and the lumen (white arrow) clearly observable. The main advantage of investigating cryo-fractured fibres is that the fibres' deformation is limited and allows us to examine sections with a clean break. It was noted that fractures due to the cryofracture process often occurred in the kink-band region, indicating that kinks are the weakest areas of the fibres. **Figure III-20f and 21g** show a focus on kink-bands of Type A and Type B, respectively. **Figures III-21i and k** show the corresponding inner layers of the flax cells where the areas selected are the regions at higher magnification illustrated in **Figures III-21j and 21l**, respectively.

The macrofibrils were highly deviated, following the shape of the kink, and all the layers were involved up to the lumen in both the TA and TB kink-bands. **Figure III-21j** highlights that certain macrofibrils were detached and less deviated than others, thereby creating cavities (see red arrows) between them and the other bundles of macrofibrils. These cavities are numerous and detectable in the largest TA kink-bands. On the other hand, inside the TB kink-band illustrated in **Figure III-21l**, one can notice a low number of cavities, probably due to the less drastic deviation of the macrofibrils from their natural angle.

The impact of the preparation mode and the original existence of these cavities can be debated; to better understand the internal architecture of kink-band regions and provide matching elements, the following sections aim to explore these areas by SHG and AFM microscopy.

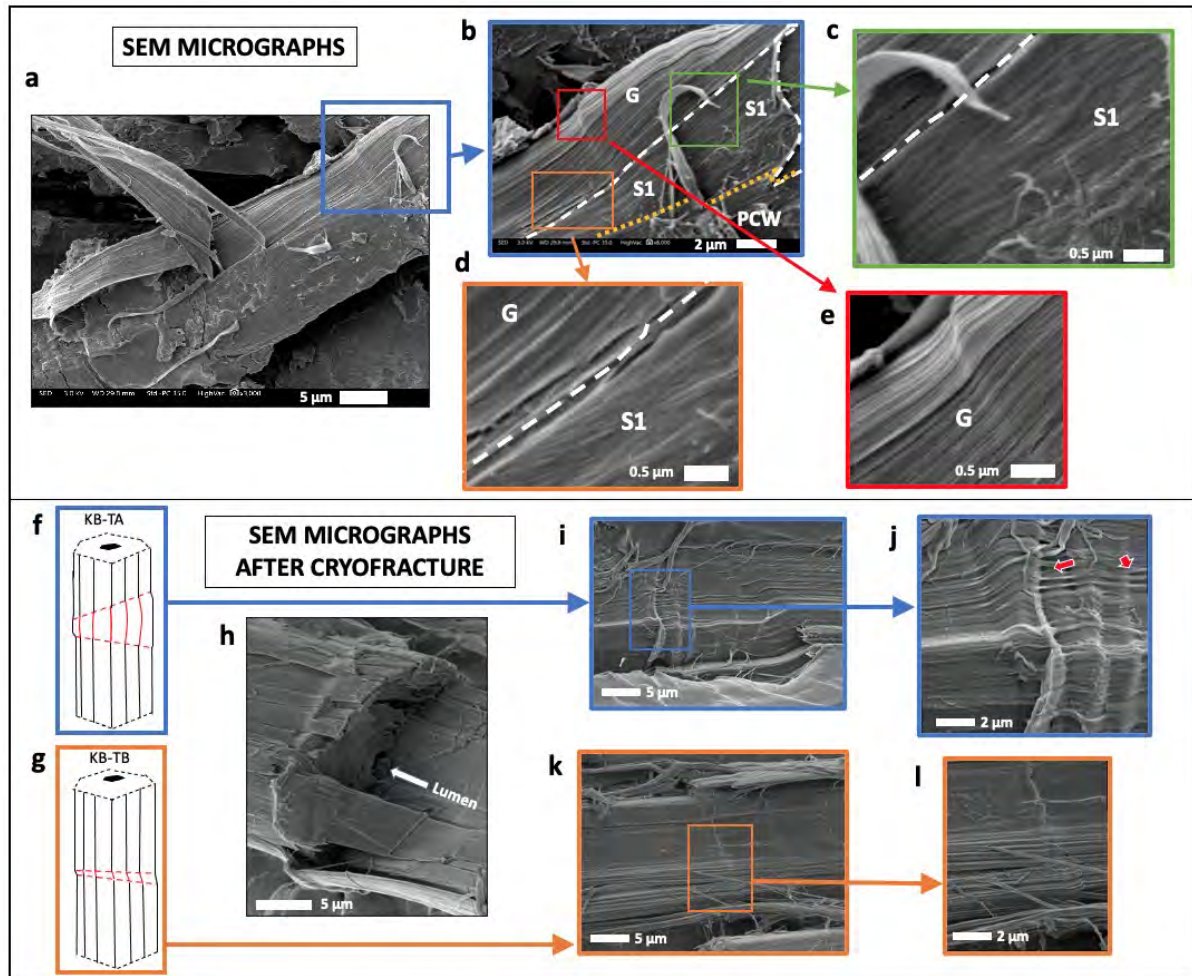


Figure III-21 SEM micrograph of a peeled elementary flax fibre (a) and magnified area showing details of the kink-band region (b); sub-details of this area are given on S_1 layer (c), S_1/G transition (d) zone and G layer structure (e). (h) is a SEM micrograph of a cryofractured fibre broken in the kink-band region, the lumen (white arrow) and the inner layers are clearly visible. The images (i, j) and (k, l) correspond to kink-bands type A (f) and B (g), respectively. It can be noted that the macrofibrils deviated and followed the shape of the kink-band in all the layers. In (j), certain macrofibrils were detached and less deviated than the surrounding macrofibrils, which led to the creation of cavities between them (indicated with the red arrows).

3.4.2 Multiphoton study of the cellulosic kink-band architecture

Multiphoton microscopy was used to deeply investigate the organisation of cellulose macrofibrils within the kink-band area; two different elementary flax fibres were analysed in air and water environments; the resulting images are shown in **Figure III-22**. Autofluorescence and SHG channels were separated to better examine the results obtained, and both autofluorescence and second-harmonic signals were visible in the two environments.

In air, the microfibril angle of the cellulose macrofibrils appears to be interrupted in the kink-band area and emits a lower second-harmonic signal, which suggests a lower cellulose organisation compared to that in the area of the fibres free of defects, in line with the investigations conducted by other teams

[132,146]. The SHG strongly depends on the polarisation angle of the laser, and various SHG signals in the kink-bands can be collected by changing the polarisation angle with the HWP; however, the detected signals are lower than those in the remaining part of the fibre.

Few studies have examined the impact of moisture on the structure and mechanical behaviour of elementary plant bast fibres; in fact, the hygroscopicity has been principally studied only when plant fibres are used in composites to characterise the final product [147]. Using the small-angle X-ray diffraction technique, Astley and Donald noted that the MFA in flax fibres increased from 11° in a dry state to 15° in a wet state [87].

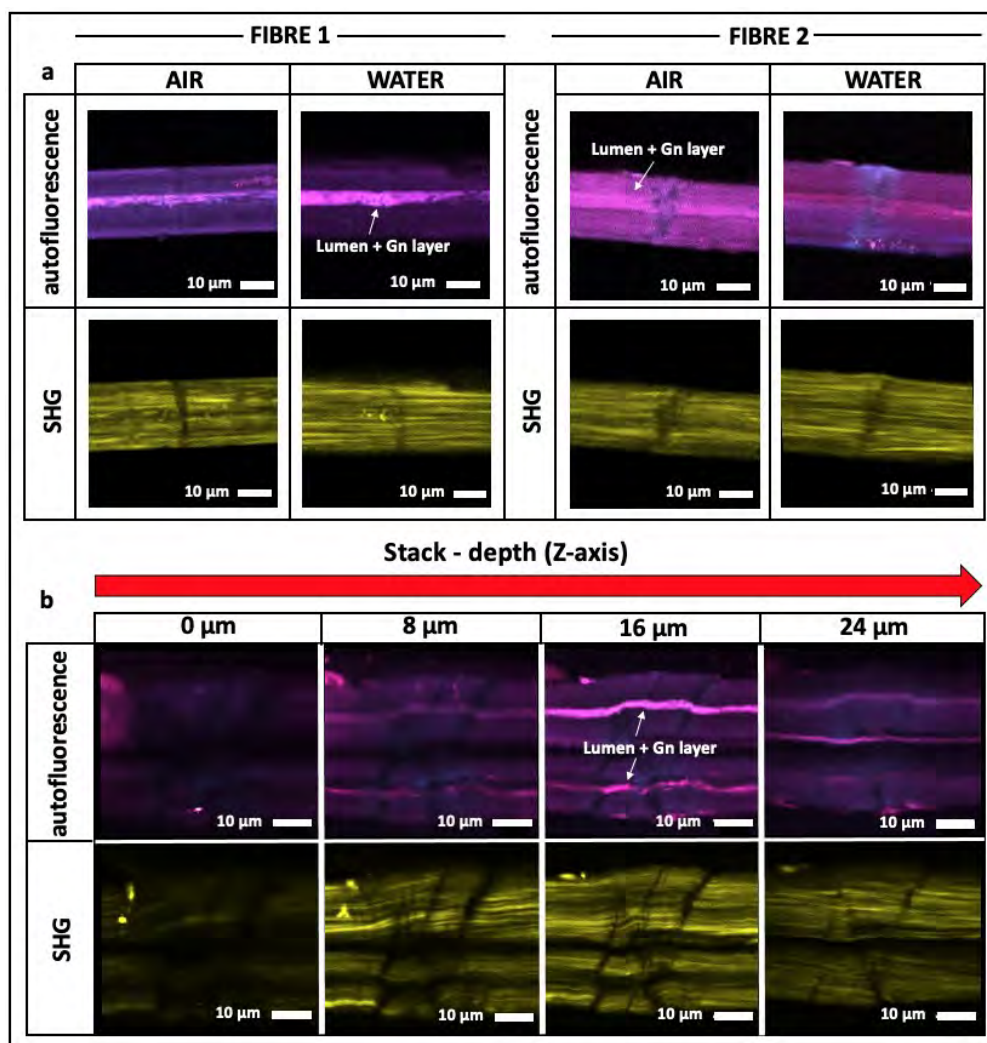


Figure III-22 SHG microscopic imaging on two elementary flax fibres (a), mounted in air and water, with the signals collected considering the autofluorescence (merge channels of R460/60, T460/60, R550/88 and T550/88 TND) and SHG channels. The autofluorescence channels 460/60 (blue) and 550/88 (magenta) highlight the lumen coupled with the Gn layer, which is primarily responsible for the fluorescence signal, in the middle of the fibre; in contrast, the SHG channel shows the second-harmonic emission due to the macrofibrils, and it can be noted that the MFA in the air and water environments is the same. The kink-band region, however, exhibits a higher SHG emission in water than that in air, due to the more orderly macrofibril network. In (b), a bundle of three fibres, two of which are in foreground, immersed in water was investigated at different depth. Kink-bands area show a different macrofibril orientation in the SHG channel, as well as the presence of a lumen+Gn layer in the autofluorescence channel.

In the present study, one can argue that there is a difference in contrast between the kink-band region and the rest of the fibre (**Figure III-22a**). The dark area between the kink-band and defect-free areas was less contrasted in the water environment than that previously observed in air.

Toba *et al.* and Céline *et al.* examined fibre bundles (wood and flax, hemp and sisal) through XRD and Fourier transform infrared spectroscopy in attenuated total reflectance mode (FTIR-ATR) [148,149]. In both of these studies, the authors first examined the wet samples and successively the dehydrated state, and they found that the crystallinity increased owing to the sorption of water. This increase in crystallinity linked with sorbed water was also observed by Nakamura *et al.*, who examined cotton by using differential scanning calorimetry and XRD [150]. Nakamura *et al.* [150], followed by Céline *et al.* [149], suggested that the amorphous phase of cellulose likely became more crystalline with moisture. The increase in crystallinity when the fibres were in a wet state likely occurred due to the hydrogen bonds that water formed with cellulose or hemicellulose, which broke after dehydration, thereby causing relaxation of the cellulose structure and a consequent decrease in crystallinity.

The SHG observations in the kink-band areas support the hypothesis that an amorphous region may evolve towards a more crystalline region after wetting, resulting in a more ordered structure that led to the collection of a higher SHG signal corresponding to a lower contrast (with the remaining fibre). However, a second hypothesis for the smaller difference in contrast when considering the fibres mounted in water is a partial re-organisation of the macrofibril network, which was previously disoriented during the formation of the kink-band and due to the swelling of the fibre.

In **Figure III-22b**, the SHG was used to analyse a bundle consisting of three elementary fibres, two of them visible in the foreground and the third one hidden by the two, mounted in water. Here, 4 images along the Z-axis were acquired with a step of 8 μm . Measurements were recorded in water. Different macrofibril orientations in the SHG channel, along with the lumen+Gn layer on the autofluorescence channels, can be observed. On both foreground fibres, the lumen appears progressively, approximately in the middle plane of the fibre. This latter phenomenon is highly visible due to the autofluorescence channels in blue/cyan (R460/60 and T460/60) and magenta (R550/88 and T550/88 TNDD), which highlight the Gn layer around the lumen that follows the shape of the kink-band. This fluorescent signal is attributed to the remaining cytosolic fluorescent components or cytochrome components liberated after cell death [109,110].

Occasionally, it was observed an accumulation of the fluorescent material at the lumen/Gn level in the kink-band region, as shown in **Figure III-23**, or irregular interruptions of the fluorescence signal in this layer along the fibre length, which can be attributed to a localised reduced thickness of the Gn cell wall or a localised modification of the composition that can lead to lower fluorescence emission. Interestingly, it is possible to note that even this innermost layer deviates following the kink-band. The images reported in **Figures III-22** and **24** demonstrate the continuity of the lumen along the kink-band area and allow the detection of darker areas, with less SHG response, throughout the fibre thickness.

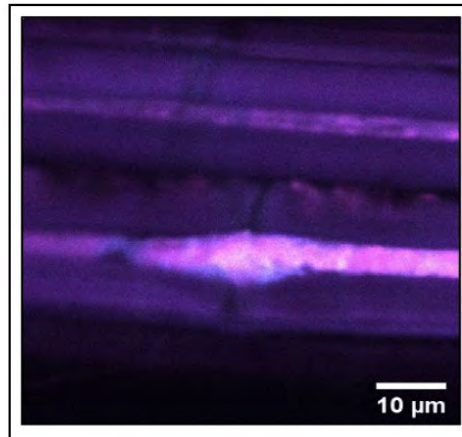


Figure III-23 SHG investigation; in the kink-band area, material accumulation from the Gn layer has occurred.

This finding demonstrates that the kink-band is not only a volumetric and localised geometric defect in the fibre periphery but also in the entire volume of the fibre, including the G and Gn layers.

To evaluate the MFA in the kink-band regions, **Figure III-24** shows a focus of SHG analysis in the bundle and one of the elementary fibres already illustrated in **Figure III-22**, both mounted in a water environment; **Figures III-24a** and **24b** correspond to the TA and TB kink-bands, respectively. MFA values are generally included between 0° and 10° in defect-free areas (**Section 2** of this **Chapter**); here, with this complementary study, it was observed that stronger deviations exist in kink-band regions, but they are mainly not an increase in the helix angle of the microfibrils to the fibre axis but rather an additional radial angular offset (**Figure III-24**). Nevertheless, in connection with the literature, in the present study was denoted MFA as the whole microfibril angle between the fibre longitudinal axis and the macrofibril orientation.

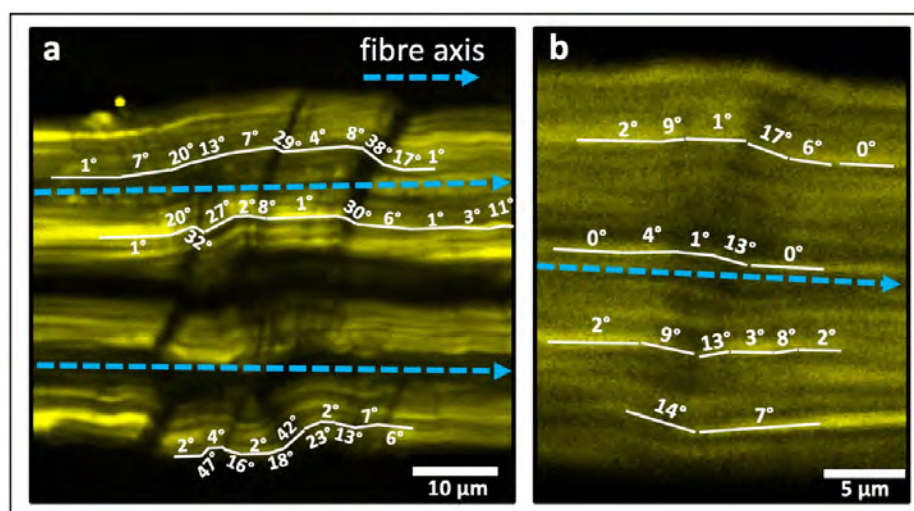


Figure III-24 SHG imaging of a bundles of three elementary flax fibres with two visible fibres in foreground **(a)** and a single elementary fibre **(b)** mounted in water where TA and TB kink-bands are identified, respectively. The MFA is approximately and manually estimated, following the macrofibrillar orientation and taking the fibre axis as a reference (blue arrow). The difference in terms of values between TA **(a)** and TB **(b)** is clearly observable.

The MFA was manually estimated to range from 6° to 47° and 4° to 17° for type A (**Figure III-24a**) and type B kink-bands (**Figure III-24b**), respectively. These values are well correlated with the MFA reported by Thygesen and Gierlinger [132], who examined hemp kink-bands through Raman polarisation.

Although the lack of spatial resolution of the SHG microscopy may lead to misinterpretation, it allows the *in situ* investigation of the local MFA, as the macrofibrils are clearly visible in the acquired images. In contrast, when the MFA is measured using the X-ray scattering diffraction technique, various limitations are encountered: i) the values are deduced by fitting the signals, ii) they are a mean of the whole fibre bundle, and iii) $\text{MFA} < 8^\circ\text{--}9^\circ$ cannot be measured without specific calibration. These limits can be overcome using SHG microscopy, as the MFA is directly measured.

In this study, variability was noted between the angles of deviation in the large (TA) and small (TB) kink-bands, influencing the entire macrofibrillar network. In the type B kink-band, the deviation angle of the macrofibrils is lower, and the network is still ordered even inside the kink-band. In contrast, the type A kink-band exhibits dark areas in which the network is not detected even when the fibre is mounted in water, possibly linked to the presence of detached macrofibrils that create cavities, as previously evidenced by SEM observations.

3.4.3 AFM PF-QNM mapping to explore the mechanical properties and topography of kink-band areas

The micromechanical properties of the kink-band are a crucial aspect. Nevertheless, although several papers suggest that kink-bands are the weakest point, structurally or mechanically speaking, relevant information regarding the mechanical behaviour of this region compared to that in the defect-free areas of the same fibre is not available in the literature.

The AFM PF-QNM technique and other very similar fast force-distance curve modes can be used to evaluate the indentation modulus of plant cell walls at the micro- and nanoscale levels [36,38,39,151–153]; however, to the best of our knowledge, until now, mechanical information pertaining to the kink-band areas of bast fibres has not been provided. Although the AFM technique has been applied in other fields to investigate kink-bands in collagen [154] and polymeric fibres [155], conventional AFM modes have been applied and do not provide mechanical information.

Figure III-25 shows two maps of the indentation modulus of kink-band regions in a bundle consisting of at least two single flax fibres (**Figure III-25a**) and an elementary fibre (**Figure III-25b**). In the bundle, three homogenous areas were selected in the kink-band, indicated by blue squares, and these areas were considered to calculate the mean indentation modulus inside the kink-band region. In addition, four areas (black squares) were selected to calculate the mean indentation modulus in a homogeneous area without defects. Similar work was performed in the single fibre kink-band by

selecting two areas inside the kink-band (red squares) and three areas outside (black squares). All the regions of interest were carefully selected in the areas of the image that showed no evidence of accumulated material or roughness generated during the sample preparation, especially during the cutting step with the ultramicrotome.

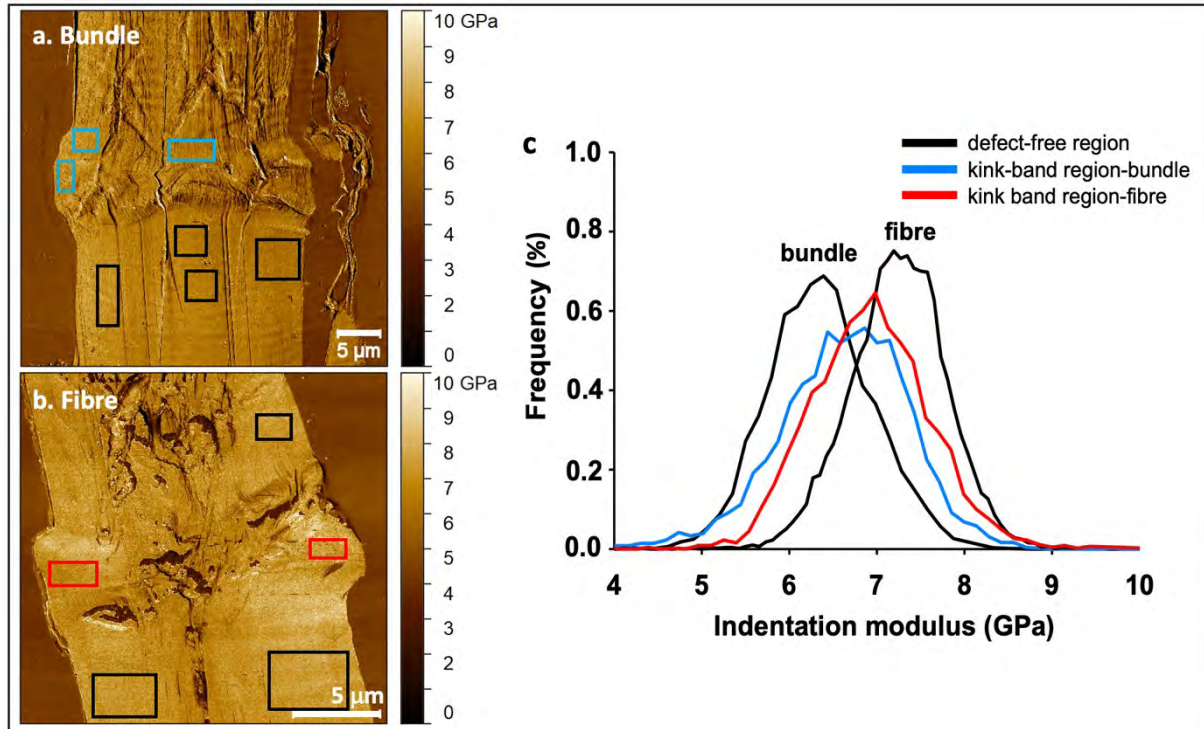


Figure III-25 Indentation moduli of a bundle consisting of at least two flax fibres (a) and of a single fibre (b) cut along their length and with a well-defined kink-band area; the blue and red squares represent the areas used to calculate the mean indentation modulus inside the defects, and the black squares represent the areas used to calculate the mean indentation modulus in the defect-free area. The graphic on the right represents the frequency distributions of the calculated indentation modulus in fibre and bundle. Approximately 7,000 and 24,800 measurements points were used for the kink-band region and defect-free areas, respectively.

A small difference is observed in the indentation modulus calculated on the defect-free areas of the two fibre elements, approximately 6.2 GPa for the bundle and 7.3 GPa for the elementary fibre (mean indentation modulus calculated using these and other images not shown in this study: 6.9 ± 1.2 GPa), which could be due to a difference in the MFA or the cutting angle. In all cases, the indentation modulus distributions of the kink-band region and the region without defects are similar, with values of approximately 6.8–7.0 GPa for the kink-band areas (mean indentation modulus calculated using these and other images not shown in this study: 6.5 ± 1.5 GPa).

The small difference likely occurs as the topography is considerably more inhomogeneous inside the kink-band and affects the values of the indentation moduli. If two neighbouring points with the same indentation modulus have a marked difference in the topography at the scale of the tip radius, their indentation moduli are expected to be underestimated or overestimated due to an erroneous, implicitly

used contact area in the indentation stiffness formulae [48,156]. The fact that the indentation modulus is similar in all areas, while the apparent MFA measured by SHG is not the same, could be mainly explained by the fact that the measured surface is parallel to the microfibril direction and their rotation in the kink-bands is in this plane.

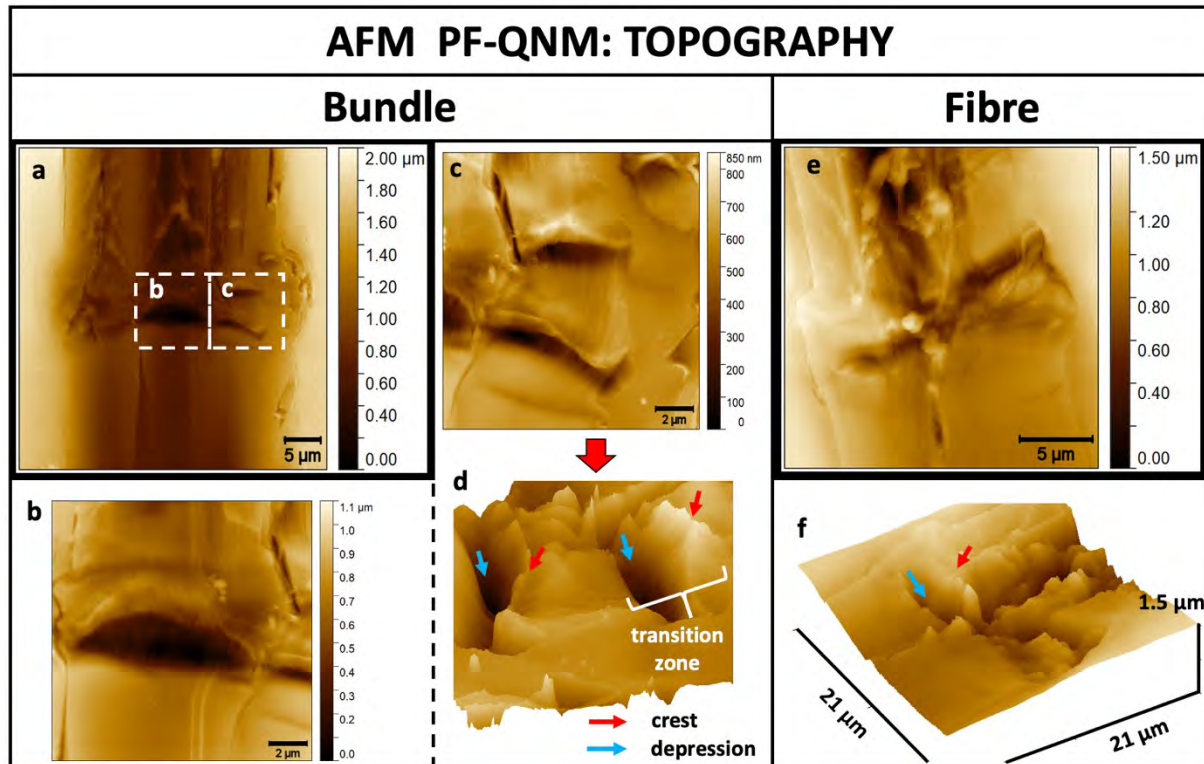


Figure III-26 Topography images (a) in the kink-band region of Figure III-25a with a focus on two areas (white dashed squares) in (b) and (c); (d) 3D topography of the same area presented in (c) where a system of crest-depression is identified inside the kink-band region with red and blue arrows. (e) Topography of the single fibre showed in Figure III-25b and (f) the associated 3D topography where the same crest-depression system already noted in the bundle is observable (blue and red arrows).

Figure III-26a shows the topography of the bundle, and specific areas analysed in detail are indicated with white dashed squares. **Figures III-26b, c** show the details of the area affected; the kink-band topography exhibits a particular morphology corresponding to a transition region, which involves depression of the cell wall alternated by a crest-like structure, as illustrated in the 3D topography (**Figure III-26d**) and indicated by blue and red arrows, respectively. Similar morphology was also observed in **Figures III-26e, f**, which show the topography and the 3D of the single fibre previously analysed in **Figure III-25b**.

This particular crest-depression system seems to be a specific feature of TA kink-bands. However, the hypothesis that it can be attributed to a pull-out phenomenon occurring during the cutting of the sample with the diamond knife cannot be completely ruled out due to the greater misalignment of the microfibril with the cutting direction.

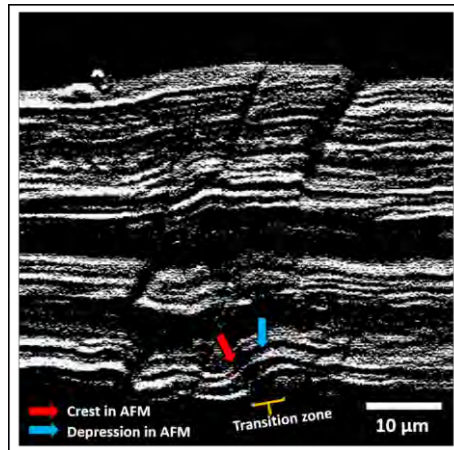


Figure III-27 SHG microscopic image of a kink-band in a bundle of flax fibres; the transition zone with a crest (red arrow) and depression (blue arrow) identified in the AFM topographic images is assumed to be in morphological contrast to the SHG analysis. Fibre bundle mounted in water.

The crest-depression structure can be correlated with the image of the bundle obtained using the SHG microscopy technique (**Figure III-27**), in which certain folds are visible. In contrast to SHG microscopy, which performs measurements within the core of the fibre, AFM measurements are performed at the surface of the fibre cut in two parts along its length, albeit above or below the lumen. It was assumed that the structures observed in the AFM likely resulted from the cutting of the kink-bands. Nevertheless, the crests in the AFM could correspond to the area with the most misaligned macrofibrillar network in the SHG.

3.5 Kink-band areas, a complex and sensitive structure

Through this study, a set of structural and mechanical information was obtained using three different techniques. In TA kink-band areas, heterogeneous zones located in the transition zones between kink-band and defect-free areas were highlighted by SEM (**Figure III-21j**) and confirmed with SHG and AFM observations. In these regions, there is no or very poor SHG emission signal (**Figure III-27**), indicating a more disordered structure. These observations are in line with literature assessments and, in particular, with the hypothesis of Zhang *et al.* [138], where the authors noted that the kink-band region included a main cavity consisting of several voids assembled and separated by membranes, also associated with the presence of small pores regrouped in the area close to the kink. By using AFM, it is possible to further explore these defect regions inside the kink-band zone.

According to this goal, **Figure III-28a** shows the same bundle of **Figures III-25a** and **26a-d**, with the areas analysed in detail represented by white dashed squares.

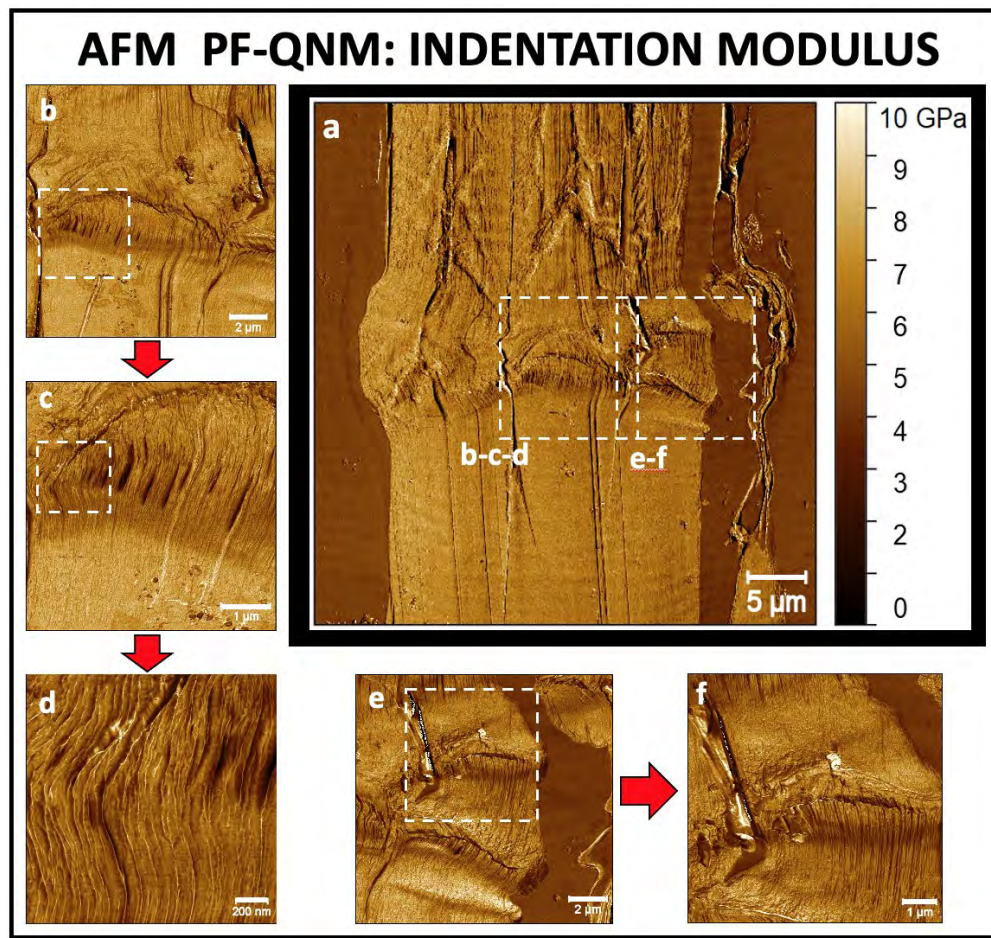


Figure III-28 Indentation modulus of several areas at different scales of the flax fibre bundle and kink-band area: **(a)** whole bundle and areas investigated (white squares); **(b)** and **(c)** focus on one of the central defects and **(d)** focus on the macrofibrils network; **(e)** and **(f)** other defects in the fibre on the right, which highlight a well-ordered network of macrofibrils in the transition zone.

In **Figures III-28b-d**, inhomogeneities at the transition zones located at the limit between the kink band and the defect-free areas are clearly highlighted. Macrofibrils have a highly ordered structure in the depression regions, even though they are deflected with a well-defined angle; however, at the top of the crest, the macrofibrillar network appears less ordered, and it is impossible to distinguish the single macrofibrils from each other (**Figures III-28b, e and f**).

The cavities that alternate with the crest-like inhomogeneities may suggest a weaker point at which the stress during tensile loading may accumulate until failure [157]. The observations made here on a TA kink-band contrast with the much smaller defects and cavities observed on the TB kink-band (**Figure III-29**). This observation can support the hypothesis of Aslan *et al.* [136]: the large kink-bands are likely the areas where failures begin because they exhibit the most considerable heterogeneities. The indentation modulus maps shown in **Figures III-28b-d** indicate that, in some cases, a discontinuity may occur between macrofibrils, which may result in a break with the lines having a lower indentation modulus. In the topography, these lines, which appear as a detachment between the macrofibril bundles,

correspond to small depression regions, as observed in the SEM micrographs presented in **Figures III-21i, j**.

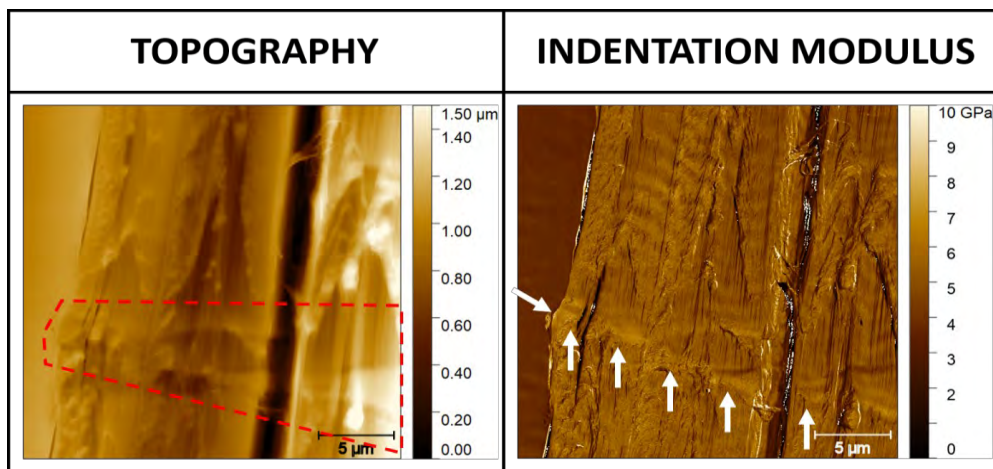


Figure III-29 Topography and indentation modulus acquired using the AFM PF-QNM technique, by analysing another small kink-band region in the same fibre bundle as that examined in the study. The kink-band region is highlighted as a red line and through white arrows in the topography and indentation modulus map, respectively.

Therefore, the kink-band areas show more or less disordered structures depending on their morphology, with sometimes marked cavities resulting from the deformations at the origin of the formation of kink-bands. The latter also leads to very significant changes in the local MFA values, as shown by SEM and SHG (**Figure III-21e** and **24**). Nevertheless, cell wall mechanical properties are little affected, regardless of the considered area and the kink-band type (**Figure III-25a, b** and **29**).

Thanks to these analyses, it was possible to measure the G transverse indentation modulus ranging from 6.2 to 7.3 GPa, which includes both kink-band and defect-free areas; these values are significantly lower than the local longitudinal indentation modulus obtained by Arnould *et al.* by using AFM in PF-QNM mode [39], confirming the highly anisotropic structure of fibres [82]. Here, AFM PF-QNM measurements can be used to directly determine the transverse indentation modulus of flax cell walls. Our results are well correlated with the direct measurements obtained by nanoindentation on wood [33] or sisal and hemp [82] but are more reliable due to the large number of measurement points (between 11,800 and 20,000 points for each image) and the method of sample preparation, which allows direct testing of the cell wall. Considering wood cell walls and by tilting the fibres to estimate their different stiffness tensor components, Jäger *et al.* [106] calculated the transverse indentation modulus of spruce wood cell walls to be 6.02 ± 0.38 GPa, which is in accordance with the presented values, given the difference in the chemical composition and MFA.

Therefore, the kink-band areas exhibit (almost) unchanged G cell wall mechanical performance compared to defect-free zones but an altered ultrastructure, whether in terms of porosities or MFA changes, suggesting that they appear after the cell wall structuration and explaining the differences in mechanical behaviour observed on fibres with a large number of defects [133,135]; the cavities can also

lead to easy-going breaks, as observed after cryofracture (**Figure III-21h**), the ruptures occurring preferentially in the kink-band areas. This is also the case when flax fibres are mixed with a thermoplastic matrix [74]. It is important to keep in mind that the properties estimated through AFM PeakForce are local properties, which in this study were measured in homogenous areas (**Figure III-25**) and below the scale of the cell wall; by definition, the stiffness of cavities cannot be estimated, even if this latter could have an impact on the mechanical properties or behaviour of the whole fibre element.

3.6 Three investigative techniques but also three scales of measurement; what are the cell wall elements measured?

The use of three different techniques with different resolutions raises questions about the nature of the objects measured in each case. Several models for the ultrastructure of plant fibres have been reported in the literature. However, conclusions are sometimes contradictory when describing the hierarchy from a fibril to the fibre bundle in terms of the elementary unit with the relative diameter [158–160] and when describing the ultrastructure of a single elementary fibre and the cellulose microfibril orientation inside the layers [7,127,105,161,162].

In the classical attribution currently used in biology [163], several glucan chains (18–40 units) constitute a single elementary fibril of crystalline cellulose, and several elementary fibrils are regrouped in a structure known as a microfibril, which has a diameter of a few nanometres [164–167]. Despite the disagreement pertaining to the smallest unitary fibril structure and the terminology (for instance, the term “elementary fibril” is often used to indicate a microfibril), it is generally accepted that microfibrils have a diameter ranging from 2 to 4 nm [130,131,145], although some researchers have reported on microfibrils having a diameter of approximately 20 nm for certain plants [167,168]. Nevertheless, this aspect is irrelevant for our results, and furthering this debate is beyond the scope of this study.

In contrast, it has been confirmed that several microfibrils are grouped to form bundles named macrofibrils (or mesofibrils). These structures have been examined using several analytical techniques, such as AFM, SEM or transmission electron microscopy (TEM), and it has been noted that they have a diameter ranging from 14 to 200 nm [128–130].

Furthermore, the SEM, SHG microscopy, and AFM techniques can help to understand the hierarchy between the micro/macrofibrils and the relationship with the MFA. **Figure III-30** shows the comparison between the three techniques used to investigate the thickness of the micro/macrofibrils, and the corresponding results are shown in the graphics on the right. SEM microscopy can resolve the elements at the nanometre scale, and a single fibrillar unit (profile in white) has a thickness of approximately 150 nm, typical of macrofibrils.

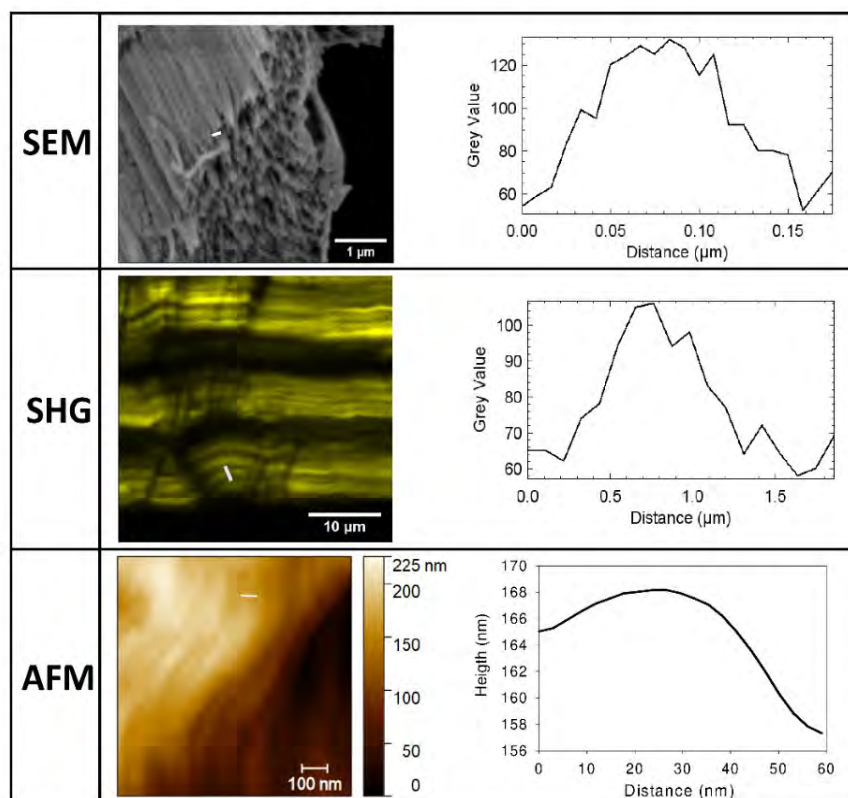


Figure III-30 SEM micrograph, SHG image and topographic map obtained using the AFM PF-QNM. The images are compared to measure the fibril diameter. The grey value in the Y-axis of the SEM and SHG profiles indicates the brightness of the pixels in the image.

In contrast, SHG microscopy exhibits bands with a thickness of approximately 1.0 μm , which is extremely large. However, since the SHG response depends on the order and geometry of the structure, the signal is likely the result of a whole separate bundle of macrofibrils.

AFM has the highest resolution compared to the other techniques used in this study, and can correctly resolve an object of a few nanometres [128,129,169]. The smallest fibril structure examined in this study has a size range of 40–60 nm (**Figures III-30-32**); however, in the literature, microfibrils have been defined to have a diameter of approximately 4–10 nm. In addition, the tip of the AFM probe has a finite dimension that leads to the well-known ‘dilation or convolution effect’ [170,171], i.e., the size of an isolated object measured by AFM is enlarged by the size of the tip diameter. Moreover, the microfibrils may be embedded or coated with a slight layer of the cell wall matrix, making them appear larger than they are. In this study, the tip radius ranges from 40 to 55 nm; consequently, the size of the objects measured is comparable to that of the microfibrils, in line with the findings of Donaldson [130]. In particular, Donaldson reported that the smallest microfibril found in the wood had a diameter of 14 nm; the measurements were performed using field emission scanning electron microscopy (FESEM), which, in this case, can resolve objects of a few nanometres, similar to the AFM technique.

Thus, AFM confirms its potential use as a powerful structural investigation tool. In **Figure III-32**, 6 microfibrils are grouped to form a single macrofibril visible from the drawn profile traced. The

microfibrils, as well as the associated macrofibrils, are well distinguishable on the image of topography and the corresponding profile.

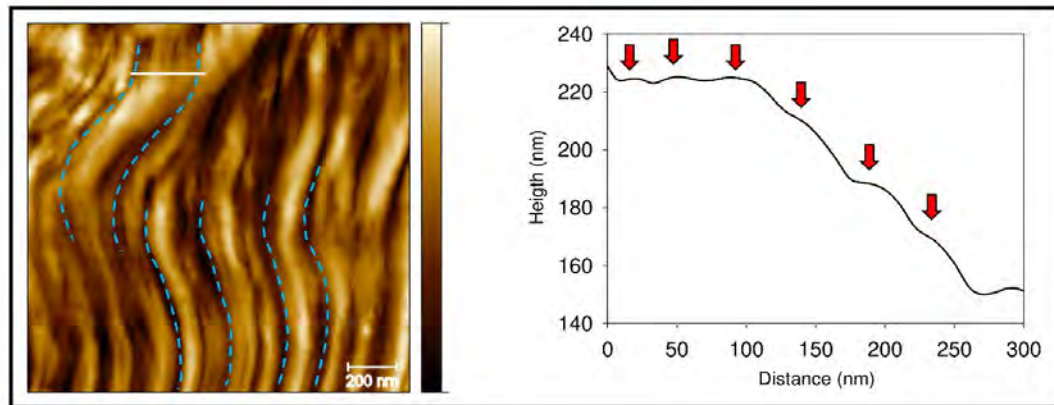


Figure III-31 Topography of the area selected in **Figure III-28d** after image processing for the local contrast to clearly highlight the bundles. The profile line (white) is shown in the graphic on the right, and 6 microfibrils can be identified (red arrows). The dotted lines indicate the edge of certain macrofibrils.

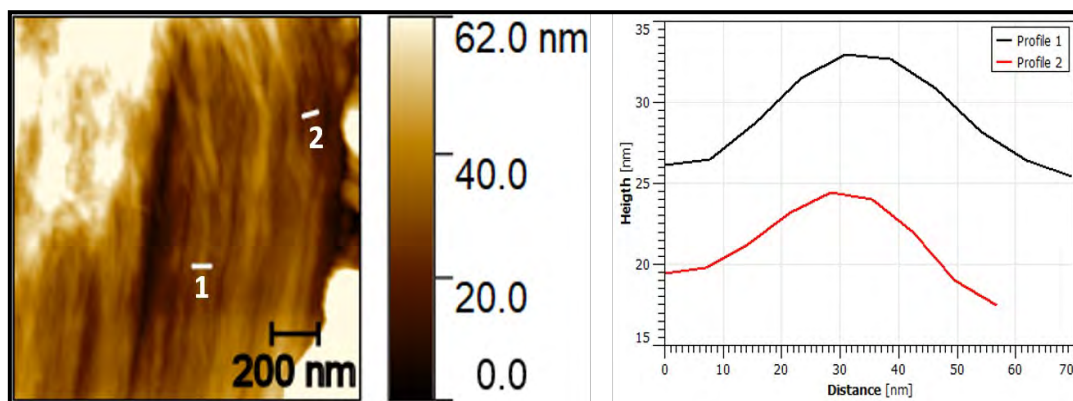


Figure III-32 Topography of a small area selected from **Figure III-28f**; two profiles are considered to measure the microfibril diameter.

3.7 Conclusions

In the present section, cutting-edge techniques, such as AFM PF-QNM and SHG, were combined to study the structural and mechanical properties of flax fibre kink-band regions. SEM analysis was also performed to consolidate and provide additional understanding elements. The main conclusions of this integrated study are as follows: SEM and AFM investigations evidenced the presence of cavities in large kink-bands, which was supported by a low SHG signal, proving a deficiency of crystalline cellulose or a simply more disordered network in these specific zones after the formation of the kink-band.

In kink-band areas, strong deviations of MFA were visually highlighted with the three techniques. SEM exhibited significant MFA evolution in the G layer, and these observations were quantified through

SHG imaging; interestingly, these changes were more pronounced in TA kink-bands (6° – 47°) than in TB kink-bands (4° – 17°).

Despite its deviation, continuity of the lumen in areas affected by kink-bands was demonstrated through SHG and AFM observations, which suggests that the kink-band also involves the inner structure of the cell.

Deep mechanical characterisation of kink-band transverse stiffness was addressed using AFM in PF-QNM mode; no substantial differences were observed between the kink-band and defect-free regions.

This original combination of techniques may give rise to a debate on the size and nature of the objects measured, which is different according to the tool used, from nanofibrils through AFM to aggregates of microfibrils by using multiphoton microscopy.

The elements provided in this section contribute to a better knowledge of these areas of defects; using an integrated approach, relevant information was obtained on the MFA in this specific zone; more than just the cell wall mechanical properties, weakness of kink-band areas is attributed to defects in local structure, inducing an easier rupture under stress. The present work does not pretend to be exhaustive. In future work, it would be interesting to widen the panel of defects studied by focusing on their origins. Indeed, environmental conditions, abiotic stress during growth or the process of fibre extraction can also influence the shape and morphology of the kink-band region.

Bibliography

- [1] J. Merotte, A. Le Duigou, A. Bourmaud, K. Behlouli, C. Baley, Mechanical and acoustic behaviour of porosity controlled randomly dispersed flax/PP biocomposite, *Polym. Test.* 51 (2016) 174–180. <https://doi.org/10.1016/j.polymertesting.2016.03.002>.
- [2] L. Pil, F. Bensadoun, J. Pariset, I. Verpoest, Why are designers fascinated by flax and hemp fibre composites?, *Compos. Part A Appl. Sci. Manuf.* 83 (2016) 193–205. <https://doi.org/10.1016/j.compositesa.2015.11.004>.
- [3] M. Miao, N. Finn, Conversion of Natural Fibres into Structural Composites, *J. Text. Eng.* 54 (2008) 165–177. <https://doi.org/10.4188/jte.54.165>.
- [4] A. Kicińska-Jakubowska, E. Bogacz, M. Zimniewska, Review of Natural Fibers. Part I—Vegetable Fibers, *J. Nat. Fibers.* 9 (2012) 150–167. <https://doi.org/10.1080/15440478.2012.703370>.
- [5] A. Duval, A. Bourmaud, L. Augier, C. Baley, Influence of the sampling area of the stem on the mechanical properties of hemp fibers, *Mater. Lett.* 65 (2011) 797–800. <https://doi.org/10.1016/j.matlet.2010.11.053>.
- [6] M.P. Ansell, L.Y. Mwaikambo, The structure of cotton and other plant fibres, in: S.J. Eichhorn, J.W.S. Hearle, M. Jaffe, T. Kikutani (Eds.), *Handbook of Textile Fibre Structure*, Woodhead Publishing, 2009: pp. 62–94. <https://doi.org/10.1533/9781845697310.1.62>.
- [7] A. Bourmaud, J. Beaugrand, D.U. Shah, V. Placet, C. Baley, Towards the design of high-performance plant fibre composites, *Prog. Mater. Sci.* 97 (2018) 347–408. <https://doi.org/10.1016/j.pmatsci.2018.05.005>.
- [8] P. Wambua, J. Ivens, I. Verpoest, Natural fibres: can they replace glass in fibre reinforced plastics?, *Compos. Sci. Technol.* 63 (2003) 1259–1264. [https://doi.org/10.1016/S0266-3538\(03\)00096-4](https://doi.org/10.1016/S0266-3538(03)00096-4).
- [9] N. Graupner, D. Labonte, H. Humburg, T. Buzkan, A. Dörgens, W. Kelterer, J. Müssig, Functional gradients in the pericarp of the green coconut inspire asymmetric fibre-composites with improved impact strength, and preserved flexural and tensile properties, *Bioinspir. Biomim.* 12 (2017) 1–10. <https://doi.org/10.1088/1748-3190/aa5262>.
- [10] C. Rihouey, F. Paynel, T. Gorshkova, C. Morvan, Flax fibers: assessing the non-cellulosic polysaccharides and an approach to supramolecular design of the cell wall, *Cellulose.* 24 (2017) 1985–2001. <https://doi.org/10.1007/s10570-017-1246-5>.
- [11] K. Rogers, The cell, Britannica Educational Pub. in association with Rosen Educational Services, New York, NY, 2011: pp.55–60.
- [12] B.D. Lazić, B.M. Pejić, A.D. Kramar, M.M. Vukčević, K.R. Mihajlovski, J.D. Rusmirović, M.M. Kostić, Influence of hemicelluloses and lignin content on structure and sorption properties of flax fibers (*Linum usitatissimum* L.), *Cellulose.* 25 (2018) 697–709. <https://doi.org/10.1007/s10570-017-1575-4>.
- [13] M.S. Zamil, A. Geitmann, The middle lamella—more than a glue, *Phys. Biol.* 14 (2017) 015004. <https://doi.org/10.1088/1478-3975/aa5ba5>.
- [14] M. Sfiligoj, S. Hribernik, K. Stana, T. Kree, Plant Fibres for Textile and Technical Applications, in: S. Grundas (Ed.), *Advances in Agrophysical Research*, InTech, 2013: pp. 369–398. <https://doi.org/10.5772/52372>.
- [15] R. Raghavan, R.-B. Adusumalli, G. Buerki, S. Hansen, T. Zimmermann, J. Michler, Deformation of the compound middle lamella in spruce latewood by micro-pillar compression of double cell walls, *J. Mater. Sci.* 47 (2012) 6125–6130. <https://doi.org/10.1007/s10853-012-6531-y>.
- [16] A. Bourmaud, D. Siniscalco, L. Foucat, C. Goudenhooff, X. Falourd, B. Pontoire, O. Arnould, J. Beaugrand, C. Baley, Evolution of flax cell wall ultrastructure and mechanical properties during the retting step, *Carbohydr. Polym.* 206 (2019) 48–56. <https://doi.org/10.1016/j.carbpol.2018.10.065>.
- [17] D. Siniscalco, O. Arnould, A. Bourmaud, A. Le Duigou, C. Baley, Monitoring temperature effects on flax cell-wall mechanical properties within a composite material using AFM, *Polym. Test.* 69 (2018) 91–99. <https://doi.org/10.1016/j.polymertesting.2018.05.009>.

- [18] A.S. Dombia, M. Castro, D. Jouannet, A. Kervoëlen, T. Falher, L. Cauret, A. Bourmaud, Flax/polypropylene composites for lightened structures: Multiscale analysis of process and fibre parameters, *Mater. Des.* 87 (2015) 331–341. <https://doi.org/10.1016/j.matdes.2015.07.139>.
- [19] A. Bourmaud, G. Ausias, G. Lebrun, M.-L. Tachon, C. Baley, Observation of the structure of a composite polypropylene/flax and damage mechanisms under stress, *Ind. Crops Prod.* 43 (2013) 225–236. <https://doi.org/10.1016/j.indcrop.2012.07.030>.
- [20] A. Monti, A. El Mahi, Z. Jendli, L. Guillaumat, Mechanical behaviour and damage mechanisms analysis of a flax-fibre reinforced composite by acoustic emission, *Compos. Part A Appl. Sci. Manuf.* 90 (2016) 100–110. <https://doi.org/10.1016/j.compositesa.2016.07.002>.
- [21] J. Beaugrand, S. Guessasma, J.-E. Maigret, Damage mechanisms in defected natural fibers, *Sci. Rep.* 7 (2017) 1–7. <https://doi.org/10.1038/s41598-017-14514-6>.
- [22] S. Guessasma, J. Beaugrand, Damage Kinetics at the Sub-micrometric Scale in Bast Fibers Using Finite Element Simulation and High-Resolution X-Ray Micro-Tomography, *Front. Plant. Sci.* 10 (2019) 194. <https://doi.org/10.3389/fpls.2019.00194>.
- [23] M.S. Zamil, H. Yi, V.M. Puri, Mechanical characterization of outer epidermal middle lamella of onion under tensile loading, *Am. J. Bot.* 101 (2014) 778–787. <https://doi.org/10.3732/ajb.1300416>.
- [24] K. Charlet, A. Beakou, Interfaces within flax fibre bundle: Experimental characterization and numerical modelling, *J. Compos. Mater.* 48 (2014) 3263–3269. <https://doi.org/10.1177/0021998313508871>.
- [25] L. Qin, L. Lin, F. Fu, M. Fan, Micromechanical properties of wood cell wall and interface compound middle lamella using quasi-static nanoindentation and dynamic modulus mapping, *J. Mater. Sci.* 53 (2018) 549–558. <https://doi.org/10.1007/s10853-017-1185-4>.
- [26] J.E. Jakes, C.R. Frihart, J.F. Beecher, R.J. Moon, P.J. Resto, Z.H. Melgarejo, O.M. Suárez, H. Baumgart, A.A. Elmustafa, D.S. Stone, Nanoindentation near the edge, *J. Mater. Res.* 24 (2009) 1016–1031. <https://doi.org/10.1557/jmr.2009.0076>.
- [27] W. Gindl, H.S. Gupta, T. Schöberl, H.C. Lichtenegger, P. Fratzl, Mechanical properties of spruce wood cell walls by nanoindentation, *Appl. Phys. A.* 79 (2004) 2069–2073. <https://doi.org/10.1007/s00339-004-2864-y>.
- [28] R. Wimmer, B.N. Lucas, Comparing Mechanical Properties of Secondary Wall and Cell Corner Middle Lamella in Spruce Wood, *IAWA J.* 18 (1997) 77–88. <https://doi.org/10.1163/22941932-90001463>.
- [29] O. Arnould, R. Arinero, Towards a better understanding of wood cell wall characterisation with contact resonance atomic force microscopy, *Compos. Part A Appl. Sci. Manuf.* 74 (2015) 69–76. <https://doi.org/10.1016/j.compositesa.2015.03.026>.
- [30] B. Clair, R. Arinero, G. Lévêque, M. Ramonda, B. Thibaut, Imaging the Mechanical Properties of Wood Cell Wall Layers by Atomic Force Modulation Microscopy, *IAWA J.* 24 (2003) 223–230. <https://doi.org/10.1163/22941932-90001591>.
- [31] L. Muraille, V. Aguié-Béghin, B. Chabbert, M. Molinari, Bioinspired lignocellulosic films to understand the mechanical properties of lignified plant cell walls at nanoscale, *Sci. Rep.* 7 (2017) 44065. <https://doi.org/10.1038/srep44065>.
- [32] D. Ren, H. Wang, Z. Yu, H. Wang, Y. Yu, Mechanical imaging of bamboo fiber cell walls and their composites by means of peakforce quantitative nanomechanics (PQNM) technique, *Holzforschung.* 69 (2015) 975–984. <https://doi.org/10.1515/hf-2014-0237>.
- [33] M. Eder, O. Arnould, J.W.C. Dunlop, J. Hornatowska, L. Salmén, Experimental micromechanical characterisation of wood cell walls, *Wood Sci. Technol.* 47 (2013) 163–182. <https://doi.org/10.1007/s00226-012-0515-6>.
- [34] A. Jäger, Th. Bader, K. Hofstetter, J. Eberhardsteiner, The relation between indentation modulus, microfibril angle, and elastic properties of wood cell walls, *Compos. Part A Appl. Sci. Manuf.* 42 (2011) 677–685. <https://doi.org/10.1016/j.compositesa.2011.02.007>.
- [35] S. Malek, L.J. Gibson, Multi-scale modelling of elastic properties of balsa, *Int. J. Solids Struct.* 113 (2017) 118–131. <https://doi.org/10.1016/j.ijsolstr.2017.01.037>.
- [36] A. Bourmaud, J. Mérotte, D. Siniscalco, M. Le Gall, V. Gager, A. Le Duigou, F. Pierre, K. Behlouli, O. Arnould, J. Beaugrand, C. Baley, Main criteria of sustainable natural fibre for efficient unidirectional biocomposites, *Compos. Part A Appl. Sci. Manuf.* 124 (2019) 105504. <https://doi.org/10.1016/j.compositesa.2019.105504>.

- [37] H. Dhakal, A. Bourmaud, F. Berzin, F. Almansour, Z. Zhang, D.U. Shah, J. Beaugrand, Mechanical properties of leaf sheath date palm fibre waste biomass reinforced polycaprolactone (PCL) biocomposites, *Ind. Crops Prod.* 126 (2018) 394–402. <https://doi.org/10.1016/j.indcrop.2018.10.044>.
- [38] C. Goudenhoofft, D. Siniscalco, O. Arnould, A. Bourmaud, O. Sire, T. Gorshkova, C. Baley, Investigation of the Mechanical Properties of Flax Cell Walls during Plant Development: The Relation between Performance and Cell Wall Structure, *Fibers*. 6 (2018) 6. <https://doi.org/10.3390/fib6010006>.
- [39] O. Arnould, D. Siniscalco, A. Bourmaud, A. Le Duigou, C. Baley, Better insight into the nano-mechanical properties of flax fibre cell walls, *Ind. Crops Prod.* 97 (2017) 224–228. <https://doi.org/10.1016/j.indcrop.2016.12.020>.
- [40] A. Bourmaud, H. Dhakal, A. Habrant, J. Padovani, D. Siniscalco, M.H. Ramage, J. Beaugrand, D.U. Shah, Exploring the potential of waste leaf sheath date palm fibres for composite reinforcement through a structural and mechanical analysis, *Compos. Part A Appl. Sci. Manuf.* 103 (2017) 292–303. <https://doi.org/10.1016/j.compositesa.2017.10.017>.
- [41] J. Gao, J.S. Kim, N. Terziev, O. Allegretti, G. Daniel, Chemical and ultrastructural changes in compound middle lamella (CML) regions of softwoods thermally modified by the Termovuoto process, *Holzforschung*. 68 (2014) 849–859. <https://doi.org/10.1515/hf-2013-0221>.
- [42] H.P.S. Abdul Khalil, A.F.I. Yusra, A.H. Bhat, M. Jawaid, Cell wall ultrastructure, anatomy, lignin distribution, and chemical composition of Malaysian cultivated kenaf fiber, *Ind. Crops Prod.* 31 (2010) 113–121. <https://doi.org/10.1016/j.indcrop.2009.09.008>.
- [43] A. Day, K. Ruel, G. Neutelings, D. Crônier, H. David, S. Hawkins, B. Chabbert, Lignification in the flax stem: evidence for an unusual lignin in bast fibers, *Planta*. 222 (2005) 234–245. <https://doi.org/10.1007/s00425-005-1537-1>.
- [44] A. le Duigou, A. Bourmaud, E. Balnois, P. Davies, C. Baley, Improving the interfacial properties between flax fibres and PLLA by a water fibre treatment and drying cycle, *Ind. Crops Prod.* 39 (2012) 31–39. <https://doi.org/10.1016/j.indcrop.2012.02.001>.
- [45] A. Bourmaud, M. Gibaud, A. Lefeuvre, C. Morvan, C. Baley, Influence of the morphology characters of the stem on the lodging resistance of Marylin flax, *Ind. Crops Prod.* 66 (2015) 27–37. <https://doi.org/10.1016/j.indcrop.2014.11.047>.
- [46] K. Radotić, J. Simić-Krstić, M. Jeremić, M. Trifunović, A study of lignin formation at the molecular level by scanning tunneling microscopy, *Biophys. J.* 66 (1994) 1763–1767. [https://doi.org/10.1016/S0006-3495\(94\)81007-0](https://doi.org/10.1016/S0006-3495(94)81007-0).
- [47] N. Terashima, T. Awano, K. Takabe, M. Yoshida, Formation of macromolecular lignin in ginkgo xylem cell walls as observed by field emission scanning electron microscopy, *C. R. Biol.* 327 (2004) 903–910. <https://doi.org/10.1016/j.crv.2004.08.001>.
- [48] G. Stan, R.F. Cook, Mapping the elastic properties of granular Au films by contact resonance atomic force microscopy, *Nanotechnology*. 19 (2008) 235701. <https://doi.org/10.1088/0957-4484/19/23/235701>.
- [49] S.J. Hanley, D.G. Gray, Atomic Force Microscope Images of Black Spruce Wood Sections and Pulp Fibres, *Holzforschung*. 48 (1994) 29–34. <https://doi.org/10.1515/hfsg.1994.48.1.29>.
- [50] A. Kundu, D. Sarkar, N.A. Mandal, M.K. Sinha, B.S. Mahapatra, A secondary phloic (bast) fibre-shy (bfs) mutant of dark jute (*Corchorus olitorius* L.) develops lignified fibre cells but is defective in cambial activity, *Plant Growth Regul.* 67 (2012) 45–55. <https://doi.org/10.1007/s10725-012-9660-z>.
- [51] S. Alix, L. Lebrun, S. Marais, E. Philippe, A. Bourmaud, C. Baley, C. Morvan, Pectinase treatments on technical fibres of flax: Effects on water sorption and mechanical properties, *Carbohydr. Polym.* 87 (2012) 177–185. <https://doi.org/10.1016/j.carbpol.2011.07.035>.
- [52] J. Biagiotti, D. Puglia, J.M. Kenny, A Review on Natural Fibre-Based Composites-Part I: Structure, Processing and Properties of Vegetable Fibres, *J. Nat. Fibers*. 1 (2004) 37–68. https://doi.org/10.1300/J395v01n02_04.
- [53] J.M. van Hazendonk, E.J.M. Reinerik, P. de Waard, J.E.G. van Dam, Structural analysis of acetylated hemicellulose polysaccharides from fibre flax (*Linum usitatissimum* L.), *Carbohydr. Res.* 291 (1996) 141–154. [https://doi.org/10.1016/S0008-6215\(96\)00160-7](https://doi.org/10.1016/S0008-6215(96)00160-7).
- [54] R.F. Evert, *Esau's Plant anatomy: meristems, cells, and tissues of the plant body : their structure, function, and development*, Wiley-Interscience, Hoboken, N.J., 2006.

- [55] D. Crônier, B. Monties, B. Chabbert, Structure and Chemical Composition of Bast Fibers Isolated from Developing Hemp Stem, *J. Agric. Food Chem.* 53 (2005) 8279–8289.
- [56] L. Marrot, A. Lefeuvre, B. Pontoire, A. Bourmaud, C. Baley, Analysis of the hemp fiber mechanical properties and their scattering (Fedora 17), *Ind. Crops Prod.* 51 (2013) 317–327. <https://doi.org/10.1016/j.indcrop.2013.09.026>.
- [57] E. Gümüşkaya, M. Usta, M. Balaban, Carbohydrate components and crystalline structure of organosolv hemp (*Cannabis sativa* L.) bast fibers pulp, *Bioresour. Technol.* 98 (2007) 491–497.
- [58] F. Khan, S.R. Ahmad, Chemical modification and spectroscopic analysis of jute fibre, *Polym. Degrad. Stab.* 52 (1996) 335–340. [https://doi.org/10.1016/0141-3910\(95\)00240-5](https://doi.org/10.1016/0141-3910(95)00240-5).
- [59] A. Roy, S. Chakraborty, S.P. Kundu, R.K. Basak, S.B. Majumder, B. Adhikari, Improvement in mechanical properties of jute fibres through mild alkali treatment as demonstrated by utilisation of the Weibull distribution model, *Bioresour. Technol.* 107 (2012) 222–228. <http://dx.doi.org/10.1016/j.biortech.2011.11.073>.
- [60] S. Karimi, P.M. Tahir, A. Karimi, A. Dufresne, A. Abdulkhani, Kenaf bast cellulosic fibers hierarchy: a comprehensive approach from micro to nano., *Carbohydr. Polym.* 101 (2014) 878–885. <https://doi.org/10.1016/j.carbpol.2013.09.106>.
- [61] A. Ashori, J. Harun, W.D. Raverty, Mohd.N.Mohd. Yusoff, Chemical and Morphological Characteristics of Malaysian Cultivated Kenaf (*Hibiscus cannabinus*) Fiber, *Plast. Tech. Eng.* 45 (2006) 131–134. <https://doi.org/10.1080/03602550500373782>.
- [62] C. Zhou, Y. Ohtani, K. Sameshima, M. Zhen, Selection of plant population of kenaf (*Hibiscus cannabinus* L.) as a papermaking raw material on arid hillside land in China, *J. Wood Sci.* 44 (1998) 296–302. <https://doi.org/10.1007/BF00581310>.
- [63] L. Bacci, S. Di Lonardo, L. Albanese, G. Mastromei, B. Perito, Effect of different extraction methods on fiber quality of nettle (*Urtica dioica* L.), *Text. Res. J.* 81 (2011) 827–837. <https://doi.org/10.1177/0040517510391698>.
- [64] A. Bourmaud, H. Dhakal, A. Habrant, J. Padovani, D. Siniscalco, M.H. Ramage, J. Beaugrand, D.U. Shah, Exploring the potential of waste leaf sheath date palm fibres for composite reinforcement through a structural and mechanical analysis, *Compos. Part A Appl. Sci. Manuf.* 103 (2017) 292–303. <https://doi.org/10.1016/j.compositesa.2017.10.017>.
- [65] N. Saadaoui, A. Rouilly, K. Fares, L. Rigal, Characterization of date palm lignocellulosic by-products and self-bonded composite materials obtained thereof, *Mater. Des.* 50 (2013) 302–308. <https://doi.org/10.1016/j.matdes.2013.03.011>.
- [66] F.B. Daher, S.A. Braybrook, How to let go: pectin and plant cell adhesion, *Front. Plant Sci.* 6 (2015). <https://doi.org/10.3389/fpls.2015.00523>.
- [67] C. Baley, Y. Perrot, F. Busnel, H. Guezenc, P. Davies, Transverse tensile behaviour of unidirectional plies reinforced with flax fibres, *Mater. Lett.* 60 (2006) 2984–2987. <https://doi.org/10.1016/j.matlet.2006.02.028>.
- [68] G. Coroller, A. Lefeuvre, A. Le Duigou, A. Bourmaud, G. Ausias, T. Gaudry, C. Baley, Effect of flax fibres individualisation on tensile failure of flax/epoxy unidirectional composite, *Compos. Part A Appl. Sci. Manuf.* 51 (2013) 62–70. <https://doi.org/10.1016/j.compositesa.2013.03.018>.
- [69] F. Barthelat, H.D. Espinosa, An Experimental Investigation of Deformation and Fracture of Nacre—Mother of Pearl, *Exp. Mech.* 47 (2007) 311–324. <https://doi.org/10.1007/s11340-007-9040-1>.
- [70] M. Tanguy, A. Bourmaud, J. Beaugrand, T. Gaudry, C. Baley, Polypropylene reinforcement with flax or jute fibre; Influence of microstructure and constituents properties on the performance of composite, *Compos. B. Eng.* 139 (2018) 64–74. <https://doi.org/10.1016/j.compositesb.2017.11.061>.
- [71] N. Graupner, H. Fischer, G. Ziegmann, J. Müssig, Improvement and analysis of fibre/matrix adhesion of regenerated cellulose fibre reinforced PP-, MAPP- and PLA-composites by the use of Eucalyptus globulus lignin, *Compos. B. Eng.* 66 (2014) 117–125. <https://doi.org/10.1016/j.compositesb.2014.05.002>.
- [72] J. Padovani, D. Legland, M. Pernes, A. Gallos, C. Thomachot-Schneider, D.U. Shah, A. Bourmaud, J. Beaugrand, Beating of hemp bast fibres: an examination of a hydro-mechanical treatment on chemical, structural, and nanomechanical property evolutions, *Cellulose.* 26 (2019) 5665–5683. <https://doi.org/10.1007/s10570-019-02456-3>.

- [73] F. Berzin, J. Beaugrand, S. Dobosz, T. Budtova, B. Vergnes, Lignocellulosic fiber breakage in a molten polymer. Part 3. Modeling of the dimensional change of the fibers during compounding by twin screw extrusion, *Compos. Part A Appl. Sci. Manuf.* 101 (2017) 422–431. <https://doi.org/10.1016/j.compositesa.2017.07.009>.
- [74] A. Le Duc, B. Vergnes, T. Budtova, Polypropylene/natural fibres composites: Analysis of fibre dimensions after compounding and observations of fibre rupture by rheo-optics, *Compos. Part A Appl. Sci. Manuf.* 42 (2011) 1727–1737. <https://doi.org/10.1016/j.compositesa.2011.07.027>.
- [75] B. Duchemin, A. Thuault, A. Vicente, B. Rigaud, C. Fernandez, S. Eve, Ultrastructure of cellulose crystallites in flax textile fibres, *Cellulose*. 19 (2012) 1837–1854. <https://doi.org/10.1007/s10570-012-9786-1>.
- [76] A.B. Wardrop, Cell wall organization in higher plants I. The primary wall, *Bot. Rev.* 28 (1962) 241–285. <https://doi.org/10.1007/BF02860816>.
- [77] G.J. Ritter, The microstructure of cellulose fibers, United States Department of Agriculture, Forest Service, Forest Products Laboratory, Madison, Wisconsin, 1942.
- [78] M. Ioelovich, Cellulose: nanostructured natural polymer, LAP LAMBERT Academic Publishing. (2014).
- [79] C. Baley, Analysis of the flax fibres tensile behaviour and analysis of the tensile stiffness increase, *Compos. Part A Appl. Sci. Manuf.* 33 (2002) 939–948. [https://doi.org/10.1016/S1359-835X\(02\)00040-4](https://doi.org/10.1016/S1359-835X(02)00040-4).
- [80] A.N. Netravali, Biodegradable natural fiber composites, in: R.S. Blackburn (Eds.), *Biodegradable and Sustainable Fibres*, R.S. Blackburn, Woodhead Publishing, 2005: pp. 271–309.
- [81] A. Bourmaud, C. Morvan, A. Bouali, V. Placet, P. Perré, C. Baley, Relationships between micro-fibrillar angle, mechanical properties and biochemical composition of flax fibers, *Ind. Crops Prod.* 44 (2013) 343–351. <https://doi.org/10.1016/j.indcrop.2012.11.031>.
- [82] A. Bourmaud, C. Baley, Rigidity analysis of polypropylene/vegetal fibre composites after recycling, *Polym. Degrad. Stab.* 94 (2009) 297–305. <https://doi.org/10.1016/j.polymdegradstab.2008.12.010>.
- [83] L. Donaldson, Microfibril Angle: Measurement, Variation and Relationships – A Review, *IAWA J.* 29 (2008) 345–386. <https://doi.org/10.1163/22941932-90000192>.
- [84] M. Müller, C. Czihak, M. Burghammer, C. Riekkel, Combined X-ray microbeam small-angle scattering and fibre diffraction experiments on single native cellulose fibres, *J. Appl. Crystallogr.* 33 (2000) 817–819. <https://doi.org/10.1107/S0021889800099751>.
- [85] M. Müller, C. Czihak, G. Vogl, P. Fratzl, H. Schober, C. Riekkel, Direct Observation of Microfibril Arrangement in a Single Native Cellulose Fiber by Microbeam Small-Angle X-ray Scattering, *Macromolecules*. 31 (1998) 3953–3957. <https://doi.org/10.1021/ma980004c>.
- [86] C. Wang, N. Wang, S. Liu, L.-P. Choo-Simth, H. Zhang, Z. Zhi, Investigation of Microfibril Angle of Flax Fibers Using X-Ray Diffraction and Scanning Electron Microscopy, *J. Nat. Fibers*. (2018) 1–10. <https://doi.org/10.1080/15440478.2018.1546639>.
- [87] O.M. Astley, A.M. Donald, A Small-Angle X-ray Scattering Study of the Effect of Hydration on the Microstructure of Flax Fibers, *Biomacromolecules*. 2 (2001) 672–680. <https://doi.org/10.1021/bm005643l>.
- [88] H.L. Bos, A.M. Donald, In situ ESEM study of the deformation of elementary flax fibres, *J. Mater. Sci.* 34 (1999) 3029–3034.
- [89] B. Thomas, D. McIntosh, T. Fildes, L. Smith, F. Hargrave, M. Islam, T. Thompson, R. Layfield, D. Scott, B. Shaw, C.L. Burrell, S. Gonzalez, S. Taylor, Second-harmonic generation imaging of collagen in ancient bone, *Bone Rep.* 7 (2017) 137–144. <https://doi.org/10.1016/j.bonr.2017.10.005>.
- [90] V. Zubkovs, F. Jamme, S. Kascakova, F. Chiappini, F. Le Naour, M. Réfrégiers, Single vs. two-photon microscopy for label free intrinsic tissue studies in the UV light region, *Analyst*. 139 (2014) 2663–2667. <https://doi.org/10.1039/C4AN00203B>.
- [91] G. Cox, E. Kable, Second-Harmonic Imaging of Collagen, in: D.J. Taatjes, B.T. Mossman (Eds.), *Cell Imaging Techniques: Methods and Protocols*, Humana Press, Totowa, NJ, 2006: pp. 15–35. https://doi.org/10.1007/978-1-59259-993-6_2.
- [92] R.M. Williams, W.R. Zipfel, W.W. Webb, Interpreting Second-Harmonic Generation Images of Collagen I Fibrils, *Biophys. J.* 88 (2005) 1377–1386. <https://doi.org/10.1529/biophysj.104.047308>.

- [93] Y. Goulam Houssen, I. Gusachenko, M.-C. Schanne-Klein, J.-M. Allain, Monitoring micrometer-scale collagen organization in rat-tail tendon upon mechanical strain using second harmonic microscopy, *J. Biomech.* 44 (2011) 2047–2052. <https://doi.org/10.1016/j.jbiomech.2011.05.009>.
- [94] R.M. Brown, Jr., A.C. Millard, P.J. Campagnola, Macromolecular structure of cellulose studied by second-harmonic generation imaging microscopy, *Opt. Lett.* 28 (2003) 2207–2209. <https://doi.org/10.1364/OL.28.002207>.
- [95] S. Psilodimitrakopoulos, I. Amat-Roldan, S. Santos, M. Mathew, A. Thayil K. N., D. Zalvidea, D. Artigas, P. Loza-Alvarez, Starch granules as a probe for the polarization at the sample plane of a high resolution multiphoton microscope, in: A. Periasamy, P.T.C. So (Eds.), *Multiphoton Microscopy in the Biomedical Sciences VIII*, San Jose, CA, 2008: p. 68600E. <https://doi.org/10.1117/12.763168>.
- [96] V. Gager, D. Legland, A. Bourmaud, A. Le Duigou, F. Pierre, K. Behloul, C. Baley, Oriented granulometry to quantify fibre orientation distributions in synthetic and plant fibre composite preforms, *Ind. Crops Prod.* 152 (2020) 112548. <https://doi.org/10.1016/j.indcrop.2020.112548>.
- [97] M.-F. Devaux, D. Legland, Grey level granulometry for histological image analysis of plant tissues, in: A. Méndez-Vilaz (Ed.) *Microscopy. Advances in Scientific Research and Education*, Formatex Research Center, 2014: pp. 681–688.
- [98] M.F. Devaux, B. Bouchet, D. Legland, F. Guillon, M. Lahaye, Macro-vision and grey level granulometry for quantification of tomato pericarp structure, *Postharvest Biol. Technol.* 47 (2008) 199–209. <https://doi.org/10.1016/j.postharvbio.2007.06.017>.
- [99] P. Soille, *Morphological Image Analysis: Principles and Applications*, 2nd ed., Springer-Verlag, Berlin Heidelberg, 2004. <https://doi.org/10.1007/978-3-662-05088-0>.
- [100] P. Soille, ed., *Morphological Texture Analysis: An Introduction*, in: K. R. Mecke, D. Stoyan (Eds.), *Morphology of Condensed Matter: Physics and Geometry of Spatially Complex Systems*, Mecke, K. & Stoyan, D., Springer-Verlag, Berlin Heidelberg, 2002: pp. 215–237. <https://doi.org/10.1007/3-540-45782-8>.
- [101] D. Legland, M.-F. Devaux, B. Bouchet, F. Guillon, M. Lahaye, Cartography of cell morphology in tomato pericarp at the fruit scale, *J. Microsc.* 247 (2012) 78–93. <https://doi.org/10.1111/j.1365-2818.2012.03623.x>.
- [102] F.S. Pavone, P.J. Campagnola, eds., *Second Harmonic Generation Imaging*, 1 edition, CRC Press, Boca Raton, 2013.
- [103] O. Nadiarnykh, R.B. LaComb, P.J. Campagnola, W.A. Mohler, Coherent and incoherent SHG in fibrillar cellulose matrices, *Opt. Express.* 15 (2007) 3348. <https://doi.org/10.1364/OE.15.003348>.
- [104] P.J. Campagnola, A.C. Millard, M. Terasaki, P.E. Hoppe, C.J. Malone, W.A. Mohler, Three-Dimensional High-Resolution Second-Harmonic Generation Imaging of Endogenous Structural Proteins in Biological Tissues, *Biophys. J.* 82 (2002) 493–508. [https://doi.org/10.1016/S0006-3495\(02\)75414-3](https://doi.org/10.1016/S0006-3495(02)75414-3).
- [105] J.-C. Roland, M. Mosiniak, D. Roland, Dynamique du positionnement de la cellulose dans les parois des fibres textiles du lin (*Linum usitatissimum*), *Acta Bot. Gall.* 142 (1995) 463–484. <https://doi.org/10.1080/12538078.1995.10515271>.
- [106] A. Jäger, K. Hofstetter, Ch. Buksnowitz, W. Gindl-Altmutter, J. Konnerth, Identification of stiffness tensor components of wood cell walls by means of nanoindentation, *Compos. Part A Appl. Sci. Manuf.* 42 (2011) 2101–2109. <https://doi.org/10.1016/j.compositesa.2011.09.020>.
- [107] A. Lefeuvre, A. Bourmaud, C. Morvan, C. Baley, Elementary flax fibre tensile properties: Correlation between stress–strain behaviour and fibre composition, *Ind. Crops Prod.* 52 (2014) 762–769. <https://doi.org/10.1016/j.indcrop.2013.11.043>.
- [108] M. Dochia, C. Sirghie, R.M. Kozłowski, Z. Roskwitalski, Cotton fibres, in: R. M. Kozłowski (Ed.), *Handbook of Natural Fibres*, Elsevier, 2012: pp. 11–23. <https://doi.org/10.1533/9780857095503.1.9>.
- [109] R.F. Evert, *Esau's Plant anatomy: meristems, cells, and tissues of the plant body : their structure, function, and development*, Wiley-Interscience, Hoboken, N.J., 2006.

- [110] V.P. Skulachev, V.N. Anisimov, Y.N. Antonenko, L.E. Bakeeva, B.V. Chernyak, V.P. Elichev, O.F. Filenko, N.I. Kalinina, V.I. Kapelko, N.G. Kolosova, B.P. Kopnin, G.A. Korshunova, M.R. Lichinitser, L.A. Obukhova, E.G. Pasyukova, O.I. Pisarenko, V.A. Roginsky, E.K. Ruuge, I.I. Senin, I.I. Severina, M.V. Skulachev, I.M. Spivak, V.N. Tashlitsky, V.A. Tkachuk, M.Yu. Vyssokikh, L.S. Yaguzhinsky, D.B. Zorov, An attempt to prevent senescence: A mitochondrial approach, *Biochim. Biophys. Acta Bioenerg.* 1787 (2009) 437–461. <https://doi.org/10.1016/j.bbabbio.2008.12.008>.
- [111] R.H. Berg, Evaluation of spectral imaging for plant cell analysis, *J. Microsc.* 214 (2004) 174–181. <https://doi.org/10.1111/j.0022-2720.2004.01347.x>.
- [112] G.D. Love, C.E. Snape, M.C. Jarvis, I.M. Morrison, Determination of phenolic structures in flax fibre by solid-state ¹³C NMR, *Phytochemistry*. 35 (1994) 489–491. [https://doi.org/10.1016/S0031-9422\(00\)94788-5](https://doi.org/10.1016/S0031-9422(00)94788-5).
- [113] A.K. Mohanty, S. Vivekanandhan, J.-M. Pin, M. Misra, Composites from renewable and sustainable resources: Challenges and innovations, *Science*. 362 (2018) 536–542. <https://doi.org/10.1126/science.aat9072>.
- [114] M.K. Deyholos, S. Potter, Engineering bast fiber feedstocks for use in composite materials, *Biocatal. Agric. Biotechnol.* 3 (2014) 53–57. <https://doi.org/10.1016/j.bcab.2013.09.001>.
- [115] A. Le Duigou, P. Davies, C. Baley, Environmental Impact Analysis of the Production of Flax Fibres to be Used as Composite Material Reinforcement, *J. Biobased Mat. Bioenergy*. 5 (2011) 153–165. <https://doi.org/10.1166/jbmb.2011.1116>.
- [116] B. Madsen, E.K. Gamstedt, Wood versus Plant Fibers: Similarities and Differences in Composite Applications, *Adv. Mater. Sci. Eng.* 2013 (2013) 1–14. <https://doi.org/10.1155/2013/564346>.
- [117] B. Focher, A. Marzetti, H.S.S. Sharma, Changes in the structure and properties of flax fibre during processing, in: *The Biology and Processing of Flax*, Sharma H. S. S. Van Sumere C. F. (Eds.), M Publications, Belfast, 1992: pp. 329–342.
- [118] M. Hughes, G. Sèbe, J. Hague, C. Hill, M. Spear, L. Mott, An investigation into the effects of micro-compressive defects on interphase behaviour in hemp-epoxy composites using half-fringe photoelasticity, *Compos. Interfaces*. 7 (2000) 13–29. <https://doi.org/10.1163/156855400300183551>.
- [119] L.G. Thygesen, M.R. Asgharipour, The effects of growth and storage conditions on dislocations in hemp fibres, *J. Mater. Sci.* 43 (2008) 3670–3673. <https://doi.org/10.1007/s10853-008-2587-0>.
- [120] C.R. Nodder, A Study of Flax and Kindred Fibres, *J. Text. Inst.* 13 (1922) 213–219. <https://doi.org/10.1080/03684504.1922.11673746>.
- [121] A. Thuault, S. Eve, P. Jouannot-Chesney, J. Bréard, M. Gomina, Interrelation Between the Variety and the Mechanical Properties of Flax Fibres, *J. Biobased Mat. Bioenergy*. 7 (2013) 609–618. <https://doi.org/10.1166/jbmb.2013.1396>.
- [122] X. Zeng, S.J. Mooney, C.J. Sturrock, Assessing the effect of fibre extraction processes on the strength of flax fibre reinforcement, *Compos. Part A Appl. Sci. Manuf.* 70 (2015) 1–7. <https://doi.org/10.1016/j.compositesa.2014.12.004>.
- [123] A. Hernandez-Estrada, H.-J. Gusovius, J. Müssig, M. Hughes, Assessing the susceptibility of hemp fibre to the formation of dislocations during processing, *Ind. Crops Prod.* 85 (2016) 382–388. <https://doi.org/10.1016/j.indcrop.2016.01.006>.
- [124] K. Nyholm, P. Ander, S. Bardage, G. Daniel, W. Science, Dislocations in pulp fibres – their origin, characteristics and importance – a review, *Nord Pulp Paper Res. J.* 16 (2001) 376–384.
- [125] B. Clair, A. Dejardin, G. Pilate, T. Alméras, Is the G-Layer a Tertiary Cell Wall?, *Front. Plant Sci.* 9 (2018) 623. <https://doi.org/10.3389/fpls.2018.00623>.
- [126] T. Gorshkova, P. Mikshina, A. Petrova, T. Chernova, N. Mokshina, O. Gorshkov, Plants at Bodybuilding: Development of Plant “Muscles”, in: *A. Geitmann, J. Gril (Eds.), Plant Biomechanics: From Structure to Function at Multiple Scales*, Springer, Cham, 2018: pp. 141–163. https://doi.org/10.1007/978-3-319-79099-2_7.
- [127] C. Baley, C. Goudenhooff, M. Gibaud, A. Bourmaud, Flax stems: from a specific architecture to an instructive model for bioinspired composite structures, *Bioinspir. Biomim.* 13 (2018) 026007. <https://doi.org/10.1088/1748-3190/aaa6b7>.
- [128] J. Fahlén, L. Salmén, Cross-sectional structure of the secondary wall of wood fibers as affected by processing, *J. Mater. Sci.* 38 (2003) 119–126. <https://doi.org/10.1023/A:1021174118468>.

- [129] E. Balnois, F. Busnel, C. Baley, Y. Grohens, An AFM study of the effect of chemical treatments on the surface microstructure and adhesion properties of flax fibres, *Compos. Interfaces*. 14 (2007) 715–731. <https://doi.org/10.1163/156855407782106537>.
- [130] L. Donaldson, Cellulose microfibril aggregates and their size variation with cell wall type, *Wood Sci Technol*. 41 (2007) 443–460. <https://doi.org/10.1007/s00226-006-0121-6>.
- [131] J.J. Lyczakowski, M. Bourdon, O.M. Terrett, Y. Helariutta, R. Wightman, P. Dupree, Structural Imaging of Native Cryo-Preserved Secondary Cell Walls Reveals the Presence of Macrofibrils and Their Formation Requires Normal Cellulose, Lignin and Xylan Biosynthesis, *Front. Plant Sci*. 10 (2019) 1398. <https://doi.org/10.3389/fpls.2019.01398>.
- [132] L.G. Thygesen, N. Gierlinger, The molecular structure within dislocations in *Cannabis sativa* fibres studied by polarised Raman microspectroscopy, *J. Struct. Biol*. 182 (2013) 219–225. <https://doi.org/10.1016/j.jsb.2013.03.010>.
- [133] L.G. Thygesen, M. Eder, I. Burgert, Dislocations in single hemp fibres—investigations into the relationship of structural distortions and tensile properties at the cell wall level, *J. Mater. Sci*. 42 (2007) 558–564. <https://doi.org/10.1007/s10853-006-1113-5>.
- [134] A. Khodayari, A.W. Van Vuure, U. Hirn, D. Seveno, Tensile behaviour of dislocated/crystalline cellulose fibrils at the nano scale, *Carbohydr. Polym*. 235 (2020) 115946. <https://doi.org/10.1016/j.carbpol.2020.115946>.
- [135] C. Baley, Influence of kink bands on the tensile strength of flax fibers, *J. Mater. Sci*. 39 (2004) 331–334.
- [136] M. Aslan, G. Chinga-Carrasco, B.F. Sørensen, B. Madsen, Strength variability of single flax fibres, *J. Mater. Sci*. 46 (2011) 6344–6354. <https://doi.org/10.1007/s10853-011-5581-x>.
- [137] J. Beaugrand, S. Guessasma, J.-E. Maigret, Damage mechanisms in defected natural fibers, *Sci. Rep*. 7 (2017). <https://doi.org/10.1038/s41598-017-14514-6>.
- [138] H. Zhang, T. Sui, L.G. Thygesen, P. O'Brien, A.M. Korsunsky, Multi-modal Microscopy Characterisation of Nodal Markings in Flax Fibre, in: *Proceedings of the World Congress on Engineering (WCE)*, London, U.K., 2015.
- [139] J. Sliseris, L. Yan, B. Kasal, Numerical modelling of flax short fibre reinforced and flax fibre fabric reinforced polymer composites, *Compos. B. Eng*. 89 (2016) 143–154. <https://doi.org/10.1016/j.compositesb.2015.11.038>.
- [140] T. Nilsson, P.J. Gustafsson, Influence of dislocations and plasticity on the tensile behaviour of flax and hemp fibres, *Compos. Part A Appl. Sci. Manuf*. 38 (2007) 1722–1728. <https://doi.org/10.1016/j.compositesa.2007.01.018>.
- [141] L. Benabou, Kink Band Formation in Wood Species Under Compressive Loading, *Exp. Mech*. 48 (2008) 647–656. <https://doi.org/10.1007/s11340-007-9098-9>.
- [142] M. Eder, N. Terziev, G. Daniel, I. Burgert, The effect of (induced) dislocations on the tensile properties of individual Norway spruce fibres, *Holzforschung*. 62 (2008) 77–81. <https://doi.org/10.1515/HF.2008.011>.
- [143] R. Coste, M. Soliman, N.B. Bercu, S. Potiron, K. Lasri, V. Aguié-Béghin, L. Tetard, B. Chabbert, M. Molinari, Unveiling the impact of embedding resins on the physicochemical traits of wood cell walls with subcellular functional probing, *Compos. Sci. Technol*. 201 (2021) 108485. <https://doi.org/10.1016/j.compscitech.2020.108485>.
- [144] B. Madsen, M. Aslan, H. Lilholt, Fractographic observations of the microstructural characteristics of flax fibre composites, *Compos. Sci. Technol*. 123 (2016) 151–162. <https://doi.org/10.1016/j.compscitech.2015.12.003>.
- [145] A. Bourmaud, D. Siniscalco, L. Foucat, C. Goudenhooff, X. Falourd, B. Pontoire, O. Arnould, J. Beaugrand, C. Baley, Evolution of flax cell wall ultrastructure and mechanical properties during the retting step, *Carbohydr. Polym*. 206 (2019) 48–56. <https://doi.org/10.1016/j.carbpol.2018.10.065>.
- [146] D. Dai, M. Fan, Investigation of the dislocation of natural fibres by Fourier-transform infrared spectroscopy, *Vib. Spectrosc*. 55 (2011) 300–306. <https://doi.org/10.1016/j.vibspec.2010.12.009>.
- [147] A. Céline, S. Fréour, F. Jacquemin, P. Casari, The hygroscopic behavior of plant fibers: a review, *Front. Chem*. 1 (2014). <https://doi.org/10.3389/fchem.2013.00043>.

- [148] K. Toba, H. Yamamoto, M. Yoshida, Crystallization of cellulose microfibrils in wood cell wall by repeated dry-and-wet treatment, using X-ray diffraction technique, *Cellulose*. 20 (2013) 633–643. <https://doi.org/10.1007/s10570-012-9853-7>.
- [149] A. Céline, O. Gonçalves, F. Jacquemin, S. Fréour, Utilisation de la spectrométrie infrarouge pour une quantification rapide du taux d'humidité dans des fibres végétales, *Revue Des Composites et Des Matériaux Avancés*. 24 (2014) 81–95. <https://doi.org/10.3166/rcma.24.81-95>.
- [150] K. Nakamura, T. Hatakeyama, H. Hatakeyama, Effect of Bound Water on Tensile Properties of Native Cellulose, *Textile Research Journal*. 53 (1983) 682–688. <https://doi.org/10.1177/004051758305301108>.
- [151] K. Casdorff, T. Keplinger, I. Burgert, Nano-mechanical characterization of the wood cell wall by AFM studies: comparison between AC- and QITM mode, *Plant Methods*. 13 (2017) 60. <https://doi.org/10.1186/s13007-017-0211-5>.
- [152] K. Casdorff, T. Keplinger, M. Rüggeberg, I. Burgert, A close-up view of the wood cell wall ultrastructure and its mechanics at different cutting angles by atomic force microscopy, *Planta*. 247 (2018) 1123–1132. <https://doi.org/10.1007/s00425-018-2850-9>.
- [153] R. Coste, M. Pernes, L. Tetard, M. Molinari, B. Chabbert, Effect of the Interplay of Composition and Environmental Humidity on the Nanomechanical Properties of Hemp Fibers, *ACS Sustain. Chem. Eng.* 8 (2020) 6381–6390. <https://doi.org/10.1021/acssuschemeng.0c00566>.
- [154] A. Stylianou, D. Yova, Surface nanoscale imaging of collagen thin films by Atomic Force Microscopy, *Mater. Sci. Eng. C*. 33 (2013) 2947–2957. <https://doi.org/10.1016/j.msec.2013.03.029>.
- [155] W. Hu, A. Buzin, J.-S. Lin, B. Wunderlich, Annealing behavior of gel-spun polyethylene fibers at temperatures lower than needed for significant shrinkage, *J. Polym. Sci. B Polym. Phys.* 41 (2003) 403–417. <https://doi.org/10.1002/polb.10372>.
- [156] K. Heinze, O. Arnould, J.-Y. Delenne, V. Lullien-Pellerin, M. Ramonda, M. George, On the effect of local sample slope during modulus measurements by contact-resonance atomic force microscopy, *Ultramicroscopy*. 194 (2018) 78–88. <https://doi.org/10.1016/j.ultramic.2018.07.009>.
- [157] H.N. Dhakal, M. Sain, Enhancement of Mechanical Properties of Flax-Epoxy Composite with Carbon Fibre Hybridisation for Lightweight Applications, *Materials*. 13 (2019) 109. <https://doi.org/10.3390/ma13010109>.
- [158] K.J. Niklas, The Cell Walls that Bind the Tree of Life, *BioScience*. 54 (2004) 831–841. [https://doi.org/10.1641/0006-3568\(2004\)054\[0831:TCWTBT\]2.0.CO;2](https://doi.org/10.1641/0006-3568(2004)054[0831:TCWTBT]2.0.CO;2).
- [159] H. Zhu, Z. Fang, C. Preston, Y. Li, L. Hu, Transparent paper: fabrications, properties, and device applications, *Energy Environ. Sci.* 7 (2014) 269–287. <https://doi.org/10.1039/C3EE43024C>.
- [160] Y. Li, X. Yi, T. Yu, G. Xian, An overview of structural-functional-integrated composites based on the hierarchical microstructures of plant fibers, *Adv. Compos. Hybrid Mater.* 1 (2018) 231–246. <https://doi.org/10.1007/s42114-017-0020-3>.
- [161] J. Biagiotti, D. Puglia, J.M. Kenny, A Review on Natural Fibre-Based Composites-Part I: Structure, Processing and Properties of Vegetable Fibres, *J. Nat. Fibers*. 1 (2004) 37–68. https://doi.org/10.1300/J395v01n02_04.
- [162] B. Domenges, K. Charlet, Direct Insights on Flax Fiber Structure by Focused Ion Beam Microscopy, *Microsc. Microanal.* 16 (2010) 175–182. <https://doi.org/10.1017/S1431927609991292>.
- [163] G. Chinga-Carrasco, Cellulose fibres, nanofibrils and microfibrils: The morphological sequence of MFC components from a plant physiology and fibre technology point of view, *Nanoscale Res. Lett.* 6 (2011) 417. <https://doi.org/10.1186/1556-276X-6-417>.
- [164] H. Meier, Chemical and morphological aspects of the fine structure of wood, *Pure Appl. Chem.* 5 (1962) 37–52. <https://doi.org/10.1351/pac196205010037>.
- [165] A. Frey-Wyssling, The ultrastructure of wood, *Wood Sci. Technol.* 2 (1968) 73–83.
- [166] J. Blackwell, F.J. Kolpak, The Cellulose Microfibril as an Imperfect Array of Elementary Fibrils, *Macromolecules*. 8 (1975) 322–326. <https://doi.org/10.1021/ma60045a015>.
- [167] M.A.S. Azizi Samir, F. Alloin, A. Dufresne, Review of Recent Research into Cellulosic Whiskers, Their Properties and Their Application in Nanocomposite Field, *Biomacromolecules*. 6 (2005) 612–626. <https://doi.org/10.1021/bm0493685>.

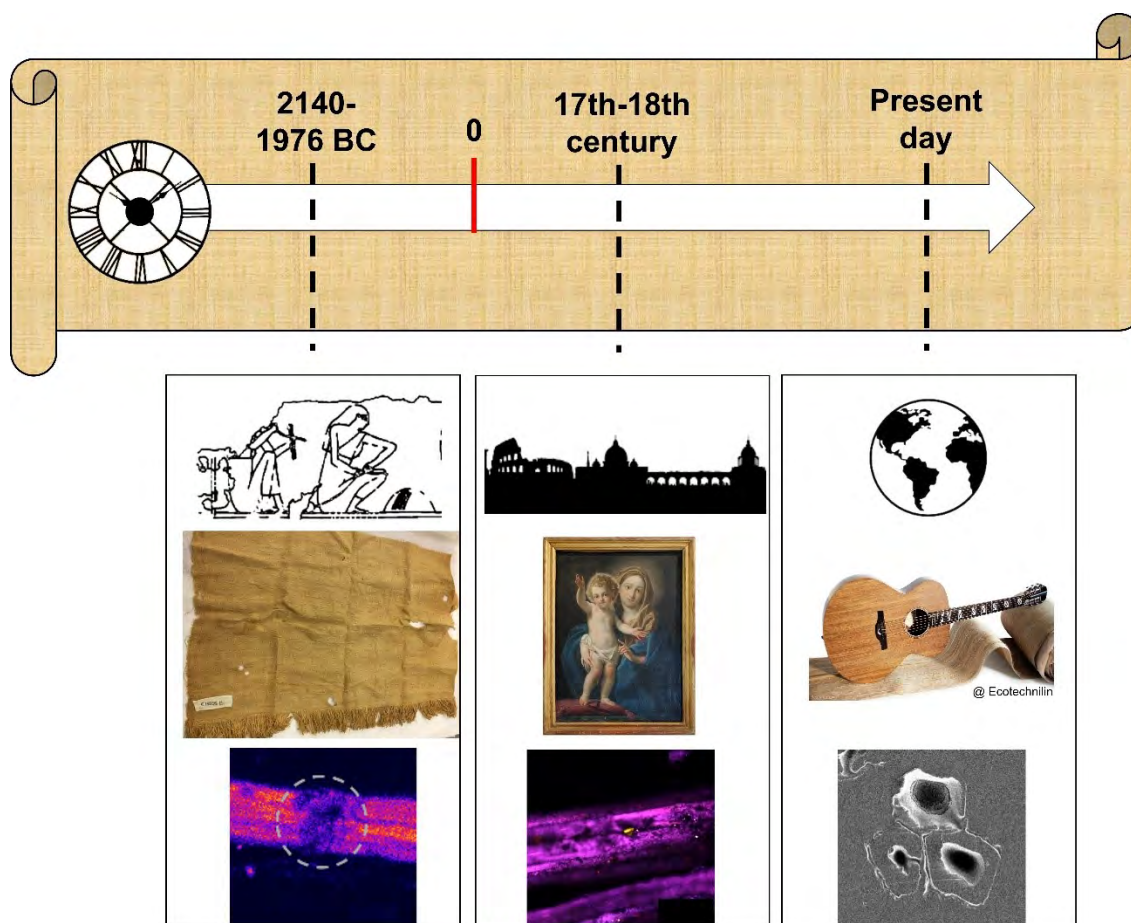
- [168] J. Summerscales, N.P.J. Dissanayake, A.S. Virk, W. Hall, A review of bast fibres and their composites. Part 1 – Fibres as reinforcements, *Compos. Part A Appl. Sci. Manuf.* 41 (2010) 1329–1335. <https://doi.org/10.1016/j.compositesa.2010.06.001>.
- [169] G. Raj, E. Balnois, C. Baley, Y. Grohens, Adhesion Force Mapping of Raw and Treated Flax Fibres Using AFM Force-Volume, *J. Scan. Probe Microsc.* 4 (2009) 66–72. <https://doi.org/10.1166/jspm.2009.1010>.
- [170] S. Hanley, J. Giasson, J. Revol, D. Gray, Atomic force microscopy of cellulose microfibrils: comparison with transmission electron microscopy, *Polymer*. 33 (1992) 4639–4642. [https://doi.org/10.1016/0032-3861\(92\)90426-W](https://doi.org/10.1016/0032-3861(92)90426-W).
- [171] J.C. Thimm, D.J. Burritt, W.A. Ducker, L.D. Melton, Celery (*Apium graveolens* L.) parenchyma cell walls examined by atomic force microscopy: effect of dehydration on cellulose microfibrils, *Planta*. 212 (2000) 25–32.



CHAPTER IV. Ageing and degradation



Graphical Abstract



A. Melelli, D. Shah, G. Hapsari, R. Cortopassi, S. Durand, O. Arnould, V. Placet, D. Benazeth, J. Beaugrand, F. Jamme, A. Bourmaud, Lessons on textile history and fibre durability from a 4000-year-old Egyptian flax yarn, *Nat. Plants.* (2021). <https://doi.org/10.17863/CAM.71495>.

A. Melelli, G. Roselli, N. Proietti, A. Bourmaud, O. Arnould, F. Jamme, J. Beaugrand, A. Migliori, G. Di Girolami, P. Cinaglia, C. Santulli, Chemical, morphological and mechanical study of the ageing of textile flax fibres from 17th/18th-century paintings on canvas, *J. Cult. Herit.* (under review).

A. Melelli, D. Pantaloni, E. Balnois, O. Arnould, F. Jamme, C. Baley, J. Beaugrand, D.U. Shah, A. Bourmaud, Investigations by AFM of Ageing Mechanisms in PLA-Flax Fibre Composites during Garden Composting, *Polymers.* 13 (2021) 2225. <https://doi.org/10.3390/polym13142225>

1. Lessons on textile history and fibre durability from a 4000-year-old Egyptian flax yarn

1.1 Introduction

Flax has a long and fascinating history. This plant was domesticated around 8,000 BCE [1], in the Fertile Crescent area [2], first for its seeds and then for its fibres [1,3]. Although, its uses existed long before domestication, residues of flax yarn dated 30,000 years ago have been found in the Caucasus area [4]. However, it is Ancient Egypt which laid the foundations for the cultivation of flax as a textile fibre crop [5]. Today, flax fibres are used in high-value textiles, as well as natural actuators [6] or reinforcements in composite materials [7].

Flax is therefore a bridge between ages and civilizations.

The most beautiful fabric pieces of flax date from Ancient Egypt (**Figure IV-1**), their highly-preserved state a result of their optimal conservation over millennia in coffins or tombs with remarkably stable moisture and thermal conditions, as well as sheltering from UV light. Flax textiles were particularly prized by the Egyptians because of its comfort and the fineness of its fibres [8].

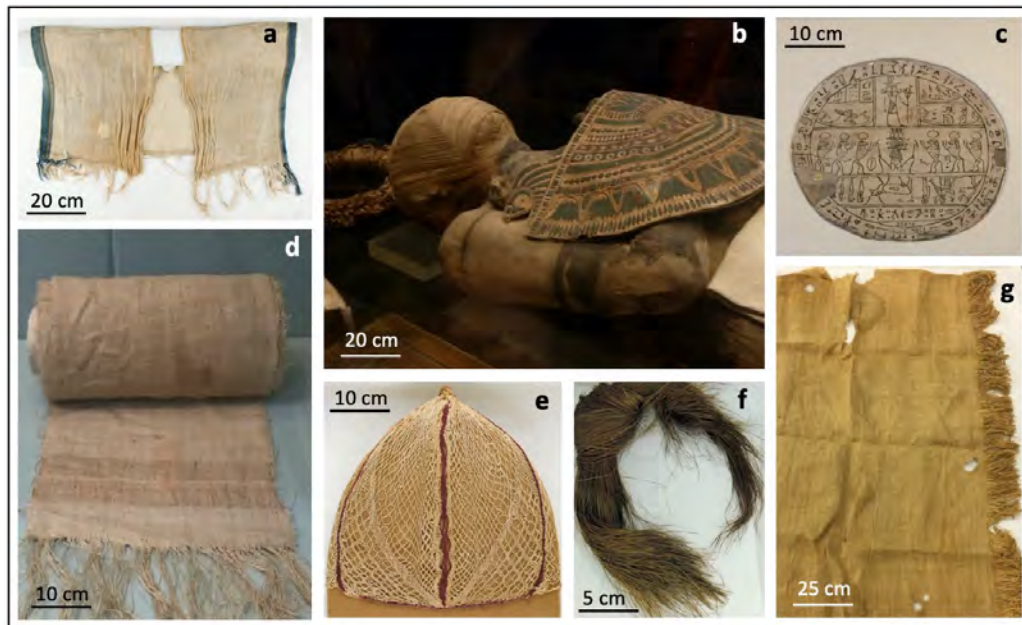


Figure IV-1 Examples of the uses of flax in ancient Egypt. Child's vest with dyed blue edges, 800–720 or 700–540 BCE (**a**); Mummy of man with flax agglomerated and stuccoed fabric, 332–30 BCE (**b**); Flax hypocephalus, 305–30 BCE (**c**); Fragment of flax shroud, 1550–1295 BCE (**d**); Hairnet cap, AD 5th or 6th century (**e**); Unspun flax hank, 1420–1230 BCE (**f**) and Mortuary linen, 2140–1976 BCE (**g**). Objects **c** and **d** are exposed at the British Museum (London—UK); **a**, **b**, **e**, **f** and **g** are exposed (**b**) or in the store room (**a**, **e**, **f** and **g**) at Le Louvre Museum (Paris-F). All images are from the authors' personal collection. Images of **a**, **e**, **f** and **g** objects were obtained with the specific permission of Le Louvre Museum.

Flax was widely used for clothing (**Figure IV-1a**) and in the fishing sector for work clothes, felucca sails and nets. The funerary uses included mummy strips (**Figure IV-1b**), funeral linen (**Figures IV-1c, d, g**) as well as ornaments (**Figure IV-1e**). In terms of cultivation, the fertile Nile valley with its light and rich or sandy soils was particularly suitable for flax. After growing, the stems were pulled out, as shown in illustrations found in the tomb of Sennedjem (Deir el Medineh, Egypt) and then probably water-retted. Over the past century or so, growth conditions have changed and varietal selection has significantly increased the crop's fibre yields [9]. It is therefore difficult to compare varieties across the ages.

Even so, an in-depth study of 407 flax genotypes of different origins has shown that regions that have been the centre of origin of the crop, such as the Mediterranean or Abyssinia, highlight haplotypes that are more unique than the temperate group and are representative of oil-seed plants [10]. According to Braun [11], the flax found in the lake dwelling does not belong to the species now cultivated (*Linum usitatissimum* L.) but to the *Linum angustifolium* which is not cultivated at the present time. Today's cultivated flax *Linum usitatissimum* L. is considered as being domesticated from the wild progenitor pale flax *Linum angustifolium* Huds. Both have phenotypic characters of great heritability, and are distinguishable by several characteristics, such as the length and width of petals, size of seeds, colour and shape of the flower, height of plants but also the number of days until emergence from the soil or flowering [12]. However, the height of the plants shown on the Egyptian bas-reliefs [13] as well as the size of the seeds found during excavation [1] suggests that the species cultivated by the Egyptians were morphologically close to those we know today.

For several decades, the development of non- or micro-destructive analysis techniques has led to numerous works on the conservation of ancient textiles. Non-destructive methods such as optical microscopy [14], or vibrational techniques [15,16] have been largely used to investigate archaeological textiles, principally to evaluate their degradation mechanisms and state of conservation. Vibrational spectroscopy studies can now benefit from synchrotron radiation [17] as well X-ray diffraction (XRD) measurement in the archaeometric study of historical textiles [18,19]. Conservation of mechanical performance and the ultrastructural differences between ancient and modern flax varieties have not been examined thus far.

Here, in order to assess the quality and durability of ancient flax fibres and relate this to their processing methods, the morphological, ultrastructural and mechanical characteristics of a yarn from an Egyptian mortuary linen, dating from the early Middle Kingdom (Eleventh dynasty, ca. 2033–1663 BCE) were examined and compared against a modern flax yarn. Advanced microscopy techniques, such as nano-tomography, multiphoton excitation microscopy and atomic force microscopy were used. Our findings reveal the cultural know-how of this ancient civilization in producing high-fineness fibres, as well as the exceptional durability of flax, which is sometimes questioned, demonstrating their potential as reinforcements in high-tech composites.

1.2 Materials

Two samples of flax yarns were studied (**Figure IV-2**), an ancient and a contemporary sample, referred to as old and modern flax, respectively, in the manuscript. The large linen tabby, bordered with a fringe (inv. E 13595, **Figure IV-2a**) was given in 1929 by Georges Daressy, former General Secretary of the Antiquity Service in Egypt, to the Louvre Museum (Paris, France). Its provenance is unknown but this piece of shroud most likely came from a tomb, because all the textiles of ancient Egypt were found in cemeteries. These cemeteries were located in the desert in order to ensure dryness and optimal conservation of the burials. Indeed, in the valley, the annual flooding of the Nile was too risky. Thus, the Egyptian climate of the desert areas, which was exceptionally dry and favourable to the proper conservation of organic materials, made it possible to find many fabrics in excellent condition.

The linen was radiocarbon dated in 2009 (Laboratoire de Mesure du Carbone 14, CEA-Saclay, Gif-sur-Yvette Cedex, France): it had been harvested between 2140 and 1976 BC (with 95.4% probability), during the 9th, 10th or 11th dynasties, a period known as the First Intermediate Period and the beginning of the Middle Egyptian Kingdom. Morphological characteristics of the ancient yarn were calculated from mass measurements and from image analysis. The linear density and twist of this old yarn are 122 tex and 180 tpm, respectively. In addition, a contemporary yarn was used (**Figure IV-2b**). It was produced from textile flax (Melina variety) cultivated in 2018 in Normandy (France) by Teillage Saint-Martin company; this flax was dew-retted conventionally over 6 weeks and then scutched and hackled [20]. Then, it was wet spun by Safilin Pionki (Poland) with a linear density and twist of 105 tex and 320 tpm, respectively.

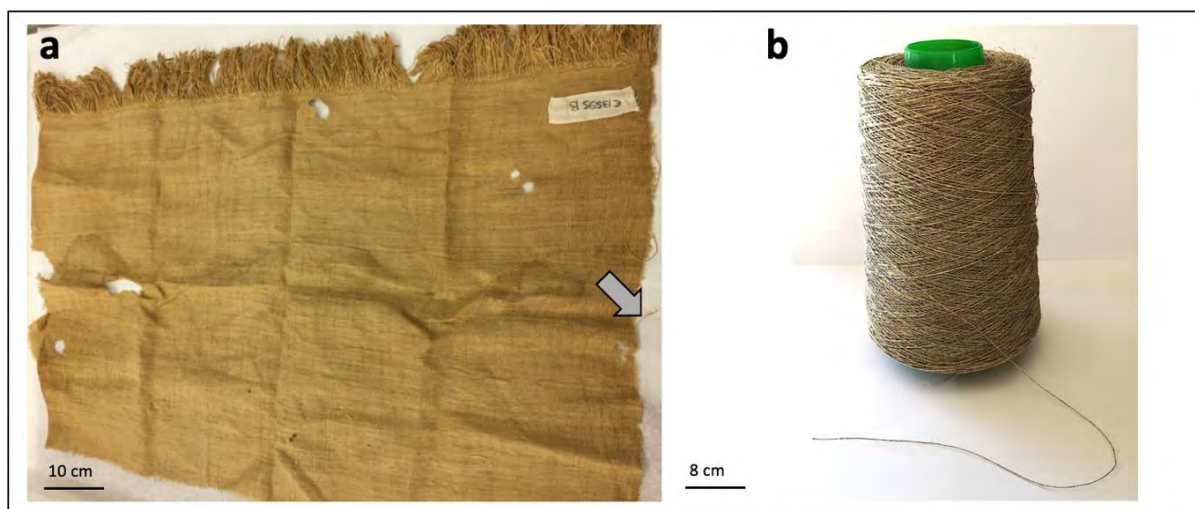


Figure IV-2 Samples used for yarn sampling. Mortuary linen, 2140–1976 BCE (**a**) and spool of yarn, 2019 AD (**b**). The yarn collected is indicated by an arrow in (**a**). Images of an object was obtained with the specific permission of Le Louvre Museum.

1.3 Methods

1.3.1 SEM observations

For each of the two yarns, a sample of a few millimetres was used. A Jeol JSM 6460LV scanning electron microscope was used to analyse the flax yarns; secondary emission electrons were used, and the accelerating voltage was 3.0 kV. They were glued to a sample holder using a conductive adhesive and then metallized with a thin layer of gold using an Edwards Scancoat Six device for 180 s.

1.3.2 Multiphoton microscopy

Sample preparation

An elementary fibre of the modern yarn was extracted and mounted on paper support commonly used for tensile tests according to ASTM C1557 and fixed with universal glue. The sample prepared was placed between two coverslips and scanned. In contrast, the preservation state of the Egyptian yarn does not allow to extract elementary fibres, which are more brittle, so a whole collective of less than 1 cm was mounted on paper support commonly used for tensile tests but glued in the horizontal direction in order to use the aperture of 5 mm. The sample prepared was placed between two coverslips and scanned by the multiphoton microscope. The samples were mounted at 90° to the initial laser polarisation position.

Parameters

The half-wave plate was rotated to change the laser polarisation angle until to reach the maximum intensity SHG signal of both flax yarns (maximum signal reached 2°–3°). The maximum laser power percentage used was 2% for the Egypt yarn and 5% for the modern yarn to avoid the bleaching of the surface. Both autofluorescence and SHG signals were collected by GaAsP NDD (gallium arsenide non-descanned) detectors. The scan line average was 16, the scan velocity was fixed at 1 (fps) and the scan size was 512x512 pixels. All the measurements were performed at room temperature and dry ambient.

1.3.3 X-ray tomography measurements

The yarns' microstructure was characterised using X-ray nanotomography. Image acquisition was realised on an EasyTom RX Solutions micro/nano tomograph (RX Solutions, Chavanod, France). A Lanthanum hexaboride (LaB6) filament was used as cathode with a voltage of 50 keV and a current of 100 μ A, leading to a resolution of 0.5 μ m. The anode was in beryllium and has a thickness of 0.5 mm.

Resolution of the micro-CT images was set to $4.44\ \mu\text{m}/\text{pixel}$. The imager used was a Fluoroscopic High Speed imaging sub-system PaxScan 2520DX and the scintillator was produced with a direct deposition of Cesium Iodide (CsI).

To obtain optimum measurement contrast, the framerate has been set to 0.25 fps. In addition, in order to minimize the measurement noise, each projection obtained was the result of the averaging of 15 acquisitions. Finally, in order to obtain the most faithful reconstruction possible, the flax fibers were measured in 1440 different positions (angles). The yarn centering was carried out using a perforated carbon tube. The tube outside diameter was 1 mm and the inside hole diameter was 0.5 mm. A little bit of glue was used to maintain the yarns. The measured volume was 0.5 mm in diameter over a height of 0.8 mm with a resolution of 500 nm.

In order to allow maximum beam stability from the start of the measurement, the wire was preheated 3 hours before the start of the measurement. In total, each measurement therefore lasted approximately 27 hours. An X-ray radiograph is given in **Figure IV-3a** to illustrate the measurement (the yarn is hardly perceptible). The reconstruction was carried out using Xact software using the filtered back-projection method. For the noise filtering, the apodization was done using a sine window with a threshold of 75% for the low pass filter. For the border filter a Tukey window type was used with a non-filtered area of 46%. For more information on filters and the effects of reconstruction filter on CBCT image quality see [21]. Once the reconstruction has been carried out, the result is stored in the form of a slices stack.

An illustration is given **Figure IV-3b**. Finally, the analyses and reconstruction of surfaces were carried out using the VGSTUDIO MAX software as illustrated on **Figures IV-4a** and **4b** at two different scales.

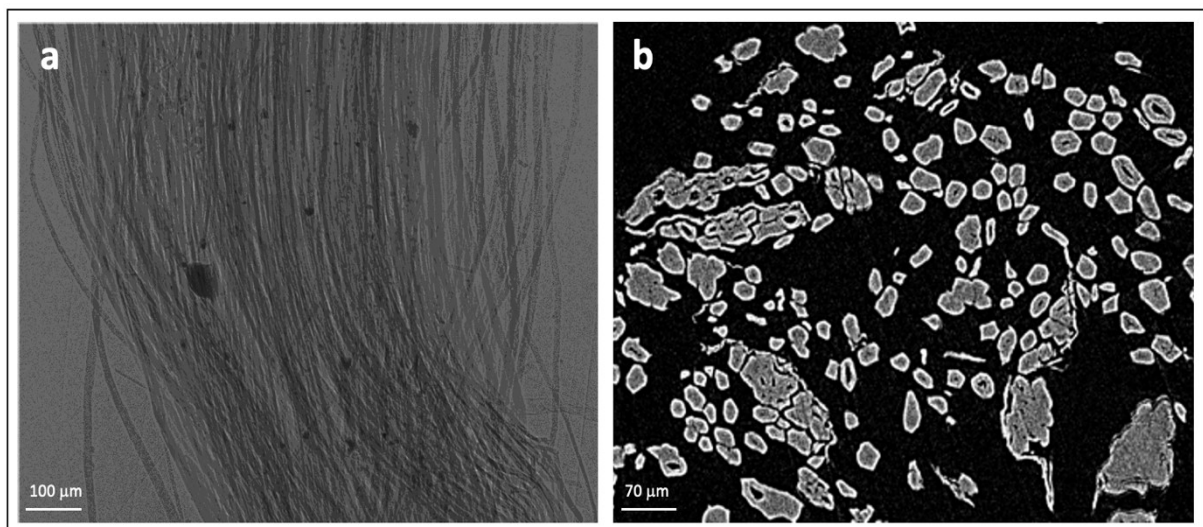


Figure IV-3 Tomographic protocol. Example of X-Ray radiograph on the modern yarn: in Z direction (**a**) and a slice after reconstruction in Y Direction (**b**).

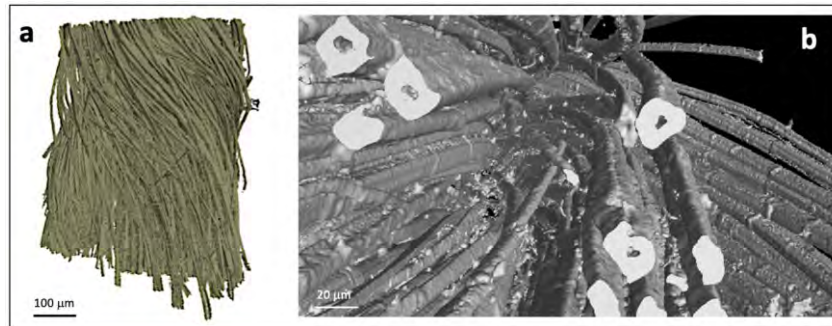


Figure IV-4 Yarn after volume reconstruction at overall **(a)** and local **(b)** scale. Nano Tomographic images were acquired from a measured volume of 0.5 mm in diameter over a height of 0.8 mm and each projection obtained was the result of the averaging of 15 acquisitions.

1.3.4 Nano-mechanical investigations

Sample preparation

A subsample of less than 1 cm was cut from the ancient flax yarn (Louvre) and modern flax yarn samples and prepared as reported in **Chapter II**.

In **Figures IV-5a, b** are reported the topography of an elementary fibre from the ancient flax yarn and the topography of a bundle from the modern one.

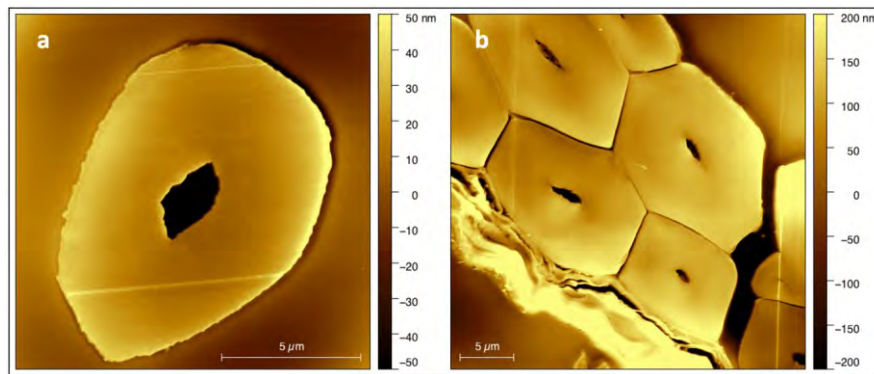


Figure IV-5 A good flatness of the images is observed; a more heterogeneous zone appears at the level of the cortical residues for modern flax **(b)**; the structure and the constituents of these regions are different from those of the fibres which can lead to disturbances during cutting. In **(a)** a single flax fibre can be seen, while in **(b)** a fibre bundle can be identified. The fibre bundle consists of individual plant cells (fibres) connected by the middle lamella (dark lines). In the lower-left part of the picture, remains of the parenchyma can be found. Two to three different areas of each sample (old and modern respectively) were measured to obtain a better statistic.

Nanoindentation parameters

Preliminary to the atomic force microscopy measurements, nanoindentation measurements with a Nanoindenteur XP (MTS Nano Instruments, Oak Bridge, Tennessee, USA) used at room temperature and equipped with a three-side pyramid indenter (Berkovich-Berko XPT-12761-0) were used to evaluate

the indentation modulus of the samples. Once the indenter touched the surface, the strain rate was set at 0.05 s^{-1} (i.e., $1 \text{ } \mu\text{N/s}$) during loading to reach a depth limit of 120 nm. The load was held at the maximum value for 60 s and then the withdraw was done with the same loading rate up to 10% of the maximum load. The Poisson's ratio was set to 0.

AFM PF-QNM investigations

The range of the stiffness of the cantilevers used was between 109 and 161 N/m and the tip radius between 15 and 30 nm at the beginning of the measurements.

The Poisson's ratio used was set to 0 as the tested cell walls are anisotropic, thus the modulus measured is the indentation modulus. The maximum fast scan velocity was selected at $8 \text{ } \mu\text{m/sec}$ and the image resolution set to 512×512 pixels.

Two to three different areas of each sample (old and modern respectively) were measured to obtain a better statistic but only one representative area for each sample is reported here (**Figures IV-5** and **6**). **Figure IV-5** shows the topography images corresponding to the investigated areas. To obtain the indentation modulus values, the entire surface of the G (or S_2) cell wall layer of each fibre was selected; indentation modulus data were automatically calculated for each point from the force-distance curves with a DMT contact model using NanoScope Analysis software (Bruker, Billerica, Massachusetts, USA).

Consequently, for each sample, the indentation modulus calculated were obtained from two or three separate images and from between 80,000 and 140,000 points for each image. **Figure IV-6** shows the calculation mask, covering the investigated area. For each sample, histograms were plotted and represented the data obtained from all the images analysed; 206,613 and 364,575 AFM force curves were used for old and modern flax indentation modulus calculation, respectively.

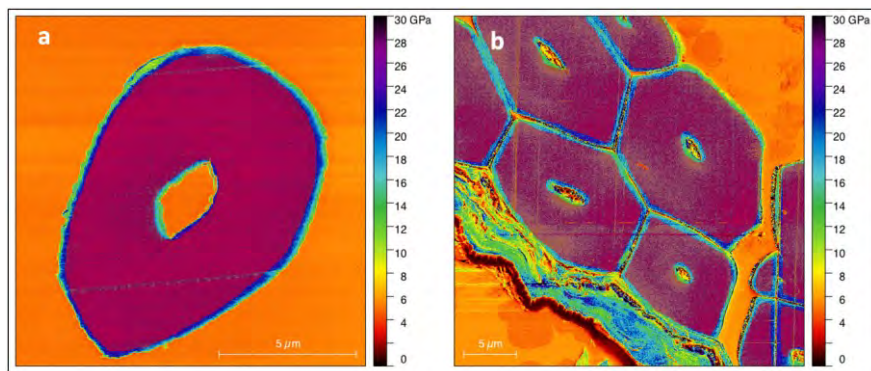


Figure IV-6 Data treatment of AFM PF-QNM investigations. The purple mask represents the areas used to collect the data. Similar calculations were performed on the other images for modern and old yarn. Two to three different areas of each sample (old and modern respectively) were measured to obtain a better statistic. The indentation modulus calculated were obtained from two or three separate images and from between 80,000 and 140,000 points for each image analysed.

1.3.5 FTIR-ATR spectroscopy

Sample preparation

A small subsample of around 5 mm from both the modern and the ancient flax yarn were directly analysed with a FTIR-ATR spectroscope.

Parameters

Spectra were acquired at room temperature with a Vertex70v vacuum Fourier Transform Infrared spectrometer (Bruker, USA) equipped with a DLaTGS detector, a KBr window, the KBr beamsplitter and an Attenuated Total Reflection golden gate accessory (germanium cell). Spectra were acquired in absorbance mode with a spectral resolution of 4 cm⁻¹ and in a range from 4000 to 600 cm⁻¹.

Both spectra from modern and old yarns were acquired with an accumulation of 64 scans after the background subtraction of a spectrum “in air” with OPUS software (Bruker, USA). The acquisition range was from 500 to 4000 cm⁻¹. The spectra were elastic baseline corrected and unit vector normalised using Opus software (Version 7.5).

1.3.6 XRD investigations

Wide-angle X-ray diffraction (WAXD) measurements were performed under ambient conditions on a Siemens D500 diffractometer CuK α radiation. Scans were collected from 2 θ = 5 to 60° with step size of 0.03° at 4 s/step. The beam was directed perpendicular to the fibre yarn length.

Crystallinity was calculated using **Eq. IV-1**, where I_{tot} is the intensity at the primary peak for cellulose I (at 2 θ = 22.5°) and I_{am} is the intensity from the amorphous portion evaluated as the minimum intensity (at 2 θ = 19.0°) between the primary and the secondary peaks (see **Figure IV-11**).

$$C = \frac{I_{\text{tot}} - I_{\text{am}}}{I_{\text{tot}}} \times 100 \quad (\text{Eq. IV-1})$$

1.3.7 NMR analysis

NMR investigations were performed on modern and old yarns according to the protocol described in [22]. Solid state ¹H/¹³C CP/MAS NMR experiments were performed on a Bruker Avance III 400 MHz spectrometer with a ¹³C frequency of 100.62 MHz by using a double resonance H/X CP/MAS 4 mm probe. The cellulose cell wall crystallinity was calculated by dividing the area of the four peaks of the crystalline region by those of the seven peaks for the cellulose C4 region. The lateral dimensions of the fibrils (LFD) and the lateral dimensions of the fibril aggregates (FLAD) were then estimated using a square model of a cross-section of cellulose microfibril. This analysis is based on the total cellulosic surfaces of amorphous cellulose and a microfibril model with cellulosic chains 0.57 nm wide [23].

1.3.8 Statistical analysis

A t-test was performed to quantify the statistical differences in fibre diameters and indentation moduli values between the old and modern fibres. P value was calculated for the two cases, with significance level $\alpha = 0.05$.

1.4 Results and Discussion

Figures IV-7a and 7d compare the overall architecture, observed by SEM, of old and modern flax yarn, respectively. Despite a lower level of twist (about 180 turns per metre (tpm) against 320 tpm for the modern flax), the old flax possesses a similar metric number (about 122 tex or 8.2 km/kg), showing the mastery of the Egyptians in manual spinning.

Figure IV-7b reveals the level of individualisation of the fibres. In the flax stem, fibres are aggregated in cohesive bundles made of several tens of fibres, the latter being more or less divided after retting and extraction stages. The old yarn is mainly made up of elementary flax fibres; the residues of cortical parenchyma and middle lamellae are very few. This demonstrates the effectiveness of the water-retting process utilised at the time as Pliny the Elder explained [24]. Water-retting enables homogeneous retting and, when it is well executed, enables the production of very fine fibres. One can notice that the low fibre yield in ancient flax varieties can also lead to easier retting and fibre division [25].

In modern flax fibre extraction processes, stems undergo field retting over several weeks. Dependent on natural weather conditions, this can lead to retting heterogeneity. As a consequence, numerous residues of pectic intermediate lamellae or cortical parenchyma are visible on the modern flax yarn (**Figures IV-5b and 7e, h**). Such residues increase roughness of the yarn and are detrimental to the sensation of comfort (e.g. softness). This is in contrast to the reputation of Egyptian flax fabrics, whose most beautiful specimens were reserved for members of high society. These observations validate the important know-how of ancient Egyptians in textile manufacturing. The scanning electron micrographs (**Figures IV-7a, b**) also reveal the excellent general conservation of the ancient fibrous yarns.

Figures IV-7g and 7h present cross-sections of the old and modern yarn observed in nanotomography and **Figure IV-7i** illustrates the analysed distribution in elementary fibre diameters for the two materials. The mean diameters are $14.3 \pm 3.3 \mu\text{m}$ for the fibres in the old yarn ($n = 523$) and $17.6 \pm 3.6 \mu\text{m}$ for the modern yarn ($n = 208$); both diameter values are consistent with typically reported values on flax fibres [26]. A significant difference in elementary fibre diameters is observed and confirmed by a student test with $P \leq 0.001$. The smaller diameters of old flax may be related to the plant variety, the weather conditions during growth (hydric stress, for example) [27], and/or even the sampling area within the stem, with larger diameter fibres being generally located in the middle section of the stem height [28]. The retting method utilised may also explain the differences and scatter in elementary fibre diameters between the old and modern flax yarn (**Figure IV-7i**).

The use of water-retting for the old flax yarn, leads to completely separated fibres and free from surface residues (**Figure IV-7b**). This further demonstrates the skill of the ancient Egyptians in obtaining fine yarns and textiles. However, it is not possible to exclude that the ageing process can also lead to degradation of these pectic residues, contributing to separate the fibres.

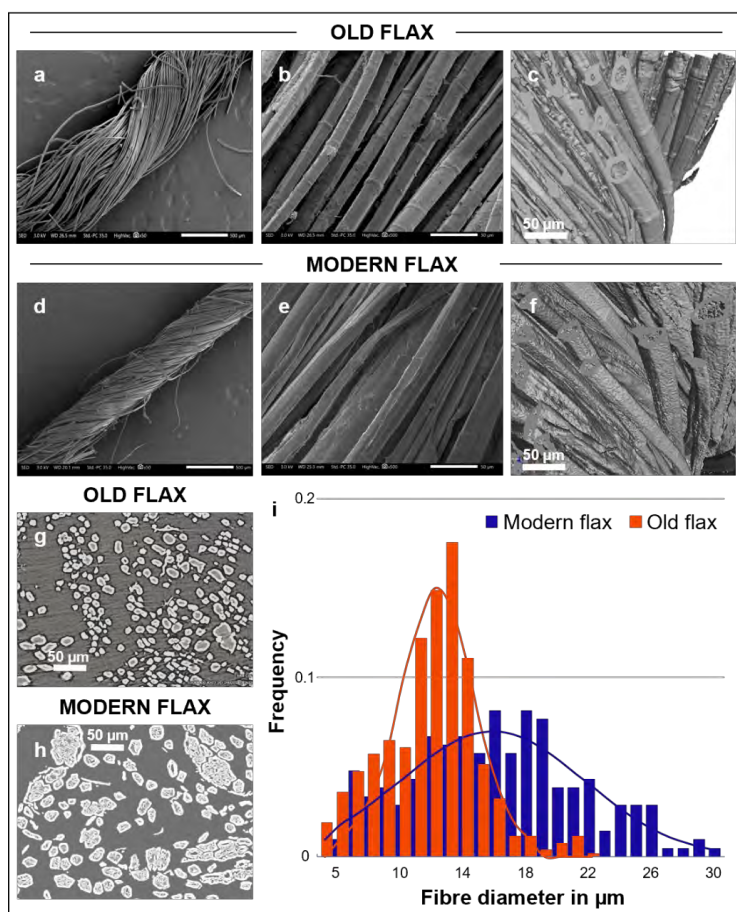


Figure IV-7 Scanning electronic microscopy and nano-tomographic images of modern and 4000-year-old flax. Overview of yarn (**a, d**) and fibres within the yarns (**b, e**); Tomographic overview of fibres highlighting the larger lumen size for old flax (**c, f**) and tomographic yarn cross-section showing the lower diameter of old flax fibres (**g, h**). Histograms (**i**) present the distribution of single fibre diameter for both old and modern flax. For SEM, at least 5 areas were investigated; nano-tomographic images were acquired from a measured volume of 0.5 mm in diameter over a height of 0.8 mm and each projection obtained was the result of the averaging of 15 acquisitions.

Differences are also visible in the size of the lumens, with SEM and tomographic images (**Figures IV-7c, f, g and h**) showing larger ones for old flax fibres. While the lumens of modern flax fibres represent only a few percent of the total surface area [29], here, old fibres possess lumens of the order of 30–40%, comparable to wood or coconut fibres [29]. It is possible to speculate that these low wall thicknesses of old flax may be due to a premature halt in the cellulose filling process of the cell walls following the intrusive growth phase [28]. This filling can be interrupted by extreme weather conditions, such as lodging or marked periods of hydric stress [30]. The artificial selection over the centuries may also be responsible for changing the shape of the fibre cells and their current diameter.

Flax fibres are characterised by their multi-layered structure and their generally polygonal shape, as well as by the presence of structural defects known as kink-bands [31], distributed along the fibre length. Notably, the relative quantity and size of these kink-bands is particularly large on old fibres (**Figure IV-7b, Figures IV-8a, b**) in comparison to modern fibres (**Figures IV-8d, e**). The origin of these defects is not well known but the plant fibre community generally attributes them to mechanical stresses induced during the extraction or processing of the stems, but also to residual stresses that may be released during periods of stem or fibre drying, possibly during the retting stage [31,32].

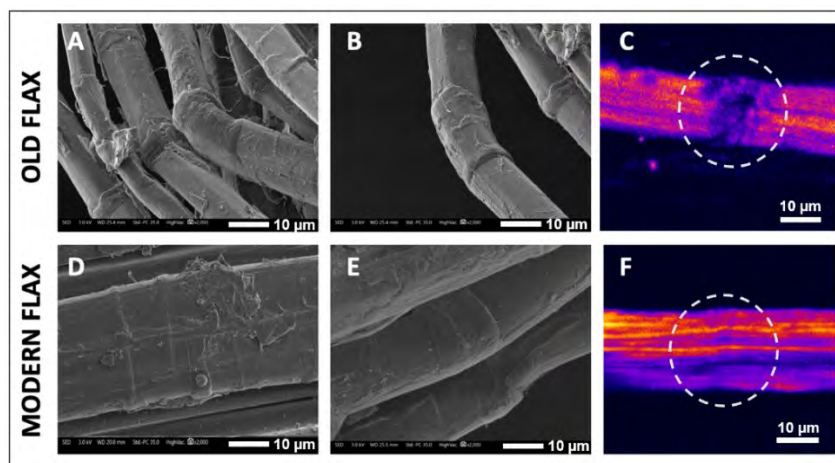


Figure IV-8 Focus on kink-band (defect) regions in the fibres. Scanning electron microscopy images showing differences between kink-bands structure and intensity in old (**a, b**) and modern (**d, e**) flax. SHG microscopy observations highlighting the local disorganisation of cellulose macrofibrils in the kink-band region (dotted grey line) for old flax (**c**) compared to modern flax (**f**). For SEM and SHG, at least 5 areas were investigated and the most representative images selected for publication.

The large quantity of kink-bands on old flax fibres may be the result of aggressive decortication, scutching or spinning processes used by the Egyptians following water-retting, but may also be caused by progressive release of internal stresses over the 4 millennia. In flax fibres, kink-bands modify the aesthetics and regularity of the fibres, and are also considered as zones of weakness, especially when utilised in a fibre-reinforced composite [33]. Kink-bands also make the fibre more susceptible and sensitive to ageing by acting as entry points for microorganisms or moisture to access the inner layers of the cell walls [34]. Kink-bands were specifically examined through multiphoton microscopy with second-harmonic generation imaging, which highlights crystalline cellulose within the plant cell walls. **Figure IV-8c** shows discontinuity and disorganisation of crystalline cellulose in the kink-band of old flax, and possibly indicate areas of low crystallinity in this region. Both these factors would cause kink-band rich ancient flax fibres to be more brittle [19]. Indeed, these old fibres have proved to be very fragile during handling, and impossible to isolate without breaking/damaging them for any single-fibre tensile testing.

Finally, atomic force microscopy tests in peak force quantitative nano-mechanical (AFM PF-QNM) mode were conducted on transverse cross sections of old and modern flax fibres. Such measurements

allow estimation of the indentation modulus of flax plant cell walls (**Figures IV-9a-e**), i.e., do not depend on the relative lumen size and are a useful measure for highlighting mechanical property gradients or heterogeneities within cell walls [35].

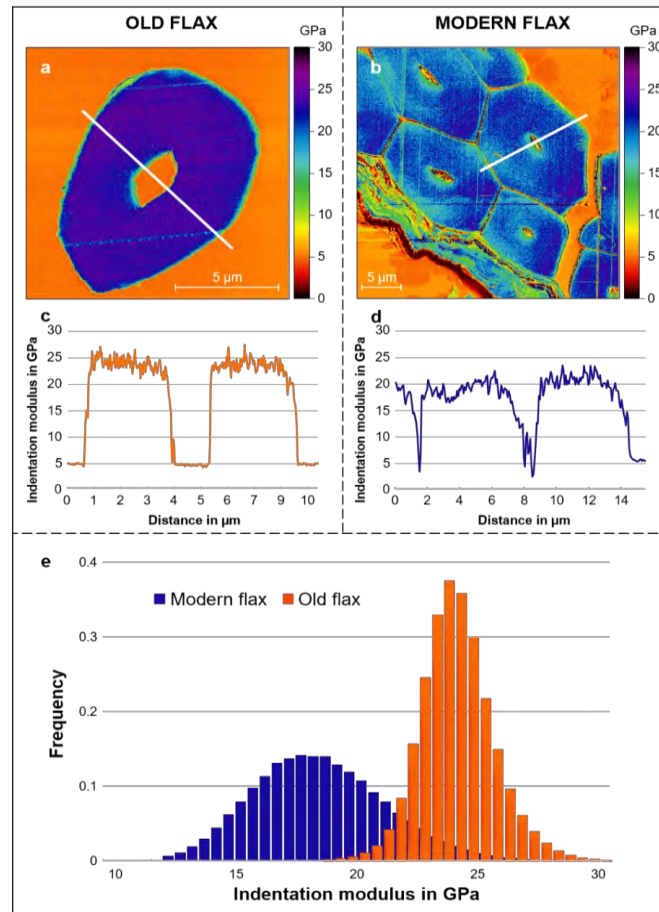


Figure IV-9 AFM peak force measurements in old and modern flax fibres. One can notice larger lumen size on old flax fibre (a) and residue of cortical parenchyma on modern flax (b). Figure (c) and (d) show the profile of indentation modulus in old and modern flax, respectively, according to the position on the white line (a and b). Distributions of indentation modulus are shown in (e).

Interestingly, it was found that the AFM mechanical properties are slightly higher for cell walls of old flax than those of modern flax, i.e., 23.7 ± 0.2 GPa and 20.3 ± 0.1 GPa, respectively; for each batch, 2,500 indentation moduli values were statistically compared, and the student t-test confirmed that the two sets of moduli are different with $P \leq 0.001$. Values of modern flax are in line with the measurements in the literature [20] and measured by nanoindentation (**Table IV-1**). Moreover, the measured indentation moduli are homogeneous in the fibre sections and show little dispersion, suggesting no ageing gradient across a fibre transverse section. Such quantitative nano-structural measurements, never before conducted on such ancient fibres, reveal the durability of these flax plant cell walls. Even though at the fibre-scale, the kink-bands are regions of pronounced damage, the cell walls themselves exhibit a moderate change in their elastic performance despite their age; only a slight increase in their stiffness, connected to the evolution of their non-cellulosic polysaccharide composition, is demonstrated.

Table IV-1 Nanoindentation modulus and hardness obtained on fibre and resin for old and modern flax samples.

Sample		Number of tests	Indentation modulus in GPa	Standard Deviation in GPa	Hardness in MPa	Standard Deviation in MPa
Old Sample	Fibre	23	23.9	± 3.48	430	± 70
	Resin	15	5.10	± 0.20	236	± 5
Modern fibre	Fibre	35	20.7	± 2.93	396	± 55
	Resin	23	5.30	± 0.25	250	± 19

Measurements by infrared spectroscopy (**Figure IV-10** and **Table IV-2**) revealed a lower intensity of peaks attributed to parietal hemicelluloses for old flax. It has been shown that the longitudinal and transverse shear moduli of the fibres [36] and especially the stiffness of the non-cellulosic matrix of the plant cell walls [37] have a major effect on the indentation modulus; our results confirm this important influence of hemicelluloses, even though they are the softest component of the cell wall, on the indentation modulus. Higher indentation modulus has previously been recorded on old wood samples and is attributed to a loss of pectins, as well as modification of the ligno-cellulosic cell wall polymers [38]. The wider literature supports the hypothesis of a significant evolution in the ageing sensitive hemicellulosic polymers over 4,000 years. Surprisingly, the lower intensity of the band at 1730 cm^{-1} in the old yarn can suggest that the Egyptian yarn did not undergo severe oxidation, but the loss of hemicellulose, highlighted by the lower intensity at 1250 cm^{-1} , was also confirmed by NMR analysis. The lower band at 1636 cm^{-1} in the old yarn also indicate a loss of absorbed water that can contribute to increase its stiffness.

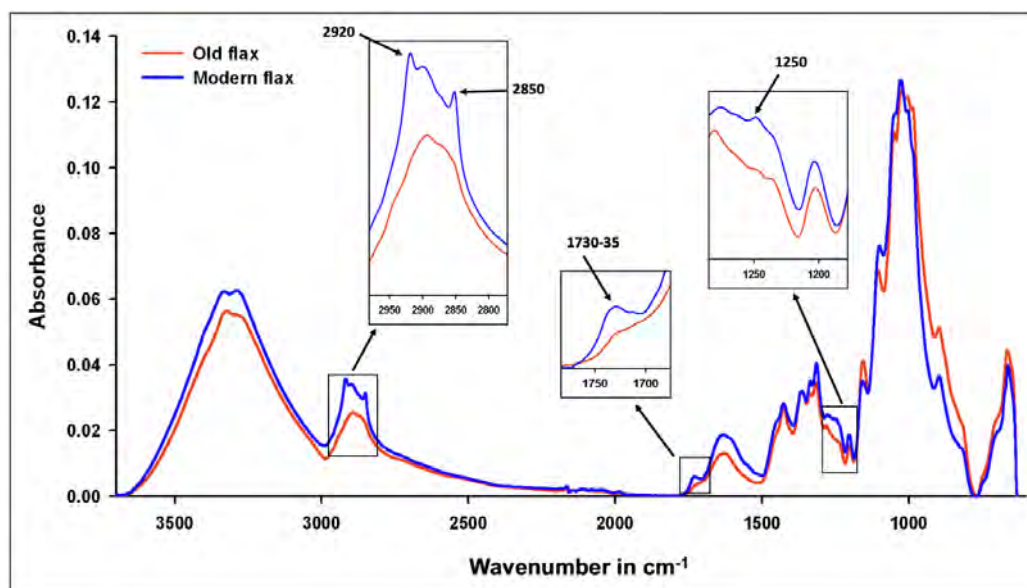


Figure IV-10 FTIR-ATR spectra of modern (blue) and red (Egyptian) flax yarn. baseline subtraction and normalization have been done. Three zones are specifically marked to better highlight differences between the spectra. The main differences between spectra of the modern and ancient flax yarns are in esters carbonyl absorbances ($\sim 1730\text{ cm}^{-1}$) due to the hemicellulose, in the absorbance at $\sim 1247\text{ cm}^{-1}$ of the C-O stretching of the hemicellulose and, around 2920 cm^{-1} and 2850 cm^{-1} , in the CH stretching of alkyl groups of cellulose and hemicelluloses [39,40]. All these peaks are extremely low in the Egyptian flax yarn compared to the modern one.

Table IV-2 Correspondence between the peaks recorded in FTIR and the main constituents of the flax cell walls. All of these data come from literature. The shaded lines correspond to the peaks highlighted in **Figure IV-10**; they underline the main differences related to peaks attributed to hemicelluloses, between spectra of the modern and old flax yarn.

Position (cm ⁻¹) in Egyptian and modern flax yarn	Position (cm ⁻¹) assigned in literature	Assignment (literature)	Reference
~ 3334 to 3286	~ 3600 to 3000	Hydrogen bonded OH (hydroxyl group) stretching vibration in cellulose, hemicellulose and lignin	[40–43]
~ 2920	~ 2920	vC–H stretching vibration in cellulose and hemicellulose	[41,42]
~ 2895	~ 2900	vC–H general organic material content of the fibre, polysaccharides	[40,44]
~ 2850	~ 2850	vC–H ₂ in cellulose, hemicellulose and lignin	[40–42, 44]
~ 1730	~ 1730–1735	Carbonyl C=O and carboxyl stretching of carboxylic acid or ester group of hemicelluloses. A high intensity of this band can also be due to degradation by oxidation process	[16,39–42,45]
~ 1635	~ 1635	Absorbed water	[40,45,46]
~ 1595 (present in modern but absent in old flax yarn)	~ 1595	vC=C aromatic in plane, lignin	[39,40,46,47]
~ 1515 present in modern but absent in old flax yarn)	~ 1510	vC–C aromatic in plane, lignin	[39, 40,47]
~ 1450	~ 1455	δC–H; δC–OH 1° and 2° alcohol	[40,41]
~ 1425	~ 1420	δOCH and δHCH in plane, crystalline cellulose	[40,48–50]
~ 1365	~ 1365–1370	δC–H and δCOH of cellulose, hemicellulose	[49,51]
~ 1334	~ 1335	δCH ₂ and δCOH, mainly cellulose	[40,44,49,52]
~ 1315	~ 1315	δCH ₂ wagging and δCOH of cellulose, hemicellulose	[50]
~1280	~1280	δCH	[51,52]
~ 1247	~ 1250	vC–O hemicellulose polysaccharides, lignin	[48,49, 50]
~ 1234	~1235	vC–O in lignin and δC–OH in cellulose	[49,52]
~ 1203	~ 1200	δC–OH; δC–CH	[40,49,52]
~ 1157	~ 1155	v _{as} C–O–C; vC–C ring breathing	[49,51]
~ 1105 for old flax yarn ~1099 for modern flax yarn	~ 1105	vC–O 2° alcohol; vC–O–C glycosidic (mainly cellulose)	[49,53]
~ 1050	~ 1050	vC–OH 2° alcohol	[53]
~ 1025	~ 1025	vC–OH 1° alcohol	[40,44,49,53]
~ 1005	~ 1005	vC–O	[49,53]
~ 985	~ 985	vC–O	[49,52]
~ 895	~ 895	v(C–O–C) in plane in β–Glycosidic bond	[16,40,44,50]

Differences in crystallinity were also checked through both nuclear magnetic resonance (NMR) and X-ray diffraction (XRD) measurements; **Figure IV-11** shows that the cellulose crystallinity measured by both NMR (58.0% for Egyptian yarn and 56.0% for the modern yarn) and XRD (59.6% for Egyptian yarn and 58.4% for the modern yarn) techniques is comparable between the ancient and modern flax yarns. By ^{13}C NMR it was also confirmed a loss of hemicellulose of the old flax, due to the disappearance of the band at 32 ppm, visible, however, in the modern one.

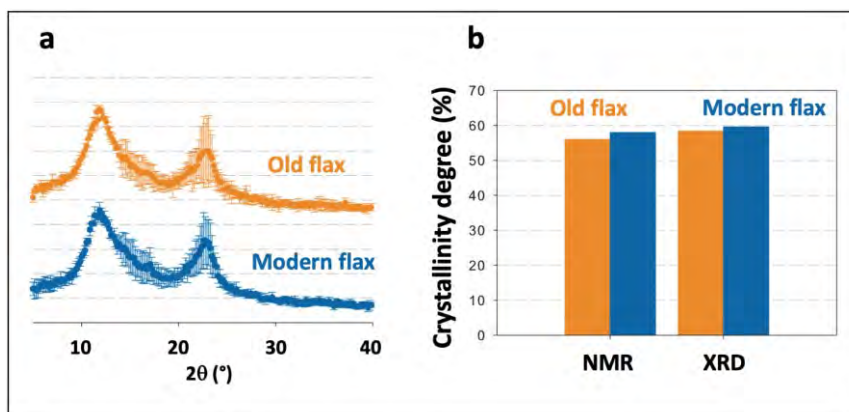


Figure IV-11 XRD spectra of old and modern flax (a) and comparison between crystallinity degree obtained through NMR and XRD investigations (b).

1.5 Conclusions

Our structural examination of 4000-year old Egyptian flax fibres in comparison to modern flax fibres has offered a number of insights on the textile know-how of the Egyptians, as well as on the temporal evolution of flax fibres. Through water retting and manual processing, the ancient Egyptians could separate the flax into very fine fibre bundles and in most cases even into single fibres to make soft and luxurious quality textiles despite fully-manual processing.

Local nanomechanical measurements show an increase in cell wall stiffness of old fibres, probably induced by the alteration of non-cellulosic polymers, as cellulose retained a crystallinity close to that of contemporary fibres. In addition, a larger presence of structural defects – stress-concentrating kink-bands with low cellulose crystallinity – is notable on the old, fragile fibres. In future and in work-in-progress, the aim is to go further by exploring the microfibrils angle (MFA) values of ancient flax (through single fibre XRD and SHG), the internal structure of kink-bands (by nanotomography) and if possible, to gain information on the *Linum* used by ancient Egyptians thanks to genetic analysis. To improve durability at the fibre scale, producing fibres with low quantities of defects is necessary, in particular if they are to be used as reinforcements of next-generation environmentally-friendly composite materials. Intriguingly, the ancient Egyptians had also dabbled their hands in making the first linen/plaster cartonnage biocomposites for death masks, a number of which survive to date (**Figure IV-1b**)

2. Chemical, morphological and mechanical study of the ageing of textile flax fibres from 17th/18th-century paintings on canvas

2.1 Introduction

Flax (*Linum usitatissimum* L.) is one of the oldest domesticated plants [1], used for its fibres and in the food sector for its seeds. In Europe, starting from the Late Middle Age, a number of plant fibres, such as hemp and flax, have played a key role as a support for paintings on canvas, especially flax for its great homogeneity and fineness coupled with excellent mechanical properties, suitable to face the stresses and deformations that paintings undergo.

One of the methods used by artists to prepare the textile support before painting is reported in Cennino Cennini's treatise, dated to circa 1400 [54]. However, each artist had his own method and used materials of different qualities often linked to his social rank and his clientele [55], though common characteristics can be found by geographical area and historical period [56].

In general, the textile layer of a canvas has the function of supporting several other layers of different natures, since pigments are not applied directly on it. For centuries, the first layer was composed of glue, usually of animal origin, as also mentioned in Cennini's treatise [54], followed by the ground layer (gypsum or calcium carbonate and glue or flour, oil and pigments), but around the 17th century, the first layer of glue, in contact with the textile support, was sometimes omitted because artists tried to preserve the recto of the canvas support from humidity [56]. Currently, it is known that animal glue promotes the growth of mould and bacteria [55,57].

Several studies have focused their attention on the mechanical properties of textile supports by measuring the vibrations or tension of canvases [58–61]. Two important methods to evaluate the state of preservation of the textile support are the calculation of the degree of polymerization (DP) of cellulose (by viscometry or GPC) [62] and the determination of the cellulose morphology and microstructural heterogeneities with solid-state nuclear magnetic resonance spectroscopy (^{13}C CP-MAS NMR). In particular, the last technique only requires small amounts of material, namely 25 μL [63,64], which corresponds to approximately 30 mg of sample. Due to the small amount of sample usually available from cultural objects such as paintings, a combination of techniques is usually necessary to have a clear evaluation of the state of preservation of artworks.

For example, scanning electron microscopy (SEM) or optical microscopy have been combined with techniques capable of obtaining information on cellulose crystallinity and chemical modifications, such as X-ray diffraction (XRD), Fourier transform infrared (FTIR) or Raman spectroscopy [19,65,66].

Furthermore, other techniques generally used in the engineering and biology fields can also be employed for the study of cultural heritage, especially regarding the study of cellulosic fibres, such as atomic force microscopy and nanoindentation, which allow us to investigate the micromechanical properties of the cell walls [67], and SHG [49], which offers data on the fibre, especially cellulose ultrastructure as presented in **Chapter III**.

This section aims to establish the state of preservation of four 17th/18th-century Italian canvases and to elucidate possible degradation using a new combination of techniques that thus far has found very limited application in the conservation field. The canvases were first imaged by optical and scanning electron microscopy to obtain information on their morphology. Successively, local mechanical properties were examined by nanoindentation and AFM techniques, while chemical information was obtained by FTIR-ATR spectroscopy and ^{13}C CP-MAS NMR to obtain an overview of the state of preservation of each canvas. Finally, SHG microscopy was used to assess the state of the fibre ultrastructure.

Our results can help curators recognize canvases in the worst condition that require immediate intervention or more in-depth investigation by conservators; at the same time, this new pairing of techniques can support the study of other ancient artefacts made of plant fibres, such as clothing and tapestries.





2.2 Samples

Yarns from four oil paintings dated between the 17th and 18th centuries were examined. The paintings are currently stored at the Civic Art Gallery of Ascoli Piceno. Details about the paintings are given in **Table IV-3**. Yarn samples were taken from the recto of each canvas in excess areas beyond the mounting frame to avoid, as much as possible, the ground and paint layers. The sample amount taken from each painting was on the order of 50 mg.

A contemporary yarn was used as a reference sample. It was produced from textile flax (Melina variety) cultivated in 2018 in Normandy (France) by the Teillage Saint-Martin company; this flax was dew-retted conventionally over 6 weeks and then scutched and hackled. Then, it was wet spun by Safilin Pionki (Poland) with a metric number of 9.7 km/kg and a targeted twist of 320 tpm.

Figure IV-2b of **Section 1** of the present chapter shows the yarn taken as reference sample, the same that was compared with the Egyptian yarn.

Table IV-3 Dimensional and historical data on four canvases on display at the Civic Art Gallery of Ascoli Piceno.

Sample	Author	Title and date	Origin	Dimensions (cm)	Picture
GB	Giulio Benso (1592–1668)	San Cristoforo (first half of the 17th century)	From the collection of Antonio Ceci, acquired by the Gallery in 1920.	74x99	
NM	Nicola Monti (1736–1795)	Madonna col Bambino (18th century)	Commissioned for the Annunziata church (Ascoli Piceno) and exposed there until 1870, then acquired by the Gallery.	100x72	
TS1	Tommaso Sciacca (1734–1795)	Crocefissione (18th century)	The two paintings were commissioned by the Camaldolese order of Sant'Angelo Magno convent (Ascoli Piceno) for the abbot's lodging and transferred into the Gallery in 1861.	104x75	
TS2	Tommaso Sciacca (1734–1795)	Santa Francesca Romana (18th century)	During the 19th century, Santa Francesca Romana painting (TS2) has undergone a re-lining intervention: a new canvas was glued to the back of the old one, which was in a bad state of preservation, to reinforce and support it.	64x46	

2.3 Experimental methods

Several microscopic and spectroscopic techniques were applied and here briefly described.

2.3.1 *Scanning Electron Microscopy (SEM)*

To examine the fibre surface morphology, a small piece of yarn approximately 5 mm long was cut from each sample, and the modern yarn was adhered to a conductive sample holder and successively gold sputter-coated (Edwards Scancoat Six device for 180 seconds) to perform SEM micrographs.

2.3.2 *Atomic force microscopy and nanoindentation*

To the best of our knowledge, no literature exists regarding the use of AFM PF-QNM to investigate archaeological objects. Conversely, nanoindentation (NI) measurements are more widespread and are done with a deeper (i.e., several tens of nanometres up to more than a hundred nanometres) indent than AFM (i.e., indentation depth of a few nanometres here). Since the minimum spatial distance between two measurement points is much smaller in AFM than in NI, the nanoindentation leads to a lower spatial resolution than that of AFM but, on the other hand, it allows to obtain more qualitative and accurate mechanical properties. NI has already been used to investigate cultural artefacts [68,69], although the available literature is still scarce.

To prepare the samples for AFM analysis, a small piece of yarn approximately 5 mm long was cut from each canvas and embedded in low viscosity epoxy resin (see **Chapter II**). At least four AFM images were obtained from each sample and the modern yarn. An averaged indentation modulus was calculated as a mean of the pixels included in the region of interest manually delimited by mask, as shown in **Figure IV-12**. Successively, a further average was calculated using the values obtained from the various figures of each yarn.

Nanoindentation measurements of the indentation modulus and hardness were performed on the same blocks of epoxy resin with embedded yarns previously prepared for AFM analysis. At least 30 points were tested for each yarn embedded in epoxy resin and representative of each canvas investigated, except for yarn TS1: here, 16 points were tested because the block had a lower number of fibres embedded and had a smaller diameter. In addition, approximately 20 points were recorded in the epoxy embedding resin of each block to check the stability of the measurements. The obtained indentation moduli were compared to the average calculated by AFM: in practice, the averaged AFM results were validated by nanoindentation, which operates at a higher scale.

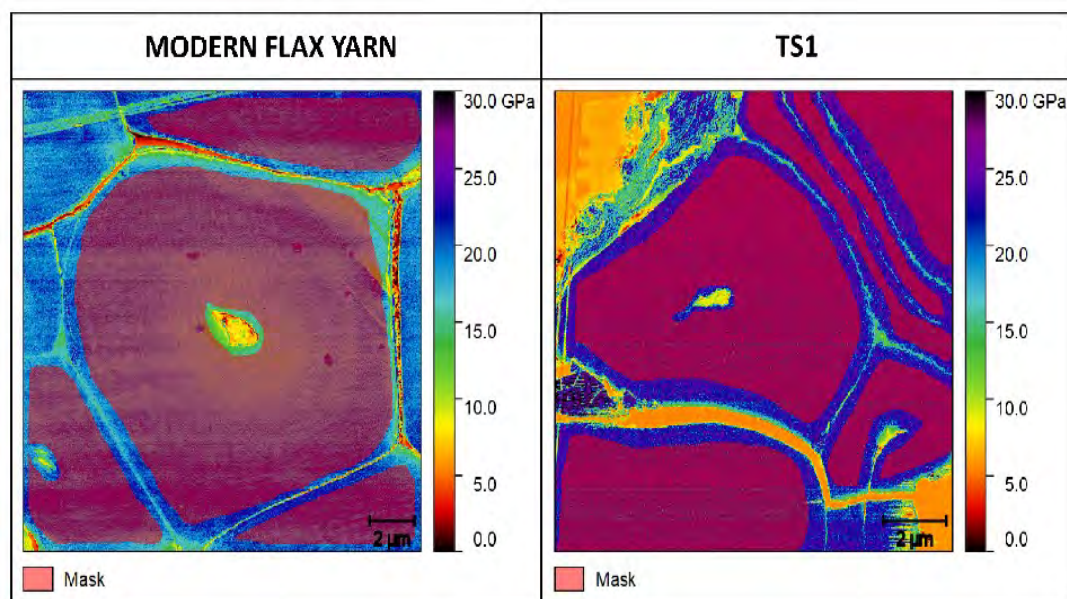


Figure IV-12 Two examples of the masks applied to AFM maps to calculate a mean value of the indentation modulus.

2.3.3 Second-harmonic generation microscopic imaging

Second-harmonic generation (SHG) is plane selective, and different levels in the Z-direction can be analysed independently from one another and allow us to investigate the inner structure of the samples, such as the angle formed by cellulose microfibrils in plant fibres [49]. For SHG analysis, a small bundle of each yarn was manually extracted and mounted on a paper frame used for traction tests according to technical standard ASTM C1557 [70]. This standard explains the preparation, mounting and testing of elementary fibres to determine tensile strength and Young's modulus; the sample support described in the technical standard is illustrated in **Chapter II**.

The ancient yarns were glued in the standard support but in the transverse direction to use a 5 mm gauge length instead of 10 mm, successively placed between two coverslips and studied with a multiphoton microscope.

2.3.4 Solid-State ^{13}C CP-MAS NMR Spectroscopy

^{13}C cross-polarisation magic angle spinning NMR spectroscopy is an NMR technique that allows samples to be studied directly in the solid-state without having to dissolve them in a suitable solvent. This allows the study of small fragments of the object and their subsequent reuse for other investigations. In addition, the rotation around the angle defined as the “magic angle” allows sharpening of the resonance lines that, in the case of solid samples, are very wide.

^{13}C CP-MAS NMR spectroscopy has been used to investigate structural changes in cellulose-based materials, allowing the determination of the crystalline/amorphous ratio and the detection of hemicellulose, cellulose oligomers and noncellulosic compounds, such as organic additives.

Flax yarns were finely cut using a microcutter and packed into 4 mm zirconia rotors with an available volume set to 25 μL and sealed with Kel-F caps. Cross-polarisation was achieved by applying the variable spin-lock sequence RAMP-CP-MAS [71]. Spectra were acquired using 1024 data points in the time domain, zero filled and Fourier transformed to a size of 4096 data points applying exponential multiplication with a line broadening of 16 Hz.

The deconvolution of ^{13}C CP-MAS spectra was performed using the dm2004 program [72], and the integrals of the resonances obtained from the deconvolution allow a semiquantitative evaluation. Each resonance was modelled by the following parameters: amplitude, position, width at half height and Gaussian line shape. Applying the best fitting procedure, the area and the chemical shift of all resonances were obtained. The sum of the integral of all resonances in each spectrum was normalised to 100. **Figure IV-13** illustrates the details of the deconvolution of C1 and C4. The crystallinity index (CI) of cellulose was calculated as a percentage of the integrals of the C-4 peaks at 86–92 ppm (C4c) and 80–86 ppm (C4a) [72]: $\text{CI}(\%) = 100 \text{ C4c}/(\text{C4c} + \text{C4a})$.

The resonance at approximately 106 ppm (C1 carbon) reveals the presence of I_α and I_β crystalline forms and can be used to evaluate the ratio $R = I_\alpha/I_\beta$, which depends on the source of the cellulose [64].

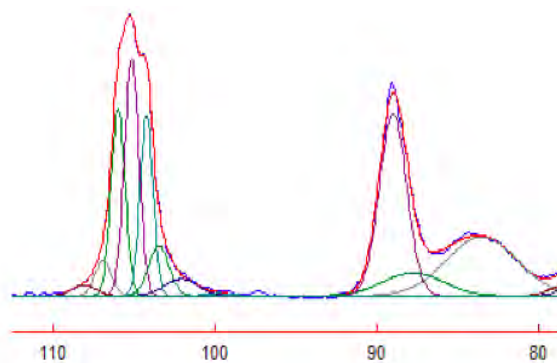


Figure IV-13 Details of the deconvolution of C1 and C4 resonances obtained for sample TS1. The profile of the C1 resonance is characterised by three sharp resonances centred at 106.6, 105.8 and 105 ppm and two very broad bands at 107 and 104 ppm. The central sharp resonance at 105.8 (magenta) is due to I_α , whereas the two lateral sharp resonances at 106.6 (green) and 105 ppm (cyan) are due to I_β .

2.3.5 Fourier-Transform Infrared Spectroscopy (FTIR)

A linear baseline correction was performed using three points at 4000, 3700 and 1800 cm^{-1} . The spectra were normalised setting the minimum absorbance measured between 4000 and 1800 cm^{-1} to 0 and the area (integral) measured between 1080 and 884 cm^{-1} to 1, since this latter is sensible to crystalline and amorphous cellulose.

Table IV-4, summarises all the setup and parameters chosen for each analysis.

Table IV-4 Summary of the techniques and parameters used

Characterization Technique	Instrument	Parameters
Scanning electron microscopy (SEM) EDX	Jeol JSM 6460LV scanning electron microscope	Accelerating voltage: 3 kV Working distance: 29.3–30.5 mm
Atomic Force Microscopy in Peak Force Nanomechanical property mapping mode (AFM PF-QNM)	Multimode 8 atomic force microscope (Bruker, USA) equipped with RTESPA-525 probes (Bruker, USA)	Spring constant (Sader method): 101–161 N/m Deflection sensitivity: calibrated on Sapphire Tip radius (relative method on Aramid fibres): 20–85 nm Peak force setpoint: 200 nN Oscillation frequency: 2 kHz Resolution: 512×512 pixels
Nanoindentation	Nanoindenter XP (MTS Nano Instruments)	Indenter: three-side pyramid indenter (Berkovich-Berko XPT-12761–0) Surface approach velocity: 10 nm/s Frequency target: 45 Hz Loading rate: 0.05 s ⁻¹ (i.e., 1 µN/s) Unloading rate: 10 µN/s Depth limit: 120 nm
Second-harmonic Generation Microscopic Imaging (SHG)	Multiphoton Nikon A1 MP+ microscope (NIKON, France) equipped with a long working distance (LWD) 16x (NA 0.80) water immersion objective (NIKON, France), a tuneable Mai Tai XF mode-5 locked Ti: sapphire femtosecond laser (SPECTRA PHYSICS, France) and a GaAsP NDD detector	Excitation wavelength: 810 nm (average power 1.5 W) Laser power used: 3% and 5% to investigate ancient and modern flax fibres, respectively to avoid bleaching Bandpass filters: 460/60 nm (autofluorescence), 550/88 nm (autofluorescence), 406/15 nm (SHG signal) Scan line average: 16 Scan velocity: 0.25 (fps) Scan size: 512×512 pixels
¹³ C CPMAS NMR	Bruker Advance III spectrometer operating at the proton frequency of 400.13 MHz	Spin rate: 12 KHz Contact time for cross polarisation: 1.5 ms Recycle delay: 3 s ¹H $\pi/2$ pulse width: 3.5 µs
FTIR-ATR	Spectrum 100 Perkin-Elmer spectrophotometer equipped with ATR system with Zinc Selenium crystal (ZnSe)	Accumulation scans : 16 Acquisition range 4000–600 cm ⁻¹ Resolution : 4 cm ⁻¹

2.4 Results and Discussion

2.4.1 Morphological description of yarns and flax fibres

Thread count is an important parameter to characterize canvases and textile fabrics, and it plays an important role in the mechanical properties of the canvases [73,74]. All the canvases except TS1 had a plane weave structure (**Figures IV-14A, D, G, J**), and GB appeared tauter than the others. GB and TS2 had similar thread counts (29/28 for the first one and 29/27 for the second one), and were coarser and more open-weave fabrics than NM (47/47) and TS1 (38/32), as shown in **Figure IV-14A**.

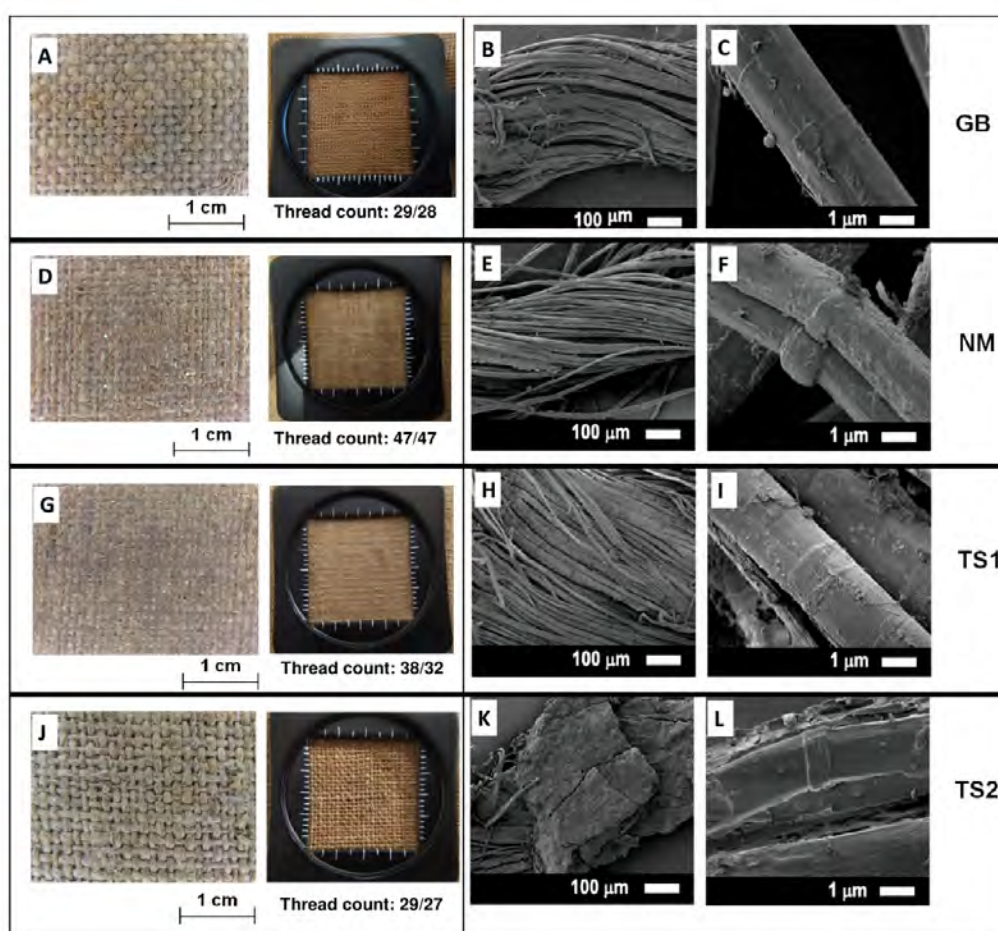


Figure IV-14 Photos and macrographs of the different yarns (**A,D,G,J** - the weave count was measured over 4x4 cm²) and SEM observations of yarns from canvas GB (**B, C**), NM (**E, F**), TS1 (**H, I**) and TS2 (**J,K**).

For all the yarns investigated by SEM, the morphology indicated that they were flax fibres due to their polygonal shape (**Figures IV-14C, F and I**) and the presence of characteristic structural defects, i.e., kink-bands (**Figures IV-14C, F, I and L**). Generally, fibres appeared well separated, although residues of middle lamellae or cortical parenchyma sometimes remained glued to the fibre surface

(**Figure IV-14B**), suggesting a possible sub-retting degree for the GB sample. Nevertheless, the overall fibre separation was good, probably thanks to the retting mode, which in the past was carried out in water, as in ancient Egypt [75]. This method consists of soaking the fibres in water for approximately two weeks before scutching them, but since the second half of the 20th century, water retting has been replaced in Europe by dew retting, which produces less pollution, even if the quality of the fibre produced is lower [76].

In all the yarns, kink-bands were highly visible, especially on yarn NM, as shown in **Figure IV-14F**. These defects are considered areas of weakness [77] and possible origins of fractures [78]. Other teams also observed that both enzymatic and acid hydrolysis start and act mainly in these regions [79,80] and can lead to fibre fragmentation. Thus, it can be assumed that cracks and porosities in kink-bands could facilitate the attack of microorganisms, which penetrate into the internal structure of the fibre to reach the lumen where they grow and then spread to the rest of the fibre cell [81].

Finally, in samples TS2, an adhesive from likely due the past re-lining intervention (**Figure IV-15a**) and large residues from the ground layer (as indicated by SEM-EDX analysis, **Figure IV-15b**) were detected. During the 19th century, in Europe, the adhesive used for re-lining interventions was glue paste, a mix of animal glue, flours and Venice turpentine or other components [55,74].

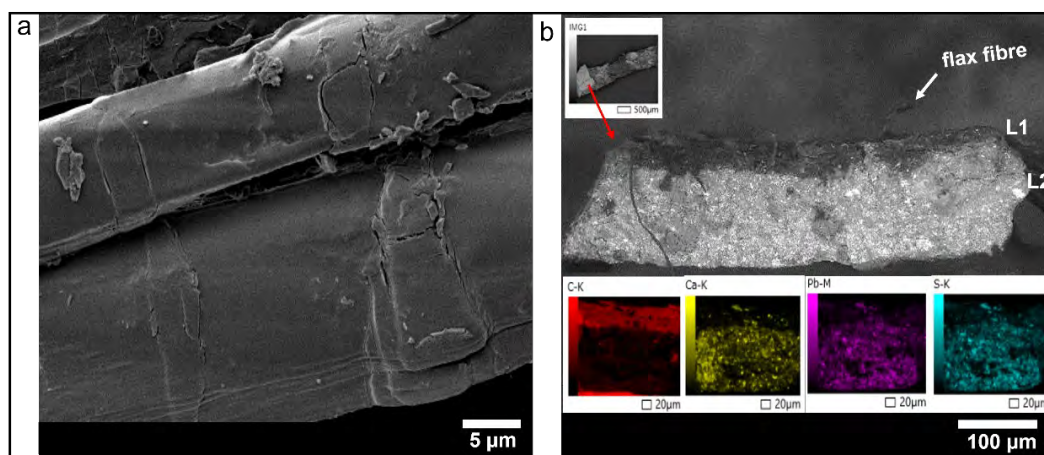


Figure IV-15 a) SEM micrograph of yarn TS2 with fibres covered by the adhesive and **(b)** SEM-EDX analysis with three layers of fibres, layer 1 (L1) made of organic material and rich in Carbon and layer 2 (L2) which is the ground layer rich in lead and probably due to lead white pigment.

The presence of this adhesive in yarn TS2 is particularly important in this case because today, it is known that glue paste can have dramatic consequences for paintings. It causes the canvas to have a greater susceptibility to humidity but also results in shrinkage and greater rigidity, and it is also highly sensitive to microbiological attack, especially in the case of animal glue [82–84].

An interesting study was recently performed by Fuster-López *et al.* in which the authors tested the glue paste on canvases and observed its ageing process [74]. They found that, in aged samples, the glue paste appeared more crystallised, dryer and sometimes delaminated. Tensile test analysis showed that the

canvases with aged glue paste were as sensitive to low relative humidity as the canvases treated with unaged glue paste. Fuster-López *et al.* also observed that the sensitivity to biodegradation, structural modification and the loss of mechanical properties were also dependent on the type of flour used in glue paste and the weave density of the linen canvas [74].

2.4.2 Investigation of local mechanical properties

Images obtained by AFM PF-QNM (**Figure IV-16**) show that ancient fibres can have a stiffness similar to that of a modern flax, which is in general approximately 18–20 GPa [67,85], and which was measured to be about 19.4 ± 0.9 GPa by AFM and 20.7 ± 2.9 GPa by nanoindentation. However, in most cases, the indentation moduli obtained from ancient yarns are higher than those obtained from the modern yarn, clearly illustrated in the profile extracted from TS1 in **Figure IV-16**, where the stiffness is calculated as approximately 24 GPa.

Despite their ageing, the flax fibres of ancient yarns still appeared homogeneous and had an intact structure (**Figure IV-16**). Nevertheless, a high indentation modulus can be indicative of a chemical change due to ageing that occurs mainly in the cell wall matrix, as reported in [38]. It should also be pointed out that the flax fibres compared in this section are neither from the same variety nor harvested at the same maturity or retted in the same manner. These differences play a central role in the mechanical properties and chemical composition of the fibres [25,86], and the results obtained must be regarded with caution.

In general, the average data obtained by both AFM and nanoindentation techniques were in agreement (**Figure IV-17a**). Yarn GB showed indentation moduli in line with those of the modern flax in both AFM (19.2 ± 3.3 GPa) and nanoindentation (19.3 ± 5.2 GPa) analyses. However, some flax fibres from this yarn showed fractures (see **Figure IV-17c**), which were probably generated during the surface preparation by the diamond knife, and their appearance could be indicative of a higher brittleness than in the modern yarn.

In canvas NM, most of the fibres appeared intact with indentation moduli of approximately 20 GPa (20 ± 6 GPa by AFM and 17.5 ± 4.5 GPa by nanoindentation), but, in the bottom right of the map shown in **Figure IV-16**, an extremely low indentation modulus (approximately 11 GPa) was recorded in one fibre, which indicates a great loss of local mechanical properties probably as a consequence of a chemical change not only in the matrix but also in the crystalline cellulose. This confirmed the suitability of the AFM technique to study aged yarns, as it is sensitive to the variable state of preservation of a canvas.

Fractures similar to those of the yarn GB were found in the yarn NM (**Figure IV-17c**), for which the lowest hardness was also recorded (**Figure IV-17b**). Paintings TS1 and TS2 were painted for the abbot's lodging and were probably exposed to similar environmental conditions.

The highest indentation moduli were recorded in yarn TS1 (23.4 ± 3.4 GPa by AFM and 23.9 ± 5.4 GPa by nanoindentation), which could correspond to a change in the chemical composition of the hemicellulose matrix, as hypothesised in a previous study [38]. Some fibres of this yarn were fractured, such as yarn GB, but with signs of biological attack highlighted by a loss of mechanical properties (~ 11 GPa) around a cavity, as illustrated in **Figure IV-17c**.

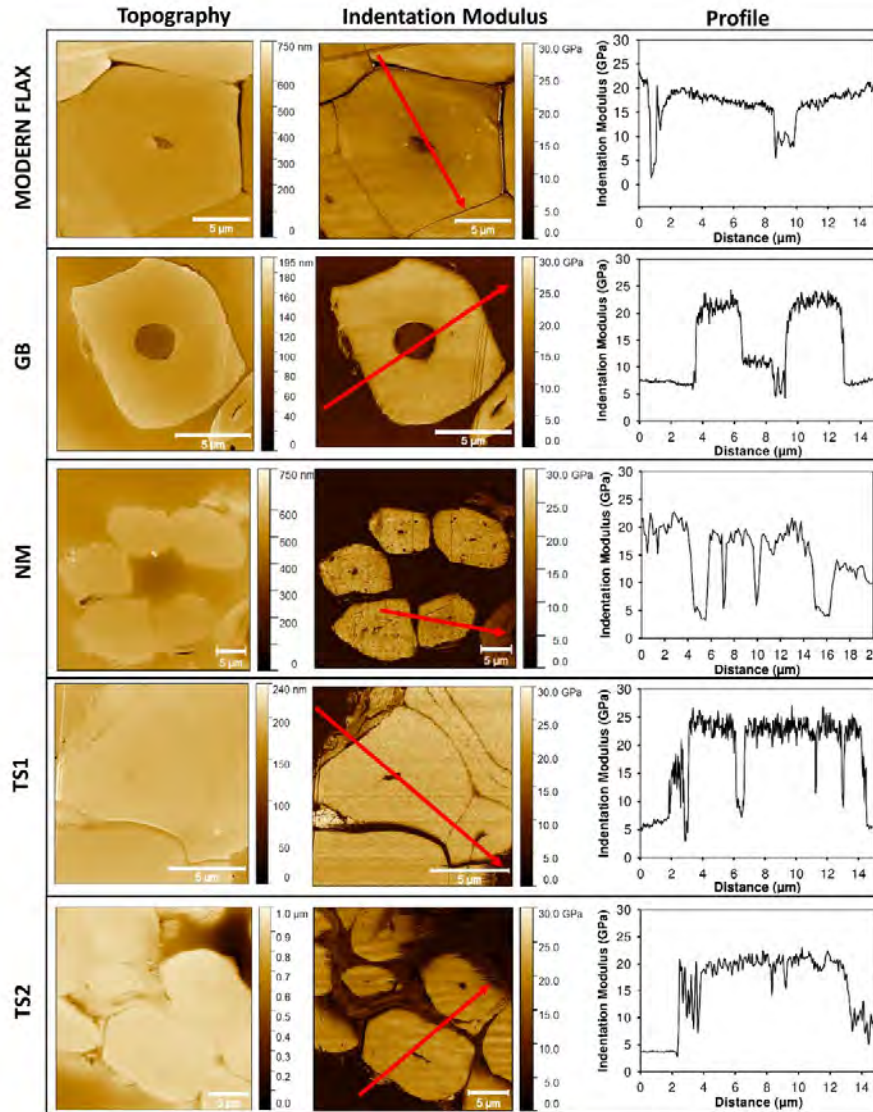


Figure IV-16 Topography and indentation modulus maps of the surface of each yarn, as obtained by AFM in PF-QNM mode. Each profile corresponds to the red line indicated on the corresponding modulus map.

In terms of morphology, the best preserved fibres were found in yarn TS2, where no fractures were noted inside the cells (**Figure IV-16**). However, this canvas underwent a past restoration intervention, and it was relined because of its poor state of preservation. In this last yarn investigated, the standard deviation of indentation moduli was comparable to that of the modern yarn (20.9 ± 3.9 GPa by AFM and 20.8 ± 3.7 GPa by nanoindentation), but the hardness is the highest recorded, probably because of

a different ageing process of the cellulose matrix caused by the coating. A hypothesis could be that the exchange of water molecules and oxygen between the fibres and the environment was reduced by the coating, leading to a different ageing process of the cells than that found in the other canvases. As previously discussed, this canvas was relined, and traces of animal glue were found by FTIR and NMR, while SEM analysis confirmed that the fibres of this canvas were coated. During the AFM analysis, some fragments were noticed on the fibre surface, probably due to the glue paste, as illustrated in **Figure IV-17c**. The fragment did not cause visible changes to the mechanical properties of the fibres, which were still homogeneous in their indentation moduli, even in their external layers (primary and S₁ cell walls).

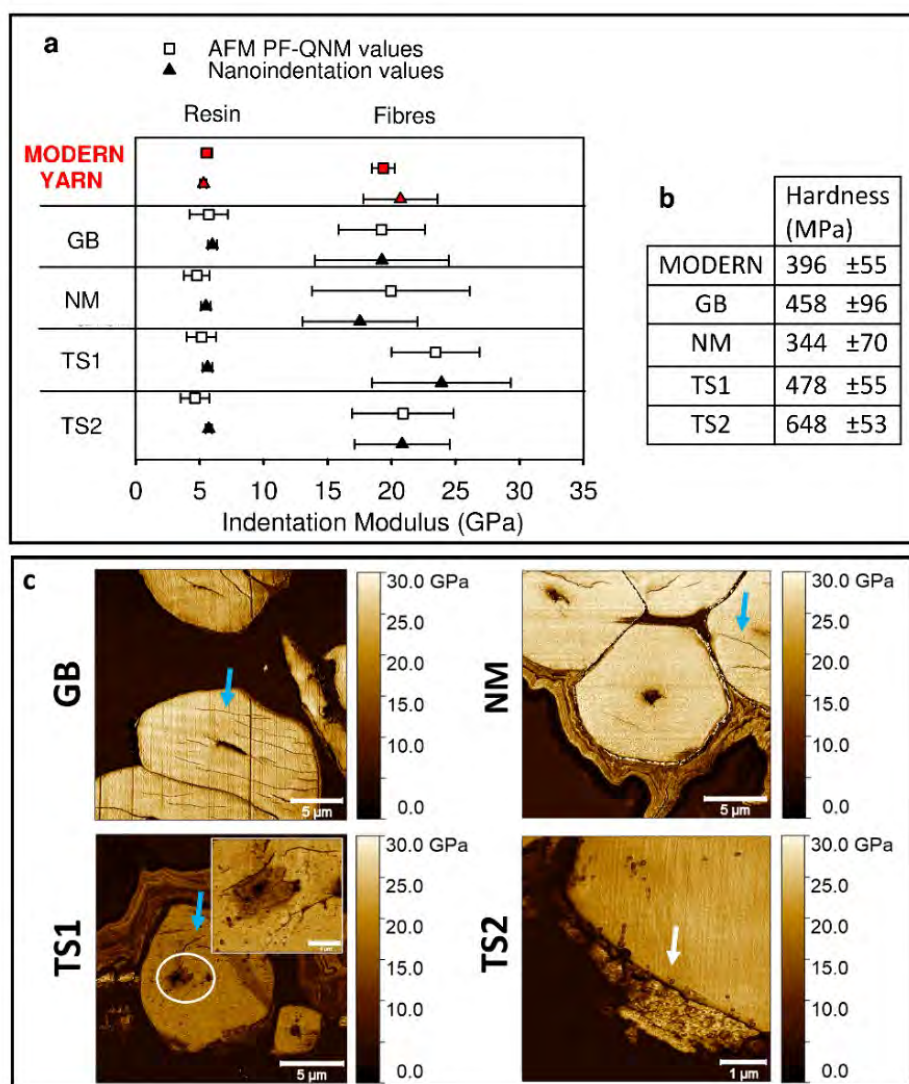


Figure IV-17 **a)** Indentation modulus obtained by AFM and nanoindentation on the different samples, **(b)** hardness values measured by nanoindentation **(c)** indentation modulus maps with fractures into the cell wall indicated by blue arrows; the white circle and zoom indicate traces of a possible biological attack near the lumen in the TS1 sample (lowered indentation modulus); the white arrow points to a fragment of a coating layer (preparation layer or re-lining intervention) in the TS2 sample (the interface with the cell wall is homogeneous, and the cell wall indentation modulus does not seem to be affected).

2.4.3 Chemical and structural modifications

FTIR results

The spectra and their attributions are reported in **Figures IV-18a, b** and **Table IV-5**, respectively. Traces of gypsum (3525 and 3394 cm^{-1}) and calcite (874 and 713 cm^{-1}) were found in samples NM, TS1 and TS2 (**Figure IV-18a**). The increase in the peak at 1735 cm^{-1} in spectra collected from the yarns of the canvases can be due to the oxidation process [87]. The band at 1595 cm^{-1} due to lignin [40,44] was noted only in the modern yarn. The absence of this peak in the canvas samples, together with the presence of the band at 2954 cm^{-1} (**Figure IV-18b**), could suggest a form of lignin degradation.

Two bands at 1577 and 1540 cm^{-1} were particularly visible in yarn TS1 (**Figure IV-18b** and **Table IV-5**), less visible in NM and probably also present in GB. These two bands are not documented in the literature for cotton or flax fibres and fabrics and are thus apparently not generated by the fibres. Zotti *et al.* observed them in ancient prints where fungal colonies were isolated, and the authors attributed these bands to a possible calcium stearate [88]. These two peaks can be an indicator of the presence of microorganisms. Furthermore, the increase in the band at $\sim 1640\text{ cm}^{-1}$ and the new band formed at 1540 cm^{-1} were also noted in linen and cotton fibres degraded after two weeks in soil and attributed to protein produced during microbial attack [89]. In biodegraded archaeological textiles, Kavkler *et al.* observed a downshift from 1430 cm^{-1} to 1420 cm^{-1} [16] of a contribution that is known to be sensitive to the cellulose lattice [90]. The shift, coupled with an increased intensity, was attributed to the presence of cellulose II [16], in line with Oh *et al.* [52]. In our yarns, both a shift and increased intensity were observed in TS1 and TS2, but only in TS1 was severe biodegradation activity confirmed by AFM (**Figure IV-17c**) and SHG (**Figures IV-20** and **21**), where cavities and partial loss of fibre cells are visible. It should also be mentioned that the peak at 1420 cm^{-1} could be the contribution of the $\nu\text{C}-\text{O}$ of calcium carbonate in calcite form [91].

The presence of a coating was observed in TS2 by SEM (**Figures IV-14L** and **15a**), and the high intensity of the amide bands at 1540 and 1644 cm^{-1} in its spectrum are indicative of a proteinaceous material, which supports the hypothesis of animal glue, probably from the glue paste.

The spectra of GB and NM are similar to that of the modern reference yarn, with the three bands at 1370 , 1335 and 1315 cm^{-1} , sensitive to the cellulose lattice [90] clearly present, which are absent in TS1 and TS2. Furthermore, the bands between 1030 and 982 cm^{-1} merge in TS1 and TS2, while, in GB and NM, the peaks can still be distinguished despite a lower intensity than in the modern yarn. The same bands merged in a broad feature and were observed in naturally aged modern fabric [92]. At the same time, the decrease in the intensity of $\text{C}-\text{O}$ vibrations between 1160 and 1030 cm^{-1} found in archaeological textiles was linked with cellulose hydrolysis [49]. In each yarn from the canvases investigated in this study, a decrease in the intensity of these bands was noted.

Additionally, the band at 898 cm^{-1} , which is indicative of the cellulose structure [90], was observed to decrease in intensity in a biodegraded archaeological cotton fabric [16]. In GB and NM, this peak is still present but small and broad; in contrast, it is totally absent in TS1 and TS2.

In conclusion, FTIR-ATR observations allowed us to confirm the presence of animal glue in TS2 and highlight that TS1 underwent the greatest modifications in the cellulose structure. In contrast, yarns from GB and NM seem better preserved.

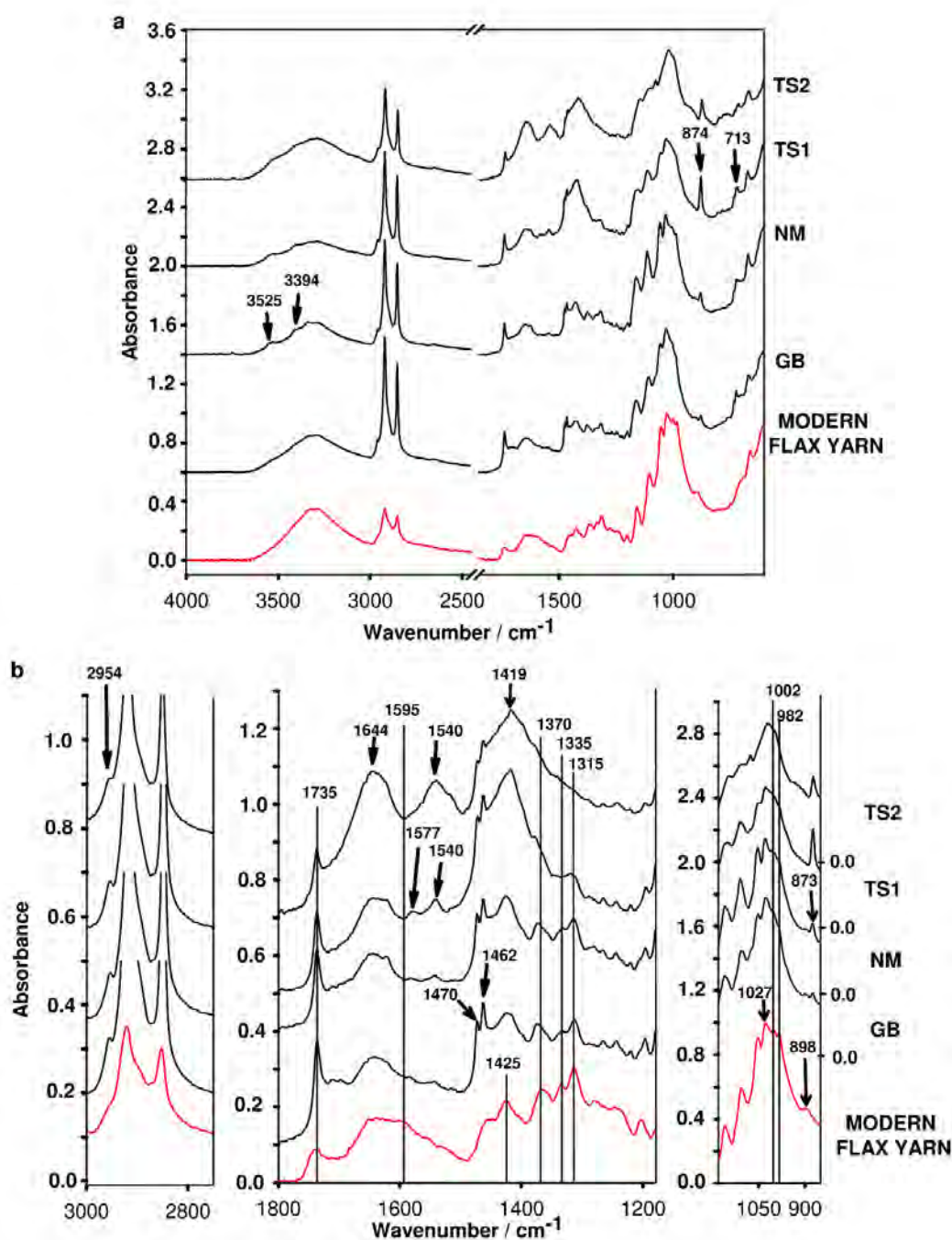


Figure IV-18 a) FTIR spectra of canvases and modern flax yarn with a break in the region between 1890 and 2550 cm^{-1} ; **(b)** focus on three regions of interest.

Table IV-5 Summary of the bands considered in the FTIR analysis.

Assignment and position Wavenumber/cm ⁻¹	Possible Attribution	MO D	GB	NM	TS1	TS2
~3525 and ~3394	vOH Gypsum [87,93]	-	-	w	w	vw
3600–3100	vOH of free cellulose/ hemicellulose/lignin [40,43]	sh	sh	sh	br	br
~2954	vCH ₃ of lignin [94]	-	w	w	w	vw
~1735	vC=O of carboxylic acid or esters groups of pectin and hemicellulose [40,43]	w, br	m, sh	m, sh	m, sh	w, sh
~1635 or ~1644 (Amide I)	δOH of absorbed water [50,95] or vC=O (Amide I) of a protein binder [96,97] or produced by microorganisms [89,98]	w, br	w, br	w, br	w, br	m, sh 1644 cm ⁻¹
~1595	vC=C aromatic in plane of lignin [40,44]	br	-	-	-	-
~1577	vC=O from oxidised phenolic lignin [99] or vCOO ⁻ of calcium stearate [88,100] with doublet at 1540 cm ⁻¹	-	vw	vw	w	-
~1540	vCOO ⁻ of calcium stearate [88,100] or vC-N and δN-H in plane (Amide II) of protein binder [96,97,101] or produced by microorganisms [89,98]	-	vw	vw	w, sh	m, sh
~1470	δCH ₂ [40,94]	-	sh	sh	sh	sh
~1462	δOH in plane [40,50]	br	sh	sh	sh	sh
~1425	δO—C—H and δH—C—H in plane [16,48,49,52]	m	m	m	s 1419 cm ⁻¹	s 1419 cm ⁻¹
~1375	δC—H and δCOH of cellulose, hemicellulose [16,49,53]	m	m	m	-	-
~1335	δCH ₂ and δCOH mainly cellulose [40,44,49,52]	w, sh	w, br	w, br	-	-
~1315	δCH ₂ wagging and δCOH of cellulose, hemicellulose [49,50,52]	m, sh	m, sh	m, sh	w, br	-
~1027	vC—O [44,49]	s, sh	s,sh	s,sh	s, br	s, br, 1019 cm ⁻¹
~1002	vC—O [49,53]	w, sh	-	vw, br	-	-
~982	vC—O [49,52]	sh	-	br	-	-
~898	vC—O—C of β-Glycosidic bond [16,40,44]	w	vw	vw	-	-
~874 and ~713	Calcite [99]	-	w	s	s	s

s= strong; m= medium; w=weak; vw= very weak; sh=sharp; br=broad

NMR results

The ^{13}C -CP-MAS spectrum can be considered as a "fingerprint" of solid cellulose components, and all four canvases exhibit typical cellulose resonances (**Figure IV-19**). The resonance at approximately 106 ppm is ascribed to anomeric carbon C1 of the glucose unit in cellulose and reveals the presence of two crystalline forms, namely, I_α and I_β . The weak shoulder at approximately 102 ppm can be attributed to the anomeric carbon of hemicellulose polysaccharides [22].

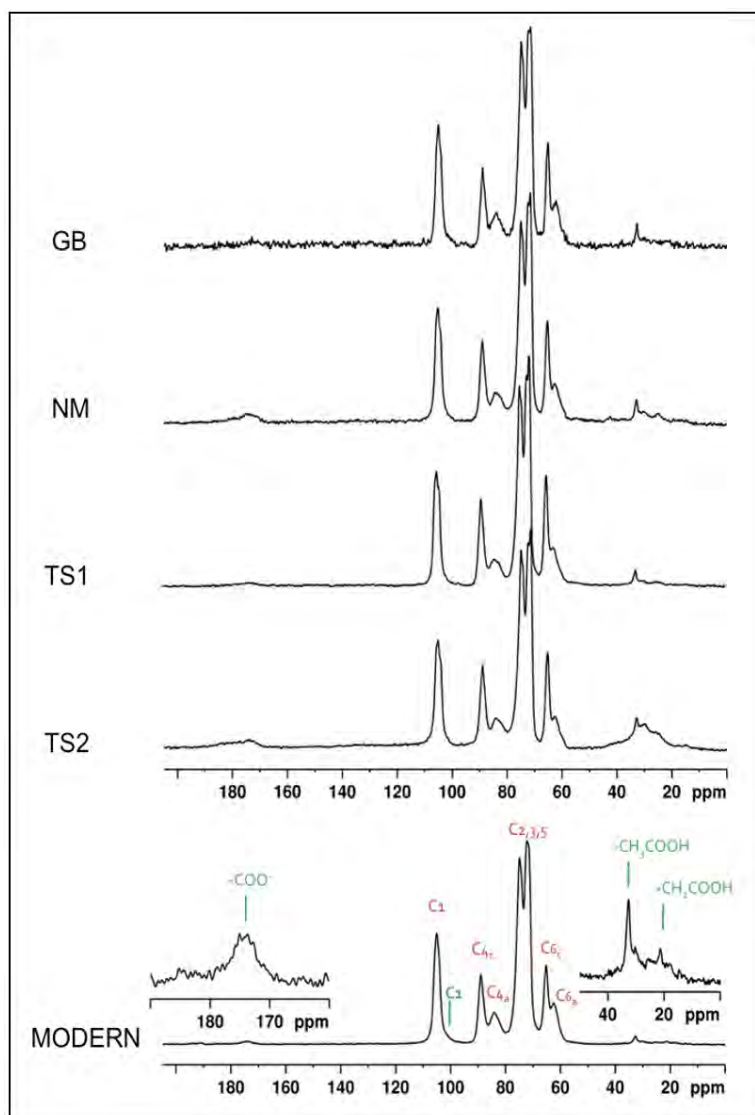


Figure IV-19 ^{13}C CP-MAS NMR spectra of canvas GB, NM, TS1 and TS2 and modern flax. On the spectrum of modern flax, a detailed assignment of the main resonances belonging to cellulose (in red) and to hemicellulose (in green) is given.

In general, the cellulose matrix exhibits easily separable resonances from crystalline and less-ordered domains for the C4 and C6 atoms of the glucose unit. Resonances at 90.3 and 66.8 ppm labelled C4c and C6c are due to C4 and C6 of the crystalline phase, whereas those at 85.4 and 64.5 ppm labelled C4a and C6a are due to C4 and C6 of the amorphous phase.

Moreover, other resonances were also identifiable: in particular, the resonance at 30 ppm ascribable to CH₂ belonging to cutin, a waxy substance that covers cell walls, the resonances at 21 ppm and 18 ppm, ascribable to the acetyl and fucose groups of hemicellulose, respectively, and resonance at 177 ppm due to carboxyl groups of hemicellulose. In **Table IV-6**, the integrals (I) of resonances obtained from the deconvolution procedure of all spectra are reported together with the crystallinity index obtained from the ratio of the integrals C4c and (C4c+C4a). The deconvolution of C1 resonance allowed us to obtain the amounts of I_α and I_β, the two allomorphs of cellulose. Our analysis showed that, in both modern and ancient flax yarns, the I_β allomorph was more abundant than the I_α allomorph. The ratio R between I_α and I_β depends on the origin of the cellulose [102]. Cellulose I_α is believed to be the dominant form in bacterial and algal celluloses, and cellulose I_β is the dominant form in higher plants, such as cotton ramie [103].

The R values for both modern and ancient flax yarns analysed in this study were found to be approximately 0.5–0.6, in accordance with the literature data on flax [104] and corresponding to the values that are usually assigned to non-lignified materials [105]. The normalised area of hemicellulose peaks at 20 and 30 ppm was found to be approximately 1.6 in modern flax, 2.4 in GB and 2.3 in TS1, while the area greatly increased in the case of canvases NM and TS2. In the case of NM, it could be probably due to a degradation process, while, in the case of canvas TS2, a change in the fingerprint of the resonances between 20–40 ppm was observed, which indicates the presence of another substance with resonances overlapping those of hemicellulose. In the same spectral region, there are resonances attributed to the protein of the animal glue.

Table IV-6 Normalised integrals of resonance (in % of total area), crystallinity index CI (in %) and R ratio of cellulose crystalline forms obtained by applying the deconvolution procedure to ¹³C CP-MAS spectra of modern flax and canvases GB, NM, TS1, TS2.

Sample	I (I _α)	I (I _β)	I (C4c)	I (C4a)	I (Hemicellulose)	I (COO ⁻)	CI	R= I _α /I _β
modern flax	5.1	9.2	8.5	6.1	1.6	0.8	57	0.55
GB	5.3	9.2	8.2	6.6	2.4	n.d.	55	0.58
NM	4.7	8.6	8.5	5.8	4.7	2.8	59	0.55
TS1	5.0	9.4	9.2	6.1	2.3	0.7	60	0.53
TS2	4.2	8.4	7.6	7.3	7.7	3.2	51	0.50

Thus, a hypothesis could be that animal glue is present on the flax fibres of yarn TS2, which was also confirmed by FTIR. The amount of carboxyl groups, which is approximately 0.8% in the modern flax, increased in canvases NM and TS2 and can be due to oxidation processes or, in the case of canvas TS2, to the presence of animal glue.

Another result concerns the crystallinity index CI. The CI value obtained for canvases GB, NM, TS1 varied in a range between 53–58%, very similar to that found in modern flax (57% in Ref [106], 55% in this study), suggesting a good state of preservation for these ancient yarns. A slight but significant decrease in crystallinity was observed in the TS2 canvas (see **Table IV-6**).

SHG results

The second-harmonic is generated in the backward and forward directions, but a previous study showed that the forward direction is more suitable to investigating the network of cellulose microfibrils present in the cell walls of plant fibres (**Chapter III, Sections 2 and 3**), so in the present study the latter one was chosen (**Figure IV-20**). The ultrastructure of flax fibres in yarns GB, NM and TS2 was well preserved and comparable to that of modern yarn (**Figures IV-20 and 21**), with a visible cellulose macrofibril network, but some pits and other forms of degradation were occasionally observed as a result of oxidation and/or hydrolysis and a possible localised biological attack (highlighted in **Figure IV-22**). In GB, traces of a different material were also found, which emitted a high-intensity second-harmonic signal, as shown in **Figure IV-20** (white arrows), but the structure of the underlying fibres was intact, as highlighted by autofluorescence channels (**Figure IV-21**, white arrows). Since the foreign material generates a second-harmonic but no fluorescence, this could suggest the presence of minerals or salts, as in the archaeological textiles studied previously [49]. The identification of this material is beyond the scope of this study. Concerning yarn TS2, despite the increased rigidity caused by glue-paste vitrification and the presence of some fractures into kink-bands, the cellulose microfibril network appeared intact under multiphoton microscopy.

All the ancient flax yarns presented sporadic degradation, identified with lacunae in the fibre structure, but yarn TS1 was in the worst state of preservation, and SHG analysis confirmed the AFM results: a severe biological attack was observed in the whole yarn. The fibre ultrastructure of this last sample was found to be highly degraded and compromised by cavities and lacunae, not only on the surface of the fibres but also into their inner structure down to the lumen.

To support the results, some additional tests were performed. Flax yarns from the four paintings were compared with modern flax fibres extracted (Bolchoï variety, cultivated in 2018 by Depestele group, see **Chapter III-Section 2.2**) and appositely used to reproduce a biological attack and acid hydrolysis and obtain a fast and approximative reference of the SH response of the two main degradation mechanisms responsible for the degradation of cellulosic fibres.

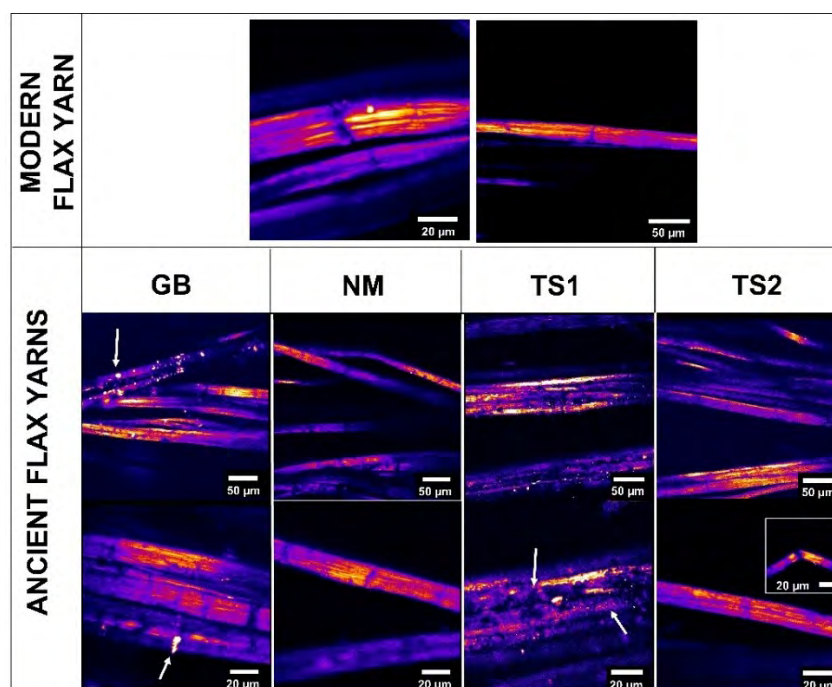


Figure IV-20 Forward SHG images of the flax yarns. GB, NM and TS2 have a generally well-preserved ultrastructure with an intact cellulose network. White arrows indicate the presence of a foreign material in GB yarn (probably minerals or salts) and cavities/pits resulting from a severe biological attack in yarn TS1. Several kink-bands with a well-defined angle are found in TS2 (square inset), suggesting brittle behaviour. A palette of false colours is used to highlight the cellulose network.

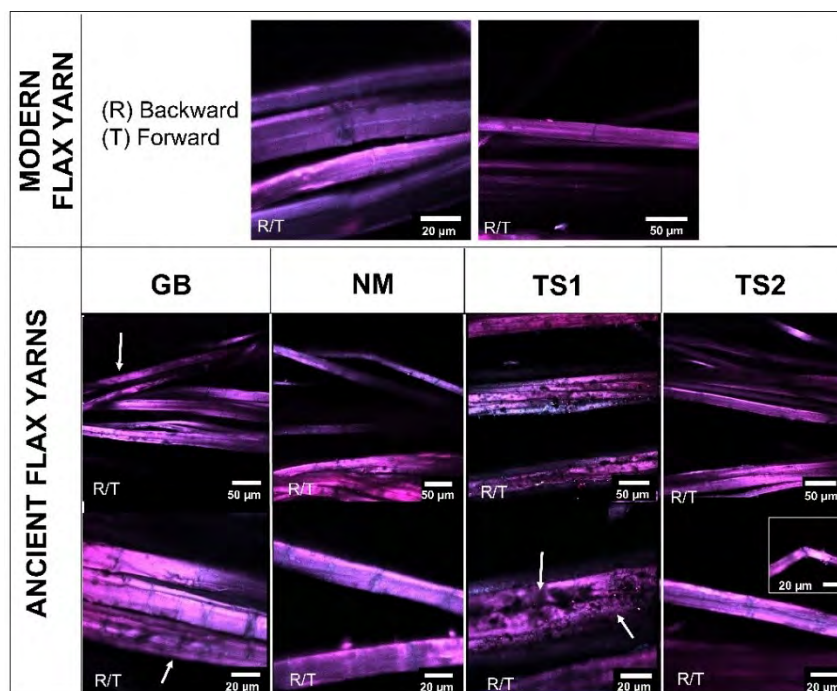


Figure IV-21 Autofluorescence maps recorded in backward (R) and forward (T) configurations. In each case, the blue/cyan (R460/60 and T460/60 TNDD) and red/magenta (R550/88 and T550/88 TNDD) channels were merged into a single image. White arrows correspond to the zones considered in **Figure IV-20** under the SHG channel. The yarn GB shows an intact fibre structure where a high second-harmonic was recorded, suggesting that salts or minerals are probably the cause of the second-harmonic signal. In TS1, fibres partially degraded and metabolised by microorganisms are also observed in the autofluorescence maps.

To reproduce a biological attack and promote a fast over-retting process, 5 g of soil were collected from the garden and put in a petri dish where 5 g of water were added. A bundle of fibres was left on the surface of the closed petri dish for 5 d at room temperature and humidity. After 5 d some fibres were extracted and mounted on paper support for SHG investigation (**Figures IV-22a, b**).

Other fibres from the same batch of Bolchoï flax variety were investigated by SHG in acidic environment. A bundle was extracted and mounted on a metal support and investigated by SHG microscopy. A solution of H_2SO_4 (1M) was then carefully injected with a syringe between the two coverslips where the sample was mounted. Fibres were left in acid environment for 8 h and images were collected before (image not shown) and after (**Figure IV-22c**) the injection of the solution.

Figure IV-22a show modern fibre under biological attack. The presence of fungal hyphae is observed with a similar SH response noted in **Figures IV-22d** from yarn NM. In **Figure IV-22b** a detail of a modern over-retted fibre with a degraded lumen due to the growth of microorganisms in the innermost layer shows lacunae comparable with fibres from TS1 (**Figures IV-22d**), and the fast acid hydrolysis in **Figure IV-22c** highlights a fibres fragmentation that has a similar degradation pattern observed in TS2 (**Figures IV-22d**).

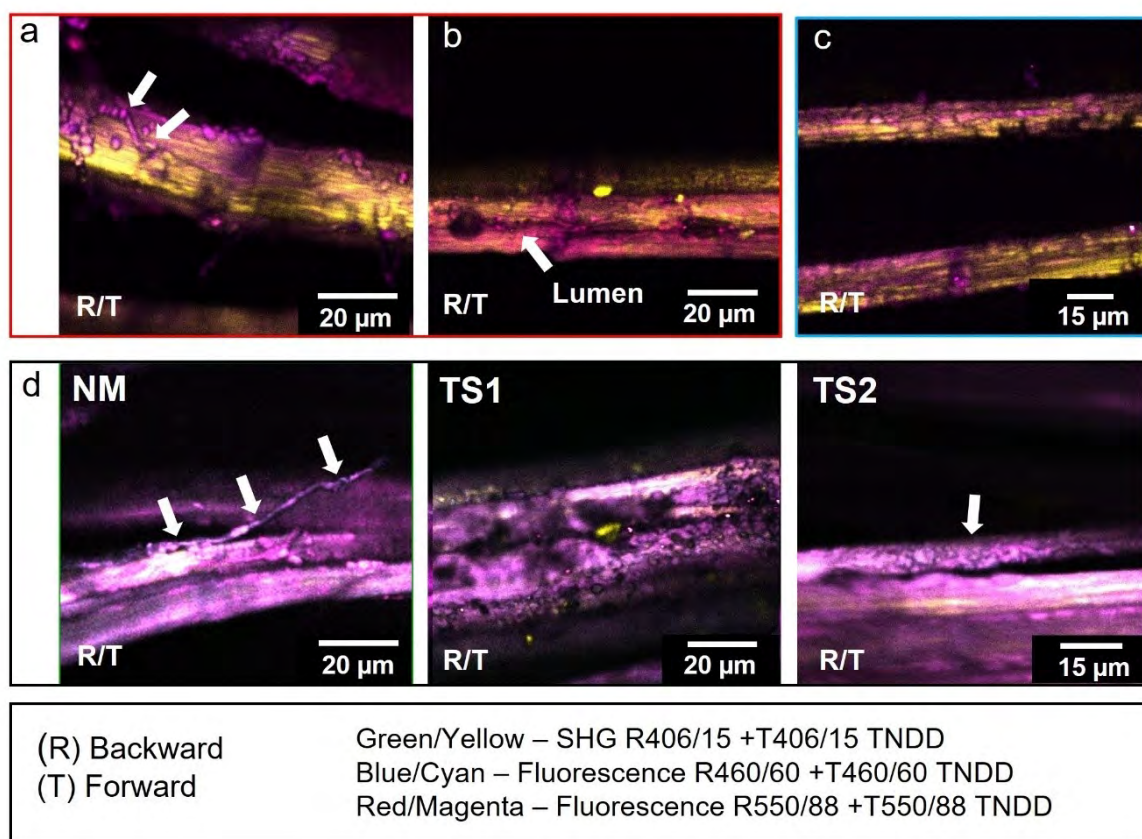


Figure IV-22 SHG images of **a)** the surface of a modern flax fibre over-retted in soil, with fungal colonization (white arrows); **b)** the same fibre with focus on the lumen; **c)** a modern flax fibre treated with H_2SO_4 (1 M) for 8 hours, which causes fibre fragmentation; **d)** fibres from yarn NM, TS1 and TS2. The white arrows in NM highlight mould on the fibre surface. TS1 shows degraded inner layers, as observed for the over-retted fibres. TS2 shows a fibre with a similar degradation as observed in **(c)**, probably due to hydrolysis. All the channels are merged in both backward and forward directions to create a single image.

2.5 Conclusions

Through this new combination of techniques, four Italian canvases dated between the 17th and 18th centuries have been investigated. The yarns extracted from each canvas were compared to a modern flax yarn to evaluate their state of preservation and highlight possible issues related to their chemical and mechanical conditions. Information on local mechanical properties obtained by nanoindentation and AFM helped to establish the state of preservation of cellulosic fibres, giving support and being complementary to chemical analyses such as FTIR and NMR. In addition, the SHG technique has proven to be fundamental to confirm the hypotheses of oxidation and biological attack formulated by the other techniques.

Yarn TS1 was found to be highly compromised by microorganisms, and future investigations should focus on assessing biological attack in the rest of the painting to avoid further degradation.

Despite the ageing, yarn GB appeared well preserved and comparable to the modern yarn. This could suggest that it was preserved in more favourable conditions before its acquisition and does not require immediate intervention.

Yarn NM showed some fibres with low mechanical properties recorded by AFM and nanoindentation, and the large amount of hemicellulose and carboxyl groups obtained by NMR suggested the presence of an oxidation process. However, thanks to the SHG, it was noted that, in this sample, the fibre ultrastructure was mainly intact.

The fibre ultrastructure of yarn TS2 was generally preserved, as well as the mechanical properties that were comparable to those of the modern sample. On the other hand, the yarn of this last painting was the most brittle, and the increased rigidity of the canvas due to the vitrification of the glue paste could be responsible for the lacunae and loss of the painting layer in the future. Furthermore, the re-lining process with glue paste could also trigger biodeterioration; however, in this case, it was observed a rather limited number of fibres with signs of mould growth.

3. Investigations by AFM of ageing mechanisms in PLA-flax fibre composites during garden composting

3.1 Introduction

Our collective need for sustainable development, driven by environmental regulations, encourages innovation in materials. Flax fibres, thanks to their specific mechanical properties, enable the design of functional, eco-friendly composite materials [29]. To design fully biodegradable or compostable composites, flax fibres must be embedded in biodegradable matrices such as poly-(butylene-succinate) (PBS), poly-(hydroxy-alkanoates) (PHA) or poly-(lactide) (PLA) [107]. In this case, an extended range of end-of-life routes can be planned, avoiding incineration, notably by recycling and by composting.

This study focuses on non-woven flax-PLA composites, due to their availability and the general interest of industry in these two bio-based components, especially for short life applications or when degradation at end of life is expected, such as specific parts for the advertising sector. During composting, degradation mechanisms of the composite material are naturally impacted by environmental conditions but also by the composite structure and the nature (physical, biochemical, thermal) of the polymer and fibre.

Composting is a bioprocess involving microorganisms and their colonization capacities as well as their arsenal of enzymatic degradation. The polymeric chains of materials can be split and, at macroscale, the composites will undergo macro- and micro-fragmentation. In compost conditions, PLA degradation is strongly affected by temperature, which substantially impacts the extent and rate of decrease in composite mass and molecular weight [108,109]. Morphologically speaking, degradation induces macro- and micro-fragmentation of the polymer matrix and, when plant fibres are incorporated, structural degradation is often boosted due to the fibres' hydrophilicity, leading to extensive interfacial damage [107]. At the composite scale, the impact of flax fibre content and preform architecture on the kinetics of degradation has been previously explored [110,111]. Moreover, mechanical properties of non-woven flax-PLA composite materials have been monitored during garden composting, showing a sudden decrease in tensile properties, but thereafter preservation of residual mechanical performance (*vis.* strength) at around 50% of initial strength even after six months in compost [107].

To our best knowledge, no existing studies focus specifically on the mechanical and structural degradation, and associated mechanisms, of the plant fibre constituents during the compost ageing process of biocomposites. Indeed, such investigations within a composite, at microscale, are challenging due to difficulties in sample preparation and the limited number of sufficiently precise and resolved

characterization tools. The development AFM PF-QNM [67] paves the way for original investigations with high precision and resolution allowing semi-quantitative indentation modulus mapping at the cell wall scale.

Here, following more than four months in a garden compost, a flax-PLA non-woven composite was examined using AFM PF-QNM technology. The mechanical properties of the composite material, its constituent flax fibres, PLA matrix and fibre-matrix interfaces, were compared before and after composting. Specifically, cross-sections of flax cell walls were mechanically mapped in different areas of composite sections to understand flax fibre degradation mechanisms within a biocomposite.

3.2 Materials

3.2.1 Flax-PLA non-woven preform

The industrial flax-PLA non-woven preform ($100 \pm 15 \text{ g/m}^2$) was provided by Ecotechnilin (Yvetot, France). This light non-woven mat is made with a needle-punching line and extracted before the napping step, prior to consolidation. PLA 3001 D from NatureWorks was used to produce films with a thickness varying from 50 to 100 μm .

3.2.2 Composite manufacturing and composting stage

Composite plates of 2 mm thickness were manufactured by a film stacking process and using thermo-compression, as described in a previous work [107]. Ten plies of flax preform were alternated with several plies of PLA to produce a sandwich by lay-up process, which was successively dried at 40 °C and at pressure of 60 kPa for 24h. A fibre volume fraction of $30 \pm 1\%$ was fixed and after thermocompression by a hydraulic press LabTech Scientific 50T (Labtech, Samutprakarn, Thailand) equipped with plates heated to 200 °C, in the composite a porosity less than 2% was achieved [107]. Dog-bone shaped samples drawn from ISO 527 were cut from these plates by a milling machine; due to the milling process, the edges of the specimen are not protected and therefore the flax fibre section is accessible (see **Figure IV-23**). Specimens were then aged in a garden compost made of green and brown plant waste [107]. Samples were buried at a depth between 20 and 40 cm; sampling was done after 125 days in the compost.

3.2.3 Sample preparation for AFM study

One composite sample was cut from a tensile specimen (**Figures IV-23c, d, e**) after 125 days of composting. The sampling region (area and orientation; **Figures IV-23e, f**) was selected to include both

‘exposed’ flax fibres (near the composite edge/surface, close to the compost) and ‘protected’ flax fibres (in the core of the composite sample). The sample was embedded in agar resin (epoxy resin agar low viscosity resin (LV); Agar scientific UK) and prepared for nanoindentation and microscopy as described in [112] (**Figure IV-23g**). Before micromechanical analysis, the sample was observed under an Olympus AX70 optical microscope equipped with a 5x (N.A. 0.15) BD objective to create a mosaic of the full surface (**Figure IV-23h**).

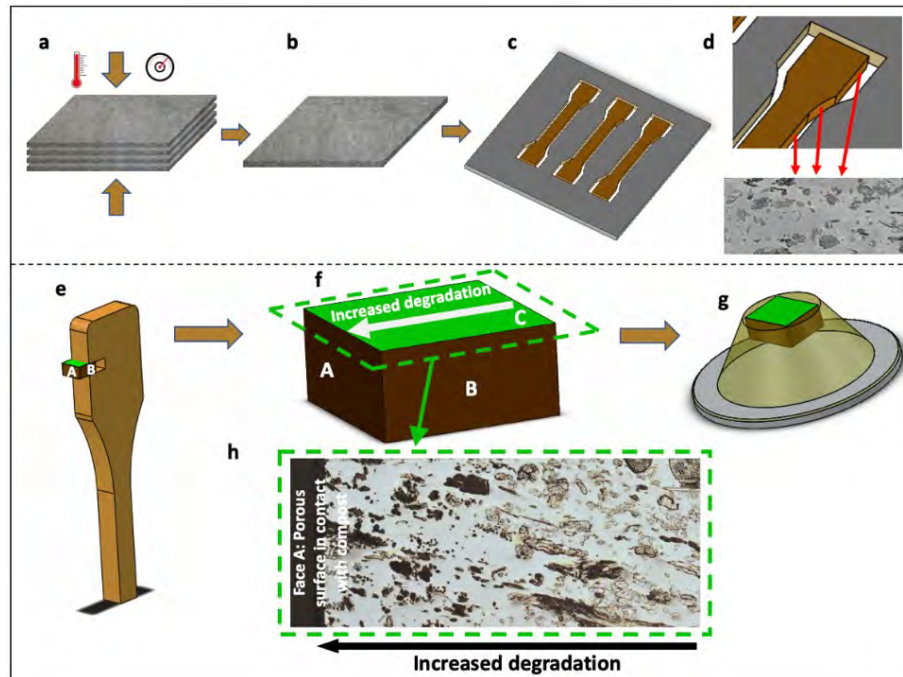


Figure IV-23 Manufacturing of the composite plates: **a)** Stacking of PLA-flax non-woven layers for hot compression, **(b)** is the obtained composite plate, **(c)** is the plate after the specimen cutting process and **(d)** focuses on the structure of the edge of the specimen with apparent flax fibres cross-section after cutting. **(e)** is a schema of the dog-bone sample indicating the region of sampling; The green face C **(f, g)** was specifically investigated in this study; the extracted sample was embedded in agar low viscosity resin and glued on an AFM sample holder **(g)**. Face A represents the most porous ‘exposed’ face **(h)**, in contact with the compost, as the dog-bone sample was cut by milling machine, whereas face B are less porous external faces in contact with thermo-compression plates, and the green face C was the one investigated by optical, electronic and atomic force microscopy.

3.3 Methods

3.3.1 Composite tensile test

Static tensile tests were performed on an Instron 5500R machine (Instron, Norwood, MA, USA) where displacement was recorded by an EIR LE-05 laser extensometer. The gauge length was 25 mm and the displacement speed was set at 1 mm/min. At least 5 valid experiments points (e.g. ignoring grip failures) were used for statistical analysis. The tangent modulus was calculated in the strain range of 0.02% to 0.15%.

3.3.2 AFM investigations

The indentation modulus is derived from the unloading part of the force-distance curve using an appropriate contact model. A DMT model was used, which corresponds to the Hertz contact model (small indentation depth compared to the tip apex radius) modified to take into account the adhesion force (mainly due to water capillarity in this case) between the tip and the sample surface [113]. The indentation modulus obtained is similar to that obtained by nanoindentation measurements, but with the required resolution to study mechanical gradient within cell wall layers [114]. For further information, see **Chapter II**.

The tip radius was adjusted between 20 and 80 nm. The image resolution was 512×512, 384×384 or 256×256 pixels depending on the aim of the image captured. The peak force amplitude was set at 30 nm for PLA measurements and between 50 and 100 nm for fibres, depending on the region investigated. At least three images were used to calculate the average moduli and roughness of PLA. The root means square (RMS) roughness was calculated after a flatten treatment (order 1) to remove the tilt of the sample beneath the tip.

3.3.3 SEM analysis

Two different samples were prepared for SEM analysis: i. a composite sample, cryo-fractured in nitrogen, for interface observation and also, ii. the sample prepared for AFM and described in **Figure IV-23** was SEM observed after AFM investigations. All samples were gold-sputtered using a Scancoat6 from Edward. Then, these samples were observed under a JEOL SEM (JSM- IT500HRSEM) at an acceleration voltage of 3 kV.

3.4 Results and discussion

3.4.1 *Evolution of overall composite microstructure with composting stage*

After spending 125 days in a garden compost, flax/PLA non-woven composites have undergone notable microstructural and mechanical property changes. As the interface region is a critical zone for stress transfer, the strength of aged composites is harshly impacted with a decrease of $51 \pm 4\%$ after composting. The degradation of the composite impacts not only its strength but also Young's modulus, which decreased by $66 \pm 7\%$ (**Figure IV-24a**).

As is visible in **Figures IV-24b** and **24c**, the degradation of the interfacial region, induced by a loss in the flax/PLA cohesion after ageing, plays an unarguable role in this drop in mechanical properties. This result is confirmed by previous results, for which a weight loss of $5.75 \pm 0.57\%$ was recorded [107] and the presence of internal porosity was observed. Looking at the position and geometry of this porosity, they appear to be mainly located at the interface between flax fibres and PLA. It is, therefore, relevant to also question the evolution in mechanical properties and ultrastructure of the flax fibres during this degradation, as they are largely responsible for the stiffness of the composite.

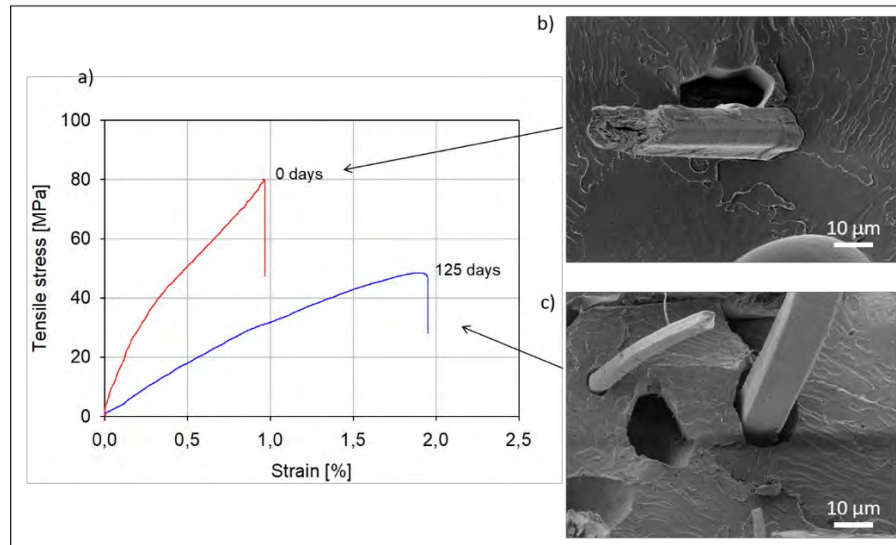


Figure IV-24 a) Mechanical property evolution of a non-woven flax/PLA composite after spending 125 days in a garden compost; (b-c) SEM micrographs of nitrogen cryo-fractured samples, showing the interface between flax fibre and PLA before (b) and after (c) compost ageing.

3.4.2 Morphology of the composite section after composting

Figure IV-25 presents a view of the investigated face (**Figure IV-25a**), as well as SEM images of flax fibres elements (**Figures IV-25b, c and d**) and PLA matrix (**Figures IV-25e, f and g**) at specific locations of the sample.

The sample was in direct contact with the compost at three faces (**Figure IV-23a**): face A and the two lateral faces B. Face A presented the worst conditions, as this face was milled during the specimen preparation resulting in a large number of fibre sections, devoid of PLA encapsulation, that are in direct contact with the compost. In contrast, as the upper and lower faces B of the specimens were in contact with platens during thermo-compression specimen manufacture, the surface and fibres would be well-permeated with PLA. Thus, the porous face A is more likely to promote the physical conditions necessary for the entry and proliferation of microorganisms [115] and, in this specific case, broken flax fibres provide an optimal access point and molecular resources for microorganisms. After 125 days in compost, degradation of PLA-flax fibre interface is noticed (**Figure IV-25d**), even in the core of the

composite, as in **Figure IV-24c**, this creates voids at the fibre-matrix interfaces, probably induced by moisture sorption and desorption of flax fibres during ageing combined with the low deformation capacity of PLA. These interfacial cavities may further facilitate the penetration of microorganisms through “channels” to the core of the sample.

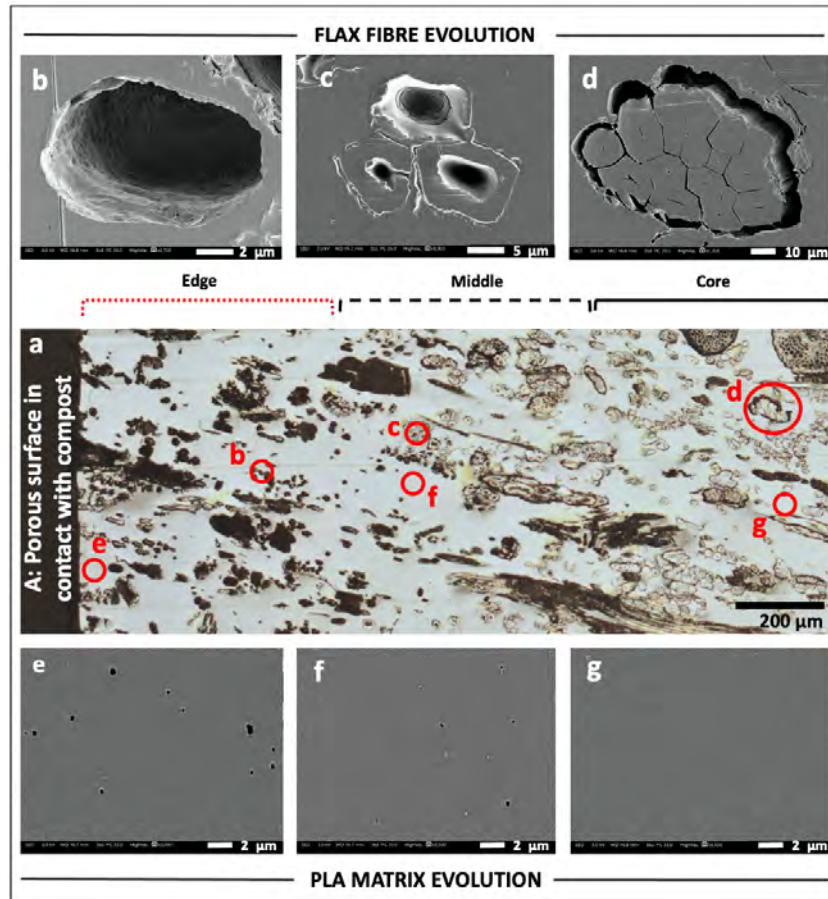


Figure IV-25 a) Optical micrograph of the investigated Face C (see **Figure IV-23**) which is divided in edge, middle and core areas following visual observation of fibre degradation; **b-d)** SEM images of fibres collected in edge, middle and core, respectively. The complete degradation of the fibres leaves phantom cavities with the same shape of the degraded fibre (**b**). Different stages of degradation can be recognised in (**c**). In (**d**) fibres in core appear intact; **e-f)** SEM images of PLA matrix investigated in edge, middle and core, respectively. Some porosities visible in edge (**e**) and middle (**f**), probably due to degradation, are absent in core (**g**). For each SEM image, corresponding investigation area is indicated with red circles in (**a**).

Figure IV-25a, one can notice that fibres closest to the compost exposed face have a black colour in contrast to that of the fibres located in the core of the material which are less accessible. Three stages of fibre degradation were identified: i. mostly black fibres at an advanced stage of degradation that often result into large empty cavities, in some cases with a cell wall residue in the periphery (**Figure IV-25b**); ii. partially degraded cell walls characterised by a grey colour often associated with channels and pits (**Figure IV-25c**), and; iii. apparently intact fibres still aggregated in bundles with a clear colour (**Figure IV-25d**). Following this observation, for the purpose of discussions in this study, the composite sample was ideally divided into three specific regions: edge, middle and core (**Figure IV-25a**).

Visually, at the SEM microscale, the PLA matrix is relatively less damaged in all three regions, though one finds an increase in porosity from the core to the edge (**Figures IV-25e-g**), with porosity size also increasing the closer they are to the edge. Development of progressive pores has already been documented for PLA, in case of immersion in a degradation medium (i.e. pH 7.4, 37 °C phosphate buffer) due to solubilisation of oligomers during 15 weeks, which is consistent with the duration of our composting stage [116]; it was evidenced that conjugated decrease of PLA molecular weight and water sorption were the key factors for this morphological degradation.

3.4.3 Assessment of the flax fibre degradation using AFM

In literature, bacteria responsible for wood and plant fibre degradation are divided into tunnelling, erosion and cavitation bacteria based on the characteristic pattern they create during their attack [81,115,117]. The tolerance limits of bacteria, especially dependent on temperature, oxygen and high values of water activity (water molecules not-chemically bonded to the material) [115], can make their proliferation difficult. However, in compost and in burial environments, optimal conditions allow bacteria to dominate over fungi [115,118]. An exception are the soft-rot fungi, particularly tolerant to these environmental conditions, which can coexist with bacteria, sometimes even degrading the same wood cell wall [119]. In general, it is possible to distinguish between fibre decay caused by fungi or bacteria, but sometimes their marks of degradation are similar especially at an advanced stage of the attack, as demonstrated in archaeological wood in burial conditions [118]. The three stages of fibre degradation previously identified (**Figures IV-25b-d**) were successively investigated by AFM, for which results are shown in in **Figure IV-26**.

After 125 days in compost, in the sample core, some fibres were found to be still intact (**Figures IV-26b, e and h**) and with an indentation modulus around 18–23 GPa, (average indentation modulus calculated also using images of different areas not shown in this manuscript: 23.2 ± 1.3 GPa) in line with indentation moduli generally found for flax fibres recorded in other papers by AFM or nanoindentation [67]. Nevertheless, one can notice a beginning of degradation in these core fibres, with low indentation modulus area around the lumen (**Figure IV-26h**, average indentation modulus calculated also using images of different areas not shown in this manuscript: 12.1 ± 1.5 GPa) inducing a bimodal distribution of indentation modulus (**Figure IV-26i**) with two main peaks around 23 and 10 GPa. A progressive degradation, with first an attack of more labile polymers such as hemicellulose and pectins can be hypothesised. It should be considered that the section investigated in this study represents only a slice of the whole sample. Fibres and fibre bundles at different planes can be more or less degraded than the one investigated, as was demonstrated by Björddal *et al.* [120] thanks to tomographic analysis. In general, degraded regions were found at the edge of the fibres (rarely),

randomly distributed in the secondary layers (typical in soft-rot decay, type I) [121] as shown in **Figure IV-27d**, or more often starting from the lumen (**Figures IV-25c and 26h**).

Fibres investigated in the middle region of the sample show more pronounced decay (**Figures IV-25c and 26g**) than those in the core (**Figure IV-25d**), with an increase of the degraded area from the lumen region. More precisely, mechanical properties of the gelatinous G layers decreased considerably (range of 5–7 GPa using the image illustrated; average indentation modulus calculated also using images of different areas not shown in this manuscript: 5.7 ± 1.2 GPa) in the degraded regions (**Figures IV-26g and 26i**). However, a part of the secondary wall in **Figure IV-26i** still appeared intact with stiffness around 18 GPa (average indentation modulus calculated also using images of different areas not shown in this manuscript: 17.9 ± 1.6).

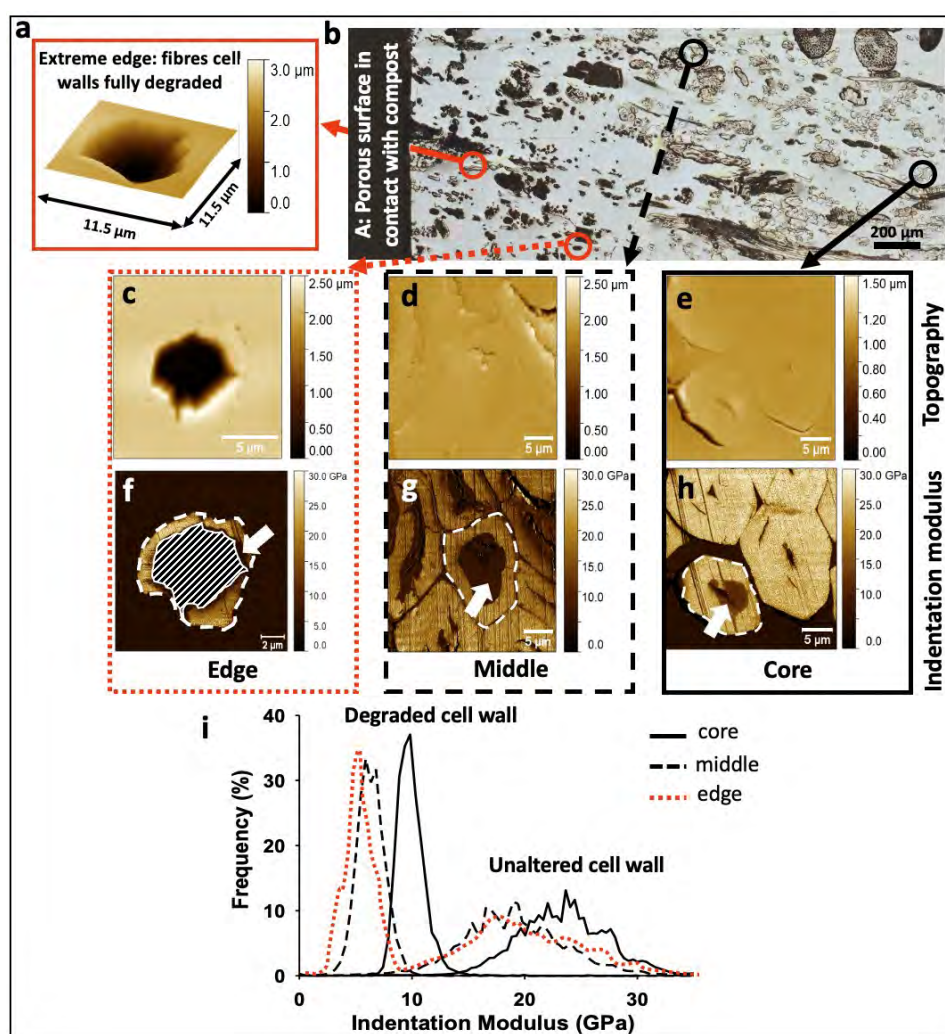


Figure IV-26 a) 3D AFM topographic image of a fully degraded fibre, located at the extreme edge of the sample; (b) Face C investigated through AFM PF-QNM; black and red circles indicate the fibres selected for AFM measurements; (c), (d) and (e) are AFM topographic images of edge, middle and core areas, respectively and (f), (g) and (h) the corresponding indentation modulus maps. (i) shows the indentation modulus distribution for each investigated region, indicated in white dot lines in (f), (g) and (h); In (f) no data was recorded in the hatched area.

The third step of fibre decay, especially in the edge of the biocomposite, consists in the complete degradation of the cell wall fragments (mean indentation modulus 4.9 ± 1.4 GPa), until only one cavity remains. Despite the advanced state of degradation of the whole cell, S₁ and the last parts of the G layer, seemed to be partially preserved at the periphery of the fibre (**Figures IV-26f and 27f**, mean indentation modulus of 19.2 ± 3.9 GPa). When fibre located at the extreme edge of the sample is considered (**Figure IV-26a**), cell walls are fully degraded. This loss of fibre material is mainly responsible for the increase in porosity of the biocomposite and its consequent loss of weight [107]. Thus, the described degradation mechanisms, from the lumen of the fibre, is a typical behaviour for tunnelling and erosion bacteria [81] but several fungi can also grow into the lumen (**Figures IV-27e and f**) and successively intrude into the rest of the fibre [122]. The progressive decrease in indentation modulus observed here, from the lumen to fibre periphery, is linked to the severity of the biological attack. It confirms also the predominant role of the lumen in plant fibre degradation; it enables the transport and propagation of water and microorganisms.

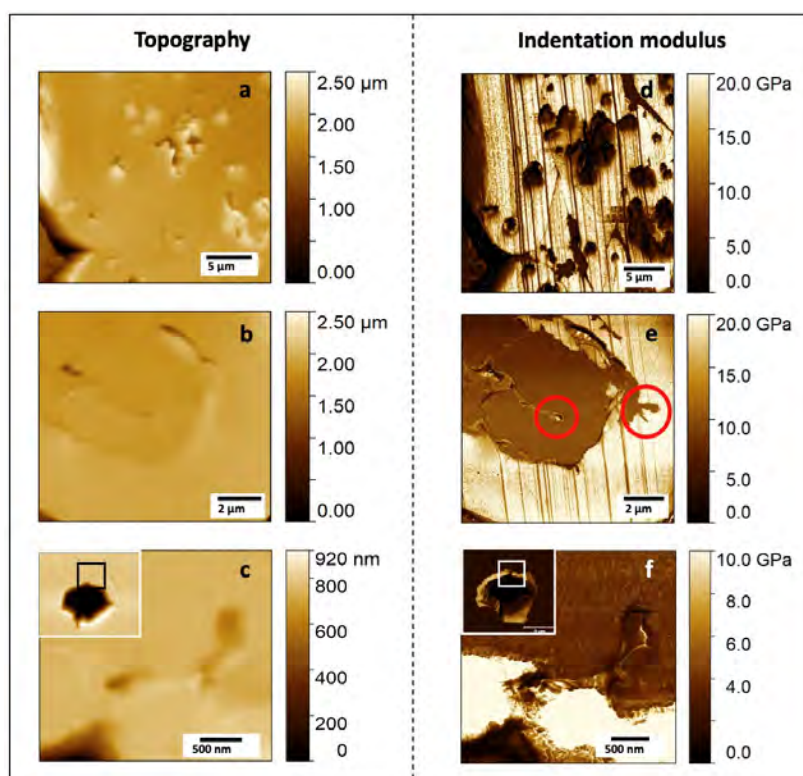


Figure IV-27 Surface topography (**a**, **b** and **c**) and indentation modulus mapping (**d**, **e** and **f**) of specific degraded areas. (**a**) and (**d**) are details of some fibres randomly degraded in G layer as typical degradation of soft-rot fungi; (**b**) and (**e**) focus on some typical degradation marks found in flax fibres, red circles highlight the presence of bacteria and a probable fungal mycelium; (**c**) and (**f**) focus on tunnel between inner and outer layers of the cell with a fungal mycelium that has grown in the exterior of the fibre and macrofibrils of the cell that are fragmented in packets with a low indentation modulus.

Moreover, flax fibres are cellulose and hemicellulose-rich and these components are high value resources for chemo-organotrophic microorganisms. Degradation is also promoted by their low lignin content, as lignin is known to inhibit the attack of fungi and bacteria.

In **Figure IV-26g** one can note that fibres investigated in the middle of the biocomposite lose their mechanical properties following the fibre shape, confirming that the gelatinous layers of flax, rich in cellulose and poor in xylan and lignin [123,124] are easily degraded; in the present case, cell wall degradation is probably initiated by structural hemicelluloses, less recalcitrant than crystalline cellulose.

3.4.4 Degradation of PLA

Contrary to flax fibres, PLA exhibits a low difference in indentation moduli between edge, middle and core regions (**Figures IV-28e, f and g**) with average values ranging from 4.7 ± 0.2 GPa to 5.2 ± 0.2 GPa. In contrast, a strong decrease in roughness, probably induced by the specific behaviour of the PLA during the cutting stage, from the core to the edge is evidenced with a ratio of 4.2 between core and edge mean values. The topography observed in the core region is comparable to that of PLA investigated in other studies [125,126], where the polymer appears as a complex matrix of fibrils, aggregated together. In the present study, the polymer formed filaments around 150–400 nm in length (**Figure IV-28d**).

During the first days of compost, the temperature under the compost can reach 60 °C [107] and this can cause a possible evolution of post-process local residual stresses as well as re-arrangement and recrystallisation of PLA during composting [107] that is visible in the core region (**Figure IV-28d**), with higher roughness, and disappeared at the edge where the degradation is more severe (**Figure IV-28b and c**). This supports the results in Xu *et al.* [125], where the authors observed a similar change in the surface topography of PLA film subjected to hydrolysis after 60 and 90 days at 60 °C. In other research, an increase in crystallisation and mineralization were noted after biodegradation and weathering process in PLA/plant fibre composites [127–129] that correlate with this phenomenon of re-crystallisation. This increase in crystallisation may induce a minor improvement in the indentation modulus as evidenced in our sample (**Figure IV-28**), even though the change in roughness may interfere with the measurement of the indentation modulus.

In the present study, the morphological change observed by AFM and decrease in RMS indicate an evolution in the organisation of PLA in the edge area in comparison to the core region, suggesting a role of microorganisms in secreting enzymes that degrade the polymers in oligomers, dimers and monomers being absorbable as nutrient [130,131]. Pits present in the PLA matrix, as observed by SEM (**Figures IV-25e, f**) or AFM (**Figure IV-28c**), are additional proof of this structural evolution, but it was not possible to attribute them to mechanical degradation caused by fungi or other types of ageing mechanisms such as self-catalysis hydrolysis [132].

A list of fungi and bacteria capable of degrading PLA are reported in [133] but, in Suyama *et al.* [134], PLA has been shown to be particularly resistant to biodegradation compared to other plastics. These authors also reported that only up to 0.04 % of bacterial colonies present in soil have the capacity to degrade PLA. Despite its low sensitivity to biodegradation, it is interesting to note that, in the

literature, PLA [131,135] and bast fibres [122,136,137] have some bacteria, such as *Bacillus brevis*, *Bacillus licheniformis*, *Paenibacillus amylolyticus*, and fungi, such as *Trichoderma viride* and *Fusarium moniliforme*, in common that are responsible of their biodegradation, but also used (or isolated) during the retting process for fibre extraction.

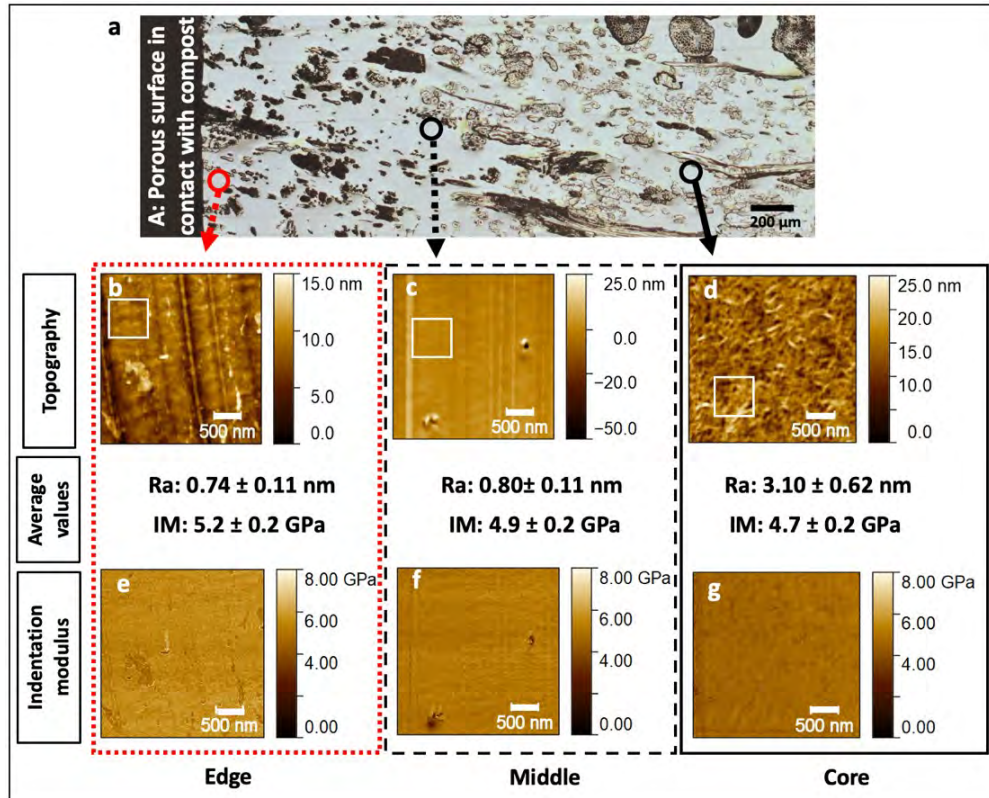


Figure IV-28 Maps of PLA topography and indentation modulus in the edge (b, e), middle (c, f) and core regions respectively (d, g). Red and black circles on the investigated composite section (a) represent the areas examined through AFM. Average values of roughness (Ra) and indentation modulus (IM) are given. Average roughness was calculated through topography acquisition in the areas delimited by white squares (55 x 55 px) and average modulus was calculated in the whole image avoiding the defects when possible (around, 65,500 force curves); at least three images were used to calculate the mean roughness and modulus in each region.

3.5 Conclusions

In the present study, the compost ageing of PLA-flax non-woven composite materials was investigated. After a period of over four months in a garden compost, flax fibres within a PLA-flax composite undergo drastic degradation with a significant decrease in indentation modulus and progressive increase in cavities from the inner part, the lumen, to the periphery of the fibre. It was shown that the lumen is a preferential degradation channel, with cell wall degradation occurring through well-known tunnelling and erosion effects. In contrast, the indentation modulus of the PLA matrix is not particularly affected, but a significant evolution in PLA morphology and change in roughness, from the core to the edge of the sample are highlighted. These phenomena are conjugated with the development of pits, induced by water ingress and microorganism attack

Bibliography

- [1] W. Van Zeist, J.A.H. Bakker-Heeres, Evidence for linseed cultivation before 6000 bc, *J. Archaeol. Sci.* 2 (1975) 215–219. [https://doi.org/10.1016/0305-4403\(75\)90059-X](https://doi.org/10.1016/0305-4403(75)90059-X).
- [2] M. Hopf, Plant remains and early farming in Jericho 1, in: G. W. Dimbleby (Ed.) *The Domestication and Exploitation of Plants and Animals*, 2nd Edition, Routledge, 2008.
- [3] C. Herbig, U. Maier, Flax for oil or fibre? Morphometric analysis of flax seeds and new aspects of flax cultivation in Late Neolithic wetland settlements in southwest Germany, *Veget. Hist. Archaeobot.* 20 (2011) 527–533.
- [4] E. Kvavadze, O. Bar-Yosef, A. Belfer-Cohen, E. Boaretto, N. Jakeli, Z. Matskevich, T. Meshveliani, 30,000-Year-Old Wild Flax Fibers, *Science*. 325 (2009) 1359–1359. <https://doi.org/10.1126/science.1175404>.
- [5] O. Heer, Prehistoric Culture of Flax, *Nature*. 7 (1873) 453.
- [6] A. Le Duigou, M. Castro, Evaluation of force generation mechanisms in natural, passive hydraulic actuators, *Sci. Rep.* 6 (2016) 18105. <https://doi.org/10.1038/srep18105>.
- [7] A.K. Mohanty, S. Vivekanandhan, J.-M. Pin, M. Misra, Composites from renewable and sustainable resources: Challenges and innovations, *Science*. 362 (2018) 536–542. <https://doi.org/10.1126/science.aat9072>.
- [8] E. Weiss, D. Zohary, The Neolithic Southwest Asian Founder Crops: Their Biology and Archaeobotany, *Curr. Anthropol.* 52 (2011) S237–S254. <https://doi.org/10.1086/658367>.
- [9] H.G. Hopkinson, Botany of Flax, *Nature*. 170 (1952) 557–559. <https://doi.org/10.1038/170557a0>.
- [10] D. Sertse, F.M. You, S. Ravichandran, S. Cloutier, The genetic structure of flax illustrates environmental and anthropogenic selections that gave rise to its eco-geographical adaptation, *Molecular Phylogenetics and Evolution*. 137 (2019) 22–32. <https://doi.org/10.1016/j.ympev.2019.04.010>.
- [11] A. Braun, Plants of Ancient Egypt, *Sci. Am.* 173 (1879) 2760.
- [12] A. Diederichsen, K. Hammer, Variation of cultivated flax (*Linum usitatissimum* L. subsp. *usitatissimum*) and its wild progenitor pale flax (subsp. *angustifolium* (Huds.) Thell.), *Genet. Resour. Crop Evol.* 42 (1995) 263–272. <https://doi.org/10.1007/BF02431261>.
- [13] T.S. Kawami, A Craft in Antiquity, *Science*. 256 (1992) 1065–1066. <https://doi.org/10.1126/science.256.5059.1065>.
- [14] S. Bruni, C. Cellamare, P. Di Lazzaro, A. Gessi, G. Marghella, L. Stante, Analysis of an archaeological linen cloth: The shroud of Arquata, *Radiat. Phys. Chem.* 167 (2020). <https://doi.org/10.1016/j.radphyschem.2019.03.052>.
- [15] H.G.M. Edwards, E. Ellis, D.W. Farwell, R.C. Janaway, Preliminary Study of the Application of Fourier Transform Raman Spectroscopy to the Analysis of Degraded Archaeological Linen Textiles, *J. Raman Spectrosc.* 27 (1996) 663–669. [https://doi.org/10.1002/\(SICI\)1097-4555\(199609\)27:9<663::AID-JRS11>3.0.CO;2-E](https://doi.org/10.1002/(SICI)1097-4555(199609)27:9<663::AID-JRS11>3.0.CO;2-E).
- [16] K. Kavkler, N. Gunde-Cimerman, P. Zalar, A. Demšar, FTIR spectroscopy of biodegraded historical textiles, *Polym. Degrad. Stab.* 96 (2011) 574–580. <https://doi.org/10.1016/j.polymdegradstab.2010.12.016>.
- [17] K. Kavkler, Ž. Šmit, D. Jezeršek, D. Eichert, A. Demšar, Investigation of biodeteriorated historical textiles by conventional and synchrotron radiation FTIR spectroscopy, *Polym. Degrad. Stab.* 96 (2011) 1081–1086. <https://doi.org/10.1016/j.polymdegradstab.2011.03.011>.
- [18] M. Müller, B. Murphy, M. Burghammer, C. Riek, M. Roberts, M. Papiz, D. Clarke, J. Gunneweg, E. Pantos, Identification of ancient textile fibres from Khirbet Qumran caves using synchrotron radiation microbeam diffraction, *Spectrochim. Acta B.* 59 (2004) 1669–1674. <https://doi.org/10.1016/j.sab.2004.07.018>.

- [19] L.K. Herrera, A. Justo, A. Duran, M.C.J. Haro, M.L. Franquelo, J.L. Perez Rodríguez, Identification of cellulose fibres belonging to Spanish cultural heritage using synchrotron high resolution X-ray diffraction, *Appl. Phys. A: Mater. Sci. Process.* 99 (2010) 391–398. <https://doi.org/10.1007/s00339-010-5626-z>.
- [20] A. Bourmaud, J. Beaugrand, D.U. Shah, V. Placet, C. Baley, Towards the design of high-performance plant fibre composites, *Prog. Mater. Sci.* 97 (2018) 347–408. <https://doi.org/10.1016/j.pmatsci.2018.05.005>.
- [21] C.C. Shaw, ed., *Cone Beam Computed Tomography*, CRC Press, Boca Raton, 2014. <https://doi.org/10.1201/b16465>.
- [22] A. Bourmaud, D. Siniscalco, L. Foucat, C. Goudenhooft, X. Falourd, B. Pontoire, O. Arnould, J. Beaugrand, C. Baley, Evolution of flax cell wall ultrastructure and mechanical properties during the retting step, *Carbohydr. Polym.* 206 (2019) 48–56. <https://doi.org/10.1016/j.carbpol.2018.10.065>.
- [23] R.H. Newman, Estimation of the lateral dimensions of cellulose crystallites using ¹³C NMR signal strengths, *Solid State Nucl. Magn. Reson.* 15 (1999) 21–29. [https://doi.org/10.1016/S0926-2040\(99\)00043-0](https://doi.org/10.1016/S0926-2040(99)00043-0).
- [24] J. André, *Nature du lin et horticulture*, in: Budé (Ed.), *Pline l’Ancien, Histoire Naturelle*, Les Belles, Paris, 1964.
- [25] C. Goudenhooft, A. Bourmaud, C. Baley, Varietal selection of flax over time: Evolution of plant architecture related to influence on the mechanical properties of fibers, *Ind. Crops Prod.* 97 (2017) 56–64. <https://doi.org/10.1016/j.indcrop.2016.11.062>.
- [26] C. Baley, A. Bourmaud, Average tensile properties of French elementary flax fibers, *Mater. Lett.* 122 (2014) 159–161. <https://doi.org/10.1016/j.matlet.2014.02.030>.
- [27] S.B. Chemiksova, N.V. Pavlencheva, O.P. Gur’yanov, T.A. Gorshkova, The effect of soil drought on the phloem fiber development in long-fiber flax, *Russ. J. Plant Physiol.* 53 (2006) 656–662. <https://doi.org/10.1134/S1021443706050098>.
- [28] A. Bourmaud, M. Gibaud, A. Lefeuvre, C. Morvan, C. Baley, Influence of the morphology characters of the stem on the lodging resistance of Marylin flax, *Ind. Crops Prod.* 66 (2015) 27–37. <https://doi.org/10.1016/j.indcrop.2014.11.047>.
- [29] A. Bourmaud, J. Beaugrand, D.U. Shah, V. Placet, C. Baley, Towards the design of high-performance plant fibre composites, *Prog. Mater. Sci.* 97 (2018) 347–408. <https://doi.org/10.1016/j.pmatsci.2018.05.005>.
- [30] C. Goudenhooft, A. Bourmaud, C. Baley, Study of plant gravitropic response: Exploring the influence of lodging and recovery on the mechanical performances of flax fibers, *Ind. Crops Prod.* 128 (2019) 235–238. <https://doi.org/10.1016/j.indcrop.2018.11.024>.
- [31] A. Hernandez-Estrada, H.-J. Gusovius, J. Müssig, M. Hughes, Assessing the susceptibility of hemp fibre to the formation of dislocations during processing, *Ind. Crops Prod.* 85 (2016) 382–388. <https://doi.org/10.1016/j.indcrop.2016.01.006>.
- [32] M. Hughes, Defects in natural fibres: their origin, characteristics and implications for natural fibre-reinforced composites, *J. Mater. Sci.* 47 (2012) 599–609. <https://doi.org/10.1007/s10853-011-6025-3>.
- [33] A. Le Duc, B. Vergnes, T. Budtova, Polypropylene/natural fibres composites: Analysis of fibre dimensions after compounding and observations of fibre rupture by rheo-optics, *Compos. Part A Appl. Sci. Manuf.* 42 (2011) 1727–1737. <https://doi.org/10.1016/j.compositesa.2011.07.027>.
- [34] J. Foulk, D. Akin, R. Dodd, Influence of pectinolytic enzymes on retting effectiveness and resultant fiber properties, *Bioresources.* 3 (2008) 155–169.
- [35] M. Eder, O. Arnould, J.W.C. Dunlop, J. Hornatowska, L. Salmén, Experimental micromechanical characterisation of wood cell walls, *Wood Sci. Technol.* 47 (2013) 163–182. <https://doi.org/10.1007/s00226-012-0515-6>.
- [36] A. Jäger, Th. Bader, K. Hofstetter, J. Eberhardsteiner, The relation between indentation modulus, microfibril angle, and elastic properties of wood cell walls, *Compos. Part A Appl. Sci. Manuf.* 42 (2011) 677–685. <https://doi.org/10.1016/j.compositesa.2011.02.007>.

- [37] M. Capron, M. Ramonda, F.F. Laurans, B. Clair, T. Alméras, O. Arnould, Mechanical characterization of developing tension wood fibre wall by atomic force microscopy, in: 8th Plant Biomechanics International Conference, Nagoya, Japan, 2015. <https://hal.archives-ouvertes.fr/hal-01436113> (accessed August 30, 2021).
- [38] T.K. Bader, K. de Borst, K. Fackler, T. Ters, S. Braovac, A nano to macroscale study on structure-mechanics relationships of archaeological oak, *J. Cult. Herit.* 14 (2013) 377–388. <https://doi.org/10.1016/j.culher.2012.09.007>.
- [39] D. Stewart, Fourier Transform Infrared Microspectroscopy of Plant Tissues, *Appl. Spectrosc.* 50 (1996) 357–365. <https://doi.org/10.1366/0003702963906384>.
- [40] P. Garside, P. Wyeth, Identification of Cellulosic Fibres by FTIR Spectroscopy - Thread and Single Fibre Analysis by Attenuated Total Reflectance, *Stud. Conserv.* 48 (2003) 269–275. <https://doi.org/10.1179/sic.2003.48.4.269>.
- [41] J. Astruc, M. Nagalakshmaiah, G. Laroche, M. Grandbois, S. Elkoun, M. Robert, Isolation of cellulose-II nanospheres from flax stems and their physical and morphological properties, *Carbohydr. Polym.* 178 (2017) 352–359. <https://doi.org/10.1016/j.carbpol.2017.08.138>.
- [42] H. Zhang, R. Ming, G. Yang, Y. Li, Q. Li, H. Shao, Influence of alkali treatment on flax fiber for use as reinforcements in polylactide stereocomplex composites, *Polym. Eng. Sci.* 55 (2015) 2553–2558. <https://doi.org/10.1002/pen.24147>.
- [43] B.D. Lazić, B.M. Pejić, A.D. Kramar, M.M. Vukčević, K.R. Mihajlovski, J.D. Rusmirović, M.M. Kostić, Influence of hemicelluloses and lignin content on structure and sorption properties of flax fibers (*Linum usitatissimum* L.), *Cellulose.* 25 (2018) 697–709. <https://doi.org/10.1007/s10570-017-1575-4>.
- [44] C. Margariti, The application of FTIR microspectroscopy in a non-invasive and non-destructive way to the study and conservation of mineralised excavated textiles, *Herit. Sci.* 7 (2019) 63. <https://doi.org/10.1186/s40494-019-0304-8>.
- [45] B.D. Lazić, B.M. Pejić, A.D. Kramar, M.M. Vukčević, K.R. Mihajlovski, J.D. Rusmirović, M.M. Kostić, Influence of hemicelluloses and lignin content on structure and sorption properties of flax fibers (*Linum usitatissimum* L.), *Cellulose.* 25 (2018) 697–709. <https://doi.org/10.1007/s10570-017-1575-4>.
- [46] C. Margariti, The application of FTIR microspectroscopy in a non-invasive and non-destructive way to the study and conservation of mineralised excavated textiles, *Herit. Sci.* 7 (2019) 63. <https://doi.org/10.1186/s40494-019-0304-8>.
- [47] V. Titok, V. Leontiev, S. Yurenkova, T. Nikitinskaya, T. Barannikova, L. Khotyleva, Infrared Spectroscopy of Fiber Flax, *J. Nat. Fibers.* 7 (2010) 61–69. <https://doi.org/10.1080/15440470903579275>.
- [48] M. Fan, D. Dai, B. Huang, Fourier Transform Infrared Spectroscopy for Natural Fibres, in: S. Salih (Ed.), *Fourier Transform - Materials Analysis*, InTech, 2012: pp.45-67. <https://doi.org/10.5772/35482>.
- [49] C. Reynaud, M. Thoury, A. Dazzi, G. Latour, M. Scheel, J. Li, A. Thomas, C. Moulhéat, A. Didier, L. Bertrand, In-place molecular preservation of cellulose in 5,000-year-old archaeological textiles, *PNAS.* 117 (2020) 19670–19676. <https://doi.org/10.1073/pnas.2004139117>.
- [50] A. Céline, S. Fréour, F. Jacquemin, P. Casari, Characterization and modeling of the moisture diffusion behaviour of natural fibres, *J. Appl. Polym. Sci.* 130 (2013) 297–306. <https://doi.org/10.1002/app.39148>.
- [51] K. Kavkler, A. Demsar, Application of FTIR and Raman Spectroscopy to Qualitative Analysis of Structural Changes in Cellulosic Fibres, *Tekstilec.* 55 (2012) 19–31.
- [52] S.Y. Oh, D.I. Yoo, Y. Shin, G. Seo, FTIR analysis of cellulose treated with sodium hydroxide and carbon dioxide, *Carbohydr. Res.* 340 (2005) 417–428. <https://doi.org/10.1016/j.carres.2004.11.027>.
- [53] M. Cintrón, D. Hinchliffe, FT-IR Examination of the Development of Secondary Cell Wall in Cotton Fibers, *Fibers.* 3 (2015) 30–40. <https://doi.org/10.3390/fib3010030>.
- [54] C. Cennini, Di Cennino Cennini Trattato della pittura messo in luce la prima volta con annotazioni dal cavaliere Giuseppe Tambroni, Company' torchi di Paolo Salviucci, Rome, 1821.
- [55] C. Giannini, Dizionario del restauro. Tecniche, diagnostica, conservazione, Nardini, Firenze, 2010, p.125.
- [56] S. Marconi, Preparazioni e Imprimiture dei dipinti su tavola e tela: materiali, metodi e storia, in: C. Maltese (Ed.), *Preparazione e finitura delle opere pittoriche-materiali e metodi : preparazioni e imprimiture, leganti, vernici, cornici*, Mursia, Milan, 1993: pp. 11–38.

- [57] A.M. Seves, Aggressione microbica alle colle da rifodero, in: G.C. Scicolone (Ed.), *Dipinti su Tela: metodologie d'indagine per i supporti cellulosici*, 2nd edition, Nardini Editore, Firenze, 2005: pp. 41–44.
- [58] S. Hackney, G. Hedley, Measurements of the Ageing of Linen Canvas, *Stud. Conserv.* 26 (1981) 1–14. <https://doi.org/10.2307/1505816>.
- [59] C.R.T. Young, R.D. Hibberd, Biaxial Tensile Testing of Paintings on Canvas, *Stud. Conserv.* 44 (1999) 129–141.
- [60] C.R.T. Young, R.D. Hibberd, The role of canvas attachments in the strain distribution and degradation of easel paintings, *Stud. Conserv.* 45 (2000) 212–220. <https://doi.org/10.1179/sic.2000.45.Supplement-1.212>.
- [61] P. Castellini, E. Esposito, B. Marchetti, N. Paone, E.P. Tomasini, New applications of scanning laser Doppler vibrometry (SLDV) to nondestructive diagnosis of artwork: mosaics, ceramics, inlaid wood, and easel painting, in: R. Salimbeni (Ed.), *Lasers in Metrology and Art Conservation*, Munich, Germany, 2001: p. 162. <https://doi.org/10.1117/12.445659>.
- [62] E. Rossi, Misure del grado di polimerizzazione per la valutazione dello stato di deterioramento di un materiale fibroso cellulosico, in: G.C. Scicolone (Ed.), *Dipinti su Tela: metodologie d'indagine per i supporti cellulosici*, 2nd edition, Nardini Editore, Firenze, 2005: pp. 25–30.
- [63] R.H. Newman, L.M. Davies, P.J. Harris, Solid-State ¹³C Nuclear Magnetic Resonance Characterization of Cellulose in the Cell Walls of *Arabidopsis thaliana* Leaves, *Plant. Physiol.* 111 (1996) 475–485. <https://doi.org/10.1104/pp.111.2.475>.
- [64] P.T. Larsson, K. Wickholm, T. Iversen, A CP/MAS ¹³C NMR investigation of molecular ordering in celluloses, *Carbohydr. Res.* 302 (1997) 19–25.
- [65] K. Kavkler, A. Demšar, Examination of cellulose textile fibres in historical objects by micro-Raman spectroscopy, *Spectrochim. Acta A Mol. Biomol. Spectrosc.* 78 (2011) 740–746. <https://doi.org/10.1016/j.saa.2010.12.006>.
- [66] T. Cerchiara, G. Chidichimo, M.C. Gallucci, R. Ferraro, D. Vuono, A. Nastro, Use of Spanish broom (*Spartium junceum* L.) canvas as a painting support: Evaluation of the effects of environmental conditions, *J. Cult. Herit.* 10 (2009) 396–402. <https://doi.org/10.1016/j.culher.2008.12.002>.
- [67] O. Arnould, D. Siniscalco, A. Bourmaud, A. Le Duigou, C. Baley, Better insight into the nano-mechanical properties of flax fibre cell walls, *Ind. Crops Prod.* 97 (2017) 224–228. <https://doi.org/10.1016/j.indcrop.2016.12.020>.
- [68] N.H. Faisal, R. Ahmed, S. Goel, G. Cross, Future of nanoindentation in archaeometry, *J. Mater. Res.* 33 (2018) 2515–2532. <https://doi.org/10.1557/jmr.2018.280>.
- [69] L. Han, X. Tian, T. Keplinger, H. Zhou, R. Li, K. Svedström, I. Burgert, Y. Yin, J. Guo, Even Visually Intact Cell Walls in Waterlogged Archaeological Wood Are Chemically Deteriorated and Mechanically Fragile: A Case of a 170 Year-Old Shipwreck, *Molecules.* 25 (2020) 1113. <https://doi.org/10.3390/molecules25051113>.
- [70] ASTM C1557-20, ASTM International, West Conshohocken, PA, 2020. <https://doi.org/10.1520/C1557-20>.
- [71] G. Metz, X.L. Wu, S.O. Smith, Ramped-Amplitude Cross Polarization in Magic-Angle-Spinning NMR, *J. Mater. Res.* 110 (1994) 219–227. <https://doi.org/10.1006/jmra.1994.1208>.
- [72] D. Massiot, F. Fayon, M. Capron, I. King, S.L. Calvé, B. Alonso, J.-O. Durand, B. Bujoli, Z. Gan, G. Hoatson, Modelling one- and two-dimensional solid-state NMR spectra, *Magn. Reson. Chem.* 40 (2002) 70–76. <https://doi.org/10.1002/mrc.984>.
- [73] L. Hammarlund, Handicraft Knowledge Applied to Archaeological Textiles, *Nord. Text. J.* (2005) 87–119.
- [74] L. Fuster-López, C. Andersen, N. Bouillon, F. Fabien, M. Rossi-Doria, M. Scharff, K. Seymour, A. Vicente-Escuder, S. Vicente-Palomino, D. Yusà-Marco, Glue-paste linings: An evaluation of some biological, chemical and mechanical aspects of a traditional technique, in: *ICOM-CC 18th Triennial Conference Preprints*, Copenhagen, 2017.
- [75] G. Vogeslang-Eastwood, Textiles, in: P.T. Nicholson, I. Shaw (Eds.), *Ancient Egyptian Materials and Technology*, Cambridge University Press, 2000: pp. 268–297.

- [76] R.M. Kozłowski, M. Mackiewicz-Talarczyk, K. Wielgusz, M. Praczyk, A.M. Allam, Bast fibres: flax, in: R.M. Kozłowski, M. Mackiewicz-Talarczyk (Eds.), *Handbook of Natural Fibres*, Woodhead Publishing, 2020: pp. 93–162. <https://doi.org/10.1016/B978-0-12-818398-4.00006-2>.
- [77] E. Martuscelli, Degradazione delle fibre naturali e dei tessuti antichi : aspetti chimici, molecolari, strutturali e fenomenologici, Paideia, 2006: pp. 85-91.
- [78] M. Aslan, G. Chinga-Carrasco, B.F. Sørensen, B. Madsen, Strength variability of single flax fibres, *J. Mater. Sci.* 46 (2011) 6344–6354. <https://doi.org/10.1007/s10853-011-5581-x>.
- [79] L.G. Thygesen, Quantification of dislocations in hemp fibers using acid hydrolysis and fiber segment length distributions, *J. Mater. Sci.* 43 (2008) 1311–1317. <https://doi.org/10.1007/s10853-007-2284-4>.
- [80] L.G. Thygesen, B.J. Hidayat, K.S. Johansen, C. Felby, Role of supramolecular cellulose structures in enzymatic hydrolysis of plant cell walls, *J. Ind. Microbiol. Biotechnol.* 38 (2011) 975–983. <https://doi.org/10.1007/s10295-010-0870-y>.
- [81] A.P. Singh, Y.S. Kim, T. Singh, Bacterial Degradation of Wood, in: Y.S. Kim, R. Funada, A.P. Singh (Eds.) *Secondary Xylem Biology*, Academic Press, 2016: pp. 169–190.
- [82] P. Ackroyd, The structural conservation of canvas paintings: changes in attitude and practice since the early 1970s, *Stud. Conserv.* 47 (2002) 3–14. <https://doi.org/10.1179/sic.2002.47.Supplement-1.3>.
- [83] K. Swerda, Painting conservation ideas, ethics, materials, and techniques in Nineteenth-century America, in: *AIC Paintings Specialty Group Postprints*, Arlington, Virginia, 2003: p. 40.
- [84] J. Coddington, C. Young, Structure and Lining: A Review, *AIC News*. 43 (2018).
- [85] C. Goudenhooft, D. Siniscalco, O. Arnould, A. Bourmaud, O. Sire, T. Gorshkova, C. Baley, Investigation of the Mechanical Properties of Flax Cell Walls during Plant Development: The Relation between Performance and Cell Wall Structure, *Fibers*. 6 (2018) 6. <https://doi.org/10.3390/fib6010006>.
- [86] C. Baley, M. Gomina, J. Breard, A. Bourmaud, P. Davies, Variability of mechanical properties of flax fibres for composite reinforcement. A review, *Ind. Crops Prod.* 145 (2020) 111984. <https://doi.org/10.1016/j.indcrop.2019.111984>.
- [87] V. Librando, Z. Minniti, S. Lorusso, Ancient and modern paper characterization by FTIR and Micro-Raman spectroscopy, *Conserv. Sci. Cult.* 11 (2011) 249–268. <https://doi.org/10.6092/issn.1973-9494/2700>.
- [88] M. Zotti, A. Ferroni, P. Calvini, Microfungal biodeterioration of historic paper: Preliminary FTIR and microbiological analyses, *Int. Biodeterior. Biodegradation*. 62 (2008) 186–194. <https://doi.org/10.1016/j.ibiod.2008.01.005>.
- [89] K. Arshad, M. Skrifvars, V. Vivod, J. Volmajer Valh, B. Vončina, Biodegradation of Natural Textile Materials in Soil, *TEK*. 57 (2014) 118–132. <https://doi.org/10.14502/Tekstilec2014.57.118-132>.
- [90] M.L. Nelson, R.T. O'Connor, Relation of certain infrared bands to cellulose crystallinity and crystal lattice type. Part II. A new infrared ratio for estimation of crystallinity in celluloses I and II, *J. Appl. Polym. Sci.* 8 (1964) 1325–1341. <https://doi.org/10.1002/app.1964.070080323>.
- [91] B.H. Stuart, P.S. Thomas, M. Barrett, K. Head, Modelling clay materials used in artworks: an infrared spectroscopic investigation, *Herit. Sci.* 7 (2019) 86. <https://doi.org/10.1186/s40494-019-0333-3>.
- [92] M. Ueland, J.M. Howes, S.L. Forbes, B.H. Stuart, Degradation patterns of natural and synthetic textiles on a soil surface during summer and winter seasons studied using ATR-FTIR spectroscopy, *Spectrochim. Acta A Mol. Biomol. Spectrosc.* 185 (2017) 69–76. <https://doi.org/10.1016/j.saa.2017.05.044>.
- [93] L. Pronti, M. Perino, M. Cursi, M.L. Santarelli, A.C. Felici, M.P. Bracciale, Characterization and Digital Restauration of XIV-XV Centuries Written Parchments by Means of Nondestructive Techniques: Three Case Studies, *J. Spectrosc.* 2018 (2018) 1–14. <https://doi.org/10.1155/2018/2081548>.
- [94] M. Zimniewska, W. Rozańska, A. Gryszczynska, B. Romanowska, A. Kicinska-Jakubowska, Antioxidant Potential of Hemp and Flax Fibers Depending on Their Chemical Composition, *Molecules*. 23 (2018) 1993. <https://doi.org/10.3390/molecules23081993>.
- [95] M.C. Seghini, F. Touchard, F. Sarasini, L. Chocinski-Arnault, J. Tirillò, M.P. Bracciale, M. Zvonek, V. Cech, Effects of oxygen and tetravinylsilane plasma treatments on mechanical and interfacial properties of flax yarns in thermoset matrix composites, *Cellulose*. 27 (2020) 511–530. <https://doi.org/10.1007/s10570-019-02785-3>.

- [96] L. Hajji, A. Boukir, J. Assouik, A. Kerbal, M. Kajjout, P. Doumenq, M.L. De Carvalho, A Multi-Analytical Approach for the Evaluation of the Efficiency of the Conservation–Restoration Treatment of Moroccan Historical Manuscripts Dating to the 16th, 17th, and 18th Centuries, *Appl. Spectrosc.* 69 (2015) 920–938. <https://doi.org/10.1366/14-07688>.
- [97] C. Sendrea, C. Carsote, E. Badea, A. Adams, M. Niculescu, H. Iovu, Non-invasive characterisation of collagen-based materials by NMR-mouse and ATR-FTIR, *UPB Sci. Bull. B Chem. Mater. Sci.* 78 (2016) 27–38.
- [98] H. Mohapatra, R. Malik, Effect of Microorganism on Flax and Linen, *J. Textile. Sci. Eng.* 06 (2015). <https://doi.org/10.4172/2165-8064.1000229>.
- [99] B. Zghari, L. Hajji, A. Boukir, Effect of Moist and Dry Heat Weathering Conditions on Cellulose Degradation of Historical Manuscripts exposed to Accelerated Ageing: ¹³C NMR and FTIR Spectroscopy as a non-Invasive Monitoring Approach, *J. Mater. Environ. Sci.* 9 (2018) 641–654. <https://doi.org/10.26872/jmes.2018.9.2.71>.
- [100] F. Kimura, J. Umemura, T. Takenaka, FTIR-ATR studies on Langmuir-Blodgett films of stearic acid with 1-9 monolayers, *Langmuir.* 2 (1986) 96–101. <https://doi.org/10.1021/la00067a017>.
- [101] D. Pellegrini, C. Duce, I. Bonaduce, S. Biagi, L. Ghezzi, M.P. Colombini, M.R. Tinè, E. Bramanti, Fourier transform infrared spectroscopic study of rabbit glue/inorganic pigments mixtures in fresh and aged reference paint reconstructions, *Microchemical Journal.* 124 (2016) 31–35. <https://doi.org/10.1016/j.microc.2015.07.018>.
- [102] R.H. Atalla, D.L. VanderHart, Native Cellulose: A Composite of Two Distinct Crystalline Forms, *Science.* 223 (1984) 283–285. <https://doi.org/10.1126/science.223.4633.283>.
- [103] B. Focher, M.T. Palma, M. Canetti, G. Torri, C. Cosentino, G. Gastaldi, Structural differences between non-wood plant celluloses: evidence from solid state NMR, vibrational spectroscopy and X-ray diffractometry, *Ind. Crops Prod.* 13 (2001) 193–208. [https://doi.org/10.1016/S0926-6690\(00\)00077-7](https://doi.org/10.1016/S0926-6690(00)00077-7).
- [104] N. Ibragimova, N. Mokshina, M. Ageeva, O. Gurjanov, P. Mikshina, Rearrangement of the Cellulose-Enriched Cell Wall in Flax Phloem Fibers over the Course of the Gravitropic Reaction, *International Journal of Molecular Sciences.* 21 (2020) 5322. <https://doi.org/10.3390/ijms21155322>.
- [105] R.H. Atalla, D.L. Vanderhart, The role of solid state ¹³C NMR spectroscopy in studies of the nature of native celluloses, *Solid State Nucl Magn Reson.* 15 (1999) 1–19. [https://doi.org/10.1016/s0926-2040\(99\)00042-9](https://doi.org/10.1016/s0926-2040(99)00042-9).
- [106] N.E. Kotelnikova, E.F. Panarin, R. Serimaa, T. Paakkari, T.E. Sukhanova, A.V. Gribanov, Study of flax fibre structure by WAXS, IR and ¹³C NMR spectroscopy, and SEM, in: Kotelnikova N. E. (Ed.), *Cellulosic Pulps, Fibres and Materials*, Elsevier, 2000: pp. 169–179. <https://doi.org/10.1533/9781845698546.169>.
- [107] D. Pantaloni, D. Shah, C. Baley, A. Bourmaud, Monitoring of mechanical performances of flax non-woven biocomposites during a home compost degradation, *Polym. Degrad. Stab.* 177 (2020) 109166. <https://doi.org/10.1016/j.polymdegradstab.2020.109166>.
- [108] Y.-X. Weng, L. Wang, M. Zhang, X.-L. Wang, Y.-Z. Wang, Biodegradation behavior of P(3HB,4HB)/PLA blends in real soil environments, *Polym. Test.* 32 (2013) 60–70. <https://doi.org/10.1016/j.polymertesting.2012.09.014>.
- [109] H.-S. Kim, H.-J. Kim, J. Lee, I. Choi, Biodegradability of bio-flour filled biodegradable poly(butylene succinate) bio-composites in natural and compost soil, *Polym. Degrad. Stab.* 91 (2006) 1117–1127. <https://doi.org/10.1016/J.POLYMDEGRADSTAB.2005.07.002>.
- [110] T. Bayerl, M. Geith, A.A. Somashekar, D. Bhattacharyya, Influence of fibre architecture on the biodegradability of FLAX/PLA composites, *Int. Biodeterior. Biodegradation.* 96 (2014) 18–25. <https://doi.org/10.1016/j.ibiod.2014.08.005>.
- [111] S. Alimuzzaman, R.H. Gong, M. Akonda, Biodegradability of nonwoven flax fiber reinforced polylactic acid biocomposites, *Polym. Compos.* 35 (2014) 2094–2102. <https://doi.org/10.1002/pc.22871>.
- [112] O. Arnould, D. Siniscalco, A. Bourmaud, A. Le Duigou, C. Baley, Better insight into the nano-mechanical properties of flax fibre cell walls, *Ind. Crops. Prod.* 97 (2017) 224–228. <https://doi.org/10.1016/j.indcrop.2016.12.020>.
- [113] K.L. Johnson, J.A. Greenwood, An Adhesion Map for the Contact of Elastic Spheres, *J. Colloid Interface Sci.* 192 (1997) 326–333. <https://doi.org/10.1006/jcis.1997.4984>.

- [114] O. Arnould, R. Arinero, Towards a better understanding of wood cell wall characterisation with contact resonance atomic force microscopy, *Compos. Part A Appl. Sci. Manuf.* 74 (2015) 69–76. <https://doi.org/10.1016/j.compositesa.2015.03.026>.
- [115] G. Caneva, M.P. Nugari, O. Salvadori, *La biologia vegetale per i beni culturali: biodeterioramento e conservazione*, 2nd ed., Nardini, 2007.
- [116] I. Grizzi, H. Garreau, S. Li, M. Vert, Hydrolytic degradation of devices based on poly(dl-lactic acid) size-dependence, *Biomaterials*. 16 (1995) 305–311. [https://doi.org/10.1016/0142-9612\(95\)93258-F](https://doi.org/10.1016/0142-9612(95)93258-F).
- [117] R.A. Blanchette, A review of microbial deterioration found in archaeological wood from different environments, *International Biodeterioration. International Biodeterioration&Biodegradation* (2000) 189–204.
- [118] Y.S. Kim, A.P. Singh, Micromorphological characteristics of wood biodegradation in wet environments: a review, *IAWA J.* 21 (2000) 135–155. <https://doi.org/10.1163/22941932-90000241>.
- [119] A.P. Singh, M.E. Hedley, D.R. Page, C.S. Han, Microbial degradation of CCA-treated cooling tower timbers, *IAWA J.* 13 (1992) 215–231.
- [120] C. Björdal, T. Nilsson, S. Bardage, Three-dimensional visualisation of bacterial decay in individual tracheids of *Pinus sylvestris*, *Holzforschung*. 59 (2005) 178–182. <https://doi.org/10.1515/HF.2005.028>.
- [121] R.A. Blanchette, A review of microbial deterioration found in archaeological wood from different environments, *Int. Biodeterior. Biodegradation*. 46 (2000) 189–204. [https://doi.org/10.1016/S0964-8305\(00\)00077-9](https://doi.org/10.1016/S0964-8305(00)00077-9).
- [122] S.N. Basu, R. Ghose, Structural Changes Brought About in the Jute Fiber by Micro-Organisms and their Enzymes, *Text. Res. J.* 32 (1962) 932–942. <https://doi.org/10.1177/004051756203201109>.
- [123] T. Gorshkova, P. Mikshina, A. Petrova, T. Chernova, N. Mokshina, O. Gorshkov, Plants at Bodybuilding: Development of Plant “Muscles”, in: A. Geitmann, J. Gril (Eds.), *Plant Biomechanics: From Structure to Function at Multiple Scales*, Springer, Cham, 2018: pp. 141–163. https://doi.org/10.1007/978-3-319-79099-2_7.
- [124] T. Gorshkova, N. Brutch, B. Chabbert, M. Deyholos, T. Hayashi, S. Lev-Yadun, E.J. Mellerowicz, C. Morvan, G. Neutelings, G. Pilate, Plant Fiber Formation: State of the Art, Recent and Expected Progress, and Open Questions, *Crit. Rev. Plant. Sci.* 31 (2012) 201–228. <https://doi.org/10.1080/07352689.2011.616096>.
- [125] H. Xu, X. Yang, L. Xie, M. Hakkarainen, Conformational Footprint in Hydrolysis-Induced Nanofibrillation and Crystallization of Poly(lactic acid), *Biomacromolecules*. 17 (2016). <https://doi.org/10.1021/acs.biomac.5b01636>.
- [126] A. Narladkar, E. Balnois, Y. Grohens, An AFM Study of Poly(L-lactic acid) and Poly(D-lactic acid) Macromolecules and Their Stereocomplexes at the Solid-Air Interface, *Macromol. Symp.* 241 (2006) 34–44. <https://doi.org/10.1002/masy.200650906>.
- [127] R. Pantani, A. Sorrentino, Influence of crystallinity on the biodegradation rate of injection-moulded poly(lactic acid) samples in controlled composting conditions, *Polym. Degrad. Stab.* 98 (2013) 1089–1096. <https://doi.org/10.1016/j.polymdegradstab.2013.01.005>.
- [128] L. Soccalingame, Étude des scénarios de fin de vie des biocomposites : vieillissement et retransformation de biocomposites PP/farine de bois et PLA/fibres de lin, *Matériaux*, Université Montpellier II-Sciences et Techniques du Languedoc, 2014.
- [129] M. Ahmad Sawpan, M.R. Islam, M.D.H. Beg, K. Pickering, Effect of Accelerated Weathering on Physico-Mechanical Properties of Polylactide Bio-Composites, *J. Polym. Environ.* 27 (2019) 942–955. <https://doi.org/10.1007/s10924-019-01405-2>.
- [130] R.J. Müller, Biodegradability of polymers: regulations and methods for testing, in: A. Steinbüchel (Ed.), *Biopolymers*, Wiley-VCH, Weinheim, 2005: pp. 365–374. <https://doi.org/10.1002/3527600035>.
- [131] X. Qi, Y. Ren, X. Wang, New advances in the biodegradation of Poly(lactic) acid, *Int. Biodeterior. Biodegradation*. 117 (2017) 215–223. <https://doi.org/10.1016/j.ibiod.2017.01.010>.
- [132] B. Laycock, M. Nikolić, J.M. Colwell, E. Gauthier, P. Halley, S. Bottle, G. George, Lifetime prediction of biodegradable polymers, *Prog. Polym. Sci.* 71 (2017) 144–189. <https://doi.org/10.1016/j.progpolymsci.2017.02.004>.

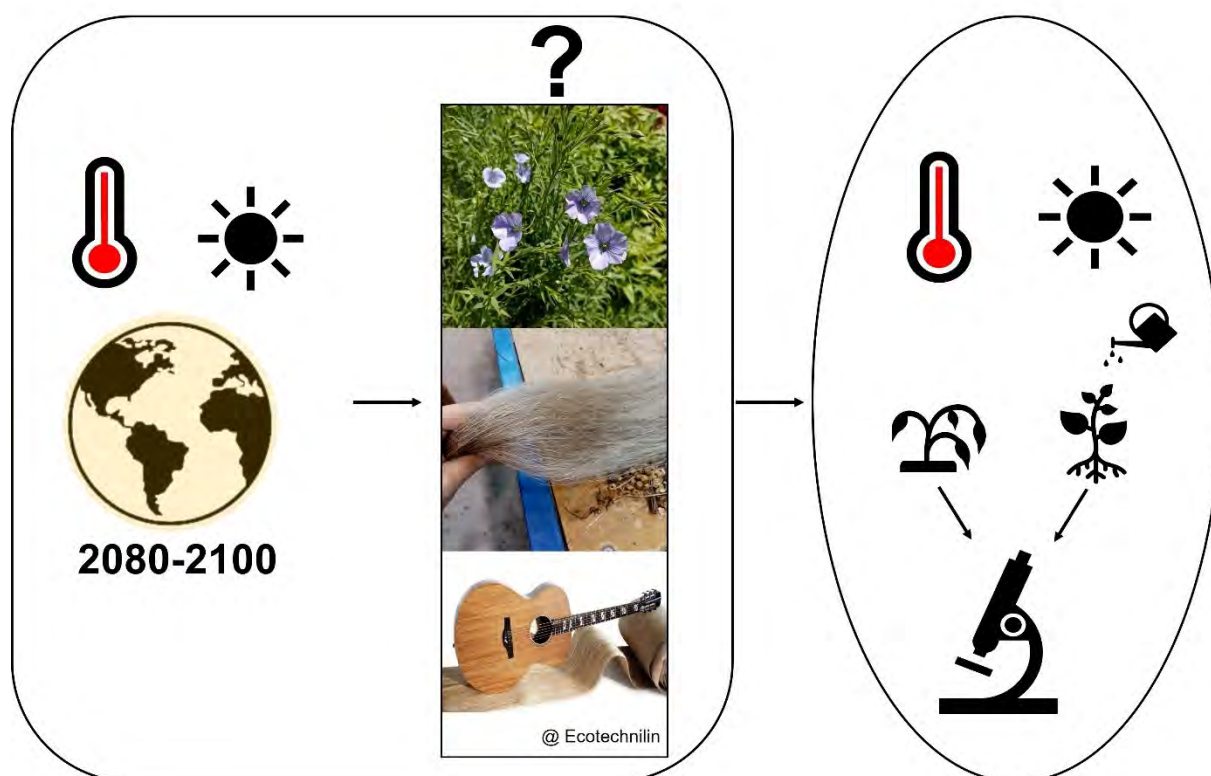
- [133] N. Butbunchu, W. Pathom-Aree, Actinobacteria as Promising Candidate for Polylactic Acid Type Bioplastic Degradation, *Front. Microbiol.* 10 (2019). <https://doi.org/10.3389/fmicb.2019.02834>.
- [134] T. Suyama, Y. Tokiwa, P. Ouichanpagdee, T. Kanagawa, Y. Kamagata, Phylogenetic Affiliation of Soil Bacteria That Degrade Aliphatic Polyesters Available Commercially as Biodegradable Plastics, *Appl. Environ. Microbiol.* 64 (1998) 5008–5011. <https://doi.org/10.1128/AEM.64.12.5008-5011.1998>.
- [135] Z. Saadi, A. Rasmont, G. Cesar, H. Bewa, L. Benguigui, Fungal Degradation of Poly(l-lactide) in Soil and in Compost, *J. Polym. Environ.* 20 (2012) 273–282. <https://doi.org/10.1007/s10924-011-0399-9>.
- [136] J. Repeškienė, A. Lugauskas, Z. Jankauskiene, Diversity of fungal species on laid and stand-retted flax, *Bot. Lith.* 13 (2007) 51–59.
- [137] C. Djemiel, E. Goulas, N. Badalato, B. Chabbert, S. Hawkins, S. Grec, Targeted Metagenomics of Retting in Flax: The Beginning of the Quest to Harness the Secret Powers of the Microbiota, *Front. Genet.* 11 (2020). <https://doi.org/10.3389/fgene.2020.581664>.



CHAPTER V. The effect of the drought stress on flax plants and fibres extracted



Graphical Abstract



A. Melelli, S. Durand, C. Alvarado, A. Kervoëlen, L. Foucat, M. Grégoire, O. Arnould, X. Falourd, F. Callebert, P. Ouagne, A. Geairon, S. Daniel, F. Jamme, A. Bourmaud, J. Beaugrand, Anticipating global warming effects: a comprehensive study of drought impact on both flax plants and fibres, *Ind. Crops Prod.* (under review)

1. Introduction

In the last 20 years, the production of textile flax fibres and tows has increased considerably, and in 2019, the Food and Agriculture Organisation of the United Nations (FAOSTAT, www.fao.org) estimated the total world production to be up to 1,000 k tons, led by France with 85% of the world textile flax fibre production [1,2]. The renewed interest in flax and other plant fibres used in areas other than textile applications, such as design and engineering, is due in part to global warming and the low environmental impact of flax fibre production, especially compared to synthetic fibres [3].

Climate change is strongly linked to greenhouse gas emissions, especially CO₂, and other types of factors, such as eutrophication, generated during the whole material lifecycle, from the production of raw materials to the end of life of the final product. Many industries and companies are focusing their efforts on reducing their footprint and adapting to new standards of the European Union but also maintaining the quality and competitive pricing of their products. For this reason, current research is focused on life cycle analysis that compares natural and synthetic materials as well as takes into account the intrinsic properties that are suitable for their use, as in the case of biocomposites reinforced with flax fibres [4–6].

However, as the production demand for plant fibres continues to grow with the goal of replacing synthetic fibres wherever possible, during the coming years, agriculture will have to increasingly contend with the effects of climate change. The reduced rainfall and the increment in temperatures implies the risk of abiotic stress such as drought, as well as various biotic stresses, for example, the emergence of new diseases and pests [7]. Moreover, this same document also reports that the risks of heavy rainfall events and flooding, which contribute to crop damage, are increasing. Thus, to meet market demand, not only for flax but also for agricultural production more generally, farmers might be forced to use more irrigation or even phytochemical products to increase crop production, which may, at the same time, contribute to the drivers of climate change (**Figure V-1**).

Focusing on France, textile flax crops are mainly located in Normandy and northern France (**Figure V-2a**). The rapid increase in flax technical fibres and production during the last two years is reported in **Figure V-2b**. It is worth noting that during 2001 and, particularly 2011, production recorded a violent decrease, and these years coincided with severe periods of drought [8,9]. Consequently, total world production was affected. Several models in the literature show the possible impact of climate change in European countries. Habets and Viennot reported a scenario with an increase in temperatures between 0.6 °C and 1.3 °C in 2021–2050 and a general decrease in rainfall in the entire country of approximately 6%, as illustrated in **Figure V-2c** with a schematic readaptation of their maps [10].

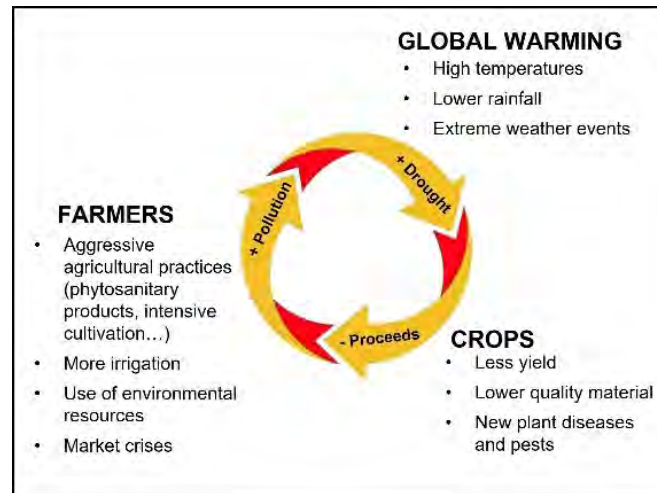


Figure V-1 Synthetic representation of interactions between climate change, agricultural markets and crop management.

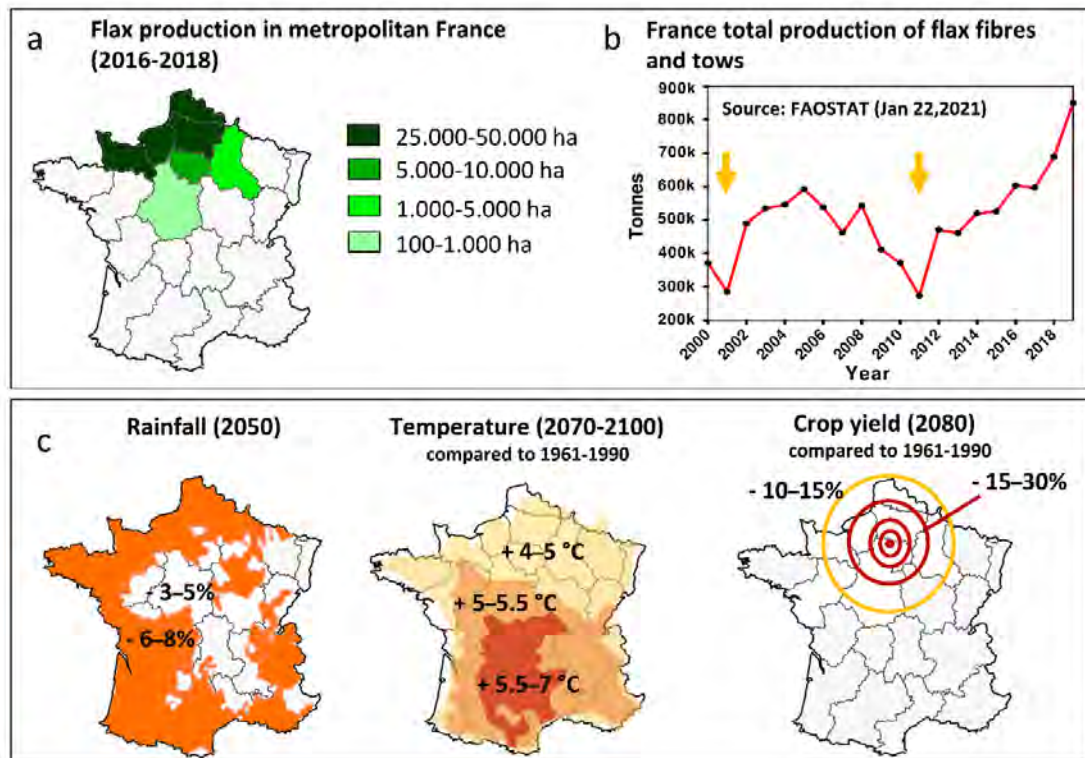


Figure V-2 a) Map of flax production in France, adapted from FrD and IAR [11], **b)** Production in France of tow and fibres between 2000–2019, data and graphic elaborated from FAOSTAT [12]. ; the yellow arrows indicate the drought that occurred in 2001 and 2011; **c)** Models of rainfall, temperature and crop yield readapted from [10] and [13]. Temperature and crop yield maps are simulations of changes compared to the years 1961-1990. Maps inspired from "PRUDENCE" and "PESTEA" EU projects [13].

The European Commission has also published an official document in which several models are proposed to forecast the years 2070 to 2100 [13]. In the worst-case scenario, if no actions are taken,

northern France could be subjected to a temperature increase of approximately 4–5 °C compared to the years 1961-1990. Moreover, in two different simulations, HadCM3/HIRHAM and ECHAM4/RCA3, compared with 1961-1990, northern France appears particularly impacted in terms of crop yield, with the highest loss of approximately 15%–30% due to drought and water deficiency [13]. **Figure V-2c** shows a schematic synthesis elaborated from the temperature and crop yield maps that can be found in the official document by Kelemen et al. (2009). All these data suggest that, in the future, flax fibre production could be particularly impacted since the cultivations are rather limited to a small area (northwestern France) that would be particularly subjected to the impact of climate change due to global warming. Thus, composite materials reinforced with plant fibres, especially flax, which appears to be a good alternative to other synthetic fibres, would no longer be sustainable in terms of CO₂ emissions, water irrigation and crop cultivation.

The effect of water deficit on plants has already been studied for several fibre plant species, such as ramie, flax or hemp. At the crop level, the consequences of particularly hot and dry years were observed with a decrease in the yield and quality of the product, as in the case of linseed oil [14]. For other species, such as hemp, drought leads to the formation of morphologically thinner and heterogeneous cell walls, probably caused by a delay in their maturity and thickening process [15].

In the case of flax, it has been observed that moderate soil drought affects plants that produce a low number of ramifications, with a reduction in the number of leaves and a decrease in stem length [16–18] and roots [19]. In the case of severe drought, cessation of metabolic processes was observed [16]. At the cell scale, flax fibres extracted from drought-stressed plants were found to be shorter than those extracted from plants grown in nonstressed conditions. Moreover, a modification of the polysaccharides was observed with a decrease in the galactose/rhamnose ratio (monosaccharides), a change in the number and length of rhamnogalacturonan-I chains and, consequently, an increase in the disorder of the cellulose microfibril network [16].

However, flax is a plant that can grow and survive in different environments, and its adaptability allows its cultivation from Russia to the Mediterranean regions [20]. The origin of this plant is ancient; it was cultivated for millennia in Mesopotamia, Syria and Egypt [21,22]. Nevertheless, these regions are particularly dry and hot, much more than the climate we find in northern France. Since flax needs approximately 400 mm of rainfall in 120 days of growth [23], depending on the water-holding capacity of the soil, and since drought or temperatures higher than 35 °C during and after flowering reduce the yield and quality of both fibres and linseed oil, certain practices were used in ancient times to compensate for the lack of water. For instance, in the ancient Near East, flax was sown in irrigated soils [21]. In the case of ancient Mesopotamia, the culture of flax was limited to very small lots rich in water and clays [21], and in ancient Egypt, flax cultivation started in November following the Nile floods [24].

At the economic level, the effect of global warming on the yield or quality of technical fibre is a growing issue. Hence, industries that cultivate and produce flax and semiproductions and industries that

employ biocomposites are demanding an increasing number of scientific studies able to predict the impact of global warming on their production.

In this context, the present work aims to investigate the consequences of drought on flax plants and the impact on the mechanical properties of elementary flax fibres for industrial batches of the same variety sown on the same date in two different selected areas of Normandy (France), one subjected to drought conditions and the other well irrigated when necessary and taken as a control, to evaluate the response to drought stress at both the plant and fibre levels. After a morphological study of the stems, synchrotron deep ultraviolet (DUV) imaging microscopy for polysaccharide and lignin biochemistry and solid-state nuclear magnetic resonance (ssNMR) analysis to decipher the ultrastructural assemblies of polymers were innovatively coupled with a multiscale mechanical assessment performed by AFM at the fibre cell wall scale and with tensile testing on elementary flax fibres extracted from the two batches.

2. Materials: flax plants and fibres

Two batches of the Damara flax industrial variety were sown at the end of March 2019 by the Depestele Group, a French company specializing in flax culture and processing, in two different growing areas located in Ernes (control; irrigated) and Fourches (at risk of drought, not irrigated), in Normandy (France). The two areas are approximately 20 km away from each other and sowing was done with the same seed rate per ha. During the whole fibre growth period, rainfall was constantly recorded until harvesting (**Figure V-3a**) together with temperature and relative humidity (**Figure V-3b**).

It is important to note that the problem of defining drought from a meteorological or agricultural point of view was already discussed in [25], with the conclusion that a lack of precipitation does not necessarily coincide with agricultural drought, expressed as the water demand of the plant. In the present study, it was defined drought as the batch that received less than 100 mm of cumulated rainfall and without irrigation, contrary to the 400 mm generally required. In contrast, the control batch was grown with nearly 250 mm of cumulative rainfall and irrigated when necessary, in order to reach the water demand of flax.

A group of approximately 100 plants were sampled from both cultivations before harvesting and at the beginning of July after approximately 103 days of growth. Fifteen stems were randomly selected to calculate height and diameter to obtain a representative sample, and the other 3 stems were randomly selected and prepared for observations at the DISCO (Dichroism, Imaging and mass Spectrometry for Chemical and biOlogical systems) beamline. The rest of the crop was harvested, and dew was retted *in situ* by the Depestele Group until the middle of August. Fibres were successively extracted using pilot (lab-scale) scutching/combing equipment equipped with a small line with three modules for breaking, scutching and combing (more precisely described in [26]). Stems passed three times through the breaking module, once in the scutching module and two times in the hackling module.

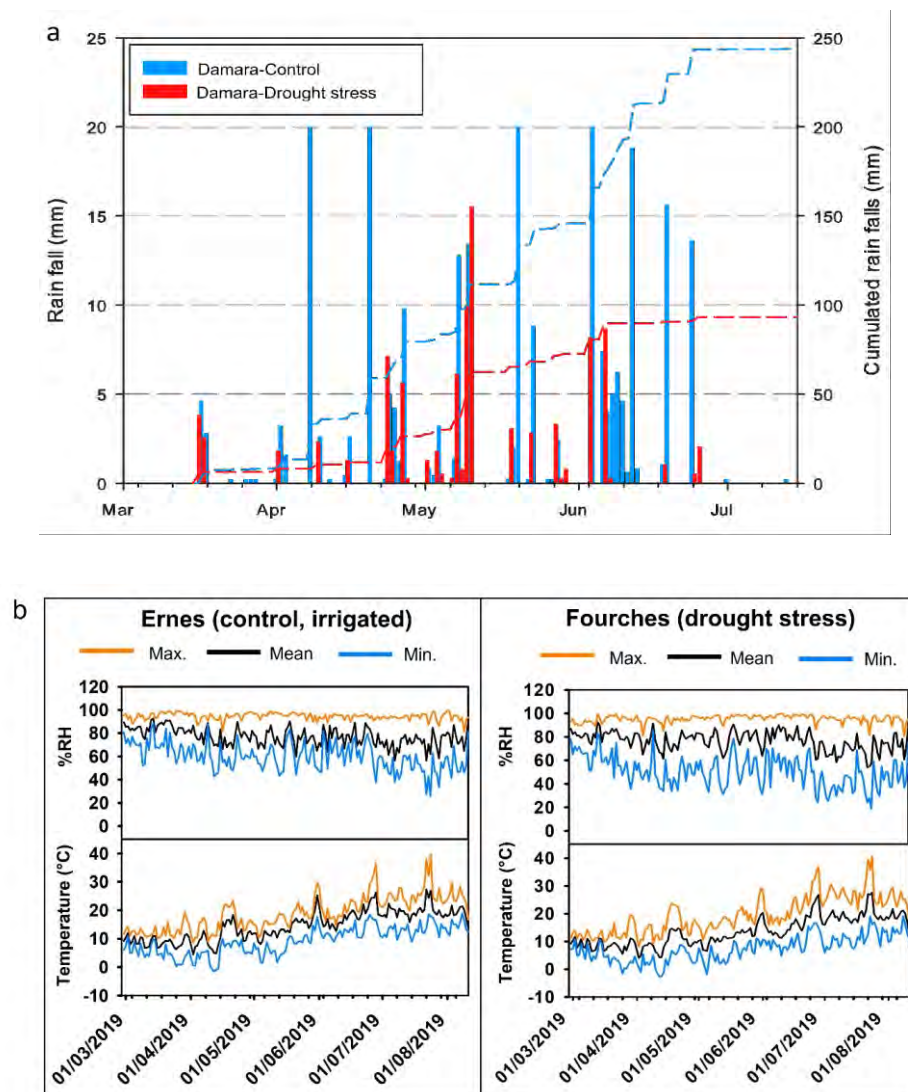


Figure V-3 a) Daily (histograms) and cumulative (dotted lines) rainfall for the two cultivation areas; b) Temperatures and relative humidity recorded during the plant growth of the two crops in selected cultivation areas.

3. Methods

3.1 DISCO Beamline Synchrotron Facility

Sample preparation

A segment of 6 cm was cut at the middle height of the plant of the three fresh stems selected from each of the two batches (**Figure V-4a**). Three small segments of 0.5 cm were successively obtained from the small portion of each individual stem, avoiding the first millimetres in direct contact with air, and then fixed at 4 °C for 24 h in a FAA (formalin acetic acid alcohol) fixative mixture of 10:5:85 v/v composed of formaldehyde (37%), glacial acetic acid (60%) and ethanol (95%). Samples were then

transferred to an automatic tissue processor (Automatic Tissue Tek VIP 3000, Sakura, MI, USA) for ethanol dehydration and successive inclusion in paraffin. Sections were successively cut with a thickness of 10 μm and placed between two quartz coverslips (Circular-Quartz, Ref. R525000, Esco Optics, USA). The sections were treated with a HistoChoice Clearing Agent (H2779, Sigma) solution to remove paraffin. To detect lignin, stem samples were stained using Wiesner (phloroglucinol-HCl) reagent as described in Bouvier d'Yvoire *et al.* [27]. Cross-sections were immediately observed using a macroscope (AZ100 M, NIKON, Japan) under bright-field conditions.

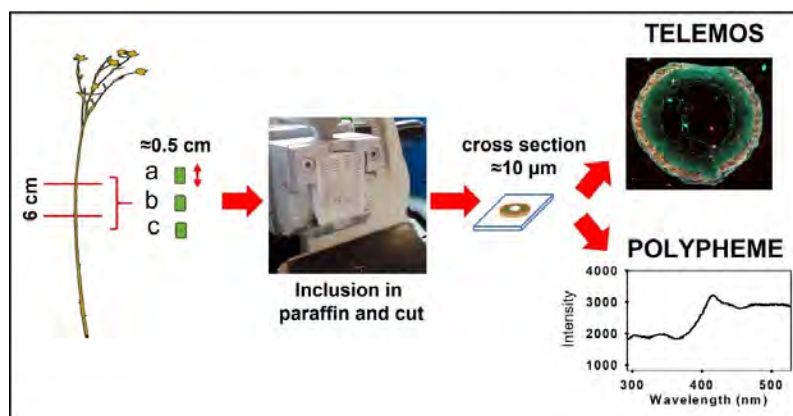


Figure V-4 Overview of the sample route analysis for Synchrotron DISCO beamline exploration.

TELEMOS parameters

As explained in detail in **Chapter II**, three different passband filters at 327–353 (assigned to the red channel, R), 420–460 (assigned to the green channel, G) and 480–550 nm (assigned to the blue channel, B) were used to detect tyrosine and tryptophan amino acids (protein), hydroxycinnamates (ferulic, p-coumaric and sinapic acids) and lignin respectively. The choice of these three filters was made after previous investigations on flax stems [28]. The suitability of the three filters has been discussed in terms of their appropriateness to capture the most important differences in the biochemical composition of flax stems under stress.

With TELEMOS, the three stems of the two batches, each with three cross-sections, were analysed in a total of 18 cross-sections, 9 from drought plants and 9 from control plants. Using ImageJ/Fiji software, segment and area tools were used to select the region of interest (ROI) and calculate the intensity of each filter in regions of the image where the beam intensity was focused, i.e., the centre of the image with the control sample (**Figure V-5**). For further information on the method, see [28]. A range of display values for each channel and each objective was fixed (10x objective: red 0–1500; green 0–2500; blue 0–2500; and 40x objective: red 0–1500; green 0–4000; blue 0–4000) to obtain similar colour intensity in images acquired with the two different objectives. Red, green and blue (RGB) channels were assigned as described in **Chapter II**, using red to better highlight tyrosine/tryptophan,

which are less fluorescent than lignin and phenolic compounds. A t-test using Sigmaplot was calculated to establish the confidence of the calculated values. The images presented in this work are composite images resulting from the sum of the three filters assigned to the RGB channels.

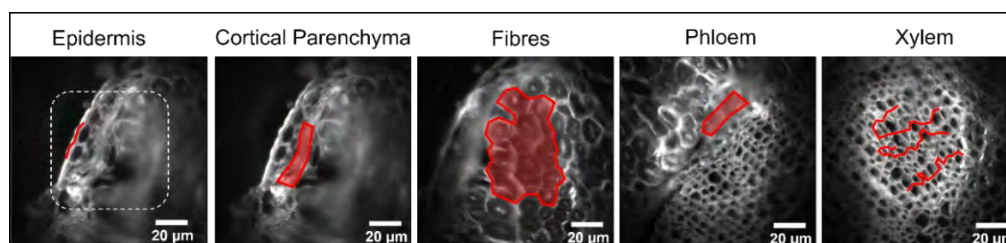


Figure V-5 TELEPOS images acquired and processed. Illustration given for the control sample. The images are 16-bit (65536 grey levels) composite images resulting from the three filters. The region of interest (ROI) where fluorescence intensity was calculated is highlighted in red. Images acquired with a 40x objective.

POLYPHEME parameters

For details on the parameters and methods used, see **Chapter II**. With POLYPHEME one cross section of a one drought-stressed stem and one cross section of a control sample were investigated. Here, an example of the corrected spectra and a table with the proposed fluorescence emission assignments are illustrated in **Figure V-6** and **Table V-1**.

Table V-1 Possible attribution of fluorescence emission collected with POLYPHEME microscope.

Emission	Main attribution	Reference
≈ 306 nm	Tyrosine	[29,30]
≈ 335 nm	Tryptophan	[29,30]
≈ 415 nm	Ferulic Acid	[30]
≈ 435 nm	Caffeic Acid	[31]
≈ 480 nm	Lignin	[30]
≈ 500–530 nm	Lignin	Disco beam line team personal communication

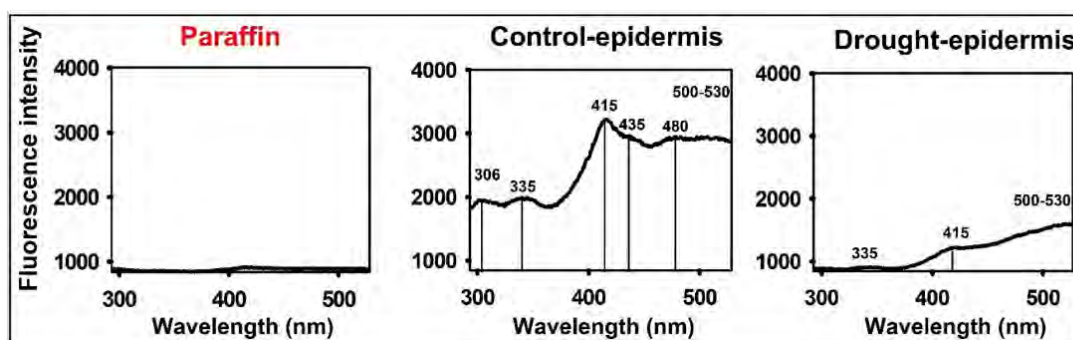


Figure V-6 Fluorescence spectra extracted from the cross section of the control and drought stem sample. Illustration of the epidermal cell type and paraffin, which does not fluoresce (background).

3.2 Single fibre tensile tests

Between 58 and 60 flax fibres were extracted from each batch and glued with universal glue on paper support according to ASTM C1557 [32], with a gauge length of 10 mm. The average diameter of each fibre (approximating the fibre to be perfectly cylindrical) was manually calculated considering five points of measurement under an optical microscope, as described in [33]. The sample elementary fibres were tensile tested by a universal MTS Synergy testing machine equipped with a load cell of 2 N under a controlled atmosphere ($T = 23 \pm 2$ °C; %RH = $50 \pm 4\%$) thanks to a Liebert Hiross indoor room cooling unit. The crosshead displacement rate was set at 1 mm/min until the fibre broke. The determination of the tensile properties, i.e., Young's modulus (E , GPa), strength at rupture (σ , MPa) and strain at rupture (ϵ_r , %) were determined by taking into account the compliance of the loading frame.

3.3 Mechanical investigation of flax cell walls by AFM and nanoindentation

AFM PF-QNM analysis

After that the stems of the two batches were scutched with the scutching line machine, several technical fibres extracted with a scutching line machine after the stem dew retting process were embedded using a low viscosity epoxy resin kit from Agar Scientific (UK) using a flat mould. The full procedure concerning the sample preparation lightly dried in an oven, the final polymerization of the blocks and the surface preparation by ultramicrotome is described in **Chapter II**.

The peak force amplitude was set at 50 nm, the maximum load was 200 nN, and a tip radius between 25 and 99 nm was obtained by calibration with a spring constant between 111 and 194 N/m following the same procedure described in **Chapter II**. The gain was set to automatic. At least 8 images of different fibres and bundles for each batch were acquired and used to calculate the mean indentation modulus. All the acquisitions were made at controlled temperature ($T = 23 \pm 2$ °C) and relative humidity (% RH = $50 \pm 4\%$).

Nanoindentation

Nanoindentation analysis was performed on the same blocks prepared for AFM, and 24 tests for the control and 38 tests for drought-stressed flax fibres were performed. Nanoindentation analysis was carried out by a Nanoindenteur XP (MTS Nano Instruments, Oak Ridge, Tennessee, USA) used at controlled atmosphere ($T = 23 \pm 2$ °C; %RH = $50 \pm 4\%$). The instrument was equipped with a three-sided pyramid indenter (Berkovich-Berko XPT-12761-0) and a 40x objective. The strain rate was set at

0.05 s⁻¹ (i.e., 1 µN/s) during loading to reach a depth limit of 120 nm. The load was held at the maximum value for 60 s, and then withdrawal was performed with the same loading rate up to 10% of the maximum load. At least 20 locations in each sample for each batch were tested.

3.4 Biochemistry

Sample preparation for biochemical analysis

Ten flax stems were cut into 3 segment equivalents in length, and the middle part was retained for further biochemical analysis. The middle segment was manually peeled, and both the flax bundles and the shive part were collected and pooled by sample nature. The content of the monosaccharides was then quantified by operating a homogenization step by cryogrinding (SPEX 6700 freezer Mill) approximately 1 g of the sample.

Monosaccharides (sugars)

The protocol was slightly modified from Barteau *et al.* [34] in the presence of inositol as an internal standard. Neutral monosaccharides were analysed as their alditol acetate derivatives [35] by gas chromatography-flame ionization detection (GC-FID) (Perkin Elmer, Clarus 580, Shelton, CT, USA). For calibration, standards of carbohydrate solutions were used. Analyses were performed in three independent assays. The total monosaccharide content is the sum of each monosaccharide amount and is expressed as the percentage of the dry matter mass.

Lignin

The lignin content was quantified in homogenised powdered particles of samples. Lignin was assessed by spectrophotometry following the acetyl bromide method [36] on samples of approximately 20 mg in mass weight per assay. The chemicals were laboratory grade from Sigma Aldrich, and the analyses were performed with four independent assays, with the lignin content expressed as a percentage of the dry matter mass.

Protein

The total C and N contents of the samples were determined on cryogrinded powders via the Dumas method using an elemental analyser (VarioMicro, ELEMENTAR). Protein contents were determined from N contents multiplied by a 5.7 coefficient usually applied for non-reserve proteins. Experiments were run in triplicate with a calculated experimental error of less than 5%.

Hydroxycinnamic acids

Ester-linked phenolics from bast fibre and shives were analysed after mild alkaline hydrolysis according to the protocol in [37]. For this purpose, 1 mL of 1 N NaOH was added to the ground samples (approx. 10 mg per assay) in centrifuged tubes and incubated for 4 h at 40 °C in a ventilated oven. Tubes were then centrifuged to discard the remaining particles, and the reaction media was acidified with 200 µL of 6 M HCl. After centrifugation (12,000 rpm, 10 min), supernatants were deposited onto a solid-phase extraction cartridge (Waters Sep-Pak Plus Short tC18 cartridges) that were preconditioned before use. Washes and elution were conducted with 1 mL solutions. The samples were then concentrated six times using an air evaporator concentrator, filtered (0.45 µm) and analysed by high-performance liquid chromatography (HPLC) combined with UV diode array detection (HPLC-DAD). The samples (2 µL) were injected onto an RP18 column (Macherey Nagel 2 × 50 mm 2.7 µm particle size, Nucleoshell RP18plus) with a flow rate of 0.3 mL.min⁻¹. The eluents were 0.1% formic acid in water (A) and 0.1% formic acid in acetonitrile (B), with a gradient of B until 60%. Peak assignment from chromatograms was performed at 320 nm according to their retention time by comparison with well-characterised samples of maize bran and UV absorption spectra [38]. A calibration curve with ferulic acid at different concentrations was used for quantification.

The supramolecular organisation of macromolecules was investigated by two complementary techniques: i) ¹³C NMR cross polarisation-magic angle spinning (CPMAS), and ii) variable contact time cross-polarisation magic angle spinning ¹³C VCT-CPMAS.

3.5 ¹H and ¹³C NMR CPMAS

Solid-state NMR (ssNMR) spectra were registered on a Bruker Advance III 400 spectrometer on rehydrated AIM to approximately 30% (w/w) with ultrapure H₂O. Spectra were recorded at a proton frequency of 400.13 MHz and a carbon frequency of 100.62 MHz. A double resonance 1H/X CPMAS 4 mm probe was used. The magic-angle-spinning (MAS) rate was fixed at 12 kHz, and each acquisition was recorded at room temperature (293 K). CPMAS experiments were realised using a 90° proton pulse of 3.3 µs, a contact time of 1.5 ms and a 10 s recycling time for an acquisition of 34 ms during which dipolar decoupling (SPINAL64) of 37.8 kHz was applied. Typically, 2048 scans were accumulated per spectrum. Chemical shifts were calibrated with external glycine, assigning the carbonyl at 176.03 ppm. The approach developed by [39] was used to evaluate the cellulose crystallinity from the deconvoluted C4 peaks in the region 77–92 ppm. In the crystalline part of the region (Cr), the Larsson *et al.* method was performed thanks to the use of three Lorentzian peaks corresponding to cellulose Cr(I_α) (89.1 ppm), cellulose Cr(I_α+I_β) (88.2 ppm) and cellulose Cr(I_β) (87.2 ppm) [39]. An additional Gaussian peak representing the paracrystalline (PCr) contribution (88.1 ppm) is also used.

Three peaks were used in the amorphous C4 region: two Gaussian peaks corresponding to accessible surface cellulose C4 (AS; 82.7 and 83.7 ppm) and another peak corresponding to inaccessible surface C4 (IAS; 83.4 ppm). The proportion of crystalline cellulose in the different samples was determined by dividing the area of the three peaks of the crystalline region by those of the six peaks for the cellulose C4 region. The lateral dimensions of the fibrils (LFD) and the lateral dimensions of the fibril aggregates (LFAD) were then estimated assuming a square cross-section of cellulose microfibrils. These estimates assumed that all amorphous cellulose was on the fibril surface. The cellulosic chain width was taken as 0.57 nm [40].

The chemical shift, half-width and area of peaks were determined using a least-squares fitting method using Peakfit® software (Systat Software Inc., USA).

3.6 ¹³C VCT-CPMAS

By varying the contact time τ of cross-polarisation (20 points between 10 μ s and 9000 μ s, with 512 accumulations per experiment), the dynamics of cross-polarisation were investigated. It is often presumed that magnetisation in ¹³C rises exponentially with time constant T_{CH} and then decays with time constant $T_{1\rho}^H$ so that the two time constants can be extracted by fitting a dual exponential function [41]. Nevertheless, it has become clear that the rising part of the curve is too complex to be described by a single exponential but rather comprises a rapid and a slower phase. Depolarisation of ¹³C in the rotating frame is described by single-phase kinetics. The cross-polarisation kinetics were fitted with the following formula (Eq. V-1) [41], and minimization was performed with the Excel solver:

$$I(\tau) = I_0 e^{-\tau/T_{1\rho}^H} * \{1 - \lambda e^{-\tau/T_{HH}} - (1 - \lambda) e^{-3\tau/2T_{HH}} e^{-\tau^2/2T_{CH}^2}\} \quad (\text{Eq.V-1})$$

where $I(\tau)$ is the area of the carbon peak according to the contact time τ ,

I_0 is the maximum carbon signal intensity (associated with the optimal contact time),

λ is a parameter that depends on the number of protons (n) carried by carbons ($\lambda=1/(n+1)$), T_{CH} is the mean dipolar coupling between carbon and proton covalently link, T_{HH} is the spin diffusion between the two proton reservoirs, and $T_{1\rho}^H$ is the rotating-frame spin–lattice relaxation time.

4. Results

4.1 Impact of drought on overall stem architecture

The first observations were performed by collecting data on the height and diameter of 15 stems sampled at plant maturity. Despite the same seeding rate, the difference in height between the stems selected from the two batches was significant (t-test with $p \leq 0.001$) and was approximately 28%, with

average length values of 81.8 ± 4.3 cm and 59.0 ± 6.5 cm for normal and droughted stems, respectively. In contrast, the difference in diameter, measured every 5 cm until the first branches, was less pronounced but still significant (**Figure V-7**), especially in the middle and bottom of the stems. In the present study, control stems presented a height in line with the height of the Damara variety measured for 2019 in other flax lots [42].

An important criterion to evaluate drought stress in flax plants is the yield after fibre extraction. In this case, the plants grown under drought conditions had a yield of 4.49 t/ha and a scutching yield of 13.8% against 7.19 t/ha and scutching yield of 17.2% of the control one; in general, the yield in terms of tonnes for the Damara variety is 8.54 t/ha, and the scutching yield should be approximately 20–28% under normal conditions [42].

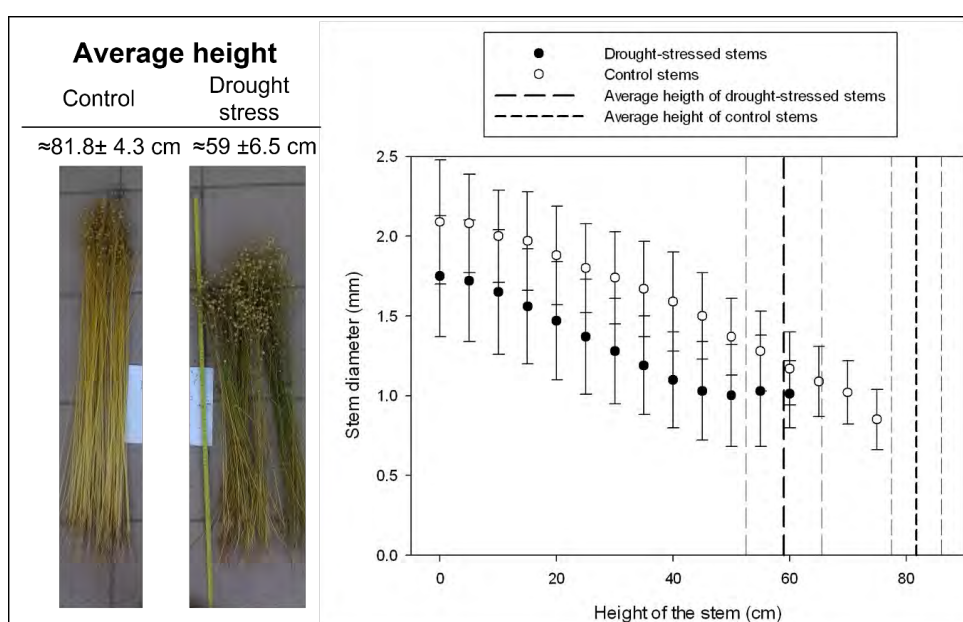


Figure V-7 The height and diameter of 15 stems from the two batches with the relative standard deviations.

4.2 Impact of drought on biochemical composition of the stem

An overview of a cross-section of a control or drought stem does not show a huge major contrast between the two batches. Wiesner staining revealed coniferaldehyde end groups in lignin by red–purple colouration. An overview of a cross section of a control and drought stem does not show huge differences contrasted between the two batches (**Figure V-8**) but highlight the xylem rich area on both control and drought stressed stems. Higher fluorescence emission in DUV fluorescence collected at 480–550 nm suggests more lignin in the drought-stressed stems (**Figures V-9a-f**), but it is contradicted by direct lignin quantification with the acetyl bromide method. No significant difference in lignin content appeared in the bast fibre region under naked eye observation (**Figure V-8**).

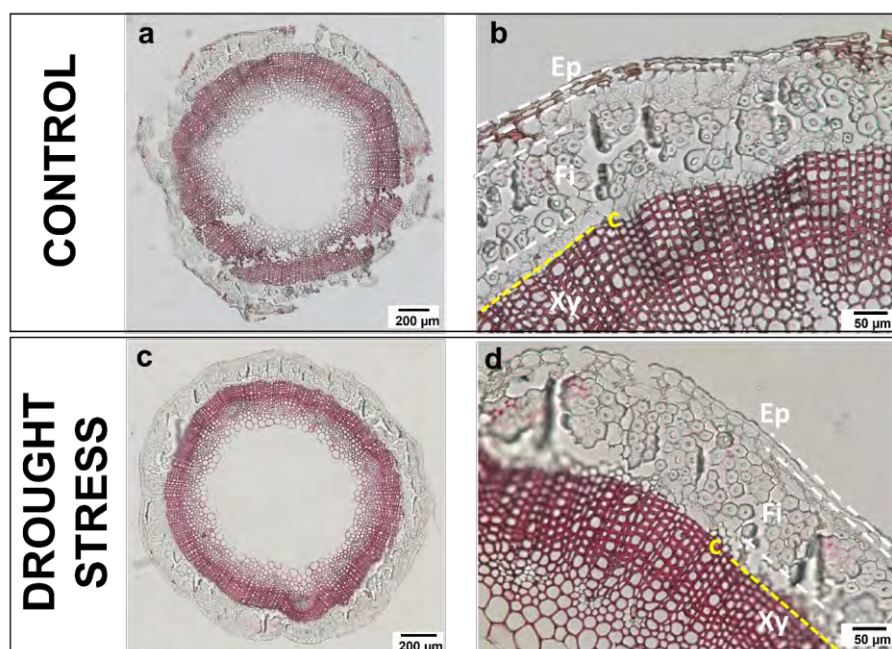


Figure V-8 Overview of control and drought-stressed cross sections. Lignin is highlighted by phloroglucinol staining, and xylem is particularly rich in lignin. Three main tissues of interest are labelled here: Ep=epidermis, Fi= fibres, and Xy= xylem in white. The cambium (c) is highlighted in yellow. The cortical parenchyma between epidermis and fibres and the phloem between the fibres and the cambium are not considered in this case because they do not show any strong staining and their cells are too small to be evaluated. Objective 5x (a-c) and using 5x digital zoom (b-d).

Using synchrotron DUV, fluorescence imaging showed similar results obtained from images acquired under 40x (**Figure V-9e**) and 10x (**Figure V-9f**) objectives with TELEMOS microscope. The mean values from the control and drought-stressed plants were calculated using the three sections from each of the three stems.

Despite the important standard deviation, the fluorescence intensity collected between 480–550 nm, attributed to lignin, appeared higher in the epidermis of the stressed stems, while the cortical parenchyma did not show any particular changes, except that a higher variability was observed in the control stems than in the stressed stems. The bast fibres were particularly interesting because in the drought-stressed stems, it was observed a higher fluorescence intensity at 480–550 nm, attributed mostly to lignin (**Figure V-9f**). Additionally, the fluorescence intensity due to tyrosine and tryptophan (327–353 nm) appeared higher in the drought-stressed fibres, but the p value calculated with the t-test indicated a nonsignificant difference, and for this reason, complementary direct biochemical analyses were performed. The phloem region from the control stems, as in cortical parenchyma, was demonstrated to have greater variability than that in the drought-stressed stems, especially regarding protein and phenolic compounds. In the xylem of the drought-stressed stems, a higher fluorescence intensity due to lignin and protein was noticed when calculated under the 40x objective. This trend was also recorded for the phenolic compounds.

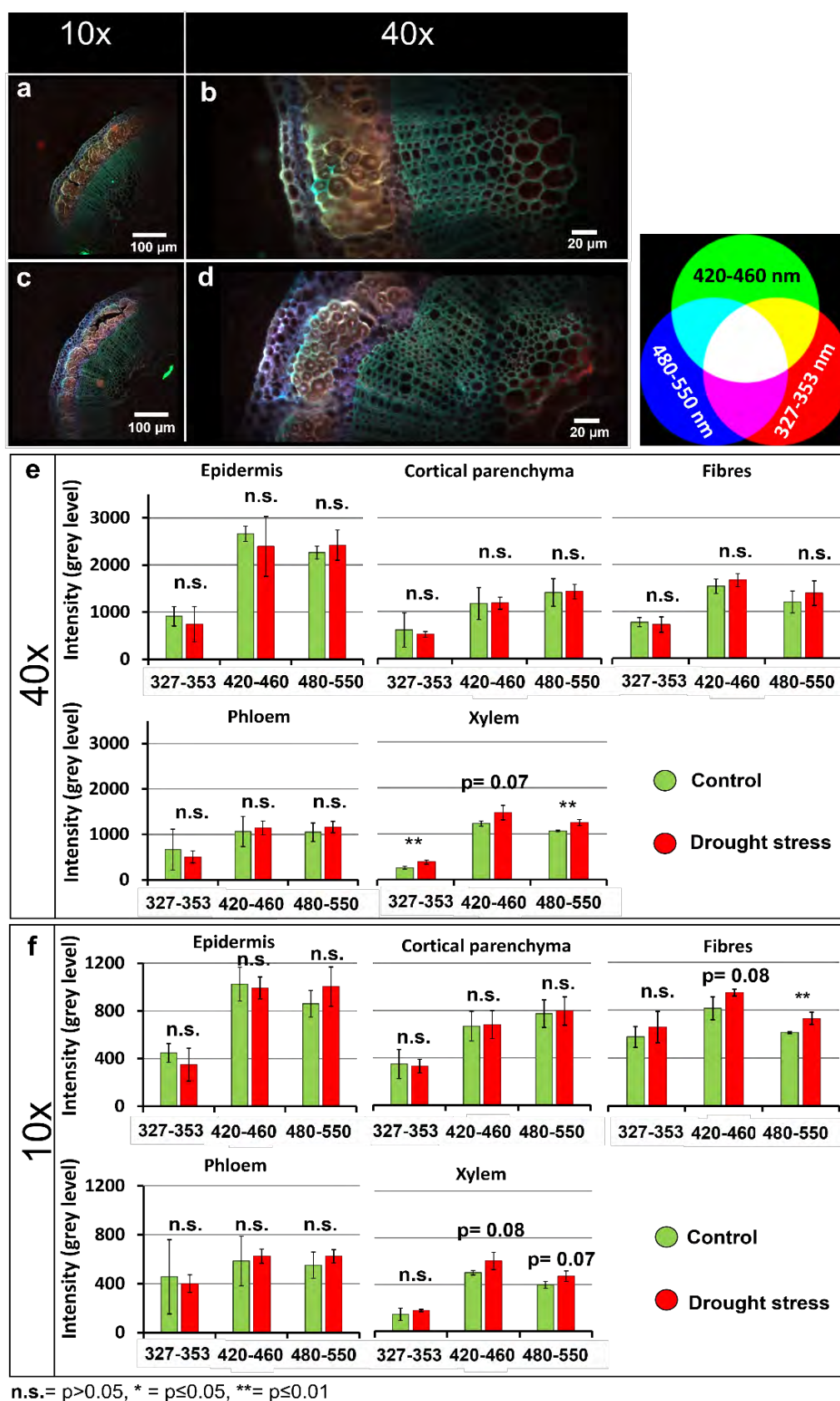


Figure V-9 TELEMOS images under 10x and 40x objectives with the three channels merged to create a single image in RGB of **a-b)** control stems and **c-d)** stressed stems. **e-f)** Graphs of the mean and standard deviation of the fluorescence intensity values calculated in each tissue considered.

The results obtained under DUV imaging were confirmed using POLYPHEME, recording a map of spectra of two cross-sections, one for each batch, chosen from the dataset. **Figure V-10** shows averaged spectra, normalised using the integrals of the three main signals 300–340 nm (attributed to protein), 415 nm (attributed to ferulic acid) and 500–530 nm (attributed to lignin) and decomposed in three different mappings.

Signals attributed to protein (red map) seemed less well distributed in the drought stem cross-section. In the cortical parenchyma of the control stem, a high concentration of protein was observed, while in the drought-stressed stem, the distribution was inhomogeneous, and the fluorescence was apparently less intense. Only some of the drought-stressed fibres gave protein autofluorescence, while in the control stem, the fluorescence was extended to all the fibres.

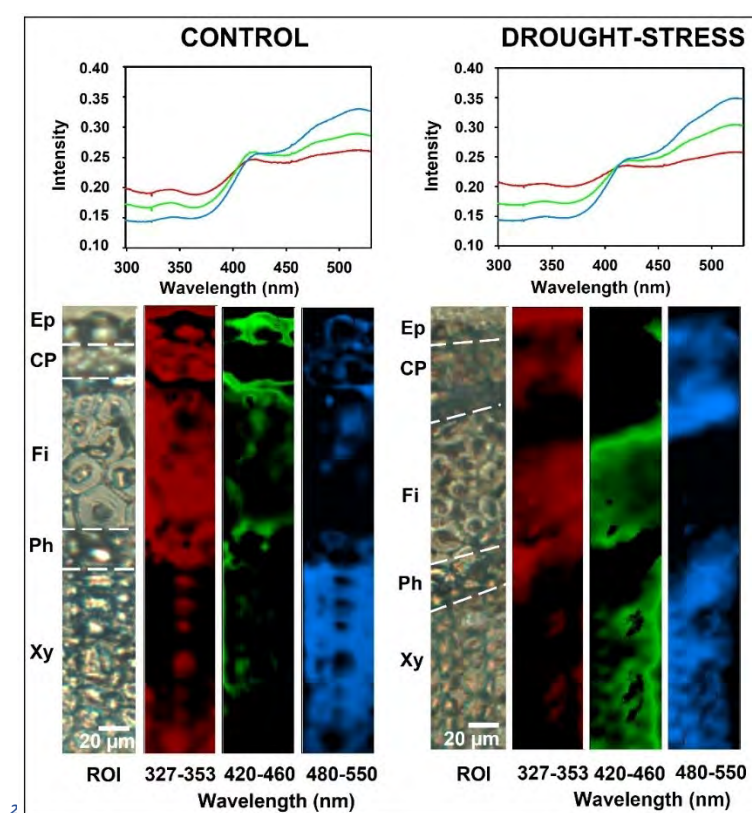


Figure V-10 Two cross sections of the stems were investigated under fluorescence microspectroscopy (POLYPHEME). The spectra were averaged and normalised and three mappings were extracted to highlight signals attributed to protein (red), phenolic compound (green) and lignin (blue) distributions. Ep=epidermis, CP=cortical parenchyma, Fi=fibres, Ph=phloem, and Xy=xylem.

The distribution of fluorescence attributed to phenolic compounds (green map) and lignin (blue map) is more interesting. In the control stem, the epidermis was rich in phenolic compounds, while no fluorescence was recorded in the stressed stem. On the other hand, technical fibres and xylem of the drought-stressed stem appeared much more enriched in phenolic compounds than those of the control stem. Fluorescence attributed to lignin content did not seem to visibly change in the xylem of the two

batches, but lignin was observed to be less localised and better distributed in the cortical parenchyma and epidermis cells of the drought-stressed stem.

4.3 Impact of drought on fibres composition and structure

Biochemical analysis of fibres extracted with GC-FID quantification showed a decrease of approximately 10% in total monosaccharide, approximately 15% of uronic acid and approximately 13% in glucose expressed in dry matter material for drought-stressed fibres (**Figure V-11** and **Table V-2**). Lefeuvre *et al.* [43] attributed arabinose, rhamnose and galactose to RG-I and xylose, mannose and glucose to “hemicellulose”. In contrast to Lefeuvre *et al.*, Akin *et al.* [44] attributed glucose to cellulose content and designed the rest as noncellulosic polysaccharides, abbreviated as NCP [44]. These last authors calculated a ratio between glucose and the sum of xylose, rhamnose, galactose, mannose and arabinose (NCP), to which a small amount of fucose was added. In the present study, glucose was assumed to be indicative of cellulose.

In drought-stressed flax fibres, the mannose content was increased by 28% and the ratio of Glucose/NCP in stressed flax bundles was lower, 4.9 in stressed fibres compared to 6.5 in control fibres as reported in **Table V-2**. This is probably due to both a higher quantity of NCP and a slight decrease in cellulose. These observations are consistent with those of Lefeuvre *et al.*, who reported an increase in hemicellulose polysaccharides [43].

Regarding lignin, a significant increase of 29% was quantified, in line with data obtained under DUV analyses, particularly by TELEMOS, which recorded a higher lignification in stressed fibres in response to abiotic stress. One must recall that both autofluorescence and biochemical analyses have the same limitation, i.e., values are calculated on signals including the middle lamellae surrounding the elementary fibres, describing then the bundle. Middle lamellae are known to be enriched in lignin [45] and can therefore cause an overestimation of the lignin content when speaking about elementary fibre in biochemical or fluorescence analyses.

Another important piece of information is obtained with the galactose/rhamnose (Gal/Rha) ratio, which is an indicator of ramification in the matrix and RG-I [43,46]. In the present study, the Gal/Rha ratio calculated was 3.8 in the control fibres versus 2.8 in the stressed flax fibres. According to Lefeuvre *et al.* [43], this lower ratio means that the ramification is less extended, arguably with a shorter galactose side chain length. Notably, long side galactose chains were purified from bast fibre G layer [47].

Regarding the protein, despite the large standard deviation, the multispectral imaging showed a trend towards a higher content in the drought-stressed fibres, whereas the direct protein content quantified with the Dumas method clearly shows an increment of almost 50% in the stressed fibres.

Shives extracted from non-retted stems showed an increased amount of xylose in drought-stressed stems, while, unlike fibres, the amount of glucose barely changed between the two batches. Furthermore, a

drastic decrease in the amount of lignin and protein in the xylem of drought-stressed stems compared to the control flax plants was observed.

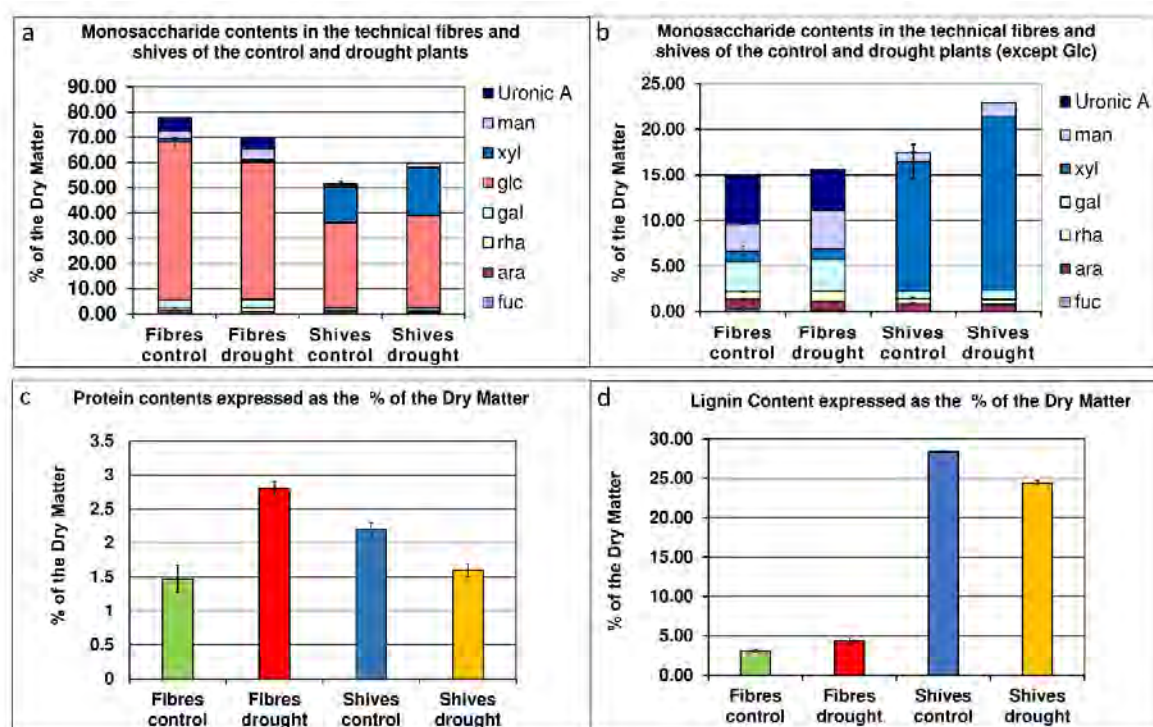


Figure V-11 Biochemical analysis of monosaccharide with **a)** or without **b)** glucose, protein **c)** and lignin **d)** and content in fibres and shives (xylem). Values are given in % of dry mass. xyl: xylose; glc: glucose; gal: galactose; man: mannose; rha: rhamnose; ara: arabinose; fuc: fucose; and Uronic A: uronic acid.

Table V-2 Detailed data of sugar analysis from fibres and shives. xyl: xylose; glc: glucose; gal: galactose; rha: rhamnose; ara: arabinose; fuc: fucose; and man: mannose. Gal/Rha and glucose/noncellulosic polysaccharide (NCP) ratios are also reported, SD standard deviation. All values are given in % of the dry mass.

FIBRES											
%	fuc	ara	rha	gal	glc	xyl	man	Uronic Acid	total sugars	Gal/Rha	Glc / NCP
Control	0.31	1.06	0.85	3.27	62.8	1.17	2.99	5.32	77.8	3.84	6.5 : 1
SD	0.17	0.04	0.59	0.26	1.85	0.13	0.03	0.80	3.81	-	-
Drought-stressed	0.11	1.00	1.18	3.36	54.3	1.17	4.17	4.50	69.9	2.86	4.9 : 1
SD	0.00	0.11	0.12	0.16	0.34	0.11	0.03	0.28	0.21	-	-
SHIVES											
Control	0.06	0.85	0.53	0.82	33.95	14.22	0.98	/	51.40	/	/
SD	0.00	0.07	0.07	0.03	0.43	1.89	0.04	/	1.66	/	/
Drought-stressed	0.04	0.73	0.58	0.95	36.71	19.15	1.45	/	59.62	/	/
SD	0.08	0.06	0.10	0.02	1.63	0.59	0.07	/	2.43	/	/

Direct quantification of some hydroxycinnamic acids linked in the cell wall by ester bridges has been performed on technical fibres and shives (**Table V-3**). This quantification includes ferulic acid as a form of monomer (major component) or one dimer (the 8–5' benzofuran) and both coumaric and sinapic acids. A slight increase in FA, sinapic and *p*-coumaric acids can be monitored in bast fibre from the drought-stressed plants and a decrease in *o*-coumaric acid. No traces of dimer of 8–5' ferulic acid dimer can be found in technical fibres. For shives, *o*-coumaric acid was not detected, and a dimer of 8–5' ferulic acid was quantified in a similar amount in the drought and control plant shives. A general slight decrease is observed in ferulic acid, *p*-coumaric and sinapic acids in drought plant shives.

In addition to biochemical quantifications, ssNMR investigations were conducted. Flax fibres from the two batches did not show differences in crystalline cellulose content under NMR analysis, with a value of approximately 55–57%; however, the Nuclear Magnetic Relaxation Time Analyses $T_{1\rho}^H$ demonstrated a higher value of almost 50% in fibres extracted from drought-stressed plants compared to that of control samples. This value is due to the molecular organisation in the range of a few nanometres (2–30 nm) around the cellulose fibres, and a higher value in drought-stressed fibres could suggest a more organised structure in components other than crystalline cellulose, i.e., pectin or hemicellulose (**Table V-4**) which appeared altered in the drought-stressed fibres, as discussed above. However, at the ultrastructural level, the cellulose LFD and LFAD parameters, representing the size parameters of both cellulose fibril and fibril aggregates, remained on the same order for both the control and drought-stressed fibres.

Table V-3 Amounts of hydroxycinnamics (monomers and dimer) released by mild alkaline hydrolysis of the control and drought technical fibres and shives. Values are expressed as % of dry matter. FA-E: ferulic acid in E or Z isomers; pCA: coumaric acid; oCA: o-coumaric acid; SA: sinapic acid; and DiFA8–5'C 8,5'-DiFerulic acid benzofuran form. DM is the dry matter.

	in % of the DM	FA-E	pCA	SA	oCA	DiFA8–5'C
Technical fibres	Control	1.5×10^{-5}	1.4×10^{-5}	1.6×10^{-6}	2.7×10^{-6}	0
	SD	1.6×10^{-6}	5.4×10^{-7}	8.5×10^{-8}	1.4×10^{-7}	0
	Drought	1.9×10^{-5}	2.1×10^{-5}	1.8×10^{-6}	7.0×10^{-7}	0
	SD	5.9×10^{-7}	1.1×10^{-6}	1.2×10^{-7}	1.3×10^{-7}	0
Shives	Control	3.6×10^{-5}	3.3×10^{-5}	2.5×10^{-6}	0	5.3×10^{-7}
	SD	1.8×10^{-6}	2.4×10^{-6}	1.2×10^{-7}	0	1.3×10^{-7}
	Drought	1.7×10^{-5}	2.2×10^{-5}	1.2×10^{-6}	0	6.4×10^{-7}
	SD	2.7×10^{-7}	3.5×10^{-8}	7.1×10^{-8}	0	1.8×10^{-7}

Table V-4 NMR data. Relaxation times associated with C_4 phase areas for control and drought-stressed samples, $T_{1\rho}^H$ is the spin lattice in the rotating frame relaxation times for protons. Crystallinity index (CI), LFD and LFAD are the crystallinity ratios obtained from the C_4 and C_6 region deconvolution of ^{13}C CP/MAS spectra, the lateral fibril dimension, the lateral fibril aggregate dimension and the hemicellulose content, respectively.

	$T_{1\rho}^H$ (ms)	
	Control	Drought
C_4	20	36
^{13}C CP/MAS		
CI (%)	57	55
LFD (nm)	4.6	4.5
LFAD (nm)	20	19.2

4.4 Impact of drought on fibres and cell wall mechanical properties

Mechanical properties were investigated at the single fibre scale by tensile testing but also at the cell wall scale by AFM PF-QNM and NI. **Table V-5** shows the tensile properties obtained on the two batches of fibres as well as the number and diameters of the fibres considered.

Previous results showed that drought stress has a clear impact on flax fibre biochemical content but also on their morphology. The diameters measured under an optical microscope on approximately 60 fibres demonstrated a significant difference ($p < 0.5$) between the control ($19.3 \pm 4.5 \mu\text{m}$) and drought-stressed fibres ($16.1 \pm 3.5 \mu\text{m}$), tested using Welch's t-test. However, neither the morphology nor the biochemical modifications seem to affect the longitudinal mechanical properties, which are still comparable between the two batches. Interestingly, these mechanical performances are fully in line with literature data collected on 50 batches of single flax fibres [48], characterised with the same protocol and equipment in our lab (**Figure V-12**); our batches have an average Young's modulus very similar to the average value of these 50 batches of elementary fibres and a strength at break slightly higher.

Table V-5 Mean diameters and tensile properties of individual flax fibres tensile-tested in tension.

	Number of fibres	Diameter (μm)	Young's Modulus (GPa)	Strength at break (MPa)	Elongation at break (%)
Control	58	$19.3 \pm 4.4^*$	$55.2 \pm 25.4^{\text{n.s.}}$	$1268 \pm 588^{\text{n.s.}}$	$2.37 \pm 0.62^{\text{n.s.}}$
Drought stressed	58	$16.1 \pm 3.5^*$	$57.3 \pm 23.6^{\text{n.s.}}$	$1230 \pm 515^{\text{n.s.}}$	$2.26 \pm 0.61^{\text{n.s.}}$

* statistically significantly different ($p < 0.5$), n.s.= not significant

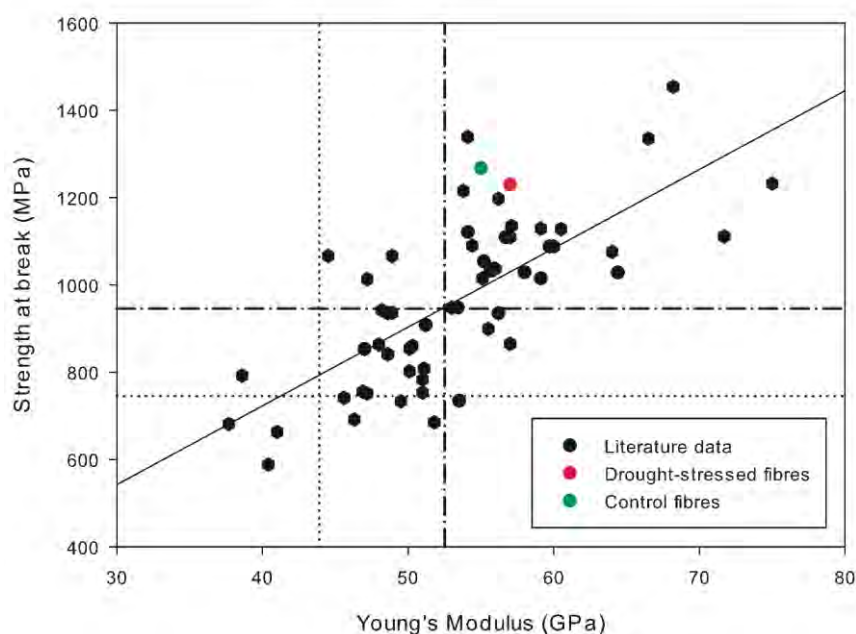


Figure V-12 Comparison of the tensile Young's modulus and strength at break of the control and stressed flax fibres with literature data [48].

Thus, at the elementary fibre scale, the tensile properties were not significantly affected, and they maintained their potential as composite material reinforcement, although the crop yield of the fibres extracted from the stressed plants was drastically reduced; this stability of flax fibre mechanical performance has already been demonstrated on a panel of 4 varieties with significantly different fibre yields [49].

At the cell level, the topography and indentation modulus obtained by AFM of fibres from control and stressed batches are reported in **Figure V-13**. The average indentation modulus obtained by AFM PF-QNM in control flax fibres was 19.3 ± 1.4 GPa and 19.0 ± 1.4 GPa in drought-stressed fibres, resulting in a nonsignificant difference (p value $> \alpha$), without any mechanical gradient in the G or S₁ layers in both cases. In light of the significant biochemical variations between the control and drought samples, this lack of contrast in indentation modulus emphasizes the hypothesis of a compensation effect of the plant metabolism to maintain its internal mechanical specifications in accordance with the *in-planta* function. Further experiments run with nanoindentation confirmed the results obtained by AFM with an average indentation modulus of 19.1 ± 3.5 GPa and 19.5 ± 2.7 GPa obtained for control and drought-stressed fibres, respectively, with again a nonsignificant difference (p value $> \alpha$).

This stability in the indentation modulus, obtained by both nanoindentation and AFM tests, provides pertinent indications of a poor evolution of both cellulose macrofibrils (crystallinity and MFA) and possible moderate changes in the polysaccharidic matrix ultrastructure, which can impact the transverse and shearing cell wall properties and, consequently, the indentation modulus. Conversely, the hardness

(H) measured is contrasted, being statistically significant between drought-stressed and control fibres (341 ± 34 MPa in stressed fibres against 296 ± 35 MPa in control), with a clear higher hardness recorded in the drought fibres (**Table V-6**). Gindl *et al.* [50] and Stanzl-Tschegg *et al.* [51] have evidenced that the hardness of plant cell walls is a good indicator of noncellulosic polymer evolution; here, hardness measurements confirm the biochemical changes, which has been shown to be more sensitive than the indentation modulus to highlight matrixial changes.

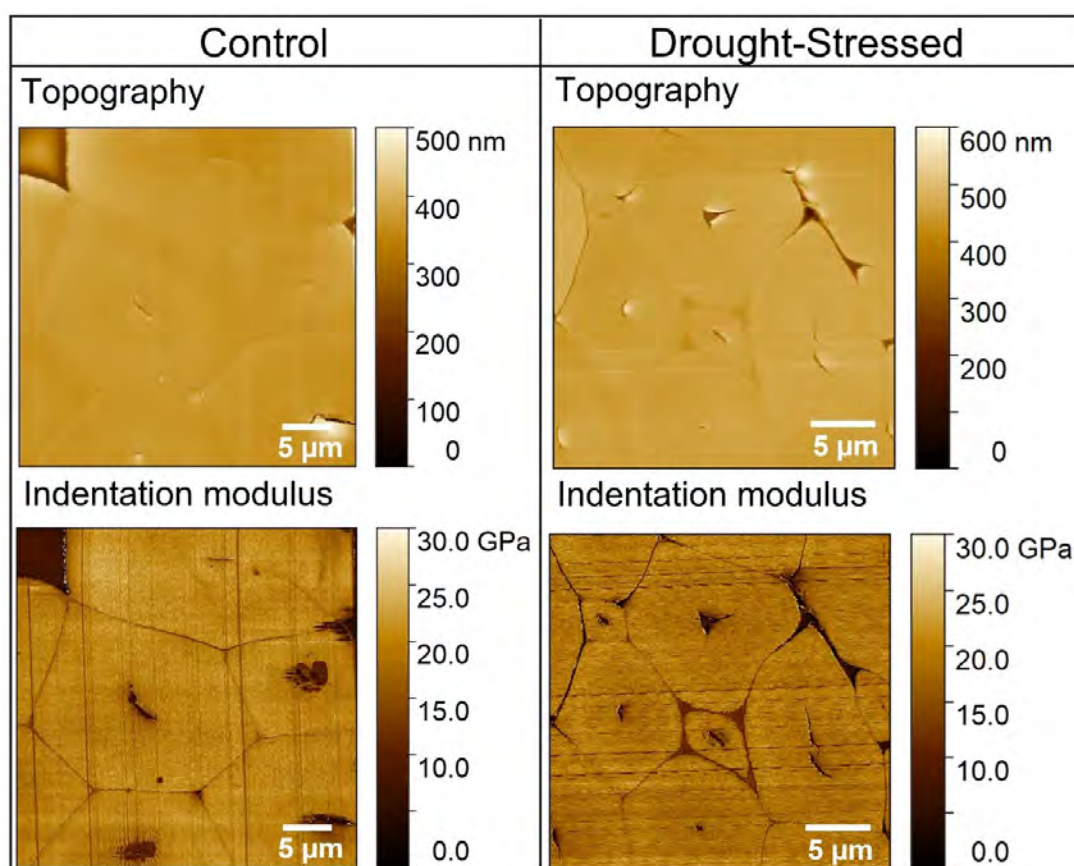


Figure V-13 Indentation modulus mapping and topography of control and drought-stressed flax cell walls obtained by AFM PF-QNM experiments.

Table V-6 mean values of indentation modulus and hardness recorded by AFM and nanoindentation.

Characterisation technique	Control	Drought-stressed
AFM PF-QNM		
Indentation Modulus (GPa)	19.3 ± 1.4 ^{n.s.}	19.0 ± 1.4 ^{n.s.}
Nanoindentation		
Indentation Modulus (GPa)	19.1 ± 3.5 ^{n.s.}	19.5 ± 2.7 ^{n.s.}
Hardness (MPa)*	296 ± 35 *	341 ± 34 *

* statistically significant (p value < 0.5), n.s.= not significant

5. Discussion

All the results obtained in this work are summarised in **Table V-7**. Flax plants grown under drought conditions have undergone important modifications in terms of morphology, as indicated by a reduction of both the height and stem diameters. This was already observed for linseed by Kariuki *et al.* [17], who also documented an important decrease in the number of leaves under water stress.

Abot *et al.* studied *Cannabis sativa* under water stress conditions and recorded a delay in stem maturity for stressed stems [15]. Conversely, it was observed that other plants anticipated their maturity by trying to shorten their growing cycle to prevent drought stress during critical periods, such as flowering [52,53]. In drought-stressed flax plants, it was observed delays in flowering and maturation (not shown in this paper).

Under drought stress, it is known that flax plants reduce their fibre diameter, and both the fibre number and length are affected [16]. This fact, together with the reduced height and diameter of the plant, has a direct impact on the fibre yield and can explain the lower fibre yield obtained from drought-stressed plants (13% versus 17% under normal conditions, and approximately 20–28% in the literature). A similar loss of yield was already reported in Lefeuvre *et al.* for drought-stressed stems of the Marilyn flax variety [43].

Histochemical analysis with phloroglucinol demonstrated a slight colouring of flax fibres from the two batches, but no differences between the drought and control fibres were detected in their cell walls or in their middle lamellae, where lignin is arguably mainly present.

Lignin is a complex polyphenolic constituent of different monolignols with the role of providing stiffness to the plant as a mechanical function as well as hydrophobicity [54] and, in the case of stress, serving as encrusting polymers with the aim of increasing the resistance of plants to unfavourable environments. Indeed, hyperlignification was also observed in the growth of other plant species under drought stress [55,56], and a role of a physical barrier was observed in stressed maize leaves, where higher lignification was attributed to the plant response to limit water transpiration [57]. However, hyperlignification due to stress is not systematic in all tissues of the plant, and it also differs among the plant species investigated [58]. Nevertheless, since the lignin content in flax fibres is very low, it is difficult to link the presence of lignin to the stiffness of the cell wall. Thanks to UV fluorescence analysis and direct biochemical quantification, it was possible to deeply investigate proteins (especially tyrosine and tryptophan) and hydroxycinnamic acids. Tyrosine and tryptophan are amino acids belonging to protein and are essential for plant metabolism. Indeed, tyrosine, as a tyrosine phosphorylation, is linked to the capacity of cell division, which is reduced when the plant undergoes drought conditions [59,60]. Furthermore, protein tyrosine phosphatase is a negative regulator of the phytohormone abscisic acid (ABA), which is responsible for the movement of stomata and, under drought stress, induces their closure [60,61]. Tryptophan is an amino acid used for the synthesis of protein and other compounds with

a different role in plant growth, resistance and reproduction; in particular, it is the precursor of auxin biosynthesis, a hormone directly linked to growth capacity [62,63]. Extensive research on wheat growth under drought stress conditions showed that plants had an increase in both tryptophan and tyrosine in their leaves [64].

Table V-7 Summary table of observations divided by techniques.

Flax plant DAMARA variety (2019)	Drought-stressed (Fourches)	
Rainfall	<100 mm cumulated rainfall	
Height (mm)	59.0 ± 6.5 (-28%) *	
Technical fibre Yield	13.8 % (-3.4 %) *	
DUV imaging	Fibres (10x)	Xylem (40x)
	Protein: + (n.s.)	Protein: 384.9 ± 46 (+32.5%)*
	Phenolic: + (n.s.)	Phenolic: + (n.s.)
DUV microspec.	Lignin: 729.5±51.7 (+16%)*	Lignin: 1244.6 ± 66 (+14.6%)*
	Fibres	Xylem
	Prot.: less intense, less homogeneous PC: more intense, well distributed Lignin: ND	Prot.: less intense, less homogeneous PC: more intense, well distributed Lignin: n.s.
Total Monosaccharides * (% dry mass)	Fibres 69.89 ± 0.21 (-10%) (Glc= -13%, Man= +28%)	Xylem 59.62 ± 2.43 (+14%) (Xyl= +26%, Man= +33%)
Lignin * (% dry mass)	Fibres 4.37 ± 0.40 (+29%)	Xylem 24.4 ± 0.30 (-14%)
Protein * (% dry mass)	Fibres 2.8 ± 0.1 (+47%)	Xylem 1.6 ± 0.1 (-27%)
Hydroxycinnamic *	Fibres +12%/+30% (except oCA= -74%)	Xylem -35%/-50% (except DFA8-5C= +17%)
¹³ C NMR CP/MAS		
CI (%)	55 % (n.s.)	
LFD & LFAD	4.5 (n.s.); 19.2 (n.s.)	
¹³ C VCT-CP/MAS	T _{1ρ} ^H = + 45–50% *	
Diameter fibres (µm)	16.1 (-17%) *	
Tensile test		
Young's modulus (GPa)	54.4 ± 22.8 (n.s.)	
Strength at break (MPa)	1180 ± 503 (n.s.)	
AFM PF-QNM		
Indentation Modulus (GPa)	19.0 ± 1.4 (n.s.)	
Nanoindentation		
Indentation Modulus (GPa)	19.5 ± 2.7 (n.s.)	
Hardness (MPa)	341 ± 34 * (+13%)	

* statistically significantly different (p<0.5), n.s.= not significant, ND= not determined

A large increase in tyrosine and tryptophan was also observed for tree stems of elm and oak wood species subjected to moderate to extremely severe drought conditions [65].

Hydroxycinnamic acids are well known to be antioxidants [66], and their biosynthesis directly involves tyrosine and phenylalanine, which are their precursors [67,68]. At the same time, lignin is biosynthesised from hydroxycinnamic acids [69,70]. In flax plants, hydroxycinnamic acids play several roles, such as cross-linking and mechanical support, and are directly involved in the plant response to biotic and abiotic stress. [71]. Most likely, for these reasons, other teams found that the amount of hydroxycinnamic acids seems to increase when plants grow under drought stress [67,72].

In general, the cutin and waxes in the external part of leaves and stems of plants, which can generate autofluorescence [73], are partially responsible for water transpiration, and their thickness seems to increase with drought, as in the case of tea leaves [74].

In the epidermis of drought-stressed flax stems examined here, a slightly higher fluorescence intensity of lignin was observed than that in control stems, while the fluorescence intensity of protein and hydroxycinnamic acids tended to decrease (**Figures V-9 e, f and 10**).

In cortical parenchyma, the difference in thickness was evident and apparently higher in the stressed stems with also larger cells, as one can note in **Figures V-9a-d**. Control stems, on the contrary, had a dense, thin and more compact cortical parenchyma. In terms of molecular distribution, high variability was found in the cortical parenchyma of the control, while the stressed stems showed a more homogeneous response in all three stems investigated, especially regarding tyrosine and tryptophan (**Figures V-9e, f**). As in cortical parenchyma, phloem showed extremely high variability in controlled plants, while the standard deviation was reduced in the stressed stems. Unfortunately, in the literature, there is a lack of information regarding the response of these tissues to drought stress. The greatest differences between the two flax batches were found in the xylem and fibres. In the xylem, it was observed an increase in fluorescence intensity in all three filters for the stressed stems, especially for the filter assigned to protein (327–353) and lignin (480–550), as reported in **Figures V-9e, f**. This seems to be in line with the literature because a higher xylem lignification appears to be beneficial for drought-stressed plants of other species [55,56,58]. However, to the best of our knowledge, there is no literature on flax xylem lignification under drought stress. Nevertheless, UV fluorescence results were contradicted by direct biochemical quantification, where a lower content of protein, lignin and hydroxycinnamic acids was measured in drought xylem than in the control flax plants (**Tables V-3 and Figures V-11c, d**). A hypothesis to explain this discrepancy relies on the method of quantification.

The specificity of the fluorescence of lignin has already been questioned [28,31], and an hypothesis is that nonlignin molecules capable of fluorescing in the range of 480–550 nm may have overestimated the lignin amount by the autofluorescence method. On the other hand, the direct method of quantification can be influenced by the contrasting affinity of reagents with fine molecule structures. For instance, lignin quantification by acetyl bromide may be sensitive to the lignin ratio of G/H and S monomers, and when lignin is stained by phloroglucinol [75] in flax, it shows a contrasting location and distribution

compared to safranin-based quantification [76]. Quantification for accurate and specific measurements of complex structures is still a challenge.

Similar limitations of both techniques were also observed for the quantification of protein and hydroxycinnamic acids. Deep UV fluorescence investigations allow the detection of only a few amino acids capable of fluorescing, such as tryptophan, while the biochemical method is based on the quantification of all the azote contents of the sample and reflects all 20 amino acids constituting proteins. Thus, if the draught samples have a high protein content but are not enriched in aromatic amino acids that can fluoresce, then DUV imaging may underestimate the real amount of protein.

In stressed xylem, for example, the biochemical quantification approach also recorded a lower amount of protein than the control one (**Figure V-11c**). It is possible to conclude that although drought stress could have caused an enrichment in tryptophan and tyrosine in the xylem observed under fluorescence, the overall amount of protein calculated by direct quantification, therefore also considering nonaromatically enriched amino acids, probably decreased.

Contrary to protein, for the analysis of hydroxycinnamic acids, direct quantification can only quantify ester bonds, and only certain forms, but does not exhaustively quantify all hydroxycinnamics. For this reason, in this case, DUV quantification is certainly more representative of the overall hydroxycinnamic acids if the two methods are compared.

Regarding flax fibres, under DUV light, a higher fluorescence intensity for all three filters was recorded in stressed flax fibres (**Figures V-9e, f**) and fluorescence microspectroscopy clearly shows enrichment, especially in hydroxycinnamic acids (**Figure V-10**). The higher amounts of protein, hydroxycinnamic acids and lignin were confirmed by direct quantification (**Figures V-11c, d** and **Table V-3**). An increase in lignin was expected in response to drought stress, as already reported in the literature for both flax and hemp fibres [15,43], but no literature data have been found on protein and hydroxycinnamic acids.

Monosaccharides were also investigated and linked to cellulose and hemicellulose. Biochemical analysis by wet chemistry (GC-FID) also demonstrated a moderate decrease in glucose content for stressed flax, probably compensating for the biosynthesis of mannose, whose content increased. In extracted drought-stressed flax fibres, Lefevre *et al.* found more xylan as a structured polysaccharide and a decrease in gel/matrix polysaccharides (rhamnogalacturonan and homogalacturonan), a decrease in uronic acid, a decrease in the Gal/Rha ratio and a decrease in total sugars extracted in acid compared with control flax fibres [43]. The presented results are generally in line with their observations (**Figures V-11a, b** and **Table V-2**), and a lower Gal/Rha ratio in drought-stressed fibres means a modification in the RG-I polymer responsible for the order of the microfibril network [16].

Increased quantities of mannose and galactose were observed by Bowne *et al.* in leaf tissues of wheat growth under drought conditions, and the authors hypothesised that mannose and galactose are correlated with plant defence in an attempt to avoid loss of water in unfavourable environmental conditions [64]. This may also be a valid explanation in the case of flax fibres.

Rihouey *et al.* reported on flax fibres that mannose is currently known only in the form of glucomannans and that glucomannans play a main structural role in fibre cells I [77]. In the present study, mannose was the main monosaccharide that changed between the two batches and became more abundant in the drought-stressed fibres. Because mannose content is extremely low in both lots compared to glucose and glucomannans are mainly located in the G layer [78–80], as illustrated in **Table V-8**, the stressed flax fibres are apparently enriched in glucomannans.

Table V-8 Flax fibre cell wall layers and approximative composition readapted from [78–80].

Fibre cell wall layer	Approximative composition
PW	~ 25–30% Cellulose ~ 30% Hemicellulose (xyloglucan and less amount of arabinoxylan) ~ 30% Pectins (homogalacturonan and less amount of RG-I and RG-II) ~ 5% Proteins
S₁	~ 40% Cellulose ~ 25% Hemicellulose (mainly xylan, small amount of glucomannans) ~ 5% Pectins (homogalacturonan) ~ 20–30% Lignin
G	~ 80–90% Cellulose ~ 5–10% Pectins (mainly RG-I, probably also a small amount of homogalacturonan) Traces of xyloglucans; small amount of glucomannans and proteins, including arabinogalactans

The amount of glucose, on the other hand, decreases in drought-stressed fibres and the xyloglucan content first, which are calculated with the ratio $\text{Glc/Xyl}=1.5$ with the rest of glucose after the estimation of glucomannans [77], and xylans then, which are calculated with the remaining xylose content [77], probably decrease as well because in both batches investigated here, the xylose is constant. Thus, hemicelluloses in the S₁ layer are particularly reduced in drought-stressed fibres and probably partially replaced by other molecules, such as lignin, protein and hydroxycinnamic acids. Regarding pectins, using the Gal/Rha ratio, it was found that drought-stressed fibres had a smaller ratio and, consequently, the stressed fibres had RG-I with shorter galactan chains [43,46]. This result confirms the results obtained by Lefeuvre *et al.* [43], who observed the same smaller ratio in drought-stressed flax fibres than in the controls.

Despite all these important biochemical modifications at the stem and fibre levels, the mechanical properties of flax fibres in terms of both indentation measured at the nanoscale level and Young's moduli measured by tensile testing were preserved, and stressed and control fibre mechanical properties were comparable at both the local and fibre scales (**Figures V-12 and 13**). Our results are in agreement with

the study of Lefeuvre *et al.*, where batches of flax fibre growth under drought and control conditions were measured by tensile testing, and the authors did not observe any significant differences [33]. It can be argued that tensile test behaviour and properties are mainly driven by cellulose content and arrangement due to the poor MFA and high crystalline cellulose content of flax fibres; consequently, changes in the polysaccharidic matrix are not easily perceptible with this method. In fact, in the present study, thanks to the NMR analysis, it was observed that the crystallinity index was the same as the microfibril network between the two batches (**Table V-4**), which can explain why the longitudinal mechanical properties of the fibres measured by the single fibre tensile test were quite the same, except for the hardness.

Hardness measured by nanoindentation was higher in the drought-stressed fibres than in the control fibres. Eder *et al.* reported that hardness is mainly due to the matrix behaviour of the fibre cell [81]. Indentation is a much more complex loading that leads to the fact that the indentation modulus depends on the longitudinal Young's modulus but also to the transverse and shear moduli [82]. Hence, indentation modulus is sensitive to the cellulose microfibrils elastic properties, such as the longitudinal Young's modulus, but also to the cell wall matrix viscoelastic properties. Despite the changes in the chemical composition and organisation of the matrix observed here, this modulus is not significantly altered. Conversely, the hardness measured by nanoindentation was higher in drought-stressed fibres than in control one. Eder *et al.* reported that the hardness is mainly due to the matrix viscoplastic (irreversible) behaviour of the cell wall [81]. Similar trends were addressed by Gindl *et al.* [50] and Stanzle-Tschegg *et al.* [51], by comparing lignification of spruce tracheids for different maturity degrees and thermally treated wood, respectively.

The longitudinal elastic modulus and strength are due to the crystalline cellulose and are unchanged as well as the indentation modulus, which depends on the viscoelastic properties of the cell wall matrix. Conversely, the hardness, which mainly depends on the viscoplastic properties of the cell wall matrix, varies between control and stressed fibres. Therefore, it can be hypothesised that biochemical changes would mainly impact the viscoplastic behaviour of the cell wall matrix.

Besides, the relationship between lignin and nanomechanical properties requires particular attention. The role of lignin in the mechanical properties of cell walls with cellulose microfibrils having a high microfibril angle has been deeply studied in wood, and a high lignin content has been observed to increase the shear modulus and strength of the matrix by filling the space between cellulose and hemicellulose [83,84,50], and the hardness measured resulted particularly sensible to the lignin concentration [50].

Following the hypothesis in Rihouey *et al.* [77], together with the observations done by Gindl *et al.* and Özpaprucu *et al.* [84,83], it is possible to hypothesise that: i) the higher amount of glucomannans and probably less branched RG-I in G layer, ii) the higher lignin content in S₁ layer and probably also iii) the lower Uronic Acid content (the more the Uronic Acid the more is the fibre strength [85]) play a central role in the increased hardness of drought-stressed flax fibres helped to improve the hardness of

drought-stressed flax fibres. However, the impact of homogalacturonans, protein and hydroxycinnamic acids on the fibre mechanical behaviour is still unclear.

6. Conclusion

In the present study, a range of deep techniques was used to investigate the morphological, biochemical and mechanical properties of flax stems and fibres when submitted to severe drought. Particular attention was given to the study of single flax fibres because of their wide use in different industrial sectors and especially as composite material reinforcements.

At the biochemical level, direct and indirect exploration of the main molecule family showed contrasts between the control and drought-stressed flax fibres. A huge increase in the protein and lignin content was found in the bast fibre drought-stressed lot, as well as an increase in hydroxycinnamates. This fact calls into question the interconnection between the cell wall polymers of drought-stressed fibres because some hydroxycinnamates are known to be able to interconnect covalently heterogeneous polymers. Additionally, the morphology of the stems and fibres was found to differ, and although the stressed flax fibres are smaller in diameter than those of plants grown under normal conditions, their mechanical properties do not seem to be impacted.

The stiffness measures, both through tensile and indentation values, do not evolve with drought stress; these properties are mainly driven by cellulose arrangement and ultrastructure, which remain quite unchanged here. In contrast, indentation hardness confirms its role as a pertinent indicator of noncellulosic component changes. Thus, thanks to the stability of their mechanical properties at the fibre scale, fibres submitted to drought are still suitable for biocomposite and textile production, although their production yield drastically decreases.

Here, a flax variety rather tolerant to drought was selected, but future work will focus on flax varieties with a higher sensitivity to drought, such as the Aretha variety. Other parameters, such as the cell wall thickness and lumen size and the number of defects along the fibres, should also be explored to better understand the mechanical properties of the drought-stressed fibres.

Bibliography

- [1] A. Gomez-Campos, C. Vialle, A. Rouilly, C. Sablayrolles, L. Hamelin, Flax fiber for technical textile: A life cycle inventory, *J. Clean. Prod.* 281 (2021) 125177. <https://doi.org/10.1016/j.jclepro.2020.125177>.
- [2] A.P. Manian, M. Cordin, T. Pham, Extraction of cellulose fibers from flax and hemp: a review, *Cellulose*. 28 (2021) 8275–8294. <https://doi.org/10.1007/s10570-021-04051-x>.
- [3] A. Le Duigou, P. Davies, C. Baley, Environmental Impact Analysis of the Production of Flax Fibres to be Used as Composite Material Reinforcement, *J. Biobased Mat. Bioenergy*. 5 (2011) 153–165. <https://doi.org/10.1166/jbmb.2011.1116>.
- [4] H.M.G. van der Werf, L. Turunen, The environmental impacts of the production of hemp and flax textile yarn, *Ind. Crops Prod.* 27 (2008) 1–10. <https://doi.org/10.1016/j.indcrop.2007.05.003>.
- [5] A. Le Duigou, P. Davies, C. Baley, Analyse du cycle de vie d'un biocomposite, *Mater. et Tech.* 98 (2010) 143–150. <https://doi.org/10.1051/mattech/2010021>.
- [6] D.U. Shah, P.J. Schubel, M.J. Clifford, Can flax replace E-glass in structural composites? A small wind turbine blade case study, *Compos. B. Eng.* 52 (2013) 172–181. <https://doi.org/10.1016/j.compositesb.2013.04.027>.
- [7] European Environment Agency, Climate change adaptation in the agriculture sector in Europe., Publications Office, LU, 2019. <https://data.europa.eu/doi/10.2800/537176> (accessed February 3, 2021).
- [8] X. Audran, L. McLeod, France facing most severe drought in 50 years, USDA foreign agricultural service, 2011.
- [9] J. Spinoni, G. Naumann, J.V. Vogt, P. Barbosa, The biggest drought events in Europe from 1950 to 2012, *J. Hydrol. Reg. Stud.* 3 (2015) 509–524. <https://doi.org/10.1016/j.ejrh.2015.01.001>.
- [10] F. Habets, P. Viennot, Évolutions constatées et prévi-sibles des principales composantes du climat ayant un effet sur l'agriculture avec un focus sur l'hydrologie, in: *Changement Climatique et Agriculture: Comprendre et Anticiper, Ici et Ailleur*, Agronomie, Environnement&Sociétés, 2015: pp. 24–32.
- [11] A. Goulard, Agria Grand Est, APM, Bâtir en balles, Blackbird, Culture In, Dedienne Multiplasturgy, Egide, Focal, LabelBreed, Notox, S.Randé/CELC, Comité Champagne, Chambre d'Agriculture de l'Aube, Construire en Chanvre, Culture in Varian, FBT Isolation, NatUp fibres, Faurecia, France Miscanthus, FRD, InterChanvre, Parexlanko, Pixabay, Mémento 2020: Panorama des marchés Fibres végétales techniques en matériaux (hors bois) en France, (2020).
- [12] Crops and livestock products: flax fibre and tow, FAOSTAT. (2021). www.fao.org (accessed August 16, 2021).
- [13] A. Kelemen, W. Munch, H. Poelman, Z. Gakova, L. Dijkstra, B. Torighelli, The climate change challenge for European regions, in: *Regions 2020*, European Commission Regional Policy, Brussels, 2009.
- [14] R. Jaime, J.M. Alcántara, A.J. Manzaneda, P.J. Rey, Climate change decreases suitable areas for rapeseed cultivation in Europe but provides new opportunities for white mustard as an alternative oilseed for biofuel production, *PLOS ONE*. 13 (2018) e0207124. <https://doi.org/10.1371/journal.pone.0207124>.
- [15] A. Abot, C. Bonnafous, F. Touchard, F. Thibault, L. Chocinski-Arnault, R. Lemoine, F. Dédaldéchamp, Effects of cultural conditions on the hemp (*Cannabis sativa*) phloem fibres: Biological development and mechanical properties, *J. Compos. Mater.* 47 (2013) 1067–1077. <https://doi.org/10.1177/0021998313477669>.
- [16] S.B. Chemikosova, N.V. Pavlencheva, O.P. Gur'yanov, T.A. Gorshkova, The effect of soil drought on the phloem fiber development in long-fiber flax, *Russ. J. Plant Physiol.* 53 (2006) 656–662. <https://doi.org/10.1134/S1021443706050098>.
- [17] L.W. Kariuki, P. Masinde, S. Githiri, A.N. Onyango, Effect of water stress on growth of three linseed (*Linum usitatissimum* L.) varieties, *Springerplus*. 5 (2016) 759. <https://doi.org/10.1186/s40064-016-2348-5>.
- [18] F.L. Milthorpe, Fibre Development of Flax in Relation to Water Supply and Light Intensity, *Ann. Bot.* 9 (1945) 31–53.

- [19] H. Mahfouze, S. Mahfouze, M. El-Enany, M. Ottai, Assessment of Flax Varieties for Drought Tolerance, *Annu. Res. Rev. Biol.* 21 (2017) 1–12. <https://doi.org/10.9734/ARRB/2017/38495>.
- [20] C. Quagliarini, Fibre vegetali da fusto, foglie, frutti e alghe, in: C. Quagliarini (Ed.), *Chimica delle fibre tessili*, 2nd ed., Zanichelli editore, Bologna, 2012: pp. 107–113.
- [21] D. Bedigian, J.R. Harlan, Evidence for cultivation of sesame in the ancient world, *Econ. Bot.* 40 (1986) 137–154. <https://doi.org/10.1007/BF02859136>.
- [22] C. Michel, M.-L. Nosch, eds., *Textile terminologies in the ancient Near East and Mediterranean from the third to the first millennia BC*, Oxbow Books, Oxford ; Oakville, 2010.
- [23] ARVALIS Institute du végétal, LIN FIBRE: Les activités d'ARVALIS institut du végétal au sein de la filière, ARVALIS, Paris, France, 2015.
- [24] G. Vogeslang-Eastwood, Textiles, in: P.T. Nicholson, I. Shaw (Eds.), *Ancient Egyptian Materials and Technology*, Cambridge University Press, 2000: pp. 268–297.
- [25] D.A. Wilhite, M.H. Glantz, Understanding: the Drought Phenomenon: The Role of Definitions, *Water Int.* 10 (1985) 111–120. <https://doi.org/10.1080/02508068508686328>.
- [26] S. Réquillé, B. Mazian, M. Grégoire, S. Musio, M. Gautreau, L. Nuez, A. Day, P. Thiébeau, F. Philippe, B. Chabbert, A. Chamussy, D.U. Shah, J. Beaugrand, V. Placet, J.-C. Benezet, A. le Duigou, M. Bar, L. Malhautier, E. De Luycker, S. Amaducci, C. Baley, A. Bergeret, A. Bourmaud, P. Ouagne, Exploring the dew retting feasibility of hemp in very contrasting European environments: Influence on the tensile mechanical properties of fibres and composites, *Ind. Crops Prod.* 164 (2021) 113337. <https://doi.org/10.1016/j.indcrop.2021.113337>.
- [27] M. Bouvier d'Yvoire, O. Bouchabke-Coussa, W. Voorend, S. Antelme, L. Cézard, F. Legée, P. Lebris, S. Legay, C. Whitehead, S.J. McQueen-Mason, L.D. Gomez, L. Jouanin, C. Lapierre, R. Sibout, Disrupting the cinnamyl alcohol dehydrogenase 1 gene (BdCAD1) leads to altered lignification and improved saccharification in *Brachypodium distachyon*, *Plant J.* 73 (2013) 496–508. <https://doi.org/10.1111/tpj.12053>.
- [28] J. Beaugrand, C. Alvarado, M.-F. Devaux, C. Rivard, S. Durand, H. Chauvet, M. Réfrégiers, F. Jamme, F. Guillon, A. Bourmaud, C. Baley, C. Goudenhoof, J. Beaugrand, Evolution of the Flax Cell Wall Composition During Development and After Gravitropism by Synchrotron Fluorescence Imaging, Preprint. (preprint). <https://doi.org/10.26434/chemrxiv.14665911.v1>.
- [29] M. Tedetti, R. Longhitano, N. Garcia, C. Guigue, F. Nicolas, M. Goutx, Fluorescence properties of dissolved organic matter in coastal Mediterranean waters influenced by a municipal sewage effluent (Bay of Marseilles, France), *Environmental Chemistry*. 9 (2012) 439–448. <https://doi.org/10.1071/EN12081>.
- [30] F. Jamme, S. Kascakova, S. Villette, F. Allouche, S. Pallu, V. Rouam, M. Réfrégiers, Deep UV autofluorescence microscopy for cell biology and tissue histology, *Biol. Cell.* 105 (2013) 277–288. <https://doi.org/10.1111/boc.201200075>.
- [31] K. Vidot, M.-F. Devaux, C. Alvarado, S. Guyot, F. Jamme, C. Gaillard, R. Siret, M. Lahaye, Phenolic distribution in apple epidermal and outer cortex tissue by multispectral deep-UV autofluorescence cryo-imaging, *Plant Science*. 283 (2019) 51–59. <https://doi.org/10.1016/j.plantsci.2019.02.003>.
- [32] ASTM C1557-20, ASTM International, West Conshohocken, PA, 2020. <https://doi.org/10.1520/C1557-20>.
- [33] A. Lefeuvre, A. Bourmaud, C. Morvan, C. Baley, Tensile properties of elementary fibres of flax and glass: Analysis of reproducibility and scattering, *Mater. Lett.* 130 (2014) 289–291. <https://doi.org/10.1016/j.matlet.2014.05.115>.
- [34] G. Barteau, W. Azoti, M. Gautreau, C. Francart, G. Alès, H. Jmal, J. Bouchet, A. Kervoëlen, J. Beaugrand, N. Bahlouli, A. Bourmaud, Recycling of wood-reinforced poly-(propylene) composites: A numerical and experimental approach, *Ind. Crops. Prod.* 167 (2021) 113518. <https://doi.org/10.1016/j.indcrop.2021.113518>.
- [35] B. Blakeney, P. Harris, R. Henry, B.A. Stone, A simple and rapid preparation of alditol acetates for monosaccharide analysis, *Carbohydr. Res.* 113 (1983) 291–299.
- [36] R. Hatfield, R.S. Fukushima, Can Lignin Be Accurately Measured?, *Crop Sci.* 45 (2005) 832–839. <https://doi.org/10.2135/cropsci2004.0238>.

- [37] S. Ho-Yue-Kuang, C. Alvarado, S. Antelme, B. Bouchet, L. Cezard, P.L. Bris, F. Legee, A. Maia-Grondard, A. Yoshinaga, L. Saulnier, F. Guillon, R. Sibout, C. Lapierre, A.L. Chateigner-Boutin, Mutation in *Brachypodium* caffeic acid O-methyltransferase 6 alters stem and grain lignins and improves straw saccharification without deteriorating grain quality, *J. Exp. Bot.* 67 (2016) 227. <https://doi.org/10.1093/jxb/erv446>.
- [38] K.W. Waldron, A.J. Parr, A. Ng, J. Ralph, Cell wall esterified phenolic dimers: identification and quantification by reverse phase high performance liquid chromatography and diode array detection, *Phytochem. Anal.* 7 (1996) 305–312.
- [39] P.T. Larsson, K. Wickholm, T. Iversen, A CP/MAS ¹³C NMR investigation of molecular ordering in celluloses, *Carbohydr. Res.* 302 (1997) 19–25.
- [40] R.H. Newman, Estimation of the lateral dimensions of cellulose crystallites using ¹³C NMR signal strengths, *Solid State Nucl. Magn. Reson.* 15 (1999) 21–29. [https://doi.org/10.1016/S0926-2040\(99\)00043-0](https://doi.org/10.1016/S0926-2040(99)00043-0).
- [41] W. Kolodziejski, J. Klinowski, Kinetics of Cross-Polarization in Solid-State NMR: A Guide for Chemists, *Chem. Rev.* 102 (2002) 613–628. <https://doi.org/10.1021/cr000060n>.
- [42] ARVALIS Institut du végétal, Lin fibre: résultats et préconisations, ARVALIS, Paris, France, 2019.
- [43] A. Lefeuvre, C. Baley, C. Morvan, Analysis of Flax Fiber Cell-Wall Non-Cellulosic Polysaccharides Under Different Weather Conditions (Marylin Variety), *J. Nat. Fibers.* 15 (2018) 539–544. <https://doi.org/10.1080/15440478.2017.1349020>.
- [44] D.E. Akin, G.R. Gamble, W.H. Morrison III, L.L. Rigsby, R.B. Dodd, Chemical and Structural Analysis of Fibre and Core Tissues from Flax, *J. Sci. Food Agric.* 72 (1996) 155–165. [https://doi.org/10.1002/\(SICI\)1097-0010\(199610\)72:2<155::AID-JSFA636>3.0.CO;2-X](https://doi.org/10.1002/(SICI)1097-0010(199610)72:2<155::AID-JSFA636>3.0.CO;2-X).
- [45] C. Lion, C. Simon, B. Huss, A.-S. Blervacq, L. Tirot, D. Toybou, C. Spriet, C. Slomianny, Y. Guerardel, S. Hawkins, C. Biot, BLISS: A Bioorthogonal Dual-Labeling Strategy to Unravel Lignification Dynamics in Plants, *Cell Chem. Biol.* 24 (2017) 326–338. <https://doi.org/10.1016/j.chembiol.2017.02.009>.
- [46] T. Gorshkova, C. Morvan, Secondary cell-wall assembly in flax phloem fibres: role of galactans, *Planta.* 223 (2006) 149–158. <https://doi.org/10.1007/s00425-005-0118-7>.
- [47] A.A. Petrova, L.V. Kozlova, I.Z. Gaifullina, B.A. Ananchenko, E.A. Martinson, P.V. Mikshina, T.A. Gorshkova, AFM analysis reveals polymorphism of purified flax rhamnogalacturonans I of distinct functional types, *Carbohydr. Polym.* 216 (2019) 238–246. <https://doi.org/10.1016/j.carbpol.2019.03.087>.
- [48] C. Baley, A. Bourmaud, Average tensile properties of French elementary flax fibers, *Mater. Lett.* 122 (2014) 159–161. <https://doi.org/10.1016/j.matlet.2014.02.030>.
- [49] C. Goudenhooft, A. Bourmaud, C. Baley, Varietal selection of flax over time: Evolution of plant architecture related to influence on the mechanical properties of fibers, *Ind. Crops Prod.* 97 (2017) 56–64. <https://doi.org/10.1016/j.indcrop.2016.11.062>.
- [50] W. Gindl, H.S. Gupta, C. Grünwald, Lignification of spruce tracheid secondary cell walls related to longitudinal hardness and modulus of elasticity using nano-indentation, *Can. J. Bot.* 80 (2002) 1029–1033. <https://doi.org/10.1139/b02-091>.
- [51] S. Stanzl-Tschegg, W. Beikircher, D. Loidl, Comparison of mechanical properties of thermally modified wood at growth ring and cell wall level by means of instrumented indentation tests, *Holzforschung.* 63 (2009) 443–448. <https://doi.org/10.1515/HF.2009.085>.
- [52] M. Farooq, M. Hussain, A. Wahid, K.H.M. Siddique, Drought Stress in Plants: An Overview, in: R. Aroca (Ed.), *Plant Responses to Drought Stress*, Springer Berlin Heidelberg, Berlin, Heidelberg, 2012: pp. 1–33. https://doi.org/10.1007/978-3-642-32653-0_1.
- [53] G.S. McMaster, W.W. Wilhelm, Phenological responses of wheat and barley to water and temperature: improving simulation models, *J. Agric. Sci.* 141 (2003) 129–147. <https://doi.org/10.1017/S0021859603003460>.
- [54] G. Neutelings, Lignin variability in plant cell walls: Contribution of new models, *Plant. Sci. J.* 181 (2011) 379–386. <https://doi.org/10.1016/j.plantsci.2011.06.012>.
- [55] M. Frei, Lignin: Characterization of a Multifaceted Crop Component, *Sci. World J.* 2013 (2013) 1–25. <https://doi.org/10.1155/2013/436517>.

- [56] U.C. Malavasi, A.S. Davis, M. de M. Malavasi, Lignin in Woody Plants under Water Stress: A Review, *Floresta Ambient.* 23 (2016) 589–597. <https://doi.org/10.1590/2179-8087.143715>.
- [57] Y. Hu, W.Ch. Li, Y.Q. Xu, G.J. Li, Y. Liao, F.-L. Fu, Differential expression of candidate genes for lignin biosynthesis under drought stress in maize leaves, *J. Appl. Genet.* 50 (2009) 213–223. <https://doi.org/10.1007/BF03195675>.
- [58] M. Cabané, D. Afif, S. Hawkins, Lignins and Abiotic Stresses, in: *Advances in Botanical Research*, Elsevier, 61, 2012: pp. 219–262. <https://doi.org/10.1016/B978-0-12-416023-1.00007-0>.
- [59] U. Schuppler, P.-H. He, P.C.L. John, R. Munns, Effect of Water Stress on Cell Division and Cdc2-Like Cell Cycle Kinase Activity in Wheat Leaves, *Plant Physiol.* 117 (1998) 667–678. <https://doi.org/10.1104/pp.117.2.667>.
- [60] D. Bartels, R. Sunkar, Drought and Salt Tolerance in Plants, *Crit. Rev. Plant Sci.* 24 (2005) 23–58. <https://doi.org/10.1080/07352680590910410>.
- [61] A. Shankar, N. Agrawal, M. Sharma, A. Pandey, G.K. Pandey, Role of Protein Tyrosine Phosphatases in Plants, *Curr. Genomics.* 16 (2015) 224–236. <https://doi.org/10.2174/1389202916666150424234300>.
- [62] D.L. Sihel, The Biosynthesis of Tryptophan, Tyrosine, and Phenylalanine from Chorismate, in: B.K. Singh (Ed.), *Plant Amino Acids: Biochemistry and Biotechnology*, 1st ed., CRC Press, 1998: 171–200. <https://doi.org/10.1201/9781482270068>.
- [63] Y. Zhao, Auxin biosynthesis and its role in plant development, *Annu. Rev. Plant. Biol.* 61 (2010) 49–64. <https://doi.org/10.1146/annurev-arplant-042809-112308>.
- [64] J.B. Bowne, T.A. Erwin, J. Juttner, T. Schnurbusch, P. Langridge, A. Bacic, U. Roessner, Drought Responses of Leaf Tissues from Wheat Cultivars of Differing Drought Tolerance at the Metabolite Level, *Mol. Plant.* 5 (2012) 418–429. <https://doi.org/10.1093/mp/ssr114>.
- [65] J. Rodríguez-Calcerrada, A.M. Rodrigues, C. António, P. Perdiguero, P. Pita, C. Collada, M. Li, L. Gil, Stem metabolism under drought stress – a paradox of increasing respiratory substrates and decreasing respiratory rates, *Physiol. Plantarum.* 172 (2021) 391–404. <https://doi.org/10.1111/ppl.13145>.
- [66] J.H. Chen, C.-T. Ho, Antioxidant Activities of Caffeic Acid and Its Related Hydroxycinnamic Acid Compounds, *J. Agric. Food Chem.* 45 (1997) 2374–2378. <https://doi.org/10.1021/jf970055t>.
- [67] D.M. Macoy, W.-Y. Kim, S.Y. Lee, M.G. Kim, Biosynthesis, physiology, and functions of hydroxycinnamic acid amides in plants, *Plant Biotechnol. Rep.* 9 (2015) 269–278. <https://doi.org/10.1007/s11816-015-0368-1>.
- [68] H.R. El-Seedi, E.A. Taher, B.Y. Sheikh, S. Anjum, A. Saeed, M.F. AlAjmi, M.S. Moustafa, S.M. Al-Mousawi, M.A. Farag, M.-E.F. Hegazy, S.A.M. Khalifa, U. Göransson, Hydroxycinnamic Acids: Natural Sources, Biosynthesis, Possible Biological Activities, and Roles in Islamic Medicine, in: *Studies in Natural Products Chemistry*, Elsevier, 55, 2018: pp. 269–292. <https://doi.org/10.1016/B978-0-444-64068-0.00008-5>.
- [69] J.M. Humphreys, C. Chapple, Rewriting the lignin roadmap, *Curr. Opin. Cell Biol.* 5 (2002) 224–229. [https://doi.org/10.1016/S1369-5266\(02\)00257-1](https://doi.org/10.1016/S1369-5266(02)00257-1).
- [70] L. Hoffmann, S. Besseau, P. Geoffroy, C. Ritzenthaler, D. Meyer, C. Lapierre, B. Pollet, M. Legrand, Silencing of Hydroxycinnamoyl-Coenzyme A Shikimate/Quinate Hydroxycinnamoyltransferase Affects Phenylpropanoid Biosynthesis, *Plant Cell.* 16 (2004) 1446–1465. <https://doi.org/10.1105/tpc.020297>.
- [71] T. Gorshkova, V.V. Salnikov, N.M. Pogodina, S.B. Chemikosova, E.V. Yablokova, A.V. Ulanov, M.V. Ageeva, J.E.G. van Dam, V.V. Lozovaya, Composition and Distribution of Cell Wall Phenolic Compounds in Flax (*Linum usitatissimum* L.) Stem Tissues, *Ann. Bot.* 85 (2000) 477–486. <https://doi.org/10.1006/anbo.1999.1091>.
- [72] D. Šamec, E. Karalija, I. Šola, V. Vujčić Bok, B. Salopek-Sondi, The Role of Polyphenols in Abiotic Stress Response: The Influence of Molecular Structure, *Plants.* 10 (2021) 118. <https://doi.org/10.3390/plants10010118>.
- [73] Y. Verherbruggen, J.L. Walker, F. Guillon, H.V. Scheller, A comparative study of sample preparation for staining and immunodetection of plant cell walls by light microscopy, *Front. Plant Sci.* 8 (2017) 1505. <https://doi.org/10.3389/fpls.2017.01505>.
- [74] M. Chen, X. Zhu, Y. Zhang, Z. Du, X. Chen, X. Kong, W. Sun, C. Chen, Drought stress modify cuticle of tender tea leaf and mature leaf for transpiration barrier enhancement through common and distinct modes, *Sci. Rep.* 10 (2020) 6696. <https://doi.org/10.1038/s41598-020-63683-4>.

- [75] A. Day, K. Ruel, G. Neutelings, D. Crônier, H. David, S. Hawkins, B. Chabbert, Lignification in the flax stem: evidence for an unusual lignin in bast fibers, *Planta*. 222 (2005) 234–245. <https://doi.org/10.1007/s00425-005-1537-1>.
- [76] F. Baldacci-Cresp, C. Spriet, L. Twyffels, A.-S. Blervacq, G. Neutelings, M. Baucher, S. Hawkins, A rapid and quantitative safranin-based fluorescent microscopy method to evaluate cell wall lignification, *Plant J.* 102 (2020) 1074–1089. <https://doi.org/10.1111/tpj.14675>.
- [77] C. Rihouey, F. Paynel, T. Gorshkova, C. Morvan, Flax fibers: assessing the non-cellulosic polysaccharides and an approach to supramolecular design of the cell wall, *Cellulose*. 24 (2017) 1985–2001. <https://doi.org/10.1007/s10570-017-1246-5>.
- [78] T. Gorshkova, T. Chernova, N. Mokshina, M. Ageeva, P. Mikshina, Plant ‘muscles’: fibers with a tertiary cell wall, *New Phytol.* 218 (2018) 66–72. <https://doi.org/10.1111/nph.14997>.
- [79] T. Gorshkova, P. Mikshina, A. Petrova, T. Chernova, N. Mokshina, O. Gorshkov, Plants at Bodybuilding: Development of Plant “Muscles,” in: A. Geitmann, J. Gril (Eds.), *Plant Biomechanics: From Structure to Function at Multiple Scales*, Springer, Cham, 2018: pp. 141–163. https://doi.org/10.1007/978-3-319-79099-2_7.
- [80] C. Goudenhooft, A. Bourmaud, C. Baley, Flax (*Linum usitatissimum* L.) Fibers for Composite Reinforcement: Exploring the Link Between Plant Growth, Cell Walls Development, and Fiber Properties, *Front. Plant Sci.* 10 (2019) 411. <https://doi.org/10.3389/fpls.2019.00411>.
- [81] M. Eder, O. Arnould, J.W.C. Dunlop, J. Hornatowska, L. Salmén, Experimental micromechanical characterisation of wood cell walls, *Wood Sci. Technol.* 47 (2013) 163–182. <https://doi.org/10.1007/s00226-012-0515-6>.
- [82] A. Jäger, Th. Bader, K. Hofstetter, J. Eberhardsteiner, The relation between indentation modulus, microfibril angle, and elastic properties of wood cell walls, *Compos. Part A Appl. Sci. Manuf.* 42 (2011) 677–685. <https://doi.org/10.1016/j.compositesa.2011.02.007>.
- [83] M. Özparpucu, N. Gierlinger, I. Cesarino, I. Burgert, W. Boerjan, M. Rüggeberg, Significant influence of lignin on axial elastic modulus of poplar wood at low microfibril angles under wet conditions, *J. Exp. Bot.* 70 (2019) 4039–4047. <https://doi.org/10.1093/jxb/erz180>.
- [84] M. Özparpucu, M. Rüggeberg, N. Gierlinger, I. Cesarino, R. Vanholme, W. Boerjan, I. Burgert, Unravelling the impact of lignin on cell wall mechanics: a comprehensive study on young poplar trees downregulated for CINNAMYL ALCOHOL DEHYDROGENASE (CAD), *Plant J.* 91 (2017) 480–490. <https://doi.org/10.1111/tpj.13584>.
- [85] A. Bourmaud, C. Morvan, A. Bouali, V. Placet, P. Perré, C. Baley, Relationships between micro-fibrillar angle, mechanical properties and biochemical composition of flax fibers, *Ind. Crops Prod.* 44 (2013) 343–351. <https://doi.org/10.1016/j.indcrop.2012.11.031>.



General conclusion and further works



The aim of this study was to relate art, engineering and flax industry. With the state-of-the-art presented in **Chapter I**, all the topics addressed in the text are slowly introduced, laying the groundwork to all the questions opened that this thesis aimed to answer. Successively, **Chapter II** describes the three principal cutting-edge techniques used during these three years of research.

Thanks to the deep investigation of the flax fibres ultrastructure in **Chapter III**, it was confirmed that kink-bands are one of the weakest points for two main reasons related to one another: i) they cause the deviation of cellulose microfibrils and ii) the detached microfibrils create cavities and inhomogeneities into the microfibril network, and, thus, into the fibre structure. Kink-bands resulted weak and fractured after a natural ageing process both in the mortuary linen dated several millennia and in some fibres of yarns from Italian paintings dated several centuries.

The extraction method plays a central role in the formation of these defects all along the fibres. The different extraction tools, which have evolved over time, can probably change the kink-band frequency along the fibre and also their shape and size. Unfortunately, no existing literature compares ancient and modern tools and their ability to create kink-bands. The new international ANR project “ANUBIS” is going to start in the year 2021; thanks to a collaboration between the University of South Brittany, INRAE, University of Cambridge, Synchrotron SOLEIL and the Oriental Archaeology French Institute in Cairo, this project will focus on kink-bands evolution and also in a more in-depth study of the ageing process of cellulosic flax fibres.

Contrary to kink-bands, middle lamellae, which are considered susceptible to fracture when plant fibres are used to reinforce biocomposite materials, have been demonstrated to be stronger than expected. The indentation modulus obtained can be either much lower or almost comparable to the indentation modulus measured in fibres cell walls, depending on the plant species and the retting process that the fibres have undergone. From this point of view, a future work that can compare middle lamellae from green and processed stems by atomic force microscopy, could better explain the micromechanical evolution of middle lamellae before and after the retting process.

Chapter IV focused on the study of the degradation mechanisms on both historical and modern objects that showed a very similar process. Thanks to the investigation of ancient flax fabrics, it was possible to confirm that the crystalline cellulose undergo slight modifications even after millennia if the artworks are preserved in favourable conditions. Contrary to the cellulose microfibrils, the polymer matrix of flax fibre cell walls, mainly composed of hemicellulose, pectin and a small amount of lignin, is more susceptible to degradation and biochemical modifications, especially under biological attack.

A biological attack is the main factor that plays an active and dramatic role, together with water, in cellulosic fibre degradation. From this perspective, the yarn from the Egyptian mortuary linen resulted much better preserved than the yarns from canvases, except for kink-bands where fractures have been

observed in almost all the fibres from the Egyptian yarn contrarily to the yarns from the canvases where these regions appeared mainly intact. The fact that no traces of fungi were observed on the fibre's surface from the Egyptian fabric, could be ascribed to the most suitable environmental conditions in which the mortuary linen was preserved.

Regarding the canvases, the oldest canvas investigated between the four considered, the '*San Cristoforo*' by Giulio Benso (GB), was subjected to a lower degradation process than the other three canvases. Clear traces of fungal colonization and fibre degradation due to hydrolysis and/or oxidation were principally found in the other three canvases and, interestingly, in the '*Crocefissione*' by Tommaso Sciacca (TS1), not only the surface of the fibre was involved, but also the internal structure appeared degraded. In this particular sample, degradation mechanisms were observed both starting from the lumen and from the surface of the fibres. Some fractured kink-bands can promote not only the penetration of bacteria and fungi, but also of water molecules, essential for biodegradation activity, in the innermost cell wall layers.

Thanks to the study of the modern biocomposite left in compost for several months, it was possible to focus on some fungi and bacteria degradation marks. In this case, bacteria were able to create tunnels and degrade the fibres starting from the lumen. An important observation of this work is that the loss of the mechanical properties principally involves the G or the P layers first and only successively the S₁ layer, which is more slowly degraded than the other two layers. The mechanical properties of the S₁ layer can be almost intact even in an advanced state of fibre degradation.

Future works should focus on identifying fungi and bacteria from degraded PLA/flax biocomposites starting from the core of a sample for a future industrial application. In parallel, thanks to the literature, it has been shown that fungi and bacteria present during the retting stage of flax stems can survive even after the fibre extraction and that some of these microorganisms are in common with artworks, and, hypothetically, also with modern flax objects. This observation opens up the question of their origin and whether some microorganisms that degrade objects made of linen are not already inside the fibres from the very beginning and develop when favourable environmental conditions are reached.

To conclude, another important link can be drawn between the past and the present days. History teaches us that changes in the flax cultivation areas and production of flax fibres were often linked to unfavourable environmental conditions and the cost/benefit ratio in terms of time and workforce that force human populations to find ways to improve the production or abandon it in favour of other types of textiles, such as wool and cotton. Nowadays, our society faces global warming and frequent extreme weather events in Europe often result in drought or sudden and abundant storms and floods. Currently, flax fibre production is mainly located in a very small area in the north-west of France, which means that the effects of climate change can have a major impact on the flax fibre production if this area is concerned. The study presented in **Chapter V** shows that, due to a moderate drought, the fibre yield is

lower and that despite biochemical changes in the flax fibre cells, the mechanical properties are still similar to those of flax plants grown under normal conditions.

However, the variety of flax must be considered in regard to the response to this type of stress since human selection resulted in some varieties being more sensitive than others to changes in environmental factors. For this reason, another future research may focus on comparing varieties and their relative response to this abiotic stress to help future industries select the more resistant fibres in case of flax cultivations in drought-risky areas.

These findings suggest a very promising and constructive relationship between art and engineering. The ANUBIS project is now designed to continue this research project and find answers to new questions opened with this work, such as the effects of the ancient extraction tools and treatments on fibres ultrastructure and morphology. Furthermore, the study of the natural ageing process of plant fibres over time and its impact on the fibre structure (in particular in kink-bands regions), achieved by the comparison between ancient and modern objects, will be one of the main topics that this project intends to address. The final objective being to better understand the flax fibres ageing behaviour to design sustainable biobased composites for tomorrow.

Conclusion générale et perspectives

Le principal objectif de cette thèse était de mettre en relation art, ingénierie et industrie de lin. Grâce à l'état de l'art présenté dans le **Chapitre I**, toutes les bases nécessaires aux questions ouvertes auxquelles cette recherche a essayé de répondre sont progressivement introduites.

Ensuite, les trois principales techniques utilisées pour cette étude sont brièvement décrites dans le **Chapitre II**.

Grâce à l'étude approfondie de l'ultrastructure des fibres de lin présentée dans le **Chapitre III**, les genoux ont démontré être des points faibles pour deux raisons principales qui se sont révélées être liées : i) ils causent une déviation des microfibrilles qui, en s'écartant du reste du réseau de microfibrilles, génère des cavités et hétérogénéités dans la structure des parois et, ii) les genoux se sont révélés être particulièrement fragiles et endommagés, même après le processus de vieillissement naturel étudié sur les deux types d'œuvres d'art examinées, que ce soit un fil de lin en provenant d'un tissu mortuaire et datant de quelques millénaires ou que ce soient des fils de lin provenant des tableaux Italiens et datant de quelques centaines d'années.

La méthode et les outils d'extraction des fibres jouent un rôle central sur la formation de ces défauts tout au long des fibres ainsi que sur leur évolution au fil du temps. De plus, leur fréquence, leur taille et leur forme géométrique varie aussi grandement selon les cas étudiés. Malheureusement, aujourd'hui il n'y a pas dans la littérature une étude qui compare les instruments d'extraction modernes aux anciens et leur faculté à créer ce type de défaut tout au long des fibres. Un nouveau projet ANR, ANUBIS, va démarrer à la fin de cette année 2021. Grâce à la collaboration entre l'Université de Bretagne Sud, INRAE, l'Université de Cambridge, le Synchrotron SOLEIL et l'Institut Français d'Archéologie Orientale, ce projet sera focalisé sur l'investigation plus approfondie du processus de dégradation des fibres de lin, grâce à l'étude de fils de lin anciens de diverses structures et origines.

Au contraire des genoux, les lamelles moyennes, qui sont souvent considérées comme des zones de rupture privilégiée quand les fibres de plantes sont utilisées dans des matériaux biocomposites, ces lamelles ont montré avoir des propriétés mécaniques plus élevées qu'attendu. Les modules d'indentation obtenus peuvent être beaucoup plus faibles ou, au contraire, quasiment similaires aux modules d'indentation des parois secondaires des fibres, en accord avec les espèces des plantes considérées et leur processus de rouissage. Forts de ce constat, un travail futur de comparaison par microscopie à force atomique des lamelles moyennes entre des tiges vertes et des fibres extraites pourrait permettre de mieux expliquer l'évolution micromécanique des lamelles moyennes avant et après rouissage.

Le **Chapitre IV** se focalise sur les mécanismes de dégradation, en étudiant des objets anciens issus du patrimoine culturel. L'étude des textiles anciens a confirmé que la partie cristalline peut se modifier de manière significative, même si un objet est préservé dans des conditions favorables comme cela

pouvait être le cas dans des tombeaux. Toutefois, ce n'est pas le cas pour la matrice non cellulosique des fibres, composée surtout par des hémicelluloses et pectines dans le cas des fibres de lin, et qui est plus susceptible de se dégrader et se modifier au niveau compositionnel, spécialement par attaque biologique. L'attaque biologique, comme l'eau, comptent parmi les principaux facteurs jouant un rôle actif et dramatique sur la dégradation des fibres cellulosiques.

De ce point de vue, le fil provenant d'un tissu mortuaire d'époque du Moyen Empire Egyptien s'est révélé être mieux préservé que les fils extraits des quatre tableaux italiens. Néanmoins il y a une exception, les genoux, dont des profondes fractures ont été observées sur quasiment toutes les fibres du fil égyptien par rapport aux autres quatre fils pour lesquels ces régions apparaissaient intactes.

Le fait que ni les champignons et ni les bactéries n'ont été observés sur la surface des fibres, peut être attribué aux meilleures conditions environnementales dans lesquelles le tissu égyptien a été préservé.

Concernant les toiles des tableaux, la toile la plus ancienne parmi les quatre considérées, issue du tableau « *San Cristoforo* » peint par Giulio Benso (GB), a subi un processus de dégradation plus faible que les trois autres. Dans les autres trois toiles, des traces de colonisation fongique et de dégradation des fibres par hydrolyse et/ou oxydation ont été trouvées, et l'attaque biologique n'était pas limitée à la surface; dans la « *Crocefissione* » peint par Tommaso Sciacca (TS1), même la structure la plus interne des fibres était dégradée. Sur ce dernier échantillon, nous avons observé des formes de dégradation soit à partir du lumen, soit à partir de la surface des fibres. Les fractures dans les genoux, qui sont parfois trouvées sur les fibres vieilles, peuvent faciliter la pénétration de bactéries et de champignons jusqu'aux couches les plus internes, ainsi que des molécules d'eau dont la présence reste une condition fondamentale pour l'activité de biodégradation. Ce travail a initié l'étude d'un biocomposite actuel dégradé en compost pendant plusieurs mois, nous nous sommes ensuite focalisés sur les mécanismes de dégradation des parois des fibres de lin par les champignons et les bactéries.

Nous avons montré que les bactéries étaient capables de créer des tunnels et dégrader les fibres par l'intérieur, à commencer par le lumen. Une observation importante à la suite de cette étude est que la perte des propriétés mécaniques est limitée dans un premier temps à la couche de parois gélatineuse (G) située à l'intérieur de la fibre ou, plus rarement, à la couche de parois primaire extérieure (P) ; au contraire la couche S_1 se dégrade de manière plus lente que les autres couches, probablement en raison de son taux de lignine plus élevé. Les propriétés mécaniques de la couche S_1 peuvent ainsi rester quasiment intactes même si la fibre est dans un état de dégradation avancé.

Dans un travail futur, il sera opportun d'identifier le type de champignons et bactéries qui sont capables de dégrader un biocomposite de PLA/lin à partir de la section intérieure d'une fibre, en vue d'une application industrielle.

En parallèle, dans la littérature il a été démontré que champignons et bactéries colonisant les plantes lors de l'étape de rouissage des tiges de lin peuvent survivre à l'extraction et que certains d'entre eux sont similaires à ceux identifiés dans les objets d'art et, hypothétiquement, même au sein des objets

fabriqués aujourd'hui. Cela soulève la question de leur origine et si certains micro-organismes qui dégradent les objets en lin ne sont pas déjà présents au sein des parois des fibres dès le début et se développent lorsque des conditions environnementales favorables sont atteintes.

Pour conclure, un autre lien important peut être tracé par l'histoire du lin entre le passé et le présent. L'histoire nous a appris que les évolutions des zones de culture du lin et de production des fibres de lin étaient surtout liées aux conditions environnementales et au rapport coût/bénéfice en termes de temps de production et de la main-d'œuvre. Cela obligeait les populations à trouver des méthodes pour améliorer la production en fibres de lin ou, au contraire, à l'abandonner en faveur d'autres textiles plus faciles à produire et/ou travailler, comme le coton et la laine.

Aujourd'hui, notre société doit faire face au réchauffement climatique et aux événements météorologiques extrêmes rencontrés en Europe. Ils sont surtout liés aux épisodes prolongés de sécheresse ou des tempêtes et inondations soudaines et abondantes qui causent la destruction des récoltes dans l'agriculture. Actuellement, la plus grande partie de la production mondiale actuelle des fibres de lin est limitée à une zone bien localisée au nord de la France. Cela signifie que dans le futur, les effets des changements climatiques pourraient affecter énormément la production des fibres de lin si cette zone est touchée par des épisodes météorologiques extrêmes, et en particulier des épisodes de sécheresse.

L'étude présentée dans le **Chapitre V** montre qu'une sécheresse modérée provoque une diminution du rendement de lin et un changement biochimique autant au niveau de la plante qu'au niveau des fibres. Malgré cette évolution de la composition biochimique des fibres, les fibres testées mécaniquement ont montré avoir des bonnes propriétés mécaniques même si les plantes ont été cultivées sous stress hydrique. Celles-ci se sont révélées comparables aux propriétés mécaniques des fibres ayant reçu des quantités conventionnelles de pluie.

Toutefois, la variété de lin joue un rôle important sur la réponse au stress hydrique car certaines d'entre elles sont plus sensibles que d'autres, ayant bénéficié de la sélection variétale très développée dans le secteur du lin depuis environ un siècle. Pour cette raison, un travail futur pourrait éventuellement comparer la réponse de deux ou plus variétés connues pour avoir une sensibilité complètement opposée au stress hydrique. Un des objectifs d'un tel travail serait de mieux comprendre les mécanismes des défenses de la plante et d'aider les chercheurs et les cultivateurs de lin à sélectionner les variétés de lin les plus résistantes, ainsi que leurs caractéristiques en prévision de cultures conduites dans des zones de potentielle sécheresse.

Les résultats de ce travail multidisciplinaire suggèrent une relation très prometteuse entre l'art et l'ingénierie ; ANUBIS est le projet désigné pour prendre la suite de cette recherche et trouver les réponses aux questions restant encore ouvertes, par exemple les effets des différents anciens instruments et méthodes d'extraction sur l'ultrastructure des fibres. Le processus de vieillissement naturel des fibres végétales au fil des siècles, l'étude de l'impact du temps sur la structure des fibres (et particulièrement dans les zones de genoux) et la comparaison entre objets anciens et modernes sont les principaux sujets

Conclusions générales et perspectives

que ce projet ambitionne d'aborder. L'objectif final étant de mieux comprendre les mécanismes de vieillissement des fibres de lin afin de concevoir des composites biosourcés durables pour demain.

Titre : Évolution de l'ultrastructure, de la composition des parois et des propriétés mécaniques des fibres de lin au fil du temps : quand l'histoire rencontre la science

Mots clés : lin, fibres, ultrastructure, vieillissement, propriétés mécaniques, histoire

Résumé : Les fibres de lin sont utilisées par la civilisation humaine depuis des millénaires. Mais le réchauffement climatique et la pollution causés par les matériaux pétro-sourcés suscitent un regain d'intérêt pour les fibres végétales et leur utilisation pour de nouvelles applications, en tant que renforts de matériaux composites par exemple.

Ce travail de recherche fait le lien entre passé et présent, en tentant de mieux comprendre le comportement des fibres de lin moderne à travers l'étude d'objets anciens.

Grâce à une combinaison originale des microscopies électronique, à force atomique et bi-photon, des investigations faites sur fibres modernes, ont mis en évidence des hétérogénéités dans leur ultrastructure, essentiellement dans les zones de genoux. Par ailleurs, ces régions ont démontré être sensibles aux mécanismes de vieillissement que ce soit dans un tissu funéraire égyptien vieux de plus de 4000 ans ou dans des toiles de tableaux Italiens,

datés entre le XVII et le XVIII siècle. Les microfibrilles de cellulose de ces fibres anciennes apparaissent quasiment intactes à travers le temps, au contraire de la matrice polymérique des parois végétales, particulièrement sensible au vieillissement, et présentant des évolutions biochimiques et mécaniques, notamment, une rigidification significative. Sur ces fibres anciennes, des signes d'attaque biologique ont été observés de manière similaire aux mécanismes relevés sur des fibres utilisées pour un biocomposite lin/PLA dégradé en compost. Ainsi, champignons et bactéries dégradent préférentiellement les hémicelluloses et la cellulose des parois cellulaires des fibres de lin. Pour conclure ce travail, les effets de sécheresse sur les plantes de lin et les fibres extraites ont été évalués, afin de se projeter vers l'avenir et de mieux comprendre des évolutions climatiques à venir sur les propriétés de cette plante, qui représente plus que jamais un pont entre les civilisations.

Title : Evolution of the ultrastructure, mechanical properties and parietal composition of flax fibres over time: when history meets science

Keywords : flax, fibres, ultrastructure, ageing, mechanical properties, history

Abstract : Flax fibres have been used by human civilization for millennia. But global warming and pollution caused by non-biodegradable materials have aroused renewed interest in plant fibres and their use in new applications, such as reinforcements of biocomposite materials.

This research is focused on drawing a line of continuity between the past and the present day, trying to understand the behaviour of flax fibres in modern objects through the study of the ancient ones.

Thanks to an original combination of atomic force, electronic and multi-photon microscopies, investigations on modern flax fibres highlighted heterogeneous in their ultrastructure, especially in kink-band area. Moreover, these regions have been proved to be sensitive to ageing mechanisms, whether in an Egyptian funerary fabric that is more than 4,000 years old or

in Italian paintings dated between the 17th and 18th centuries.

The cellulose microfibrils of these old fibres appear almost intact over time, in contrast to the polymeric matrix of the plant cell walls, which is particularly sensitive to ageing, and shows biochemical and mechanical changes, including significant stiffening. On these ancient fibres, signs of biological attack were observed in a similar way to the mechanisms noticed on fibres used for a flax/PLA biocomposite degraded in compost. Thus, fungi and bacteria preferentially degrade the hemicelluloses and cellulose of the cell walls of flax fibres. To conclude this work, the effects of drought on flax plants and extracted fibres were evaluated to look to the future and better understand the impact of possible climate changes on the properties of this plant, which represents more than ever a bridge between civilisations.